

Fund. Cosmic Physics, 1996. Vol. 17, pp. 95-281

GALACTIC RINGS

R. BUTA^{1,3} and F. COMBES²

¹ [*Department of Physics and Astronomy, University of Alabama*](#)

² [*Observatoire de Paris*](#)

³ [*Visiting Astronomer, Cerro Tololo Inter-American Observatory, National Optical Astronomy Observatories, which is operated by the Association of Universities for Research in Astronomy, Inc. \(AURA\), under cooperative agreement with the National Science Foundation.*](#)

ABSTRACT

About one fifth of all spiral disk galaxies include a ring-shaped pattern in the light distribution, and an additional one third appear to have broken or partial rings made up of spiral arms (pseudorings). These rings are a special problem in galaxy morphology with a direct bearing on the internal dynamics and evolution of disk galaxies. Morphological data have shown that rings are most often associated with bars or other common nonaxisymmetric perturbations, such as ovals. Kinematic and metric data have provided considerable evidence for intrinsic oval shapes and preferred alignments between ring major axes and bars. Photometric data have demonstrated that most rings are sites of current active star formation, and in some galaxies a ring is the *only* place where recent star formation is found. A few rings are sites of the most spectacular "starbursts" known in non-violently interacting galaxies.

Though a small fraction of observed rings may be due to collisions or mergers of galaxies, or to accretion of intergalactic gas, the vast majority of rings are probably simple resonance phenomena, caused by the actions of a rotating bar or other nonaxisymmetric disturbance on the motions of gas clouds in the disk. The evidence in support of this idea has accumulated steadily during the past 15 years, and our goal in this review is to bring together a large body of theoretical and observational results in one place. We shall see that rings are a *natural* consequence of barred galaxy dynamics, and that they are more easily understood than the bars and ovals which undoubtedly create them. However, there are interesting problems, such as the lack of any rings in some barred galaxies, the less common but by no means rare cases of rings in nonbarred galaxies, the role of mild tidal interactions, where the gas that fuels star formation in rings actually comes from, the existence of intrinsic bar/ring misalignment, and the simultaneous existence of different ring types of very different time-scales in the same galaxy. We will discuss these problems in some detail here, and indicate where the solutions may lie.

Keywords: Galaxies - structure; dynamics; evolution; rings; bars; simulations

Contents

1. [Introduction](#)
2. [Historical Overview](#)
 - 2.1 [Inner Ring Structures](#)
 - 2.2 [Outer Ring Structures](#)
 - 2.3 [Nuclear Ring Structures](#)
3. [Comparison of Ring Classifications](#)
4. [Recent Revisions to the Classification](#)
 - 4.1 [Outer Ring and Pseudoring Morphologies](#)
 - 4.2 [Inner, Outer, and Nuclear Lenses](#)
5. [Confusion of Ring Types in Nonbarred Galaxies](#)
6. [Summary of Notation for Ring and Lens Types](#)
7. [Rings and Lenses as Distinct Components of Barred Galaxy Structure](#)
8. [Rings and Nuclear Activity](#)
9. [Observations of Galactic Rings](#)
 - 9.1 [Frequency](#)
 - 9.2 [Linear and Relative Diameters](#)
 - 9.3 [Intrinsic Shapes and Orientations](#)
 - 9.4 [Photometric Properties](#)

- 9.5 [HII Regions in Ringed Galaxies](#)
- 9.6 [Neutral Hydrogen Emission from Ringed Galaxies](#)
- 9.7 [CO, IR, and Radio Continuum Emission from Ringed Galaxies](#)
- 9.8 [Kinematic Studies](#)
- 10. [Theories of Ring Formation](#)
 - 10.1 [Some Historical Points](#)
 - 10.2 [Fundamental Clues from Observations](#)
- 11. [Dynamics of Bars](#)
 - 11.1 [Bar Formation](#)
 - 11.2 [Orbits in a Barred Galaxy](#)
 - 11.3 [Bars in Early- and Late-Type Galaxies](#)
 - 11.4 [Pattern Speed Determination](#)
 - 11.5 [Angular Momentum Transport](#)
- 12. [Gas Flows in Barred Galaxies](#)
 - 12.1 [Hydrodynamics Modeling](#)
 - 12.2 [Formation of Rings](#)
 - 12.3 [Role of Viscosity](#)
 - 12.4 [Fueling the Nucleus](#)
- 13. [Self-Gravitating Hydrodynamics](#)
 - 13.1 [Stability](#)
 - 13.2 [Self-Gravitating Rings and Nuclear Spirals](#)
- 14. [Problems with Ring Formation Theory](#)
 - 14.1 [Time-scales and the Coexistence of Rings](#)
 - 14.2 [Bar-Ring Misalignment](#)
- 15. [Rings in Nonbarred Galaxies](#)
 - 15.1 [Bar Destruction, Lens, and Oval Formation](#)
 - 15.2 [Evolution Along the Hubble Sequence](#)
- 16. [Interaction Between Several Waves](#)
 - 16.1 [Nuclear Bars Inside Nuclear Rings](#)
- 17. [Tidal Interactions and Rings](#)
 - 17.1 [The Leading Arm Ringed Galaxy NGC 4622](#)
 - 17.2 [The One-Armed Outer-Ringed Galaxy NGC 4378](#)
 - 17.3 [Accretion Rings](#)
- 18. [Single-Ringed, Multi-Armed Galaxies](#)
- 19. [Conclusions](#)
- [References](#)

1. INTRODUCTION

Rings are an interesting aspect of galaxy structure. As shown by the example illustrated in [Figure 1](#), the appearance of some otherwise normal galaxies is dominated by a ring of high contrast. In the jargon of normal galaxy morphology, there are three main types of observed optical ring phenomena: nuclear rings, inner rings, and outer rings. The rings can be very striking in appearance, as in [Figure 1](#), or be merely part of the spiral pattern, which turns out to be the normal situation. Although rings appear to be a common aspect of galaxy morphology, as any casual inspection of one of several available atlases of galaxies will show, the features are hardly discussed at any length in introductory or graduate textbooks and are often treated as a mere "detail" of morphology. Yet, ringed galaxies are fundamentally interesting for a variety of reasons, not the least of which is the possible (and almost certain) association of the rings with dynamical orbit resonances. The purpose of this review is to summarize what is known about the features and the galaxies in which they are found, and in particular to try and bring together the large body of theoretical and observational results that are currently available. Since the vast majority of ringed galaxies are not violently interacting with other galaxies, it seems certain that rings are mainly a problem of internal dynamics. In fact, we believe rings may be a normal phase in the morphological evolution of many galaxies.



Figure 1. *B*-band CCD image (units mag arcsec⁻²) of [NGC 7020](#), showing the large ring near the edge of the visible disk.

The structure of this review is as follows. First, we provide a historical review to help place the subject into a proper context, and to define the basic characteristics of the main ring types. Next, we present a thorough discussion of more recent observations of ringed galaxies from a variety of approaches: morphological, photometric, kinematic, and statistical. Then we discuss rings as resonances in barred galaxies, the role of gravitational torques on their formation, the influence of periodic orbits, and the use of N-body and test-particle simulations. After this, we consider the special problem of rings in nonbarred galaxies and how they might be related to spiral modes and resonances, and the possible dissolution of bars. Next, we will consider ring formation via mild tidal encounters as opposed to the more violent encounters that are believed to cause the polar ring galaxies and collisional ring galaxies. (These latter ring types are reviewed by [Appleton and Struck-Marcell 1996](#).) Finally, we will discuss a few of the unusual examples which, though obviously barred, do not readily fit into the theoretical framework which we outline.

2. HISTORICAL OVERVIEW

2.1. Inner Ring Structures

Ring-like structures in the luminosity distribution of galaxies have been known since photography was applied to nebular research in the late 19th and early 20th centuries. The discovery of rings parallels the discovery of spiral structure in the 19th century, because some ring and pseudoring structures in several nearby galaxies were bright enough to have been seen visually with the 1.8-m speculum reflector of Birr Castle Observatory and other telescopes (see [Figure 2](#)). The accuracy of these early observations was confirmed through photographic observations with the Lick Crossley reflector in 1898-1900 by [Keeler \(1908\)](#). However, it was [Curtis \(1918\)](#) who first brought attention to a special class of spiral "nebulae" where a ring or pseudoring and a bar were characteristic parts of the structure. Four examples, [NGC 1300](#), [NGC 1530](#), [NGC 3351](#), and [NGC 5921](#) were illustrated in his classic paper, a compendium of descriptions of 762 "nebulae and clusters", of which 513 were spirals. He called the ones with a "band of matter extending diametrically across the inner parts" and "whorls" forming a "near perfect ring", " ϕ -type" spirals, "for lack of a better name." The objects Curtis first described are now recognized as "barred spirals", a term coined by [Hubble \(1926\)](#), and the near perfect ring as an "inner ring." Although Curtis referred to them as ϕ -type, a term such as θ -type is actually more appropriate since the bar never exceeds the extent of the ring (see [Figure 3](#)). ⁽¹⁾ [Hubble \(1926\)](#) would have used the term θ -type in his classification system, but Greek letters were inconvenient for catalogs in his day, so he chose the term "barred spirals" instead. Typically, the spiral structure of such a galaxy emerges from the inner ring, but [Reynolds \(1921\)](#) discovered two examples where only the θ shape was visible on his plates. Later, Hubble ([1926](#), [1936](#)) observed that the appearance of the ring in the ϕ -types was manifested by a tight spiral structure, which became more open as the spiral sequence progressed. In the ϕ -type spiral ([NGC 1433](#)) illustrated in [Figure 3](#), the ring is a tight spiral pattern that closes around the bar ends.

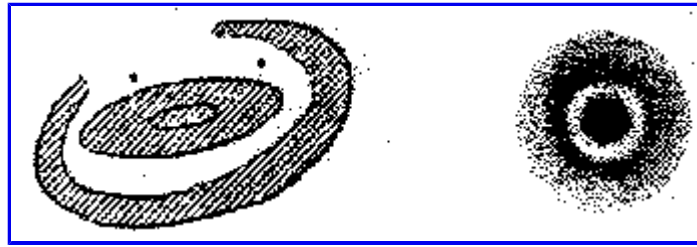


Figure 2. Visual detection of inner rings in [NGC 4725](#) (left, drawing by R. J. Mitchell in 1858; see [Parsons 1926](#)) and [NGC 4736](#) (right, drawing by [Lassell 1866](#)).



Figure 3. *B*-band CCD image of [NGC 1433](#), a " ϕ -type spiral" with a bright inner ring.

The diversity of ringed galaxies became more apparent during later phases of Hubble's nebular research. In his discussion of Hubble's revision to the standard classification system, [Sandage \(1961\)](#) described in the Hubble Atlas of Galaxies an additional category of normal spirals where the arms begin tangential to the periphery of an "internal" ring. As with the ϕ -type spirals, these rings appeared to be linked to the spiral pattern in the sense that the rings become more open towards the later spiral stages (i.e., from Sa to Sc). Some of the first examples of this kind of ringed spiral were discovered by [Shapley & Paraskevopoulos \(1940\)](#), who called them "plate spirals" because of the image conveyed by a ring which tightly wraps the nucleus in a face-on view (i.e., the appearance of a central plate or disk). The original examples of "plate spirals" were [NGC 6753](#) and the close pair [NGC 6935](#) and [NGC 6937](#), the latter now being known to contain a weak bar. Several of the examples of this kind of galaxy illustrated in the Hubble Atlas probably also have bars that are highly foreshortened (e.g. [NGC 4274](#)) or which are simply weak. Some "plate spirals" such as [NGC 6902](#) (see [Figure 4](#)) appear perfectly nonbarred in blue light but show weak bars in near infrared images. Other nonbarred ringed galaxies, such as [NGC 4736](#), have strong obvious ovals rather than conventional bars. Nevertheless, genuine examples of nonbarred ringed galaxies do exist (e.g., [NGC 7217](#), see [Figure 5](#); and [NGC 4622](#), see [Buta et al. 1992](#) and [Section 17.1](#)), although they are less common than the ϕ -types (see [Section 9.1](#)).

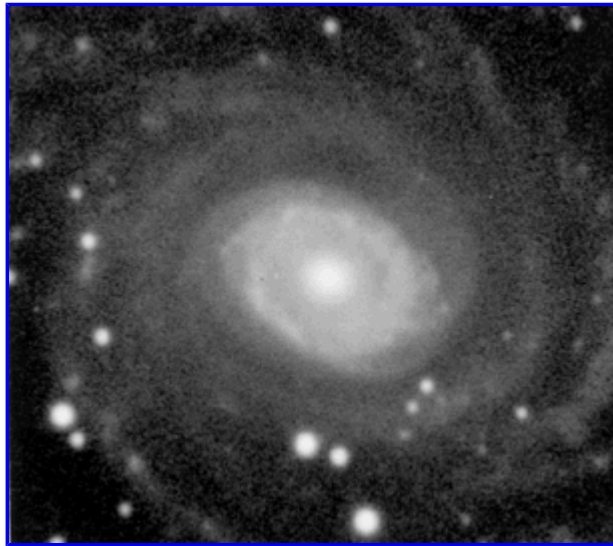


Figure 4. B-band image of [NGC 6902](#), a "plate spiral" with a bright inner ring.

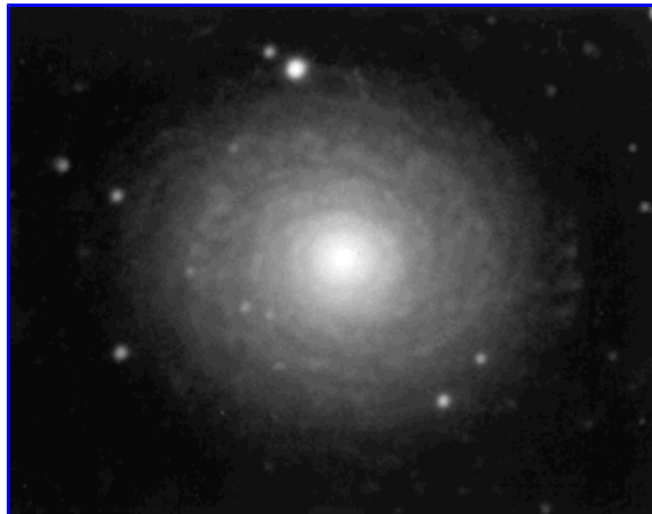


Figure 5. B-band image of [NGC 7217](#), a nonbarred ringed spiral with a bright ring and a multi-armed spiral pattern breaking from the ring.

In a personal revision of the Hubble-Sandage classification system, de Vaucouleurs ([1956](#), [1959a](#)) considered the presence or absence of a bar as a "family" characteristic and the presence or absence of an inner ring as a "variety" characteristic. The continuous variation of these characteristics at a given stage (i.e., a galaxy can be "weakly-barred" or include a partial, broken ring) led him to construct a three-dimensional classification volume ([Figure 6](#)), a well-known cross-section of which ([de Vaucouleurs & de Vaucouleurs 1964](#)) is shown in [Figure 7](#). The system is a generalization of a scheme illustrated by Sandage ([1961](#), [1975](#)), and in it pure inner rings (r) are simply the endpoint in a continuum of forms that becomes increasingly less "ringed" and more "spiral" (s) as one proceeds right to left in the classification volume. Those galaxies which are intermediate between these extremes are said to have "pseudoring", denoted by the combined symbol (rs). [Figures 8, 9, 10](#) exhibit CCD images of galaxies covering the full range of families and varieties. [Figure 7](#) also illustrates de Vaucouleurs' observations on how the morphology of the spiral structure emerging from the inner ring depends on family. In barred (SB) spirals, the spiral structure emerges from the ring as a global pattern, usually with two main arms. The ring itself is elongated along the bar axis, and has a relative size which is large compared to the extent of the outer structure (as in [NGC 1433](#), [Fig. 3](#)). In nonbarred (SA) spirals, the spiral structure typically emerges from the inner ring as a multi-armed or a non-global pattern. The ring appears to be round, and has a small size compared to the extent of the outer structure [as in [NGC 7217](#) ([Fig. 5](#)) and [NGC 6753](#) ([Figure 10](#), top)]. The mixed family (SAB) spirals have spiral patterns and rings whose characteristics are intermediate between these extremes. Of interest is the hybrid type, SAB(rs), where the inner pseudoring can have a characteristic hexagonal shape (as in [NGC 4303](#), the "model" for the central sketch in [Figure 7](#)). The hybrid nature of this form causes the center of the classification volume to contain an excess number of objects compared to other subsections ([section 9.1](#)). On the basis of a variety of indicators, [de Vaucouleurs \(1970\)](#) suggested that our Galaxy is a hybrid ringed barred galaxy of type SAB(rs)bc.

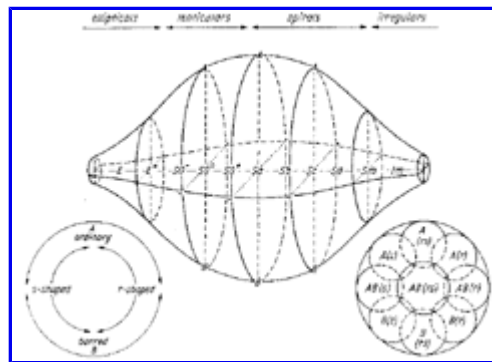


Figure 6. The three-dimensional revised Hubble classification system of [de Vaucouleurs \(1959a\)](#).

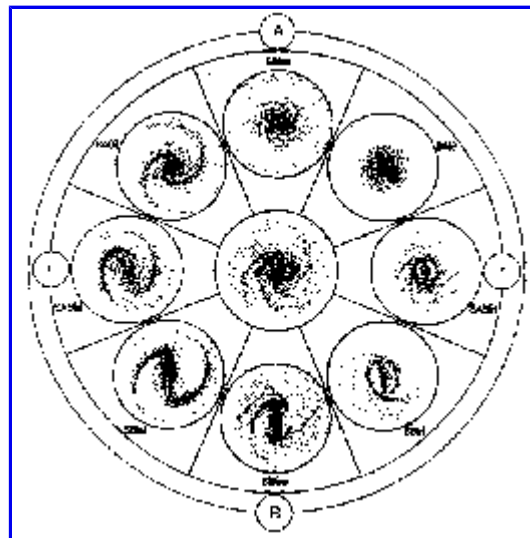


Figure 7. Cross section of revised Hubble classification system near stage Sb ([de Vaucouleurs & de Vaucouleurs 1964](#)).

There are many exceptions to the apparent "rules" in [Figure 7](#). For example, [IC 5240](#) ([Fig. 8](#), top) is an SB(r)-type spiral where *flocculent* spiral structure breaks from the inner ring, not a global pattern, which is very unusual. Nevertheless, the inner ring and bar are strong, clear features. [NGC 4622](#) (see [section 17.1](#)) and [NGC 5364](#) ([Sandage 1961](#)) are examples of SA(r) or SA(rs)-type spirals where a strong *global* two-armed pattern breaks from the inner ring. In addition, the inner ring of [NGC 4622](#) is very large compared to the extent of the spiral structure. These examples are discussed later in this review, and underscore a greater complexity of structure than can be illustrated in diagrams like [Figure 7](#).

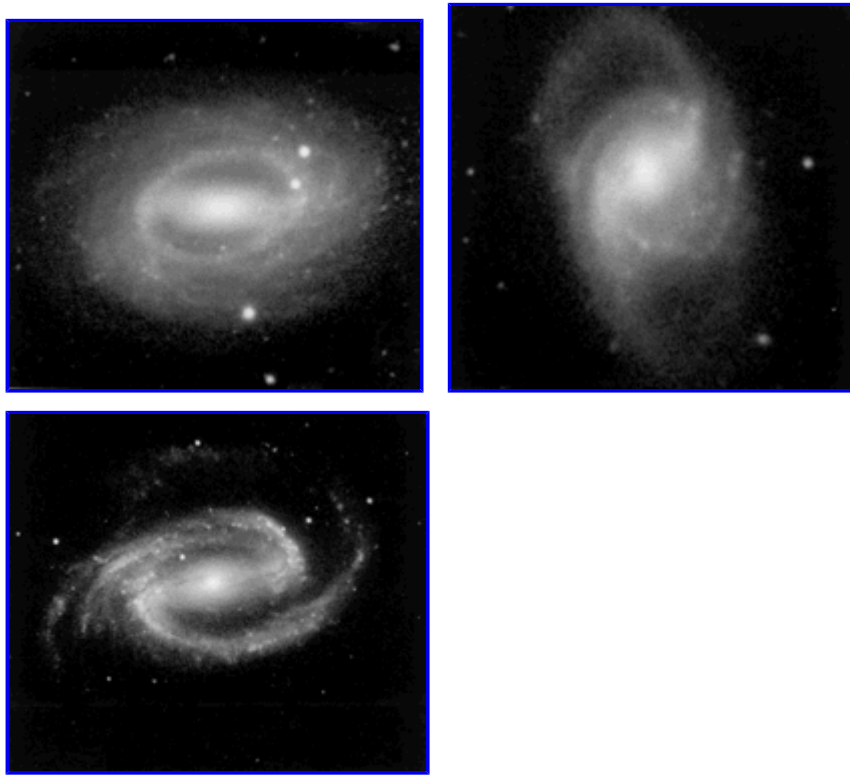


Figure 8. Examples of SB(r) ([IC 5240](#), top left), SB(rs) ([ESO 153-20](#), top right), SB(s) ([NGC 1300](#), bottom) types.

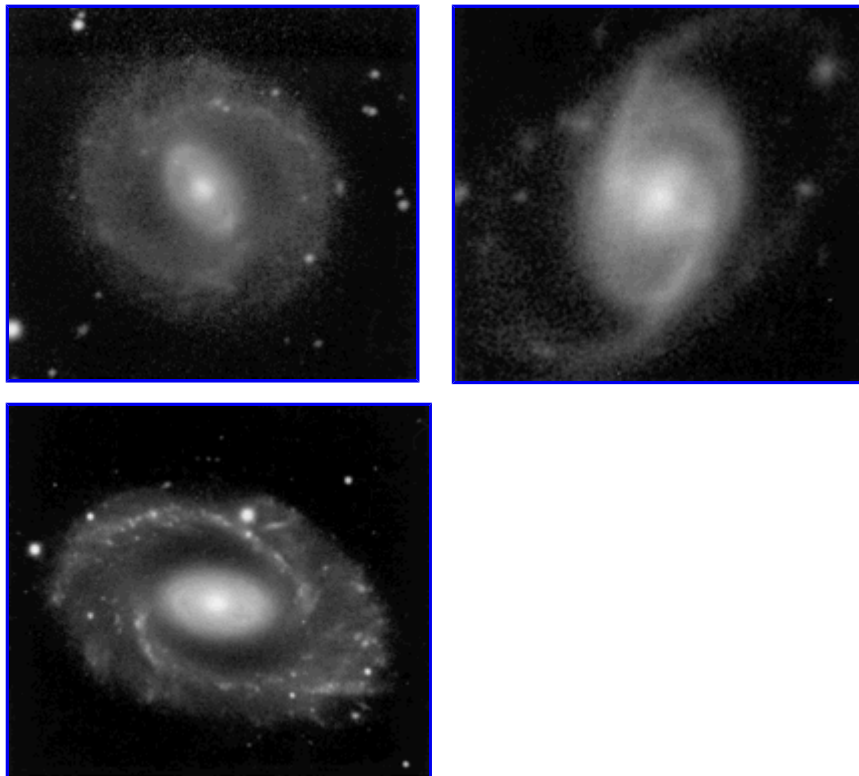


Figure 9. Examples of SAB(r) ([IC 1438](#), top left), SAB(rs) ([NGC 619](#), top right), SAB(s) ([NGC 210](#), bottom) types.

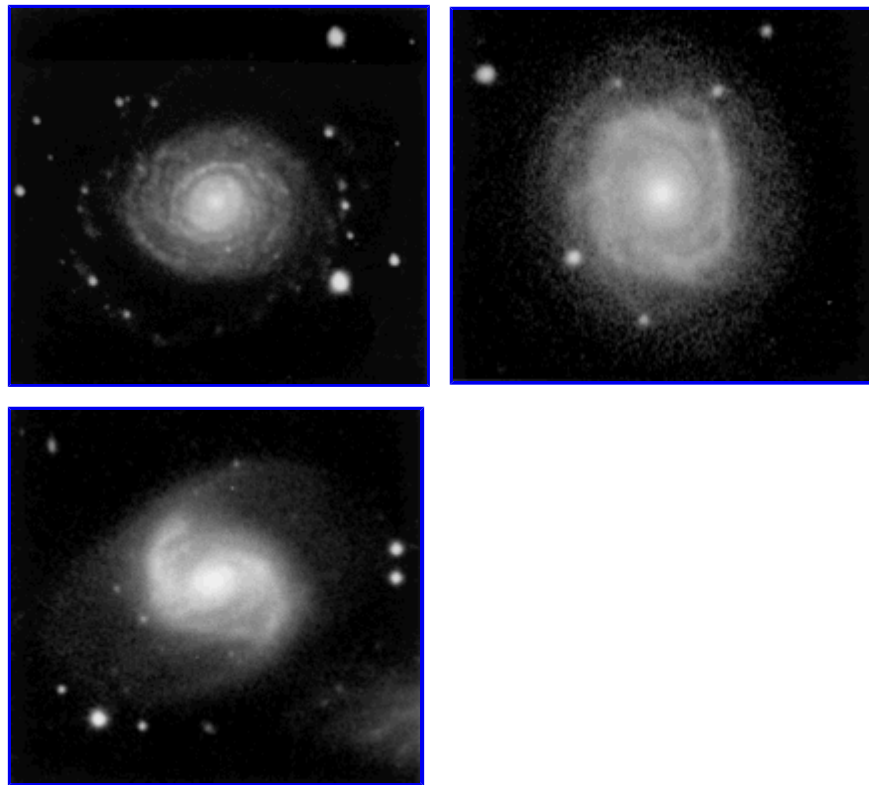


Figure 10. Examples of SA(r) (NGC 6753, top left), SA(rs) (NGC 6935, top right), SA(s) (ESO 111-10, bottom) types.

The parameter characterizing the third dimension in the classification volume is the stage T, which varies continuously in the sequence a, b, c, d, and m, with intermediate types ab, bc, cd, and dm. The stage expresses the development of spiral structure via the three principal classification criteria originally outlined by Hubble: the strength of the bulge, the degree of openness of the spiral structure, and the degree of resolution of the arms. Sandage (1961) noted that the pure ring form (r) parallels the pure spiral form (s) over the sequence Sa, SBa to Sc, SBc, but that at later stages the pure ring form is *not* common. He noted that most central rings in the Sc subclass are broken into several segments, characteristic of the (rs), pseudo-ringed variety. From a re-classification of 1500 bright galaxies taken mostly from the well-known catalog of Shapley & Ames (1932), de Vaucouleurs (1963) showed that the relative frequency of the pure ring variety (r) is highest near stage Sab, accounting for nearly 40% of the varieties observed at that stage, and that the phenomenon considerably weakened or became absent in the later spiral stages. Two late-type inner-ringed galaxies are shown in Figure 11.

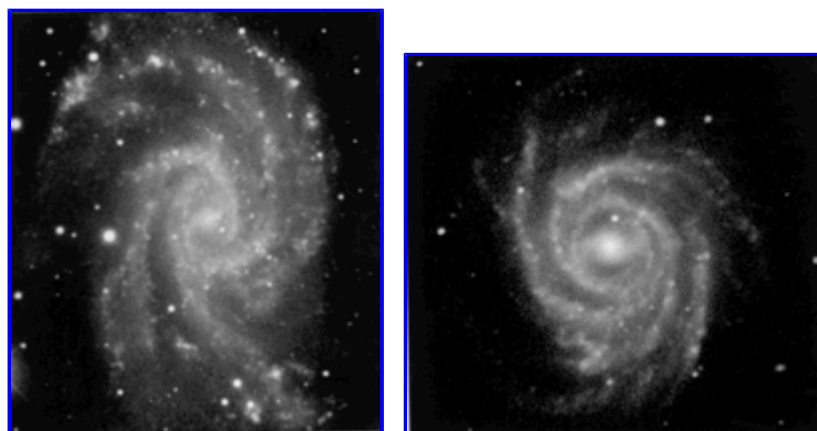


Figure 11. Examples of late-type ringed galaxies: NGC 2835 (left) and NGC 3124 (right).

Rings were also found in these early studies to be present in lenticular (S0) galaxies. In Hubble's original (1926) classification system, ringed, barred lenticulars were misclassified as SBa systems because the S0 category had not been fully recognized at the time. Sandage (1961; and more recently Sandage & Bedke 1994 = SB94) described Hubble's final classification of lenticulars. In nonbarred lenticulars, a central lens is surrounded by a faint envelope. A stage sequence (S0₁ -> S0₂ -> S0₃) is identified whereby the envelope and lens develop from a smooth luminosity distribution in early stages to a profile perturbed by a narrow, circular absorption ring. The galaxy NGC 4429,

shown in [Figure 12](#), bottom, has such an absorption ring. The region outside the absorption ring appears enhanced, giving the impression of an internal ring similar to those observed in spirals. Sandage did not associate these rings directly with the (r)-subtype, but de Vaucouleurs did classify them as inner rings. (The second, larger ring-like feature in [NGC 4429](#) was classified by de Vaucouleurs as an outer ring.) Sandage noted a gradual transition whereby the absorption ring in the later lenticular stage begins to deviate from circular patterns and take on a tightly wound spiral form as the stage sequence progresses. In barred lenticulars (and many nonbarred ones as well), rings are often found at the edge of a lens, which also develops along the stage sequence into spiral arms. In fact, Sandage noted that the structural features of barred galaxies can be characterized by "a sequence in which a simple pattern of bar and ring develops into a pattern of bar and spiral arms."

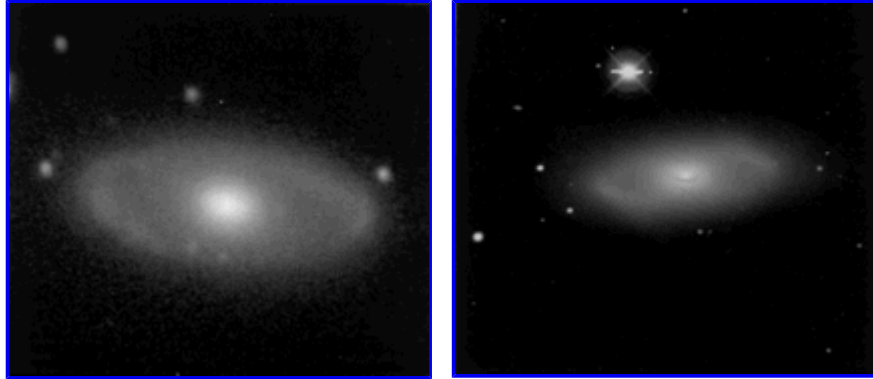


Figure 12. Examples of ringed S0 galaxies: [NGC 4553](#) (left) and [NGC 4429](#) (right).

The classification of lenticulars in the Hubble Atlas and in [SB94](#) does not recognize varieties because S0 galaxies, by definition, do not have spiral structure. However, de Vaucouleurs adopted a different interpretation and recognized family and variety for lenticulars in the same manner as for spirals, i.e., as continuous properties. Ringed, pseudoringed, and non-ringed varieties at each family are recognized in an analogous manner to spirals. The principal difference with spirals is a notable deficiency of the hybrid type, SAB(rs)0, which [de Vaucouleurs \(1963\)](#) attributed to difficulty of classification. The strongest inner rings in lenticulars are characteristic of the "late" de Vaucouleurs lenticular type $S(r)0^+$. [NGC 4553](#) ([Fig. 12](#), left) and [NGC 7187](#) ([Buta 1990b](#), [Fig. 13](#)) are two excellent examples of late, nonbarred lenticulars. [NGC 4429](#) in [Figure 12](#) is an unusual case because its "outer ring", which is actually an intermediate spiral pseudoring zone, bears an uncanny resemblance to the inner hexagonal zone of [NGC 7020](#) (see [Fig. 1](#)). The significance of this similarity is not yet clear.



Figure 13. The double ringed lenticular galaxy [NGC 7187](#), type (R)SA(r)0⁺. Note the shape difference between the two rings.

¹ [Lundmark \(1926\)](#) published a preliminary classification of "anagalactic nebulae" that also recognized ring morphologies. His spiral

category, As, included subclasses where spiral arms "form a bright ring", "Saturn-shaped" nebulae, and Curtis ϕ -type spirals. The system, however, never saw extended use. [Back](#).

2.2. Outer Ring Structures

The rings described in the previous section are called inner rings because they lie in the intermediate zone between the bulge and the spiral arms or disk. [Perrine \(1922\)](#) discovered a second type of ring structure in the southern barred galaxy [NGC 1291](#) that more properly had to be called an "outer ring" or an "external ring". [De Vaucouleurs & Buta \(1980b\)](#) note that the outer ring of [NGC 1291](#) was already visible on chart 29 of the Franklin-Adams sky charts published in 1910. It is interesting that the outer ring of [NGC 7217](#) is also plainly visible in the photograph in [Keeler \(1908\)](#). In the revised Hubble classification systems described by both [Sandage \(1961\)](#) and [de Vaucouleurs \(1959a\)](#), outer rings are denoted by the symbol (R). De Vaucouleurs commented that such a structure is often observed in lenticulars and early-type spirals but that it is not clearly related to a specific class or family. Later studies (e.g. [Kormendy 1979a](#)) have suggested that such rings may be most prevalent in barred galaxies. The relative frequency of the phenomenon seems to be greatest at stage S0/a (de Vaucouleurs 1975a; see [section 9.1](#)). Three examples of pure outer rings are illustrated in [Figure 1](#) and [Figures 13 - 14](#). As with inner rings, outer rings are closely linked to the spiral pattern, and occasionally the ring is a wrapped pair of spiral arms that nearly close together. In such cases, the ring is referred to as an outer pseudoring and is symbolized by (R'). Outer pseudorings are discussed in more detail in [section 4.1](#).

The Carnegie Atlas ([SB94](#)) emphasizes the connection between outer rings and early-type barred galaxies. In the type sequence they describe for barred S0 galaxies, the bar develops from a barely differentiated oval in the inner regions (type SB0₁), to a bar of the "ansae" type (SB0₂), to a sharp bar extending across the entire disk (type SB0₃). [SB94](#) comment that many galaxies classified as type SB0₂ or SB0_{2/3} have detached or semi-detached outer rings. The interpretation of the features is not always consistent; for example, [SB94](#) classify both [NGC 2859](#) and [4340](#) as RSB0₂, yet the ring in the latter is clearly an inner ring filled exactly by the bar.

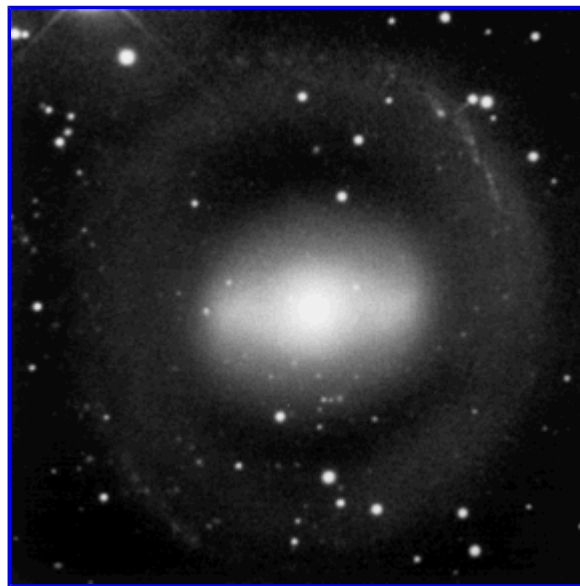


Figure 14. [NGC 1543](#), a pure outer-ringed galaxy.

2.3. Nuclear Ring Structures

The third type of ring structure, the nuclear ring, is the smallest of the three ring types. Some of the first examples were noted by [Morgan \(1958\)](#). In the presentation of his well-known spectroscopic classification system based on the forms and colors of galaxies, he isolated a class of galaxies with peculiar or complex nuclei. He described how some nuclei in spiral and barred galaxies are made up of multiple "hotspots", with type examples being [NGC 1808](#), [3351](#), [4321](#), and [5248](#). [Note that the feature in [NGC 4321](#) was already visible in a Lick Crossley photograph obtained by [Keeler \(1908\)](#), and that the feature in [NGC 3351](#) was described by [Curtis \(1918\)](#).] Concurrently with this study, [Sersic \(1958\)](#) commented on the existence of an intriguing structure in the center of the SBb galaxy [NGC 1097](#), where a "central knot is surrounded by a chain of condensations forming a single spiral arm." [Burbidge & Burbidge \(1960\)](#) later observed this object and noted that the nucleus of the galaxy is a segmented annulus consisting of bright areas and probably dust." (The center of [NGC 1097](#) had been noted long before these observations to have structure; see discussion in [Shapley & Paraskevopoulos 1940](#)). In the Hubble Atlas, [Sandage \(1961\)](#) brought attention to an intriguing case of a "nuclear spiral" in the center of the SBa galaxy [NGC 4314](#), where the nucleus is characterized by a very small spiral pattern emerging from a knotty, ring-like zone centered on a small nucleus. He observed that this internal spiral is not connected in any way with the faint external arms of the galaxy.

Surprisingly, no clear examples of nuclear rings are described in the visual observation notes of W. Parsons and co-workers ([Parsons 1926](#)), although some may have been suspected. This may be explained in part by the fact that the rings are more prominent at blue than at visual wavelengths, by their location on the steep background light gradient of the bulge, and that some of the biggest and brightest examples are in the southern hemisphere and not accessible to the latitude of Birr Castle. The nuclear structures show a diverse variety of forms ranging from true rings of "hotspots" (e.g., [NGC 6782](#) and ESO 565-11) to nuclear pseudorings (e.g., [NGC 1097](#) and [IC 4214](#)) to almost pure nuclear spirals (e.g., [NGC 4321](#), [1365](#), and [5383](#)). Several examples of nuclear rings are illustrated with ground-based CCD images in [Figure 15](#). The rings are small and generally not well-resolved by such observations, however. Barth et al. ([1995](#), [1996](#)) and [Phillips et al. \(1996\)](#) present HST images of several nuclear rings, which reveal the intricate dust lane patterns around and inside such features. Such high-resolution images reveal that even features classified as nuclear "rings" from the ground are in fact tightly wrapped spirals in many cases.

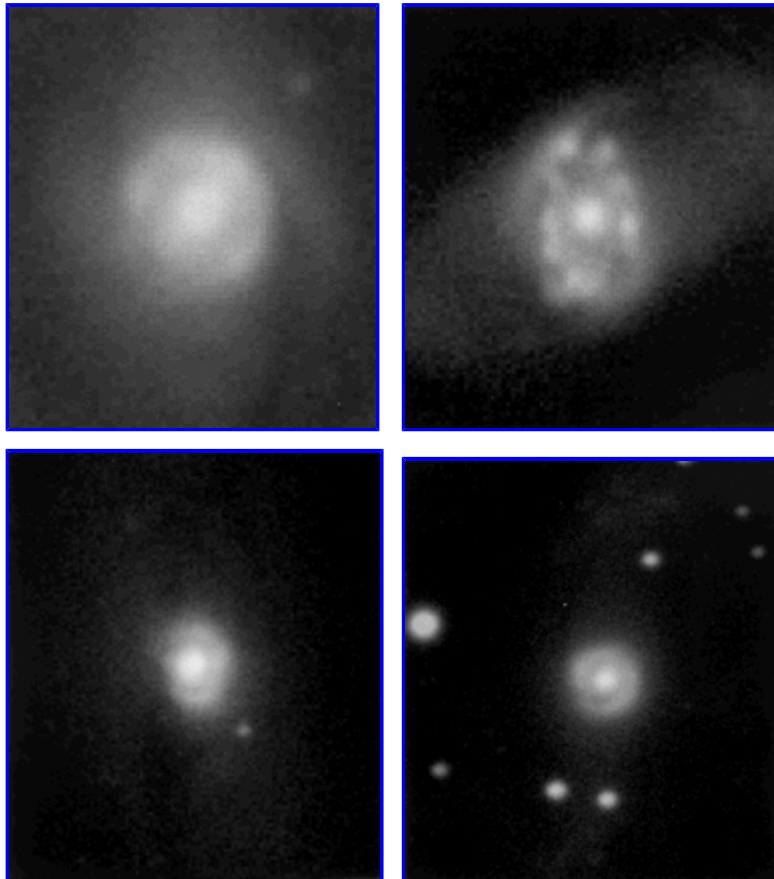


Figure 15. B-band CCD images of nuclear rings in four early-to-intermediate type galaxies: [NGC 6782](#) (top left); ESO 565-11 (top right); [NGC 1300](#) (bottom left); [NGC 1343](#) (bottom right).

The discovery of nuclear rings followed that of the previous two types of ring probably because of strong selection effects against detecting a very small, high surface brightness feature located in a region that is often overexposed on direct photographs. As the discussion implies, the phenomenon may be closely linked with the presence of a bar. This coincidence was quantified by Sersic & Pastoriza ([1965](#), [1967](#)), who found that in a carefully selected sample of 136 bright spirals over the whole sky, 20 contained the nuclear structure, and of these objects, all are either barred or weakly-barred. Unlike inner and outer rings, the nuclear ring phenomenon appears to be rare or absent in nonbarred galaxies, although this may be more a recognition difficulty than a real deficiency as noted by Buta and Crocker ([1993](#); see [section 5](#)).

3. COMPARISON OF RING CLASSIFICATIONS

The (r) and (s) varieties illustrated in [Figure 7](#) are a well-established aspect of galaxy morphology that both the Hubble-Sandage and de Vaucouleurs types recognize as a part of normal galaxy morphology. However, since most observers choose samples for follow-up work on the basis of published catalog types, it is important to note that independent classifiers do not always agree on ring classifications. For example, some galaxies classified as (r)-variety by [de Vaucouleurs \(1963\)](#) or in the Third Reference Catalog of Bright Galaxies (RC3, [de Vaucouleurs et al. 1991](#)) are classified as (s)-variety by Sandage and Tammann ([1981](#), [1987](#); hereafter RSA) and [SB94](#). In the latter sources also, outer pseudorings are generally not recognized. The disagreement results because the spiral structure in many galaxies is very ring-like. In the Carnegie Atlas, strong "near rings" such as those in [NGC 3081](#), [1433](#), [6782](#), and 7217 are noted but not formally

recognized in the classification because the rings are made of tightly wound spiral structure. In the case of [NGC 6782](#), [SB94](#) state that "the 'ring' is two inner spiral arms that start in the nucleus [hence the subtype (s) rather than (r)] and nearly overlap after each has unwrapped by about half a turn". Apparently, this effect is caused by a combination of the leading dust lanes in the bar and the tight spiral pattern that defines the inner ring in this case. In the case of [NGC 3081](#), where the "near ring" has a very high contrast in the disk, [SB94](#) state that the galaxy has "one of the most complex morphologies of the RSA galaxies. There are rings within rings at the edges of disks within disks, as intricate a structure as in nesting, concentric Russian dolls." None of these rings, however, is recognized in the Carnegie classification of SBa(s). The de Vaucouleurs classification of the galaxy is instead (R)SAB(r)0/a.

[Kostiuk \(1975\)](#) compiled a list of 143 galaxies with "outer ring-shaped structure" as seen on the prints of the first Palomar Sky Survey. This list includes mostly true rings (not pseudorings), and she identified three types of rings: RS, rings which are some type of spiral surrounding a bright main body (examples: [NGC 2859](#), [3945](#), and [4736](#)); RH, rings with a weak halo beyond the ring (examples: [NGC 4340](#), [4371](#), and [4608](#)); and R, lacking a central nucleus (now known as the conventional "ring" galaxies). This study does not distinguish inner from outer rings or early from late-type galaxies, but the sample emphasizes early types by default.

Vorontsov-Velyaminov (1987) also classifies ring phenomena in galaxies in a manner very different from the Hubble-Sandage and de Vaucouleurs systems. In his descriptive classification, there is no recognition of subclasses of rings, such as inner, outer, or nuclear types. Instead, any galaxy with a prominent ring or pseudoring, whether luminous or dark (as in the absorption rings of S0₃ galaxies) is called a ring galaxy and classified as N;R in the Morphological Catalog of Galaxies ([Vorontsov-Velyaminov et al. 1962-1968](#)). Vorontsov-Velyaminov suggested that ring galaxies form a sequence parallel to and independent of spiral galaxies, and that there is a continuous transition of forms from pure amorphous disk galaxies, N;D, to ring galaxies. These are not allowed to have a bar or spiral arms. He suggests a smooth transition also between ring galaxies with a nucleus to those without one. Thus, there is no distinction between what the others would call ringed galaxies and what are commonly referred to as collisional ring galaxies (see [Appleton & Struck-Marcell 1996](#)), unless perhaps there is a bar. Polar ring galaxies are also referred to as ring galaxies by Vorontsov-Velyaminov, who describes the edge-on cases as "lemons pierced by a needle."

Vorontsov-Velyaminov also brought attention to "double-stage" spirals, where an inner set of spiral arms is largely independent of an outer set of arms. The inner arms may be more patchy than the outer ones and merit a later classification stage than the outer arms. Many of the galaxies where this ambiguity occurs have rings or pseudorings, such as [NGC 3504](#), [NGC 1808](#), and [NGC 1433](#). In the Hubble Atlas and [SB94](#), the inner set of arms determines the Hubble type.

4. RECENT REVISIONS TO THE CLASSIFICATION OF RINGED GALAXIES

4.1. Outer Ring and Pseudoring Morphologies

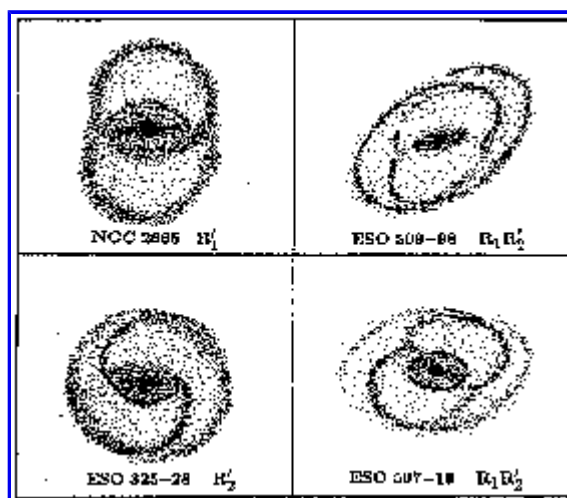


Figure 16. Schematic illustration of the "OLR subclasses" of outer pseudorings, from [Buta and Crocker \(1991\)](#).

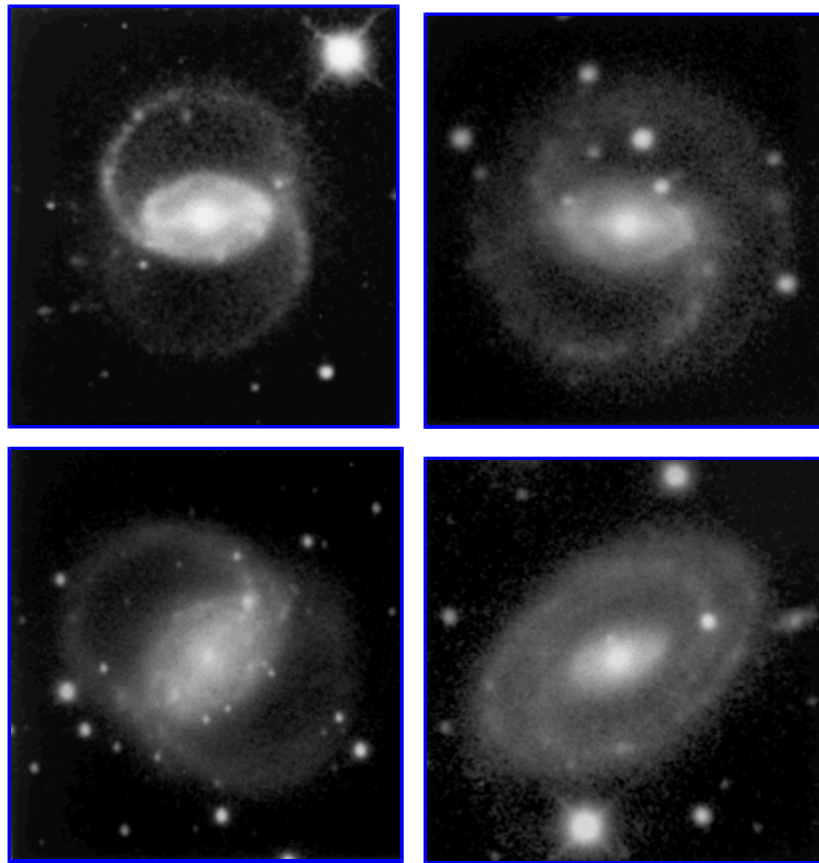


Figure 17. Examples of outer pseudorings belonging to the "OLR subclasses": [UGC 12646](#), type (R'₁)SB(r)ab (top left); [ESO 325-28](#), type (R'₂)SB(r)b (top right); [NGC 2665](#), type (R'₁)SAB(r)a (bottom left); [ESO 509-98](#), type (R₁R'₂)SB(s)a (bottom right).

The classification of ringed galaxies has had one major revision since the works of [de Vaucouleurs \(1959a\)](#) and [Sandage \(1961\)](#). The morphology of outer rings and pseudorings in barred galaxies includes subcategories that strongly resemble the gaseous rings and pseudorings that developed near the outer Lindblad resonance (OLR) in the test-particle simulations of [Schwarz \(1981\)](#); see [Buta and Crocker 1991](#)). These simulations are discussed in [section 12.2](#), but we illustrate the observed categories in this section to define the morphological symbols that we will use for what will be referred to as the "OLR subclasses."

The new subclasses are schematically illustrated in [Figure 16](#), and photographic images of several examples are shown in [Figure 17](#). Unsharp-masked images of two cases are illustrated in [Figures 18](#) and [19](#). Many barred galaxies display a pseudoring of type R'₁ defined by a 180° winding of the spiral arms with respect to the ends of a bar or oval. Often, the pseudoring displays a blunt oval shape with "dimples" at the points where the arms return to the ends of the bar. [ESO 287-56](#), shown in [Figure 18](#), is an unusually strong example of this dimpling. This image has been deprojected using an outer isophote to define the orientation of the system. At right in [Figure 18](#), an "oval of Cassini" has been fitted to the outer pseudoring of [ESO 287-56](#). This mathematical function (basically a vertical cross-section through a torus; see [Selby 1973](#)) resembles the perpendicular-aligned OLR family of periodic orbits (see [Schwarz 1981](#) and [Figure 61, section 11.2](#)), and fits the ring well.

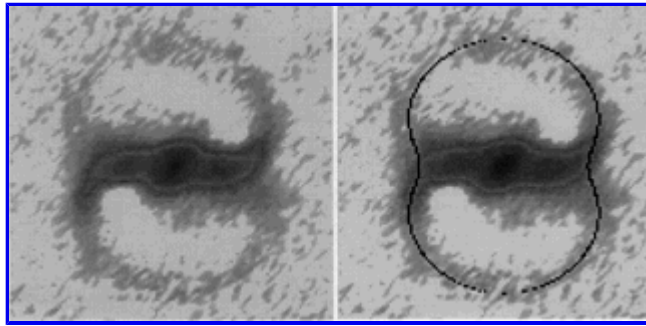


Figure 18. Deprojected, unsharp-masked images of [ESO 287-56](#), a galaxy with a "dimpled" R_1' outer pseudoring. At right an "oval of Cassini" has been plotted over the outer pseudoring to highlight the similar shape to an "OLR" orbit family.

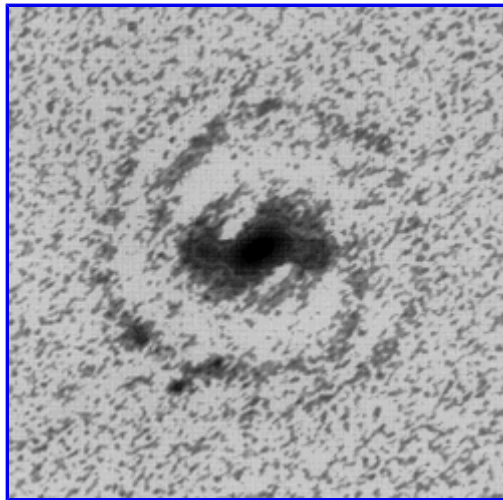


Figure 19. Deprojected, unsharp-masked of [ESO 294-16](#), a galaxy with an R_2' outer pseudoring. In this case, the pseudoring does not close along the bar minor axis line.

A substantial number of barred galaxies display a second type of feature known as an R_2' pseudoring (see lower left schematic in [Figure 16](#)). In this type, the pseudoring is defined by an $\approx 270^\circ$ winding of the outer arms with respect to the bar ends, so that in two opposing quadrants the arm pattern is doubled. The pseudoring closes roughly along the line perpendicular to the bar in the galaxy plane, and dimpling is not generally seen. When deprojected, some of the best examples of this type of feature do not necessarily close, as shown by [ESO 294-16](#) in [Figure 19](#).

Detached true outer rings do not readily fit into these subcategories because the classification depends on the character of spiral arms. However, some true rings have a dimpled shape similar to R_1' rings and are referred to as R_1 -type rings. The outer ring of [NGC 1326](#) (see [Buta & Crocker 1991](#) and [Figure 45](#)) is an example.

[Buta & Crocker \(1991\)](#) also noted a possible correlation between the presence of an R_1 or R_1' outer ring/pseudoring morphology and the existence of nuclear star formation. In an imaging survey of 29 early-type spirals, 9 out of 11 examples containing this type of outer feature included nuclear star formation in the form of blue nuclear rings, partial blue rings, or blue nuclei. In contrast, 8 out of 11 cases including a strong R_2' outer feature showed no evidence for nuclear star formation.

The R_1' and R_2' morphologies were predicted by [Schwarz \(1981\)](#) as the kinds of patterns that would be expected near the OLR in a barred galaxy. Each pattern is linked mainly to one of two major families of periodic orbits expected near the OLR. [Buta \(1985, 1986a\)](#) identified a rare combined pattern (not predicted by Schwarz) referred to in [Buta & Crocker \(1991\)](#) as the R_1R_2' morphology, where the outer arms break not from the ends of the bar, but from an R_1 -type ring. The prototype of this morphology is [ESO 509-98](#), which is illustrated schematically in [Figure 16](#) and in reality in [Figure 17](#) (see also [Buta & Crocker 1991](#)). An excellent large example is found in [NGC 1079](#) ([Buta 1995](#)). The existence of this combined type, which may be linked to the population of both main families of OLR periodic orbits, provides some of the clearest evidence of the OLR in barred galaxy morphology. We discuss the theoretical aspects of these features in more detail in [section 12.2](#).

4.2. Inner, Outer, and Nuclear Lenses

Rings are also related to other features known as lenses. Lenses are by definition rather shallow parts of the luminosity profiles which appear to have sharp edges on photographs. The photometric distinction is illustrated in [Figure 20](#). This plot shows that the difference between a ring and a lens can be in part a question of the amplitude of the enhancement over the declining background of the bulge plus disk components. This does not mean that rings and lenses are the same phenomenon, because rings can exist in the absence of a lens. Nevertheless, old ring stars may eventually populate a broader region after many orbits (see [sections 9.4](#) and [15.1](#)).

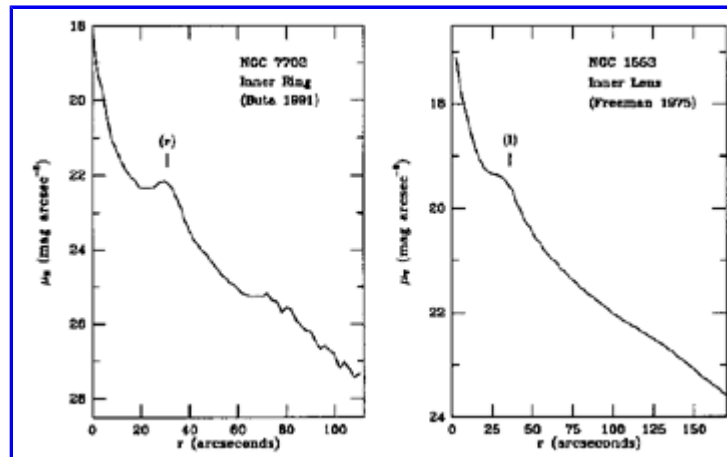


Figure 20. Photometric distinction between rings and lenses. This shows the mean major axis profiles of [NGC 7702](#) (left), which has a strong stellar inner ring, and [NGC 1553](#) (right), which has a strong inner lens. [NGC 7702](#) has a secondary bar which causes a small "bump" in the profiles for $r < 10''$, while [NGC 1553](#) has no bar.

There is a lens analogue for each type of ring, as shown in [Figure 21](#). Often, a ring is a subtle enhancement at the edge of a lens. Although lenses have been recognized for a long time (see [Sandage 1961, 1975](#); [de Vaucouleurs 1959a](#); [Freeman 1975](#); [Kormendy 1977](#); [Sandage & Brucato 1979](#); [de Vaucouleurs & Buta 1980a](#)), no specific symbol was used to denote their presence, and in published catalogues (e.g., RC1, RC2, and RC3), a lens may be classified as an inner ring (e.g., [NGC 1553](#)). [Kormendy \(1979a\)](#) proposed that lenses should be distinguished from rings, and suggested the following notation: (l) for inner lenses and (L) ⁽²⁾ for outer lenses. This notation was adopted in the Catalog of Southern Ringed Galaxies ([Buta 1995](#)), and apart from [Kormendy \(1979a\)](#) is the only major source of consistent lens classifications. [Buta \(1989\)](#) proposed the notation (nl) as an obvious extension of Kormendy's suggestion for nuclear lenses. The left panels in [Figure 21](#) show two early-type spirals with prominent inner lenses but little trace of a bar. The lower right panel shows [NGC 2983](#), an SB0⁺ galaxy with a strong outer lens, while the upper right panel shows the central region of [NGC 1317](#), an SAB galaxy with a prominent nuclear ring, a secondary bar, and a small nuclear lens surrounding the bar. In this latter case, the nuclear lens is not coincident with the edge of the nuclear ring but is coincident with the ends of the secondary bar (see [Schweizer 1980](#)). A nuclear or secondary lens in [NGC 1291](#) was also described by [de Vaucouleurs \(1975a\)](#), again surrounding a secondary bar. We discuss in [section 15.1](#) the formation and evolution of lenses.

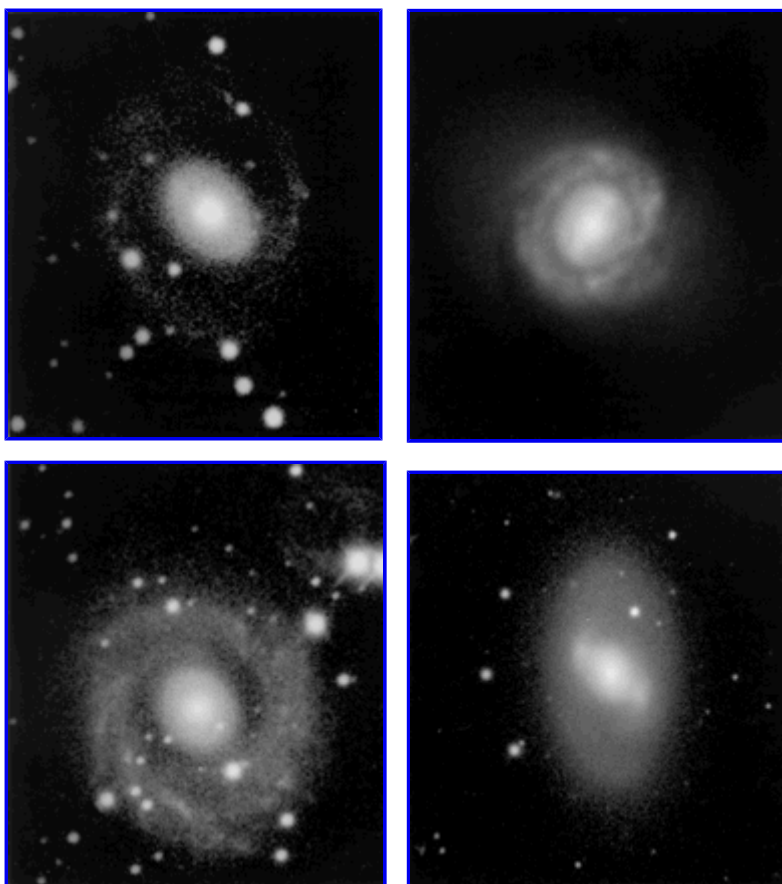


Figure 21. Examples of lenses in early-type galaxies: [ESO 264-47](#) (top left, inner lens); [NGC 1317](#) (top right, nuclear or secondary lens with secondary bar); [NGC 4909](#) (bottom left, inner lens); [NGC 2983](#) (bottom right, outer lens).

² This notation should not be confused with the classification of S0 galaxies in RC3, where "L" is used to denote a "lenticular" galaxy, as in LA(r)0⁺. [Back](#).

5. CONFUSION OF RING AND LENS TYPES IN NONBARRED GALAXIES

The classification of rings, pseudorings, and lenses into subclasses such as "inner", "outer", or "nuclear" is not always straightforward. Only for barred galaxies is it usually possible to unambiguously distinguish these different feature types. This is because the bar usually fills an inner ring or lens, if present, in one dimension. Occasionally, galaxies which appear to be nonbarred on a *B*-band image reveal a weak bar on a redder passband image, so that inner and outer features can still be distinguished. However, in some clearly nonbarred galaxies with only a single ring, it can be difficult to decide whether a ring or lens is an inner or an outer type. A confusion between inner rings and equivalent nuclear rings in nonbarred galaxies undoubtedly occurs also. Nuclear rings are easily distinguished from inner rings in SB galaxies, again because the bar usually fills the inner ring in one dimension. Without this diagnostic, however, one cannot readily distinguish an inner from a nuclear ring in an SA galaxy unless all three feature types are present. The ambiguity means that some features in SA galaxies which are really analogues of nuclear rings will be misclassified as inner rings. The inner rings in [NGC 6753](#) (Buta and Crocker 1993) and [NGC 7217](#) (Buta et al. 1995b) are probably of this nature. The high surface brightness ring in [NGC 7742](#), a very axisymmetric galaxy, has been interpreted as a nuclear ring by [Buta & Crocker \(1993\)](#) and [Wakamatsu et al. \(1996\)](#).

6. SUMMARY OF NOTATION FOR RING AND LENS PHENOMENA

Tables [1](#) and [2](#) summarize the notation and classifications that we will use for resonance ring galaxies in the remainder of this review (see [Buta 1995](#)). The classifications in [Table 2](#) are based on multicolor CCD images to be certain of the presence or absence of a nuclear ring. The list of galaxies includes virtually every conceivable combination of structures. It is noteworthy that even prototypical "grand-design"

barred spirals like [NGC 1300](#) can be included in such a list: it has a small nuclear ring inside the bar region. The list demonstrates that we can identify galaxies with up to *four* ring or pseudoring structures in co-existence. Doubled outer-ring galaxies appear to come in two types, the R_1R_2' type discussed in [section 4.1](#), and the type illustrated by [NGC 2273](#) ([van Driel & Buta 1991](#); [Figure 22](#)) where the two features are clearly separated. No theory has yet explained this latter morphology, which is so far unique. Two outer-ringed ellipticals are also listed in [Table 2](#). [Corwin et al. \(1985\)](#) classified [IC 2006](#) as (R)SA0⁻, but the object is now recognized as an elliptical galaxy with an accretion ring of neutral gas that also displays some spiral character in deep *B*-band images ([Schweizer et al. 1987a](#)). It could be classified as an (R')E type, but the ring is not a resonance feature (it is counter-rotating relative to the main stellar body). The other ringed elliptical in [Table 2](#), Hoag's object, is discussed further in [section 16](#).

TABLE I. Summary of notation for ring and lens phenomena

| Feature | symbol |
|------------------|--------------------------------------|
| nr | nuclear ring |
| nr' | nuclear pseudoring |
| r | inner ring |
| rs | inner pseudoring |
| R | outer ring |
| R' | outer pseudoring |
| R ₁ | Type 1 OLR subclass outer ring |
| R ₁ ' | Type 1 OLR subclass outer pseudoring |
| R ₂ ' | Type 2 OLR subclass outer pseudoring |
| nl | nuclear lens |
| l | inner lens |
| rl | inner ring/lens |
| L | outer lens |
| RL | outer ring/lens |

TABLE II. Examples of Types with Ring Classifications

| Object | Revised Hubble Type |
|--------------------------|---|
| NGC 210 | (R ₂ ')SAB(s)b |
| NGC 1300 | (R')SB(s,nr)b |
| NGC 1317 | (R')SAB(r'l,nr,nl)a |
| NGC 1326 | (R ₁)SAB(r,nr)0/a |
| NGC 1433 | (R ₁ ')SB(rs,nr)ab |
| NGC 1543 | (R)SB(l)0 ^o |
| NGC 1553 | SA(r)0 ^o |
| NGC 2273 | (RR)SB(rs)a |
| NGC 2983 | (L)SB(rs)0 ⁺ |
| NGC 3081 | (R ₁ R ₂ ')SAB(r,nr)0/a |
| NGC 4314 | (R')SB(l,nrr')a |
| NGC 4321 | SAB(s,nr')bc |

| | |
|-------------------------------|---|
| NGC 4622 | SA(r)ab |
| NGC 6753 | (R')SA(nr)b |
| NGC 6782 | (R ₁ ')SB(r,nr)0/a |
| NGC 7187 | (R)SA(r)0 ⁺ |
| NGC 7217 | (R')SA(rs,nr)ab |
| IC 1438 | (R ₁ R ₂ ')SAB(r,nr)a |
| IC 1993 | (R')SA(s)bc |
| IC 2006 | (R')E1 |
| IC 4290 | (R')SB(r)a |
| IC 5240 | SB(r)ab |
| ESO 287-56 | (R ₁ ')SB(s)a |
| ESO 575-47 | (R ₁ ')SB(rs)ab |
| ESO 577-3 | (R ₂ ')SB(r)ab |
| Hoag's Object | (R)E0 |

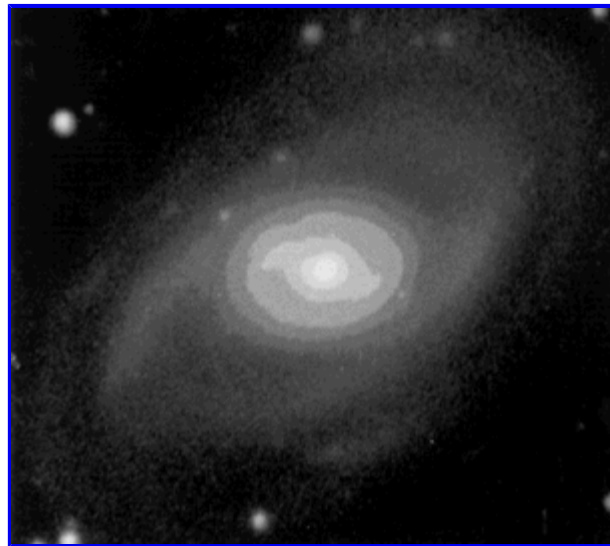


Figure 22. Illustration of [NGC 2273](#), an unusual double-outer ring galaxy. This is a V-band CCD image with some inner contouring to show the bar.

7. RINGS AND LENSES AS DISTINCT COMPONENTS OF BARRED GALAXY STRUCTURE

Tables [1](#) and [2](#) show that if one tries to recognize with classification symbols all of the various types of ring and lens features in a given galaxy, the classification can become disturbingly complex. These types do not yet even account for secondary bars! The large numbers of morphological "cells" required to describe some galaxies, and the importance of rings and lenses to barred galaxy structure, led Kormendy ([1979a, b](#)) to propose a new morphological approach to galaxy studies. Rather than assigning galaxies to morphological "cells" as in Figures [6](#) and [7](#), or in [Table 2](#), he proposed identifying a small number of building blocks, or "distinct components", in the mass distribution that might be most significant, and to characterize galaxy structure by the way these components may form, evolve, and interact over the lifetime of a system.

The main components are bulges, disks, bars, lenses, and inner and outer rings. Spiral structure was not considered by Kormendy to be a distinct component but rather an aspect of the disk because it represents a reversible perturbation from an equilibrium state (i.e., if the

generator of density waves, such as a passing companion, is removed, an equilibrium non-spiral state may be regained). Although rings are intimately connected with spiral structure, as we have amply noted, they result from dissipation processes that slowly accumulate gas into more permanent features. If the perturbation that caused a ring disappears, the ring may survive for a long time afterward. Thus, rings are justifiably distinct components in spite of their close connection to spiral structure. Using the "distinct component" approach as a basis of deductions concerning dynamics, Kormendy proposed that lenses result from bar dissolution. This idea, as well as others concerning the origin of ovals, is discussed in more detail in [section 15.1](#).

8. RINGS AND NUCLEAR ACTIVITY

Several studies have noted a preponderance of ring, pseudoring, and bar features in Seyfert galaxies. [Adams \(1977\)](#) noted that Seyferts with annular main bodies form a natural group. Later studies by [Simkin et al. \(1980\)](#), [Su & Simkin \(1980\)](#), and [Arsenault \(1989\)](#) elucidated this observation further. [Simkin et al. \(1980\)](#) used a sample of nearby Seyferts to determine that Seyferts have a preference for barred and weakly-barred systems with inner rings or pseudorings. They suggested that the nuclear activity is connected to the way a bar-like perturbation can funnel gas into the central region, causing a pile-up near the inner Lindblad resonance (ILR). As the central density increases, an ILR may grow more effective, maintaining the process. The idea has been supported by [Shlosman et al. \(1989\)](#), [Friedli & Benz \(1993\)](#), and [Heller & Shlosman \(1994\)](#). We discuss it further in [section 12.4](#).

[Su and Simkin \(1980\)](#) found a correlation between disk morphology in Seyfert 1 galaxies and the full width at zero intensity (FWZI) of the Balmer emission lines. Objects ranging from pure spirals (S), inner rings with outer spirals (RS), inner rings and outer rings (RR), inner disks and outer rings (DR), and amorphous structure (A) showed a general increase in FWZI. This was interpreted as due to the evolution of a system with a bar or oval, the gas distribution developing initially into spirals, then torqued into rings, and ending with the perturbation eventually dissolving leading to the diffusion of the rings.

[Arsenault \(1989\)](#) tried to elucidate the correspondence between nuclear activity and the presence of bars and rings by selecting samples of starburst and Seyfert galaxies and comparing the frequency of bars and rings in such systems with that in a control sample of galaxies. He concluded that bars and rings are more prevalent in AGN and starburst galaxies than in "normal" (non-AGN and non-starburst) galaxies. [Moles et al. \(1995\)](#) examined the same question using Seyfert and LINER galaxies from the catalog of [Véron-Cetty & Véron \(1991\)](#) and morphological data from RC3. Of 186 active galaxies having sufficient morphological information, 95% were found to have rings and bars. The rings and the activity were suggested to be effects that accompany the non-axisymmetrical perturbations. The debate continues, however. [Ho et al. \(1996\)](#) carried out a spectroscopic survey of nearly 500 nearby galaxies, and concluded that while bars contribute significantly to circumnuclear star formation, they do not necessarily have an obvious influence on nuclear activity.

9. OBSERVATIONS OF GALACTIC RINGS

9.1. Frequency

Perhaps the most logical next step after defining the different classes of rings is to determine how frequently these features occur in galaxies. The frequencies will help us to gauge how long-lived these ring patterns might be, and how important they are in normal galaxy structure. Unfortunately, definitive statistics, especially concerning nuclear rings, have yet to be derived owing to serious observational selection effects or inadequate samples.

The relative frequency of inner rings is the best determined of the three ring types. [De Vaucouleurs & Buta \(1980b\)](#) used revised Hubble classifications from the Second Reference Catalogue of Bright Galaxies (RC2, [de Vaucouleurs et al. 1976](#)) to deduce this frequency and attempted to account for selection effects. The main selection effects that would bias any frequency estimate are the inclination of a galaxy and the number of resolution elements in an image. The first effect is important mainly in highly inclined spiral galaxies where internal extinction prevents the ring from being detected. Any sample of randomly oriented objects would therefore underestimate the frequency of inner rings. An additional problem of high inclination is to cause an overestimate of the frequency of inner rings in nonbarred galaxies. This is because bars viewed end-on at high inclination are easily overlooked. An example is [NGC 4274](#) in the Hubble Atlas ([Sandage 1961](#)), which is classified as Sa (nonbarred), but seems an obvious end-on bar case.

The resolution effect is important because classifications in RC2 are based on heterogeneous image material, some being large-scale plates taken with large reflectors, and others being small-scale Palomar Sky Survey prints or copy plates. The small-scale images are prone to overexposure and poor resolution, so that inner rings and bars are not recognized. Thus, it is best to restrict any frequency analysis to large galaxies of low inclination.

For a sample of 618 RC2 galaxies having corrected isophotal diameter $D_0 \geq 2'$ and logarithmic axis ratio $\log R_{25} \leq 0.2$, [de Vaucouleurs & Buta \(1980b\)](#) deduced that 25% of galaxies of all types are classified as (r)-variety while 37% are classified as (rs)-variety. [Table 3](#) shows statistics of varieties based on the same restrictions but using the larger database in RC3 ([de Vaucouleurs et al. 1991](#)). This table divides the sample according to family and stage, and also includes the percentages of galaxies satisfying the diameter and inclination restrictions but for which no variety is specified. [Table 3](#) shows that among spirals, inner rings are found at the 19% level while inner pseudorings are found at the 39% level. The percentage of (r)-variety cases is higher among barred spirals than nonbarred or weakly barred spirals. Inner pseudorings and s-shapes are nearly equally frequent among SB galaxies. Among nonbarred (SA) galaxies, inner rings are

much less frequent than s-shapes, while more than half of SAB galaxies are classified as having inner pseudorings. The indication from these results is that most normal giant galaxies have an inner ring or pseudoring, and that this is especially true if a galaxy has even a weak bar. Only a small percentage of spirals do not have a variety estimate for this kind of sample. The statistics are poorer for the lenticulars (S0 or L), and a higher percentage of them do not have a variety estimate. Note that the absence of a variety estimate for either an S0 or a spiral may also indicate that no variety is applicable ([Buta 1995](#)).

TABLE III. Relative frequencies of RC3 varieties for $D_0 \geq 2'$, $\log R_{25} \leq 0.2$

| Family | $f(r)$ | $f(rs)$ | $f(s)$ | $f(N.A.)$ | N |
|--------|--------|---------|--------|-----------|-----|
| SB | 23.2% | 32.4% | 38.4% | 6.0% | 336 |
| SAB | 15.1 | 50.7 | 29.8 | 4.4 | 272 |
| SA | 15.8 | 32.1 | 46.7 | 5.5 | 165 |
| All S | 18.8 | 38.8 | 37.1 | 5.3 | 773 |
| LB | 36.1 | 19.4 | 25.0 | 19.4 | 36 |
| LAB | 13.5 | 16.2 | 35.1 | 35.1 | 37 |
| LA | 21.5 | 7.7 | 32.3 | 38.5 | 65 |
| All L | 23.2 | 13.0 | 31.2 | 32.6 | 138 |

In [Table 4](#), we examine statistics of ring frequency using volume-limited samples of RC3 galaxies. This provides a somewhat different picture of the frequency of ring phenomena. We compute the relative frequency of inner rings and pseudorings for various limiting radial velocities v_{3K} (reduced to the microwave background frame) from RC3, restricted to $\log R_{25} \leq 0.2$. For the lower redshift limits, the frequency of inner rings is about 12-13% and that of inner pseudorings is 28-34%. When the statistics are restricted by family, the frequency of rings is higher in SB galaxies than in SA galaxies, but the (s)-variety is still the dominant type. Nevertheless, volume-limited statistics still indicate that rings are observed in a large fraction of normal, massive galaxies along the Hubble sequence. Note that RC3 is not complete with regard to radial velocity measurements in most of the samples in [Table 4](#), so the statistics become less complete in addition to less reliable with increasing limiting redshift.

The effect of inclination on spiral varieties is shown in [Table 5](#), which gives the frequencies for $\log R_{25} > 0.2$. As expected, the frequencies of rings and pseudorings are considerably less, and more galaxies lack a variety estimate, due mainly to detection difficulties. [De Vaucouleurs & Buta \(1980b\)](#) investigated the effects of inclination on ring frequencies and found a general decrease for large galaxies, but that frequencies of features seen in SA and SAB galaxies can increase due to misclassification. In RC2 lenticulars, "ansae" along the major axis of an apparently nonbarred example were attributed to edge-on views of inner rings, and as a consequence the frequency of the (r)-variety unrealistically increases with inclination for such objects. It is clear now, however, that some "ansae" are probably connected to bars and not rings.

TABLE IV. Percentages of RC3 spiral varieties versus redshift, for $\log R_{25} \leq 0.2$

| $v_{3K} \leq$ | $f(r)$ | $f(rs)$ | $f(s)$ | $f(N.A.)$ | N |
|---------------|--------|---------|--------|-----------|------|
| 1400 | 12.0 | 33.7 | 45.4 | 8.8 | 249 |
| 2000 | 13.0 | 30.6 | 47.6 | 8.8 | 477 |
| 2500 | 13.3 | 28.4 | 49.3 | 9.0 | 647 |
| 3000 | 13.5 | 29.5 | 48.2 | 8.9 | 824 |
| 3500 | 14.5 | 29.7 | 46.5 | 9.4 | 1003 |
| 4000 | 14.6 | 31.6 | 44.5 | 9.4 | 1140 |
| 5000 | 16.7 | 30.8 | 40.4 | 12.1 | 1571 |
| 6000 | 17.6 | 30.1 | 39.0 | 13.2 | 1878 |
| 8000 | 19.2 | 28.5 | 37.6 | 14.7 | 2274 |
| 10000 | 19.8 | 28.2 | 36.7 | 15.3 | 2496 |
| 20000 | 20.8 | 27.8 | 35.8 | 15.6 | 2712 |

TABLE V. Percentages of RC3 spiral varieties versus redshift, for $\log R_{25} > 0.2$

| $v_{3K} \leq$ | $f(r)$ | $f(rs)$ | $f(s)$ | $f(N.A.)$ | N |
|---------------|--------|---------|--------|-----------|------|
| 1400 | 4.5 | 15.7 | 62.8 | 17.0 | 312 |
| 2000 | 5.5 | 17.5 | 60.5 | 16.5 | 595 |
| 2500 | 5.9 | 17.7 | 57.9 | 18.6 | 786 |
| 3000 | 6.7 | 18.8 | 56.4 | 18.1 | 954 |
| 3500 | 8.2 | 18.5 | 55.4 | 17.9 | 1130 |
| 4000 | 8.5 | 18.7 | 54.2 | 18.6 | 1277 |
| 5000 | 10.0 | 19.2 | 50.2 | 20.5 | 1622 |
| 6000 | 11.5 | 19.2 | 47.9 | 21.4 | 1858 |
| 8000 | 12.2 | 19.2 | 45.9 | 22.6 | 2098 |
| 10000 | 12.7 | 18.9 | 44.8 | 23.6 | 2245 |
| 20000 | 13.1 | 19.1 | 44.1 | 23.7 | 2375 |

[Kormendy \(1979a\)](#) provided another statistical study, but focussed only on SB galaxies and accounted for lenses which are not really recognized in RC2. He found that 76% of intermediate to late Hubble type SB galaxies have inner rings and pseudorings, while 54% of early type SB galaxies have inner lenses. In this analysis, inner rings and pseudorings were combined. Again, the indication is that most barred galaxies are ringed or lensed.

The distributions of inner rings and pseudorings with revised Hubble stage T (coded on the RC2 numerical scale) were described by [de Vaucouleurs \(1963\)](#) and [de Vaucouleurs & Buta \(1980b\)](#). These studies found that inner rings are most frequent among early-type galaxies while inner pseudorings are most frequent among later type galaxies. A double-peaked distribution for inner rings (with peaks at stages -1 and +2 or $S0^+$ and Sab) was also found. It is possible that some of the excess at stage $S0^+$ ($T = -1$) in those studies is due to inclusion of lenses ([Kormendy 1981](#)). In [Figure 23](#), we show the distribution of inner rings and pseudorings with type for a sample of RC3 galaxies having $v_{3K} \leq 2500 \text{ km s}^{-1}$ and $\log R_{25} \leq 0.2$. In such a volume-limited sample, the frequency of inner rings is nearly uniform in the range $-2 \leq T \leq 5$.

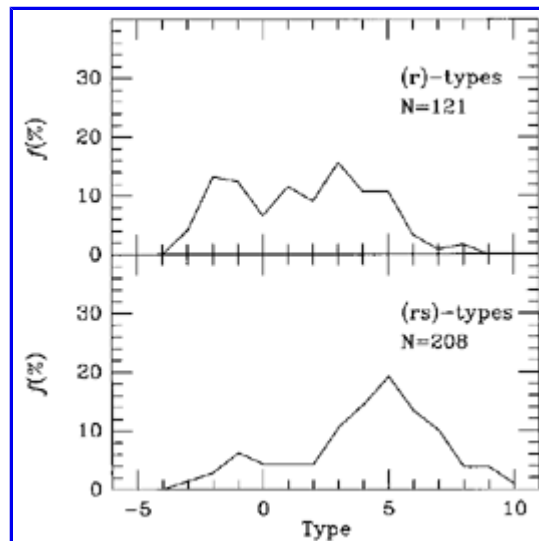


Figure 23. Relative frequency of inner rings (top) and pseudorings (bottom) as a function of RC3 Hubble type. The numbers of objects are indicated. The sample is restricted to $v_{3K} \leq 2500 \text{ km s}^{-1}$ and $\log R_{25} \leq 0.2$.

The frequencies of outer rings and nuclear rings are less well-established owing to more serious selection effects than for inner rings. [De Vaucouleurs \(1975a\)](#) first estimated the frequency of outer rings and pseudorings, and found that 4% of the galaxies in the Reference Catalogue of Bright Galaxies (RC1, [de Vaucouleurs & de Vaucouleurs 1964](#)) possess these features. The rings are most commonly observed around stage S0/a. However, though the rings seem rare, it is likely that the RC1 frequency estimate is too low. This is because of the wide range of surface brightnesses of outer rings. RC1 morphological types are based exclusively on large-scale prime focus plates, but outer rings are best detected on deep, small-scale Schmidt plates such as the SRC-J southern sky survey. Even on deep Schmidt plates, however, outer rings can be lost if there is significant galactic extinction. In [Figure 24](#), we repeat de Vaucouleurs' calculations using the more complete RC3 data. This shows the relative frequency of closed outer rings (R) and outer pseudorings (R') versus revised Hubble stage. Rings classified as (R) are most common at stage S0/a, while pseudorings (R') are more common at later types, as would be expected. Both outer rings and pseudorings are nevertheless phenomena of early-type galaxies, being rare at stages later than Sc. [Table 6](#) summarizes the percentage of outer rings and pseudorings versus radial velocity in RC3. For the lower redshift ranges, these features are found in about 10% of the entries over all types.

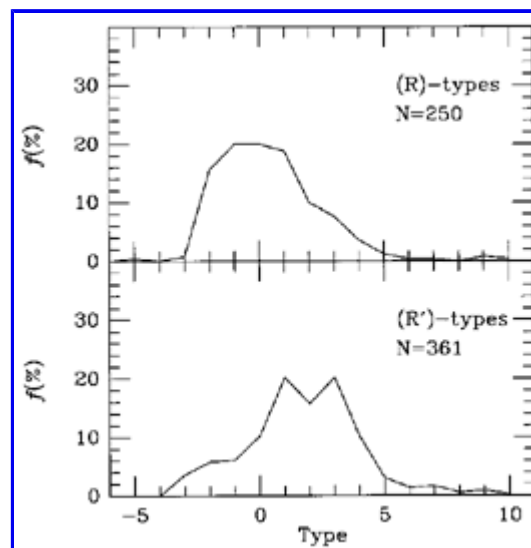


Figure 24. Relative frequency of outer rings (top) and pseudorings (bottom) as a function of RC3 Hubble type. The numbers of objects are indicated. The sample is restricted to $v_{3K} \leq 20000 \text{ km s}^{-1}$ and $\log R_{25} \leq 0.2$.

TABLE 6. Percentages of RC3 outer rings and pseudorings versus redshift, for $\log R_{25} \leq 0.2$ and all types

| $v_{3K} \leq$ | $f(R)$ | $f(R')$ | No ring | N |
|---------------|--------|---------|---------|------|
| 1400 | 4.1 | 5.2 | 90.7 | 387 |
| 2000 | 5.0 | 5.5 | 89.5 | 706 |
| 2500 | 4.6 | 5.2 | 90.1 | 953 |
| 3000 | 4.8 | 5.6 | 89.5 | 1177 |
| 3500 | 5.4 | 6.5 | 88.1 | 1404 |
| 4000 | 5.3 | 7.1 | 87.6 | 1600 |
| 5000 | 5.8 | 8.3 | 85.9 | 2176 |
| 6000 | 6.3 | 8.7 | 85.1 | 2574 |
| 8000 | 6.9 | 9.1 | 84.1 | 3119 |
| 10000 | 6.8 | 9.5 | 83.7 | 3430 |
| 20000 | 6.7 | 9.6 | 83.7 | 3749 |

For nuclear rings the problem of detection is most serious of all, not because these features are generally faint, but because they are located in the bright centers of galaxies that are easily overexposed on photographic images and where the luminosity gradient is very steep. Core overexposure and poor resolution are especially a problem with sky survey images, thus the true frequency of nuclear rings will have to be based on a CCD imaging survey of a well-defined galaxy sample. However, we believe that nuclear rings are not rare, especially in galaxies which have other rings. For example, [Buta & Crocker \(1991\)](#) found nuclear rings, some not previously known, in a small sample of galaxies chosen on the basis of the appearance of an outer ring or pseudoring. New examples of nuclear rings are turning up regularly in similar imaging surveys (e.g., [Contini et al. 1995](#)) or in radio continuum studies of active galaxies ([Wilson et al. 1991](#); [Forbes et al. 1994a, b](#); [Storchi-Bergmann et al. 1996](#)).

9.2. Linear and Relative Diameters

The diameters D_r of inner rings relative to isophotal and metric diameters of the parent galaxies are discussed in detail by [de Vaucouleurs & Buta \(1980b\)](#). The ratios $X = \log D_0/D_r$ and $Y = \log A_e/D_r$, where D_0 is the "face-on" corrected (RC2 formulation) isophotal blue diameter and A_e is the effective (half power) blue diameter, were found to depend on both family and stage as follows:

$$X = 0.54 - 0.13F + 0.036T \quad 1$$

$$Y = 0.01 - 0.13F + 0.058T \quad 2$$

where F is a family index (-1 for SA, 0 for SAB, and +1 for SB galaxies) and T is the stage index on the RC2 numerical scale. The formulae are applicable only to spirals in the type range $0 \leq T \leq 8$ (S0/a to Sdm; see [Figure 25](#)), and they indicate that inner rings and pseudorings are relatively larger in barred galaxies than in nonbarred galaxies, and in earlier types than in later types. Although relative inner ring size could thus be taken as an indicator of apparent "bar strength" at a given type, or of type at a given family, the trends shown in [Figure 25](#) reflect a complex mix of possible resonance types for nonbarred or weakly barred inner rings, differences in the mass distributions between early and late-type galaxies, and possibly even in the nature of rings in nonbarred galaxies (sections [15](#) and [17](#)).

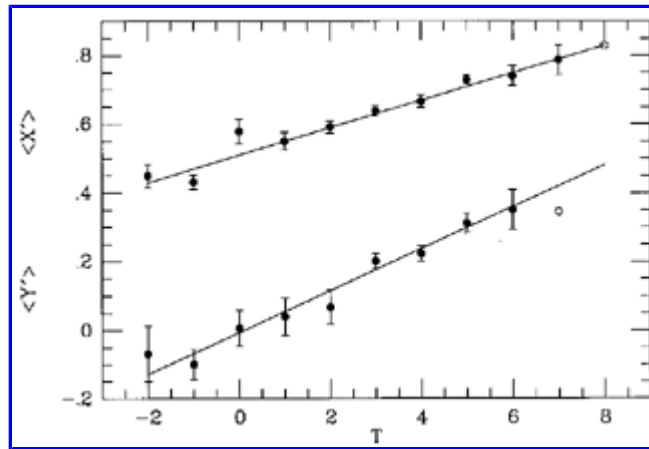


Figure 25. Mean logarithmic diameter ratios $X' = \log(D_0/D_r) + 0.13F$ and $Y' = \log(A_e/D_r) + 0.13F$ versus stage T , from [de Vaucouleurs & Buta \(1980b\)](#). Open circles are based on only one galaxy.

Absolute linear diameters D_r of inner rings and pseudorings have been studied by [Kormendy \(1979a\)](#), [Pedreros & Madore \(1981\)](#), and [Buta and de Vaucouleurs \(1982\)](#). Kormendy focussed only on a sample of 121 bright SB galaxies, and found that the basic correlation for linear inner ring and lens diameters is with the absolute magnitude M_B^0 , and hence mass, of the parent galaxy. The correlation between $\log D_r$ and M_B^0 had a slope of -5.0 within the uncertainties, which he concluded to mean that the mean surface brightness (as if all of the light is concentrated within the rings) of the galaxies is independent of luminosity. The lower mean surface brightness of later-type ringed galaxies was attributed to a variation of mass-to-light ratio with type, which he suggested implied that the mean mass density outside the core region is constant for all morphological types. He concluded that the total mass of a galaxy uniquely determines the size of a bar and all of its associated components. Kormendy also found a correlation between the sizes of outer rings, pseudorings, and lenses and absolute magnitude, but did not believe that these could provide a size scale that determines M_B^0 , because the rings contain so little light. He suggested that the sizes of outer rings are fixed by the size of the bar.

[De Vaucouleurs \(1956\)](#) first suggested that inner ring and pseudoring diameters in barred spirals might be useful as extragalactic distance indicators. He saw definite advantages to the use of such structures at the time, because rings are defined by *ridges* in the light distribution, not isophotes, and hence can be measured with better internal and external precision than isophotal galaxy diameters ([de Vaucouleurs 1959b](#)). [Pedreros & Madore \(1981\)](#) and [Buta & de Vaucouleurs \(1982\)](#) calibrated the rings as distance indicators using distance-independent indices of absolute magnitude such as the type and luminosity class. Both studies showed that inner rings become smaller with advancing stage along the Hubble sequence and with fainter luminosity class.

Using distances from the luminosity index, $\lambda_c = (T + L_c) / 10$, where T is the numerical stage (RC2 and RC3 scale) and L_c is the inclination-corrected luminosity class (also numerically coded; [de Vaucouleurs 1979](#)), and the B -band Tully-Fisher relation ([Bottinelli et al. 1980](#)), [Buta & de Vaucouleurs \(1982\)](#) derived the following formula for spirals of type Sab and later:

$$\log D_r (\text{pc}) = 3.61 + 0.15F - 0.10(T - 4) - 0.05(L_c - 3) \quad 3$$

This shows that the largest inner rings and pseudorings are found in early-type barred spirals of high luminosity. For an SB(r)ab I galaxy, the ring diameter averages about 11.5 kpc. However, for the average ringed galaxy of type SAB(r)bc II, the ring diameter is only about 4 kpc. [Pedreros & Madore \(1981\)](#) also tried a formulation using both type and luminosity class as separate parameters (rather than as the combined luminosity index) and found weakly significant differences between SB galaxies on one hand and SA+SAB galaxies on the other. Their general formulation for a moderately unbiased sample (SA+SAB+SB inclusive) gave the following formula for the apparent ring diameter (in arcseconds) reduced to a radial velocity of 5000 km s^{-1} :

$$R(5000) = -2.05L - 1.31T + 29.46 \quad 4$$

where L is the raw numerical luminosity class (not inclination-corrected). This study gave a greater dependence on luminosity class than the formulation of Buta and de Vaucouleurs, but the difference may reflect differences in the sample characteristics and calibrating distances.

[Buta & de Vaucouleurs \(1982\)](#) also considered the sizes of rings in S0 galaxies and derived a formulation based only on the Hubble type and family of the galaxy, since luminosity classes are not defined for types earlier than Sab ($T=2$). The absolute linear diameters of inner rings over the range $-2 \leq T \leq 7$ can be derived from this alternative formulation:

$$\log D_r (\text{pc}) = 3.81 + 0.15F + 0.05(T - 2.5), -2 \leq T \leq 2 \quad 5a$$

$$\log D_r(\text{pc}) = 3.81 + 0.15F - 0.12(T - 2.5), \quad 3 \leq T \leq 7$$

5b

Figure 26 shows that the reduced diameter, $\log D_r^o = \log D_r - 0.15F$, of inner rings and pseudorings from these formulae achieves a maximum of 6.1 kpc at stage Sab. A very similar trend is seen in Figure 7 of [Pedreros & Madore \(1981\)](#).

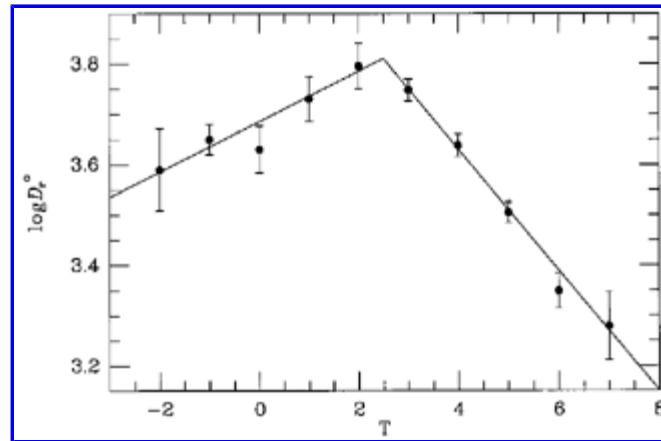


Figure 26. Mean logarithmic reduced inner ring diameter versus Hubble type, from [Buta & de Vaucouleurs \(1982\)](#).

[Buta & Crocker \(1993\)](#) have presented information on the diameters of inner, outer, and nuclear rings in a limited subset of galaxies which have at least a nuclear ring or related feature. Logarithmic means gave average diameters of 1.1, 9.5, and 22.4 kpc for nuclear, inner, and outer rings and pseudorings, respectively, in ≈ 20 SB galaxies. These are based on distances derived from radial velocities and an assumed Hubble constant of $100 \text{ km s}^{-1} \text{ Mpc}^{-1}$. The diameters of rings in weakly barred and nonbarred galaxies were also considered, and found to show greater scatter.

Many galaxies possess both inner and outer rings simultaneously. The co-existence of these features in the same galaxy provides a more dynamically interesting diameter ratio than those in equations 1 and 2. It was found by [de Vaucouleurs \(1956\)](#), [Athanasoula et al. \(1982\)](#), [Kormendy \(1982a\)](#), and [Buta \(1984, 1986a, 1995\)](#) that the ratio d_R / d_r (rings and pseudorings together) has a relatively small dispersion with a mean or median near 2.0. The largest samples, from the Catalog of Southern Ringed Galaxies ([Buta 1995](#)), gave the distributions in [Figure 27](#). Since the rings are noncircular on average (see [section 9.3](#)), the plot shows the distributions of ratios \bar{P} of geometric mean diameters rather than major axis diameters. For more than 1000 galaxies of all families, the median ratio of geometric mean ring diameters is 2.19, very similar to the outer ring to bar diameter derived by [Kormendy \(1979a\)](#). When the sample is divided by family, little dependence is found: 2.29 for SA, 2.27 for SAB, and 2.13 for SB galaxies. As noted by [Athanasoula et al. \(1982\)](#), the scatter is larger for SA galaxies than for SB galaxies.

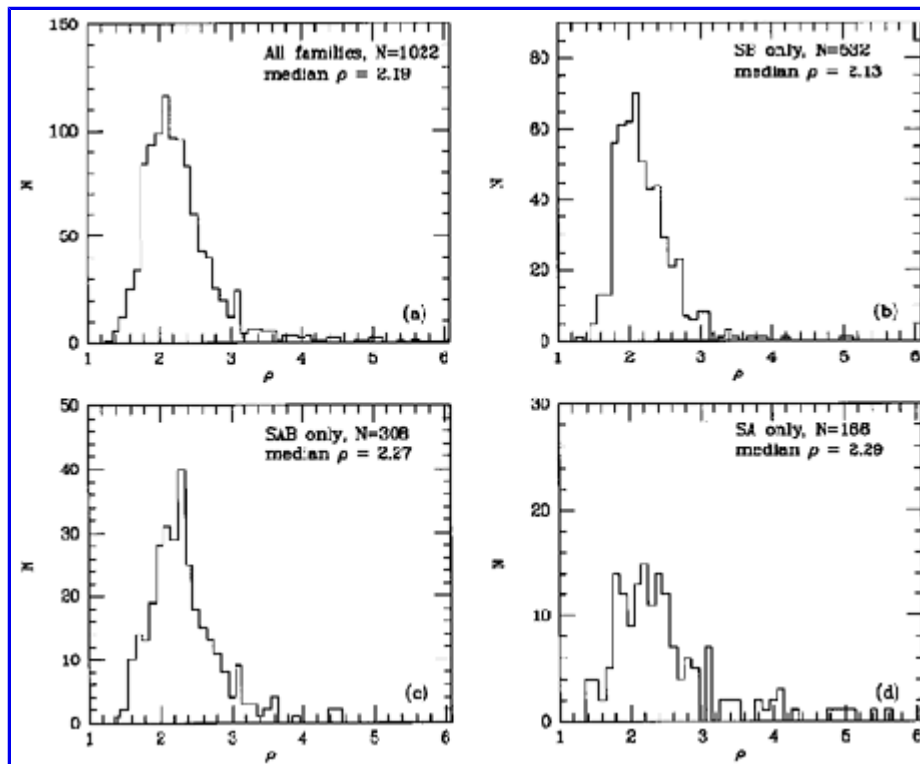


Figure 27. Distributions of ratio of geometric outer and inner ring/pseudoring diameters, from Buta (1995). The upper left panel is irrespective of family, while the other panels separate barred, weakly barred, and nonbarred galaxies.

Buta & Crocker (1993) have also considered ring ratios in systems with nuclear rings. For about 20 objects with strong bars, logarithmic averages gave ratios of 18.9, 8.7, and 2.2 for d_R / d_{nr} , d_r / d_{nr} , and d_R / d_r , respectively. No evidence for a significant type dependence of these ratios was found. Weakly-barred and nonbarred galaxies displayed considerably more scatter and possible weak type dependences in the same ratios.

9.3. Intrinsic Shapes and Orientations

Inner and Outer Rings, Pseudorings, and Lenses

Determining the intrinsic shapes and orientations of galactic rings with respect to bars is one of the most important means of connecting rings to *specific* orbital resonances. Test-particle models described in section 12.2 show that a resonance can impress its "stamp" on the morphology of a gaseous ring which forms near it, owing to the distinctive nature of periodic orbits in a bar potential. Contopoulos (1979) illustrated the properties of these orbits and showed that alignments changed by 90° across a major resonance and that orbits achieved their maximum local eccentricity near a major resonance. Schwarz (1984a) showed that model gaseous rings formed from slow secular evolution of bar-driven spiral structure, and that the gas collects into the largest periodic orbit near a resonance which does not cusp and which does not cross another orbit. Model gaseous rings took on the oval shapes and bar alignments of these orbits.

The intrinsic shapes and orientations of galactic rings have been deduced from distributions of *apparent* axis ratios and relative bar/ring position angles under the assumption of random orientations of the spin axes. De Vaucouleurs (1956; see de Vaucouleurs & Buta 1980a) produced the first catalogue of apparent major and minor axis dimensions of inner and outer rings and lenses that later could be used for this purpose (Athanasoula et al. 1982; Buta 1984). The sample included 532 galaxies of all Hubble types. Kormendy (1979a) measured diameters and angles for his small sample of SB galaxies, and was the first to really attempt to deduce intrinsic shapes from such measurements. Other sources of diameters include Pedreros & Madore (1981), who measured rings in a similar-sized sample for the distance scale, and Corwin et al. (1985), who provided measurements of ring diameters in a sample of 2000 southern galaxies. The early studies of intrinsic shapes and orientations by Kormendy (1979a), Athanasoula et al. (1982), Buta (1984, 1986a), and Schwarz (1984c) provided some evidence for oval intrinsic shapes and preferred alignments, but were not very definitive because the samples used were either too small or ill-suited to statistics, or the observational errors were not explicitly taken into account.

The Catalog of Southern Ringed Galaxies (Buta 1995 = CSRG) has provided the largest samples and the best statistics of intrinsic ring shapes and orientations. It is based on uniform searches of the Science Research Council (SRC) IIIa-J Southern Sky Survey, which is the highest quality of all of the available sky surveys. The J filter-plate match has an effective wavelength between Johnson *B* and *V* filters but is closer to *B* than *V*, thus making the plates ideal for detecting the typically blue rings (see section 9.4). Other advantages of the SRC-J

survey for ringed galaxy studies are the fine grain of the emulsion, which counters the small image scale and allows rings as small as $0'.2$ to be resolved well enough to measure at least axis ratios; and the depth of exposure of the plates, which is sufficient to reveal rings which are as faint as 1% of the night sky brightness. The principal disadvantage of the J plates is the frequent overexposure of galaxy core regions, but ESO-B and ESO-R films usually provided the necessary information in such cases.

Together, the three southern sky surveys have provided a very large database of apparent ring diameters, axis ratios, relative bar/ring position angles, and morphologies. The CSRG includes 3,692 galaxies and information on 4661 ring, pseudoring, and lens features. We illustrate in Figures 28, 29, 30 three sets of distributions from Buta (1995), where the filled circles refer to the CSRG data, and summarize in Table 7 the best current estimates of the intrinsic shapes and orientations derived under the assumption of random orientations of the spin axes (solid histograms). The principal result from these kinds of studies is that rings in galaxies are, in general, noncircular on average. The distributions in Figure 28 are for inner and outer rings, pseudorings, and lenses irrespective of family. In the analysis of Buta (1995), rings and lenses were not treated as distinct features. Selection effects in the observed distributions are discussed by Buta (1995), the main effect being inclination. For the best model fits, which allow for observational error, both inner and outer features have an average intrinsic axis ratio of ≈ 0.85 with a dispersion of ≈ 0.1 . When the samples are subdivided by family or feature subtype as in Table 7, some possibly significant differences are found. For example, both inner and outer rings, pseudorings, and lenses in SA galaxies may be rounder on average than those in SB galaxies. Inner rings and ring/lenses seem to be more oval on average than inner pseudorings, while outer rings and ring/lenses may be slightly less oval than outer pseudorings. SAB inner and outer features have characteristics that are not necessarily intermediate between those for SA and SB features.

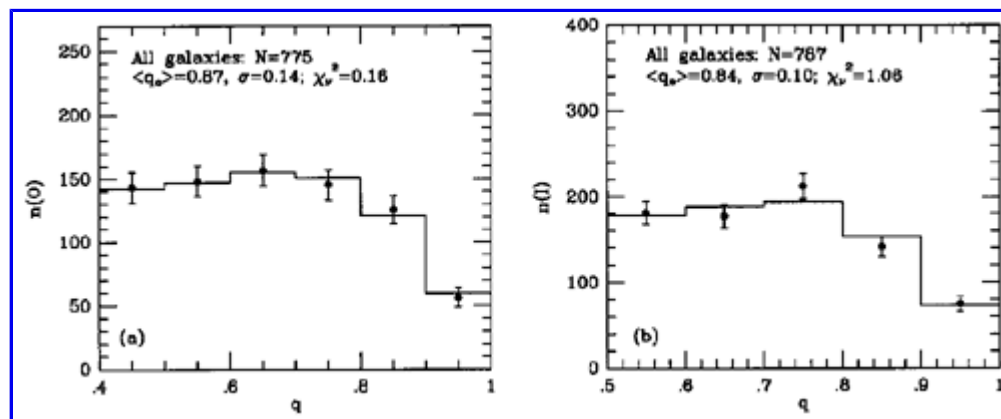


Figure 28. Model fits to observed axis ratio (q) distributions for outer ring, pseudoring, and lens features (left) and inner ring, pseudoring, and lens features (right), irrespective of family, from Buta (1995). The χ^2 per degree of freedom is indicated.

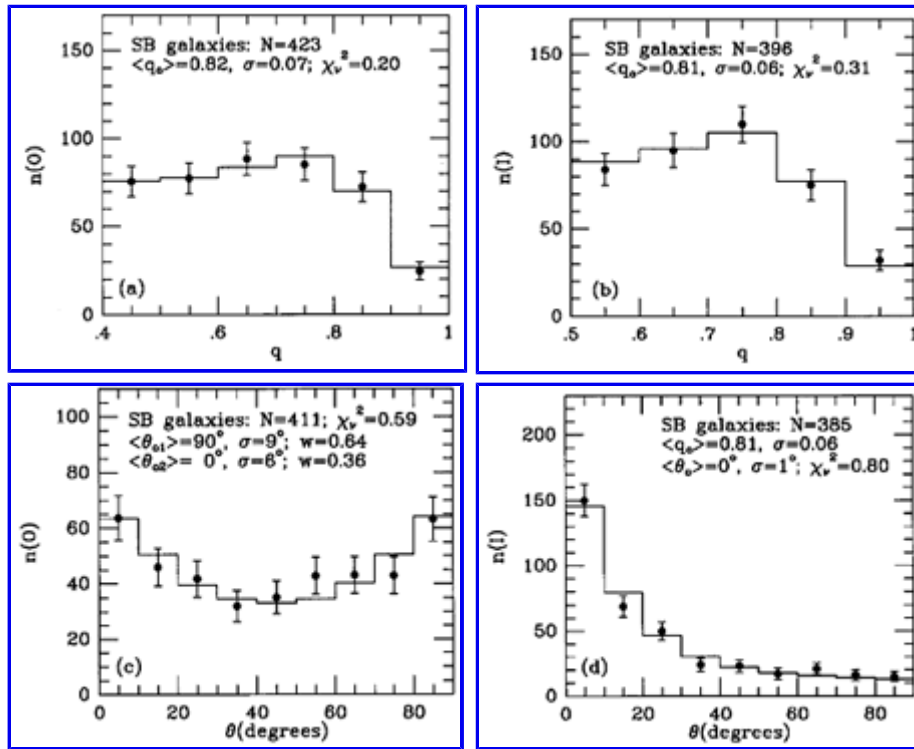


Figure 29. Model fits to observed axis ratio (q) and bar/ring position angle (θ) distributions for outer (left) and inner (right) rings, pseudorings, and lenses in SB galaxies, from [Buta \(1995\)](#).

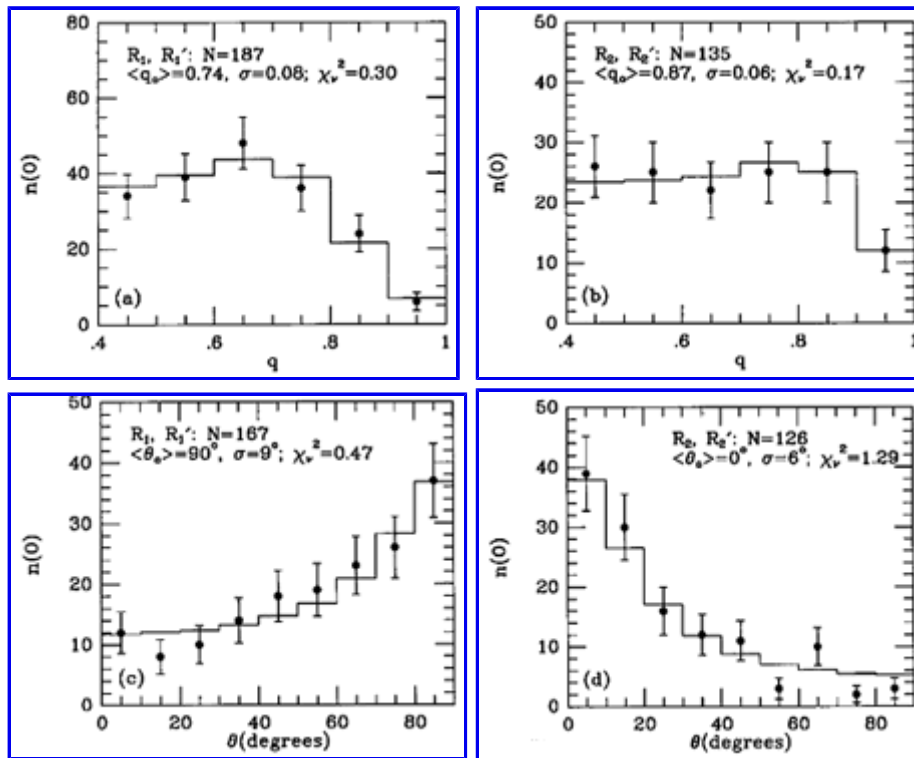


Figure 30. Model fits to observed axis ratio (q) and bar/ring position angle (θ) distributions for R_1, R'_1 and R_2, R'_2 outer features (known as the OLR subclasses), from [Buta \(1995\)](#).

The shape results for outer rings in [Table 7](#) can be compared with statistics of isophotal *disk* shapes, since outer rings are preferentially located in the outer regions of a disk. [Fasano et al. \(1993\)](#) have used a volume-limited sample of 1064 RC3 galaxies to deduce that early-type spiral galaxies have a more triaxial disk than late-types. The distribution of intrinsic shapes, inferred by inversion ([Lucy 1974](#)),

gave a peak at planar axis ratio $b/a = 0.8$, comparable to SB outer rings and pseudorings. However, the ring and disk samples are very different in nature, and the significance of the agreement in intrinsic shapes is unclear.

The distribution of relative bar/ring position angles is very interesting from these kinds of studies. The distributions are inconsistent with random alignments between bars and rings (see Figure 10 of [Buta 1986a](#)). As shown in [Figure 29](#), SB inner and outer features have about the same distribution of apparent axis ratios, and hence about the same average intrinsic shape, but the angle distributions are very different. The distribution of angles for outer features can be modeled with two populations of features having perpendicular and parallel alignments relative to the bar. The two maxima in this distribution favor that 64% of SB outer rings are aligned perpendicular to the bar and 36% are aligned parallel to the bar. The distribution of angles for inner rings favors parallel alignment exclusively. [Figure 30](#) shows that the two maxima in the angle distribution for SB outer features are connected to the "OLR" subclasses, R₁ and R₂. The latter are found to be rounder on average than the former, and their perpendicular relative alignments are strikingly illustrated. For SAB galaxies, the same two alignments are probably present, but in a greatly different proportion: 85% parallel-aligned, and 15% perpendicular-aligned.

The statistics described above give a very good indication of the properties of the average ring, but do not tell us the extremes possible for any given features. [Buta \(1986a\)](#), in a preliminary study of the CSRG data available at the time, deduced that inner rings in SB galaxies have a wide range of intrinsic axis ratios: from 0.6 to 0.95. Among low-inclination barred galaxies, extremely oval inner rings are found in [NGC 1433](#) ([Figure 3](#)), [NGC 6782](#) ([Figure 76](#)), [IC 1438](#) ([Figure 9](#)), [ESO 296-2](#), and [ESO 325-28](#) ([Figure 17](#)), while nearly circular inner rings are found in [NGC 53](#), [6761](#), and [7329](#) ([Figure 43](#)). The differences are not obviously connected to apparent bar strength (i.e., SB versus SAB).

TABLE VII. Intrinsic Shapes and Alignments of Galaxy Rings

| Feature | $\langle q_0 \rangle \pm \sigma(q_0)$ | $\langle \theta_0 \rangle \pm \sigma(\theta_0)$ | N |
|----------------------------------|---------------------------------------|---|-----|
| inner features, all families | 0.84 ± 0.10 | - | 787 |
| SB inner features | 0.81 ± 0.06 | $0^\circ \pm 1^\circ$ | 396 |
| SB(r,rl) only | 0.78 ± 0.04 | $0^\circ \pm 3^\circ$ | 251 |
| SB(rs) only | 0.88 ± 0.04 | $0^\circ \pm 1^\circ$ | 122 |
| SAB inner features | 0.78 ± 0.14 | $0^\circ \pm 8^\circ$ | 215 |
| SA inner features | 0.92 ± 0.09 | - | 172 |
| outer features, all families | 0.87 ± 0.14 | - | 775 |
| R ₁ , R' ₁ | 0.74 ± 0.08 | $90^\circ \pm 9^\circ$ | 187 |
| R ₂ , R' ₂ | 0.87 ± 0.06 | $0^\circ \pm 6^\circ$ | 135 |
| SB outer features | 0.82 ± 0.07 | $0^\circ \pm 6^\circ$ (36%) $90^\circ \pm 9^\circ$ (64%) | 423 |
| (R,RL)SB only | 0.84 ± 0.04 | $0^\circ \pm 6^\circ$ (26%) $90^\circ \pm 9^\circ$ (74%) | 152 |
| (R')SB only | 0.80 ± 0.11 | $0^\circ \pm 6^\circ$ (42%) $90^\circ \pm 9^\circ$ (58%) | 262 |
| SAB outer features | 0.94 ± 0.16 | $0^\circ \pm 6^\circ$ (85%) $90^\circ \pm 9^\circ$ (15%) | 208 |
| SA outer features | 0.97 ± 0.21 | - | 138 |

Nuclear Rings and Pseudorings

The intrinsic shapes and orientations of nuclear rings and their pseudoring counterparts cannot be obtained at the same level of precision as for inner and outer features. The reason is that most nuclear features are too small or overexposed to detect on sky survey material, and as a consequence it is currently not possible to build up the large samples required to make a definitive analysis. Less than 100 examples are currently known in galaxies ranging in type from S0 to Sc. [Buta & Crocker \(1993\)](#) have used low-inclination galaxies to deduce that nuclear rings range in intrinsic axis ratio from ≈ 0.7 to ≈ 1.0 . If oval, they are generally misaligned with the main bar at an intermediate angle between 0° to 90° , although cases of exactly parallel ([NGC 4314](#)) or perpendicular ([NGC 1317](#)) alignments are known.

9.4. Photometric Properties

Photometry of ringed galaxies is essential for a better understanding of their structure. The use of CCD's has greatly aided the studies of these galaxies in particular because some rings are so very faint. With modern detectors, the surface brightness distributions can be defined to less than 1% of the night sky in blue light. Multicolor surface photometry studies have quantified the complex luminosity and color distributions in ringed galaxies, which we describe here. Some of the studies described were not so much concerned with a ring in a particular galaxy than with other aspects, such as bars or spiral structure.

Optical Luminosity Distributions

One of the first ringed galaxies to receive serious photometric attention was [NGC 4736](#). Photoelectric drift scans by [Simkin \(1967\)](#) revealed a complex east-west luminosity profile with the inner ring as a definite extranuclear "peak" of high surface brightness. Other more detailed studies were made by [Schommer \(1976\)](#), [Boroson \(1981\)](#), and [Kent \(1986\)](#). To this day, however, no study has yet delineated the luminosity distribution of this galaxy to radii well beyond its very faint outer ring.

De Vaucouleurs (1975a) presented a photometric study of another ringed galaxy, [NGC 1291](#). Like [NGC 4736](#), [NGC 1291](#) is among the largest outer-ringed galaxies in the sky. However, it is of earlier Hubble type than [NGC 4736](#) and has no inner ring. An equivalent luminosity profile revealed a series of humps due to the strong bar and inner lens, the outer ring, and also a small nuclear bar. The latter feature is one of the first examples ever found of the nuclear bar phenomenon, which is discussed further in [section 16.1](#). The outer ring was found to have a peak surface brightness of about 24 mag arcsec⁻² in blue light, or about 20% of the night sky brightness. De Vaucouleurs was also able to model the bulge of the galaxy in terms of an $r^{1/4}$ law.

Enough ringed galaxies have been studied photometrically since these earlier studies to give a reliable indication of the range of their photometric profile shapes. Because ringed galaxies display a complex structure, usually with considerable non-axisymmetry, the most meaningful profiles are elliptically-averaged or ellipse fit profiles. [Figure 31](#) shows a montage of profiles for 10 multiple-ringed galaxies with exceptionally strong rings or pseudorings. In each case, the radius has been normalized to $r_{<25>}$, the radius where the average surface brightness is $\mu_B = 25.0$ mag arcsec⁻². Except for [NGC 1291](#) and [NGC 7217](#), these profiles are averages within elliptical annuli based on fits to an outer isophote taken to indicate the orientation of the disk. The profiles all display a multi-humped pattern where each hump is caused by a ring and in some cases a strong bar. Of the 10 objects displayed, only [NGC 7217](#) is amenable to a meaningful "decomposition" of the luminosity profile, at least over the range of surface brightnesses that could be reached with the original images. This means that properties such as bulge-to-disk ratios, disk "scale-lengths", and bulge "effective" radii and surface brightnesses are largely unknown for ringed galaxies. In the case of [NGC 7217](#), the bulge contributes perhaps 70% of the total *B*-band luminosity ([Buta et al. 1995b](#)), and with little trace of a bar or oval, it cannot be regarded as typical.

The vertical tick marks in [Figure 31](#) show the radius of the outer ring or pseudoring feature in each case, while other symbols indicate the locations of inner and nuclear rings. Inner and outer ring radii used are from the CSRG, while nuclear ring radii are from [Buta & Crocker \(1993\)](#). The normalization to $r_{<25>}$ shows that some outer features are brighter than the standard isophotal radius while others are fainter. The brightest outer ring is found in [NGC 7217](#) while the faintest is found in [ESO 565-11](#).

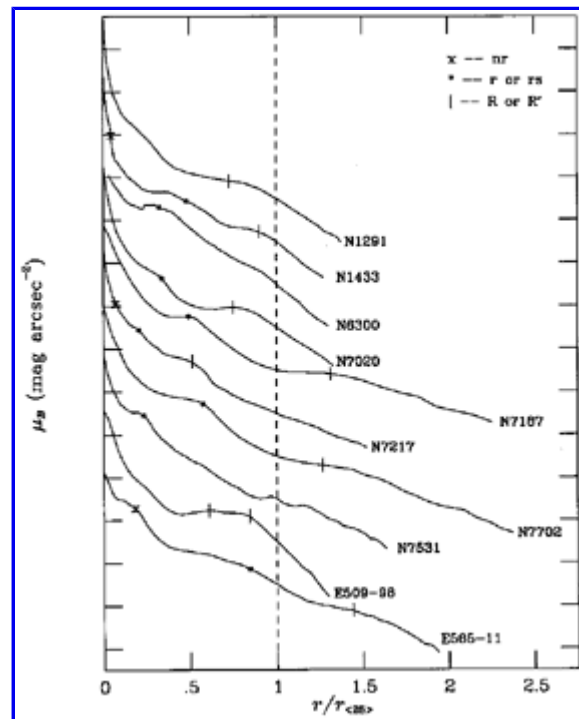


Figure 31. Azimuthally-averaged B -band luminosity profiles of classic ringed galaxies, corrected for galactic extinction. The radii are normalized to the radius, $r_{<25>}$, where the average surface brightness is $25.0 \text{ mag arcsec}^{-2}$. Locations of various types of rings (nr=nuclear ring, r,rs=inner ring or pseudoring, and R,R' = outer ring or pseudoring), are indicated with the symbols in the legend. The y-axis tick separation is $2 \text{ mag arcsec}^{-2}$.

A different normalization is used in [Figure 32](#) for those galaxies with outer rings and pseudorings only. In this figure, the radii are normalized to the radius, $r_{R,R'}$, of the outer feature. This allows us to isolate a few different groups of similar profiles. The first group includes [NGC 1433](#) and [ESO 565-11](#), which have broad humps due to the inner rings and bars, and the outer pseudorings. Both have nuclear rings, but that in [ESO 565-11](#) is much larger than the one in [NGC 1433](#). The second group consists of [NGC 1291](#), [7020](#), and [ESO 509-98](#), each of which has significant outer ring humps and lesser intermediate humps due to a bar or lens. The profile of [ESO 509-98](#) is especially interesting in that a large region interior to the outer ring (the R'₂ component of an R₁R'₂ double ring/pseudoring) is very uniform in surface brightness, while outside this radius the brightness gradient is very steep. Other published profiles which fit into this group are [NGC 2217](#) (Ohta et al. 1990), [NGC 6028](#) (Wakamatsu 1990), and probably [NGC 2859](#) (Kent 1985). The third group includes [NGC 7187](#) and [7702](#), each of which has a prominent inner ring as well as an outer ring but lack strong bars; their profiles differ clearly from the others. Groups 2 and 3 are similar in that the light distribution beyond the outer rings is exponential over the limited range shown. We cannot be certain, however, that this exponential behavior extrapolates to much larger radii. Finally, [NGC 7217](#) has a profile unlike any of the other cases, because of the significant amount of light beyond the outer ring.

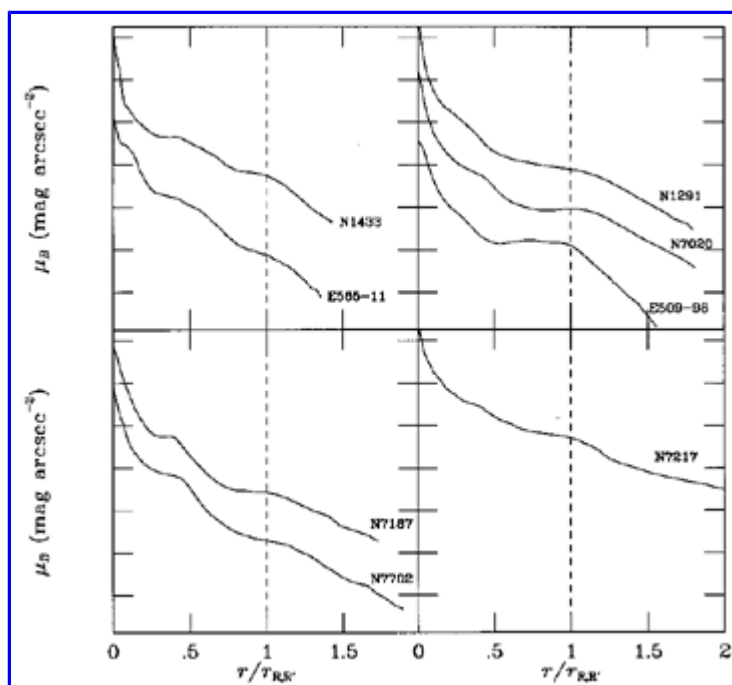


Figure 32. Profiles of ringed galaxies sorted according to similar shapes, normalized to the radius (from the CSRG) of an outer ring or pseudoring. The y-axis tick separation is $2 \text{ mag arcsec}^{-2}$.

Except for [NGC 4736](#) and [7531](#), the inner rings in most of the observed galaxies have blue light surface brightnesses of $\approx 22 \text{ mag arcsec}^{-2}$, similar to that of the (moonless) night sky brightness. The inner rings of [NGC 4736](#) and [7531](#) are about $1 \text{ mag arcsec}^{-2}$ brighter than this. Outer rings have observed surface brightnesses (corrected for galactic extinction) ranging from $\mu_B = 23.0 \text{ mag arcsec}^{-2}$ for [NGC 7217](#) (60% of night sky) to $\mu_B \approx 25.5 \text{ mag arcsec}^{-2}$ for [ESO 565-11](#) (5% of night sky), with the latter value no doubt being an upper limit since fainter examples must exist. Nuclear rings can be as bright as $\mu_B = 19.5 \text{ mag arcsec}^{-2}$ (> 10 times the night sky brightness; [Benedict 1980](#), [Benedict et al. 1992](#), [Buta 1986b](#)).

The total amount of light contained in rings is usually difficult to derive owing to the uncertain background contribution. Nevertheless, several cases have been studied and have yielded meaningful results, based either on photometric decomposition or on an approximate background interpolation from luminosity profiles. For [NGC 6300](#), [Buta \(1987a\)](#) deduced that the bright inner pseudoring contributes 25% of the B -band luminosity and 21% of the V -band luminosity. For [NGC 7702](#), [Buta \(1991\)](#) estimated the contributions of both the inner and outer rings. For the inner ring, an exponential background interpolation yielded relative contributions of 11.7%, 11.3%, 10.4%, and 9.1% in Johnson U , B , V , and Cousins R passbands. Thus, in spite of the unusual intensity of this feature, it is only a small contribution to the total luminosity. For the outer ring, no background correction was possible, and a total contribution of 12% of the blue luminosity was derived by assuming that all light beyond $R = 60''$ is due to the outer ring. In the case of [NGC 7020](#), [Buta \(1990c\)](#) derived a contribution of 17% of the total V -band luminosity for the bright outer ring over an enhanced region between $63''$ and $91''$ radius.

[Wakamatsu \(1990\)](#) derived relative outer ring fluxes by dividing galaxies at the minimum of the gap region between the inner disk and outer ring. By defining L_R^B to be the B -band luminosity of the ring plus outer disk and L_c^B to be the luminosity of the inner regions, Wakamatsu found that the ratio L_R^B / L_c^B ranges from 0.5 for [NGC 1291](#) to 1.4 for Hoag's Object, an axisymmetric outer-ringed galaxy ([Schweizer et al. 1987b](#)). [Buta \(1990c\)](#) found a ratio of 0.50 for [NGC 7020](#). Wakamatsu noted that outer rings in normal barred galaxies are much more luminous than the polar rings discussed by [Whitmore et al. \(1987\)](#).

[Buta et al. \(1995b\)](#) made an estimate of the relative flux contribution of the outer ring of [NGC 7217](#) by interpolating the background on either side of an azimuthally-averaged profile of the ring. This works well for [NGC 7217](#) because there is considerable light beyond the ring and the ring is merely a bump on a normal profile (i.e., exponential disk plus $r^{1/4}$ bulge). The outer rings and pseudorings in groups 1-3 in [Figure 32](#) cannot be separated in this manner from the background because the profiles are not standard disk plus bulge profiles. [Buta et al. \(1995b\)](#) determined that the outer ring of [NGC 7217](#) contributes only 4.4% of the total B -band luminosity.

Optical Colors

Rings appear, in general, to be sites of active star formation. This is evident on some of the earliest blue light photographs which show inner rings to be patchy. ⁽³⁾ In the Hubble Atlas ([Sandage 1961](#)), the inner rings of [NGC 1398](#), [1832](#), [3351](#), [4725](#), and [5364](#), among others, are notably patchy. The nuclear rings and pseudorings of [NGC 4321](#) and [4314](#) are also very patchy in this atlas. The few outer rings

illustrated tend to be considerably smoother, but not the outer pseudorings, as in [NGC 210](#) ([Kormendy 1979a](#); [Athanasoula & Bosma 1985](#)).

[Simkin \(1967\)](#) showed from photoelectric scans that the inner ring of [NGC 4736](#) is very blue. Color profiles in the east-west direction showed minima in $B - V$ and $U - B$ across the ring. At the ridge line, the colors were found to be $B - V = 0.58$ and $U - B = -0.37$, consistent with significant numbers of young, blue stars. [Schommer \(1976\)](#) found that the outer ring of [NGC 4736](#) has a color index of $(U - B)_0 = -0.6$, which is considerably bluer than might be expected for a feature whose luminosity distribution is relatively smooth, as if there are few HII regions and young associations. Later photoelectric measurements of the ring by [Gallagher & Wirth \(1980\)](#) gave $B - V = 0.61$ for a small region south of the center, compared to much redder colors for parts of the outer rings in [NGC 2273](#), [2859](#), and [3945](#). Gallagher and Wirth concluded that outer rings are generally stellar density enhancements, but that the ring in [NGC 4736](#) could contain many young stars.

In recent years more ringed galaxies have been observed with multicolor photography and CCD imaging and the distribution of star formation has been illustrated with profiles and color index maps. Detailed $UBVRI$ surface brightness and color index profiles of [NGC 7531](#) ([Buta 1987a](#)) are illustrated in [Figure 33](#). The inner ring causes the large secondary maxima outside the bulge at $\pm 30''$ radius along the major axis and $\pm 10''$ radius along the minor axis. These secondary maxima correspond with dips in the color indices that are very strong in $U - I$. This galaxy is an extreme case.

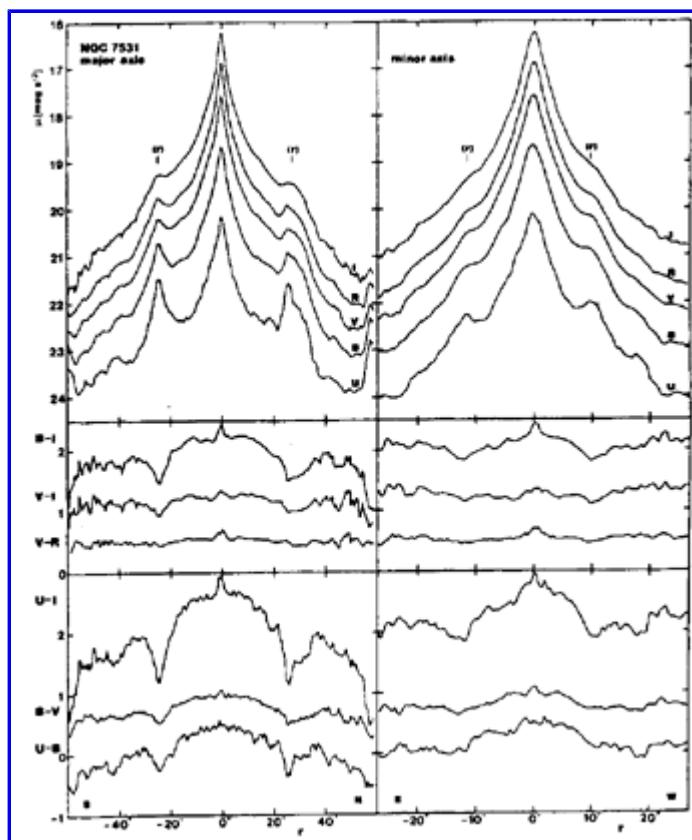


Figure 33. Surface brightness and color index profiles for [NGC 7531](#), type SAB(r)bc, from [Buta \(1987a\)](#).

Detailed color index maps have been published for many ringed galaxies, including [NGC 5364](#) ([Schweizer 1976](#)); [NGC 4314](#) ([Benedict 1980](#); [Benedict et al. 1992](#)); [NGC 1433](#), [6300](#), and [7531](#) by [Buta \(1986b, 1987a, b\)](#); [NGC 3081](#), [7020](#), [7187](#), and [7702](#) by [Buta \(1990a, b, c; 1991\)](#); [NGC 1097](#) by [Hummel et al. \(1987\)](#); [NGC 5728](#) by [Schommer et al. \(1988\)](#), 29 outer ringed and pseudoringed galaxies by [Buta & Crocker \(1991\)](#); [NGC 4622](#) by [Buta et al. \(1992\)](#); [NGC 6782](#) and [IC 1438](#) by [Byrd et al. \(1994\)](#); [NGC 3313](#), [7098](#), [IC 5240](#) by [Buta \(1995\)](#), [ESO 565-11](#) by [Buta et al. \(1995a\)](#), and [NGC 7217](#) by [Buta et al. \(1995b\)](#). [Wozniak et al. \(1995\)](#) also presented $B - I$ color index maps of a sample of galaxies having secondary bars or inner isophote twists.

A few representative cases are illustrated in [Figure 34](#) and [Figure 35](#). Most inner rings which have been studied are continuous blue enhancements, usually with imbedded discrete associations. Azimuthal variations in color index around a ring can be due to internal extinction, as in [NGC 7531](#) and [7702](#), but can also be intrinsic as in nearly face-on galaxies such as [NGC 1433](#), [3081](#), and [4622](#) (see [Figure 36](#) for the latter two cases). In [NGC 1433](#), the bright inner pseudoring is reddest in those regions immediately trailing the bar. In [NGC 3081](#), however, the inner ring is bluest in arcs at its major axis, and is reddest near its minor axis points; this kind of variation undoubtedly reflects an intrinsic oval shape in the galaxy plane. In [NGC 4622](#) ([Buta et al. 1992](#)), the bright inner ring is very blue on the west side, but quite red on the east side; this is atypical and could signify an interaction in this case.

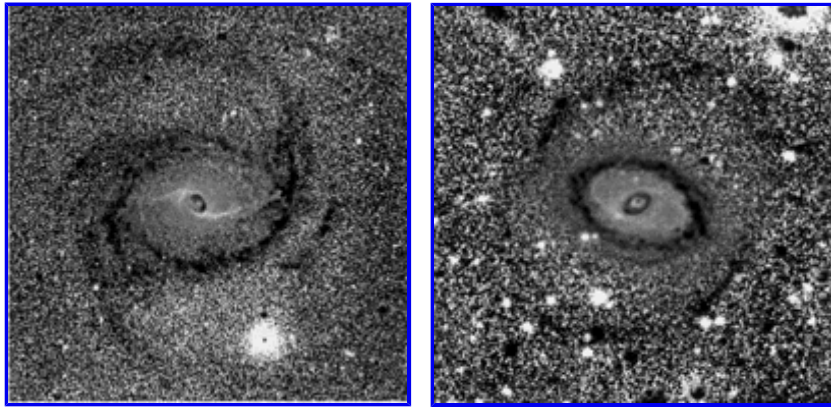


Figure 34. $B - I$ color index maps of [NGC 1433](#) (left) and [NGC 3081](#) (right). In these maps, blue features ($B - I \approx 1.0$) are dark and red features ($B - I \approx 2.5$) are light. The same coding is used in Figures [35](#), [36](#), and [76](#).

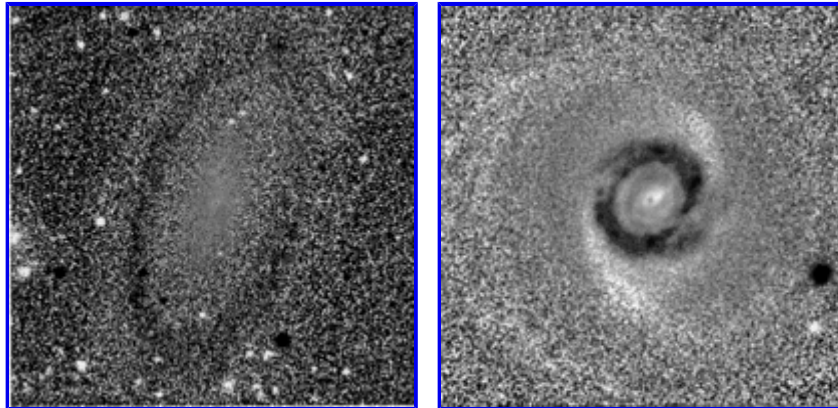


Figure 35. $B - I$ color index maps of [NGC 7020](#) (left, blue outer ring) and [NGC 1317](#) (right, blue nuclear ring).

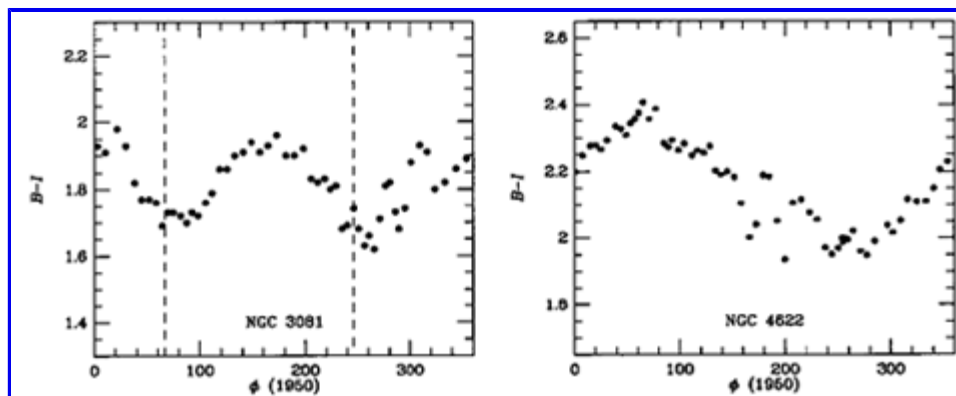


Figure 36. Azimuthal variations in $B - I$ color index around two inner rings: [NGC 3081](#) (left, weakly-barred case) and [NGC 4622](#) (right, nonbarred case). Vertical dashed lines in left panel refer to bar axis.

Although most prominent nuclear rings are blue in color index maps, red nuclear dust rings have also been identified. [Buta & Crocker \(1991\)](#) pointed out the case of [ESO 153-20](#), while [Buta et al. \(1995b\)](#), [Wozniak et al. \(1995\)](#), and [Verdes-Montenegro et al. \(1995\)](#) detected a nuclear dust ring in [NGC 7217](#) (see [Figure 37](#)). Buta et al. noted that the latter ring lies on the *inside* edge of a neutral-colored stellar nuclear ring. Wozniak et al. also discovered a nuclear dust ring in [NGC 521](#). [Vila-Vilaró et al. \(1995\)](#) discovered a partial nuclear dust ring in the Seyfert 1 galaxy [NGC 4151](#). [Higdon and Buta \(1996\)](#) illustrate a nuclear dust pseudoring in [NGC 5850](#).

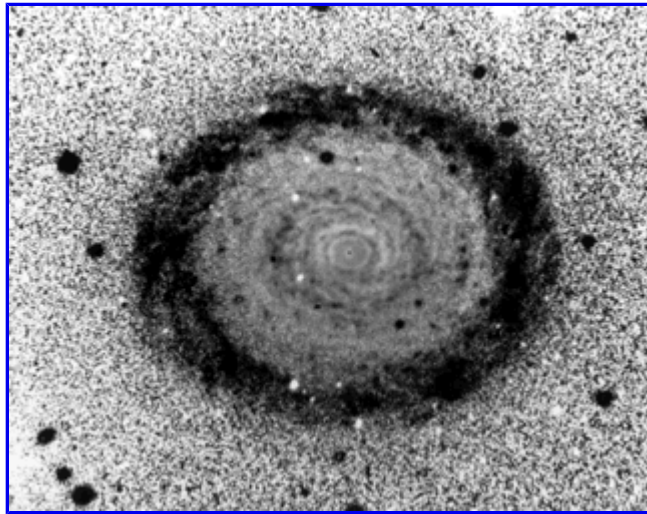


Figure 37.B - I color distribution in [NGC 7217](#), revealing the star-forming outer ring and a circumnuclear *dust* ring, from [Buta et al. \(1995b\)](#).

The star formation history of a few inner rings has been judged from color-color diagrams. Two approaches have been used. The first approach involves integrating fluxes in small circular apertures around a ring. No correction for the background light of the bulge and disk components is made, so colors in such apertures include an uncertain background contribution. In the second approach, *total, background-corrected* colors of a ring are obtained by computing an azimuthally-averaged surface brightness profile within an ellipse whose shape and orientation are the same as the ring, and interpolating a background-correction.

For [NGC 1433](#) and [7531](#), [Buta \(1986b, 1987a\)](#) used the first approach. The color-color diagram for [NGC 7531](#) is shown in [Figure 38](#). For both [NGC 1433](#) and [7531](#), the ring points scatter closely around the mean integrated galaxy sequence, which tells us that star formation has been more or less continuous in these features for a large fraction of the lifetimes of the galaxies. If the light were instead dominated by a single recent "burst" of star formation, the points would depart from the integrated galaxy sequence in a manner which would depend on the burst duration and strength, and also on the burst age ([Larson & Tinsley 1978](#); [Arimoto & Yoshii 1986](#); [Leitherer & Heckman 1995](#)). Thus, inner rings must be long-lived features in some galaxies that have had sufficient time to build up underlying old stellar components. Such an old component is evident in both [NGC 1433](#) and [NGC 7531](#).

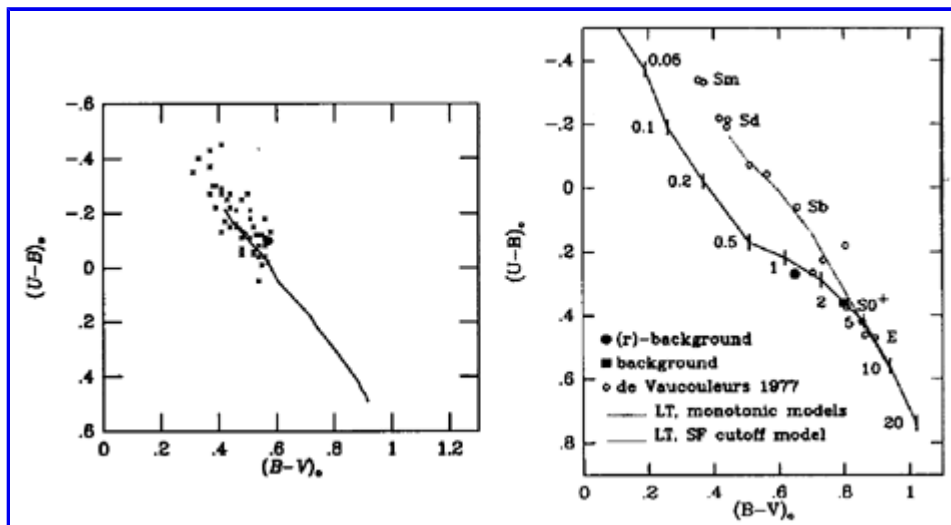


Figure 38.*left*: Two-color plot for points (crosses) within the inner ring of the Sbc galaxy [NGC 7531](#) ([Buta 1987a](#)). The solid curve is the mean color-color relation for normal galaxies from [Buta et al. \(1994\)](#); *right*: Two color relation for the inner ring of [NGC 7702](#), from [Buta \(1991\)](#); LT refers to the paper by [Larson and Tinsley \(1978\)](#).

[Buta et al. \(1995b\)](#) used the second approach for the outer ring of [NGC 7217](#). Two-color plots in the Cousins VRI system for the net colors of the outer ring are shown in [Figure 39](#) (crosses). For comparison, the integrated color sequences of a large sample of normal galaxies (from [Buta & Crocker 1992](#) and [Buta & Williams 1995](#)) are also illustrated (solid curves). The outer ring in this case has $B - V$ and $V - I$ colors bluer than the bluest late-type galaxies. Thus, the outer ring hump is dominated by a very young stellar population.

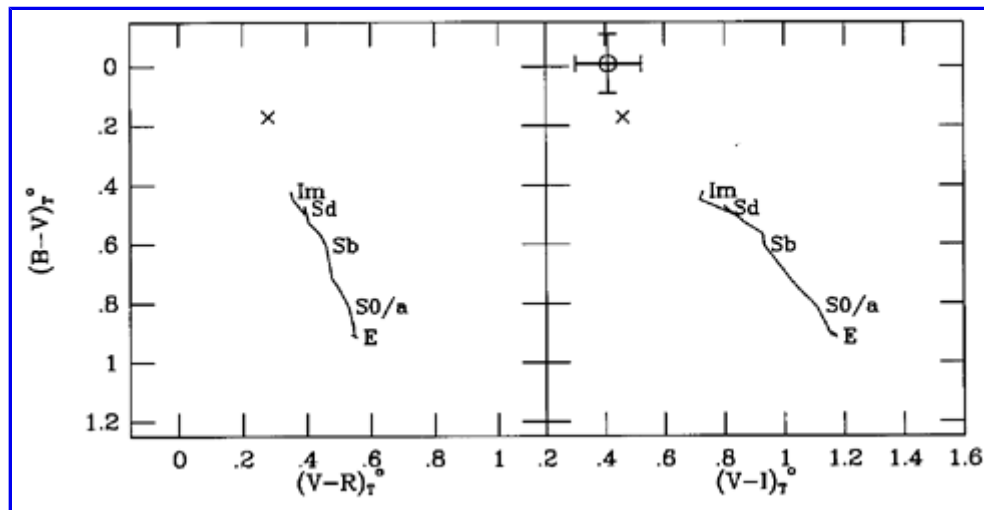


Figure 39. Two-color plot for the integrated light of the outer ring of [NGC 7217](#) (Buta et al. 1995b) and OB associations in the nuclear ring of [ESO 565-11](#) (Buta et al. 1995a). The small crosses refer to the outer ring of [NGC 7217](#). The filled circle with large error bars at upper left refers to the mean colors of 8 OB associations in the nuclear ring of [ESO 565-11](#), after background correction. The solid curves refer to a sample of RC3 galaxies (Buta & Williams 1995).

The second approach was also used for the inner ring of [NGC 7702](#) (Buta 1991). The results for this one are shown in the right panel of [Figure 38](#), where the filled circle is for the net colors of the inner ring, while the filled square is for the background underlying this ring. The additional curves in [Figure 38](#) are for model galaxies either with monotonically decreasing star formation rates or a star formation cutoff, both from [Larson & Tinsley \(1978\)](#). [Figure 38](#) shows that, while the background colors in the ring region lie close to the integrated galaxy sequence and the curve for the monotonic models, the net ring colors depart to the left of the sequence near the region where the age would be about $1-2 \times 10^9$ years in the star formation cutoff model. This suggests that the inner ring of [NGC 7702](#) is a feature which experienced a last burst of star formation over one billion years ago, and has been evolving without much further activity ever since. Thus, star formation apparently can “turn off” in rings. In support of the aging ring scenario, [Buta \(1991\)](#) described how the net inner ring profile along the major axis of [NGC 7702](#) can be represented very well by the sum of two gaussian components: a narrow, blue component and a broad, red component (see [Figure 40](#)). In the simplest interpretation, this is what would be expected of an aging ring where enhanced star formation has proceeded over a long time period. Stars born earlier in the ring would populate a broader zone than initially, while more recently formed stars would still lie near the narrower zone of gas compression.

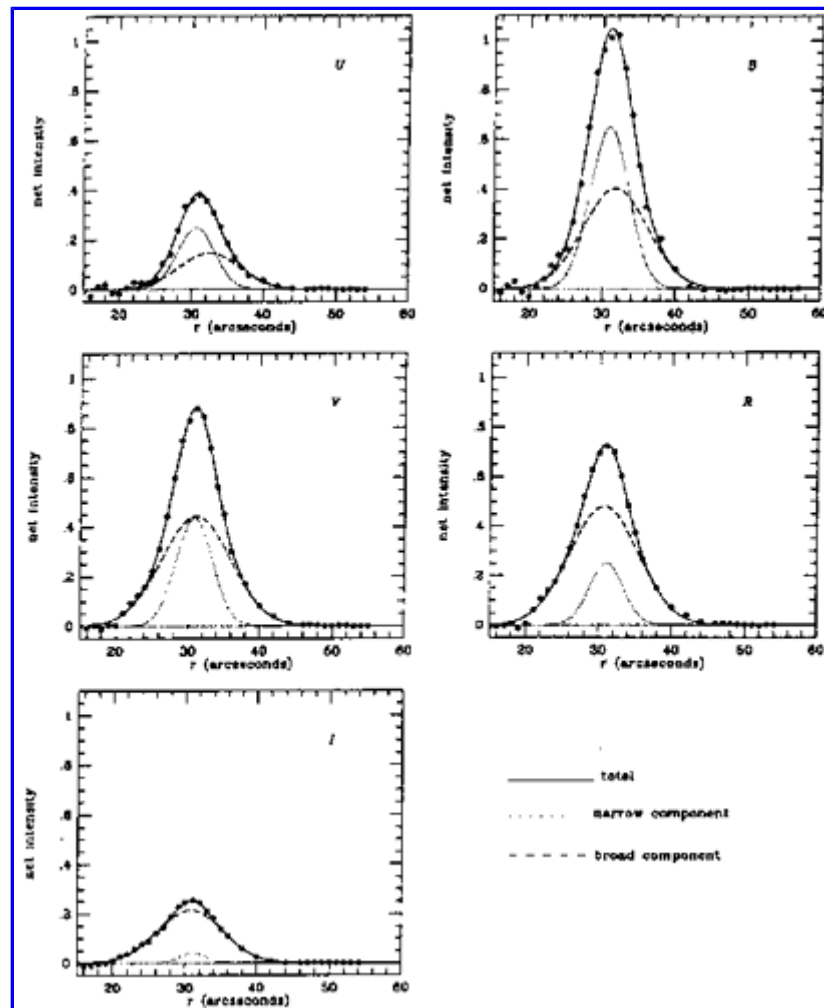


Figure 40. Diagram illustrating the possible two-component nature of the inner ring of [NGC 7702](#), from [Buta \(1991\)](#). Note that the separation of the two components has considerable uncertainty, owing to the assumed exponential background interpolation and the fairly large formal uncertainties in the Gaussian parameters.

The colors of nuclear rings require considerable care to interpret. The most extensive multicolor study of a nuclear ring was made by [Benedict et al. \(1992\)](#), who obtained optical and near-IR imaging of the nuclear ring/spiral of [NGC 4314](#). The nuclear ring was detected in all color indices and is a site of recent star formation, being prominent also at $H\alpha$ and at 6cm. Comparing IR and optical colors, Benedict et al. concluded that the nuclear ring is riddled with dust, some relatively hot. The nuclear spiral part outside the ring, on the other hand, showed evidence for an age progression, with the youngest stars in the spiral being nearest to the nuclear ring. The colors of these arms redden further away from the ring.

Because the time-scales associated with nuclear rings are likely to be short (owing to their proximity to the nuclei of galaxies), they are more prone to bursts of star formation than inner rings. That this is likely to be the case stems from the wide range of color properties of such rings. In the most extreme cases, nuclear rings represent spectacular starbursts. The best-known example is that in [NGC 1097](#) ([Hummel et al. 1987](#)). A less well-known example is that in [ESO 565-11](#) ([Buta & Crocker 1991](#); see [Figure 15](#)). The average background-corrected mean extinction-corrected colors of 8 associations in that ring is shown in [Figure 39](#). The colors are consistent with model burst populations no more than 4-5 million years old according to the models of [Leitherer & Heckman \(1995\)](#). In contrast to these cases, there also exist nuclear rings where the color enhancement is weak (see [Buta & Crocker 1991](#) for the examples of [ESO 437-67](#), [507-16](#), among others), and still others, such as in [NGC 5850](#), which are relatively neutral in color ([Higdon et al. 1996](#)), perhaps because of reddening, or perhaps because the ring is in a quiescent (post-burst) star forming phase.

Recent HST observations have elucidated the nature of star forming regions in nuclear rings. [Barth et al. \(1995, 1996\)](#) show that most nuclear rings contain bright, blue compact star clusters that usually suffer considerable extinction. The clusters are luminous enough to be called "super star clusters", a term first used for young clusters identified in starburst systems such as merger remnants ([NGC 7252](#), [Whitmore et al. 1993](#); [4038-9](#); [Whitmore & Schweizer 1995](#)) and amorphous irregulars (e.g., [NGC 1705](#); [Meurer et al. 1992](#)). [Barth et al.](#) comment that nuclear rings are the only *normal* galaxy environment where such clusters are found in large numbers. The clusters may be young globulars, and [Barth et al.](#) suggest that they will probably be disrupted eventually, or absorbed by the nuclei of the galaxies due to dynamical friction.

In the case of most outer rings, colors are difficult to measure reliably owing to the typically very low surface brightnesses of such features. We have already discussed the previous observations of [Schommer \(1976\)](#) and [Gallagher & Wirth \(1980\)](#). The colors of outer rings in [NGC 3081](#), [7020](#), and [7187](#) have also been measured, using CCD images ([Buta 1990a, b, c](#)). The mean corrected colors derived are $(B - V)_0 = 0.61, 0.78, \text{ and } 0.71$ for [NGC 3081](#), [7020](#), and [7187](#), respectively. Of these, [NGC 7020](#) is the most interesting in that all of the recent star formation is taking place in the outer ring, as shown in the $B - I$ color index map in [Figure 35](#).

³ The patchiness of the inner ring of [NGC 4736](#) was even noticed visually with the Birr Castle 1.8-m telescope in 1855. [Back](#).

9.5. HII Regions in Ringed Galaxies

The previous section showed that colors of nuclear, inner, and outer rings indicate that such features are usually sites of active star formation, particularly the inner and nuclear types. It is therefore not surprising that rings are also often concentrations of HII regions (see [Figure 41](#)). [Van der Kruit \(1976b\)](#) showed that the inner ring of [NGC 4736](#) is an intense *bounded* zone of both discrete HII regions and diffuse H α emission. In [NGC 3351](#), [Rubin et al. \(1975\)](#) and [Peterson et al. \(1976\)](#) found that HII regions are concentrated within the nuclear ring, the bright inner ring, and the outer arms, but that there was little emission from the region between the nuclear and inner rings. The same was found for the inner and nuclear rings of [NGC 5728](#) by [Rubin \(1980\)](#).

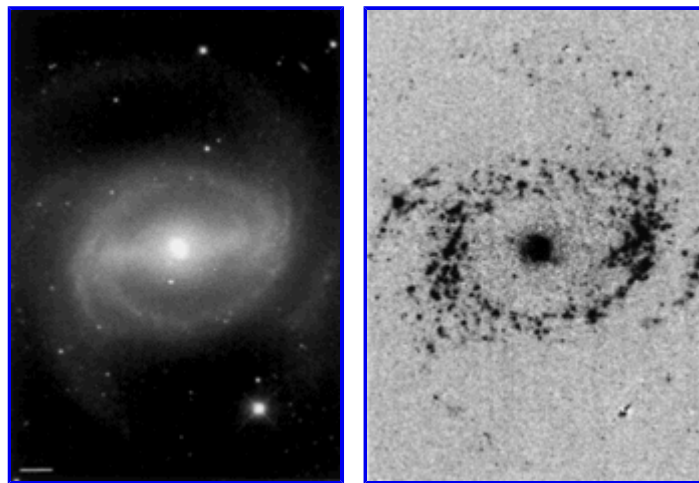


Figure 41. The distribution of HII regions in [NGC 1433](#) (right), compared to a red continuum image (left), from [Crocker et al. \(1996\)](#).

[Buta \(1984\)](#) obtained HII region distributions in 8 ringed galaxies: [NGC 1433](#), [1512](#), [3351](#), [4725](#), [4736](#), [5364](#), [6300](#), and [7531](#), based on both spectroscopy and Fabry-Perot interferometry. In the five barred spirals ([NGC 1433](#), [1512](#), [3351](#), [4725](#), and [6300](#)) of the sample, the bar regions were largely devoid of discrete HII regions, although [NGC 6300](#) was found to have diffuse H α emission in its bar region. In each case, emission is concentrated in the inner ring regions or beyond, and in a nuclear ring in three cases. In the two weakly-barred sample objects ([NGC 4736](#) and [7531](#)), the inner rings are very intense sources of H α emission and HII regions, and are the brightest regions in H α in their respective galaxies. Diffuse emission fills the entire region interior to the inner ring of [NGC 7531](#). In the one true nonbarred case, [NGC 5364](#), the inner ring includes HII regions, but is not the strongest source of emission in the galaxy.

Detector technology has improved since these early studies, and many more ringed galaxies have been imaged in H α or H α + $[NII]$, usually as parts of other studies. For example, imaging Fabry-Perot interferometry revealed a small nuclear ring of H α emission in the grand design spiral [NGC 4321](#) ([Arsenault et al. 1988](#)). This small feature is actually a spiral in broad-band images. [Pogge \(1989\)](#) imaged the ionized gas in 91 nearby non-Seyfert galaxies, and discovered a wide variety of nuclear emission morphologies. Inner rings or pseudorings were prominent in [NGC 4736](#) and [5921](#), while bright nuclear rings of emission were detected in 13 galaxies ranging from distinct rings to partial rings with "hotspots". Pogge found that the relative contribution of such rings to the total H α + $[NII]$ luminosity ranged from 1% in [NGC 4254](#) to 94% in [NGC 4314](#), and that the rings may or may not surround a nuclear emission source. This study also underscored once again the tendency for the interior regions of some inner rings (e.g., in [NGC 4736](#) and [5921](#)) to be relatively devoid of emission except for the nucleus.

[Ryder & Dopita \(1993\)](#) carried out an H α imaging survey of bright southern galaxies which included several inner-ringed galaxies: [NGC 1187](#), [1398](#), [6300](#), [5643](#), and [6744](#). They suggested that there may be a reciprocal relationship between the number of HII regions in a bar and the number in the inner ring, such that when the inner ring is well-populated with HII regions, the bar region is devoid of HII regions. The one outer-ringed galaxy in their sample, [NGC 2217](#), showed HII regions only in *parts* of the outer ring.

[Pogge & Eskridge \(1993\)](#) found from another imaging survey that the most common HII region distribution in *S0* galaxies is an HII ring. Though they refer to the observed rings only as "inner" or "outer" types, it is clear that conventional nuclear, inner, and outer rings are represented. The most interesting H α map in this paper is for [NGC 7742](#), a face-on example of a ringed SA galaxy (see [Figure 42](#)). Just as for barred galaxies, the inner ring is a strong concentration of HII regions. In their sample, the inner and nuclear rings tend to be fully populated in azimuth by HII regions, but they note that the outer rings are more sparsely populated and patchy. It is possible that some of these "gas-rich" S0's are probably early-type spirals (i.e., misclassified S0/a types).

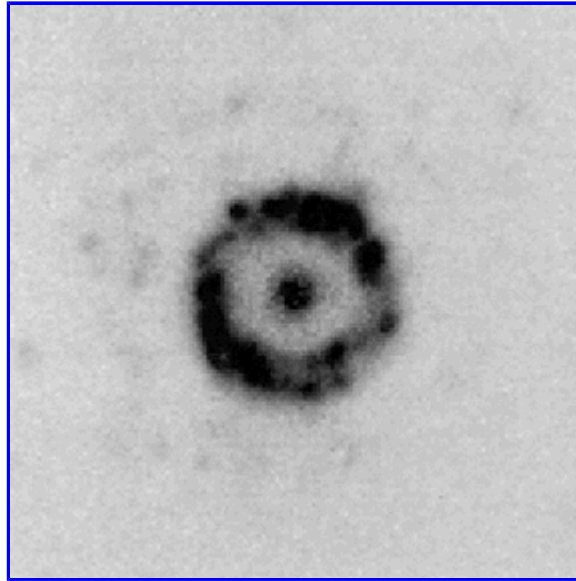


Figure 42. The distribution of HII regions in the face-on nonbarred ringed galaxy [NGC 7742](#), from [Pogge & Eskridge \(1993\)](#).

[Phillips \(1993a\)](#); see also [Kennicutt 1994](#) and [Phillips 1996](#)) surveyed the distribution of HII regions in a sample of SBb and SBc galaxies. The tendency for the bar regions of SBb galaxies to be devoid of HII regions was again noted, as well as the frequent presence of circumnuclear rings of ionized gas. He also compared the luminosity function of HII regions in inner pseudorings with that in the outer disk of a few galaxies. The outer disk HII regions in [NGC 1300](#) have a standard Type I luminosity function with no break (see [Kennicutt et al. 1989](#)), while the inner pseudoring (arms enveloping the bar in this case) appears to show a Type II luminosity function with a break, perhaps implying an upper limit to the masses of giant molecular clouds allowed in that region. Phillips also found circumnuclear star formation to be common in SBb galaxies: eleven of twelve SBb galaxies in his sample of RSA spirals include such emission.

From an H α survey of 52 RSA barred spirals, [Garcia-Baretto et al. \(1996\)](#) found nuclear ionized gas rings in 10 galaxies, three of type SBa, six of type SBb, and one of type SBbc. Their sample was chosen to have IRAS colors indicative of star formation and high dust temperatures. Most of the nuclear emission rings they identified were found to be misaligned with the primary bar.

The most detailed study of the HII region distribution in ringed galaxies has been made by Crocker, Baugus, and Buta ([1996](#), hereafter CBB). This study included H α + $[NII]$ images of 32 galaxies from the CSRG. Besides verifying the results from previous studies, [CBB](#) were able to investigate connections between HII region distributions and dynamics. The main results from the paper are as follows:

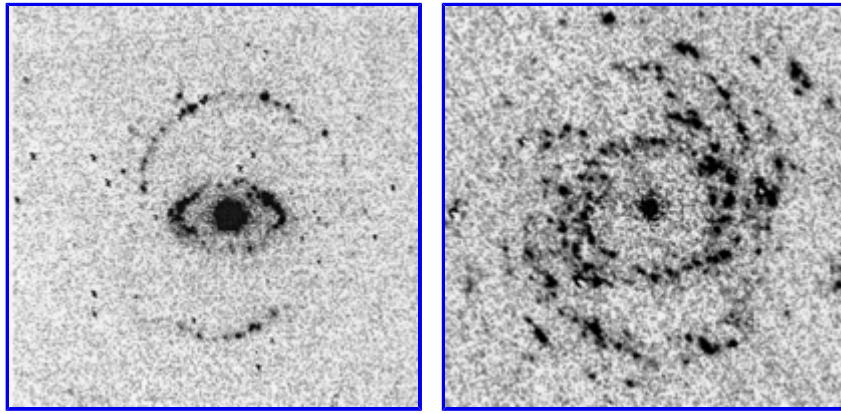


Figure 43. Distributions of HII regions in barred galaxy inner rings of different intrinsic shapes: [NGC 6782](#) (left), an example of an extremely oval inner ring (continuum axis ratio $q_C = 0.69$), and [NGC 7329](#) (right), an example of a nearly circular inner ring ($q_C = 0.94$). Both images are deprojected according to parameters in [Crocker et al. \(1996\)](#) and have been rotated so that the bar axis is horizontal.

1. The distribution of HII regions around *inner* rings is sensitive to the intrinsic shape of the ring. Extremely oval inner rings tend to have HII regions "bunched up" near the intrinsic ring major axis (see [Figure 43](#), left), while more circular rings tend to have a more even distribution of HII regions with azimuth (see [Figure 43](#), right). The effect is quantified in [Figure 44](#) via Fourier analysis for 18 galaxies whose deprojected continuum ring axis ratios (q_C) range from 0.6 to nearly 1.0. A definite correlation is in evidence with the relative 2θ Fourier amplitude F increasing with decreasing q_C . The dynamical implication of this result is that gas gathered into the rings moves along oval streamlines, and that the material slows down in the rotating reference frame near the ring major axis. This argues that inner rings lie within the corotation resonance according to [Contopoulos \(1979\)](#).

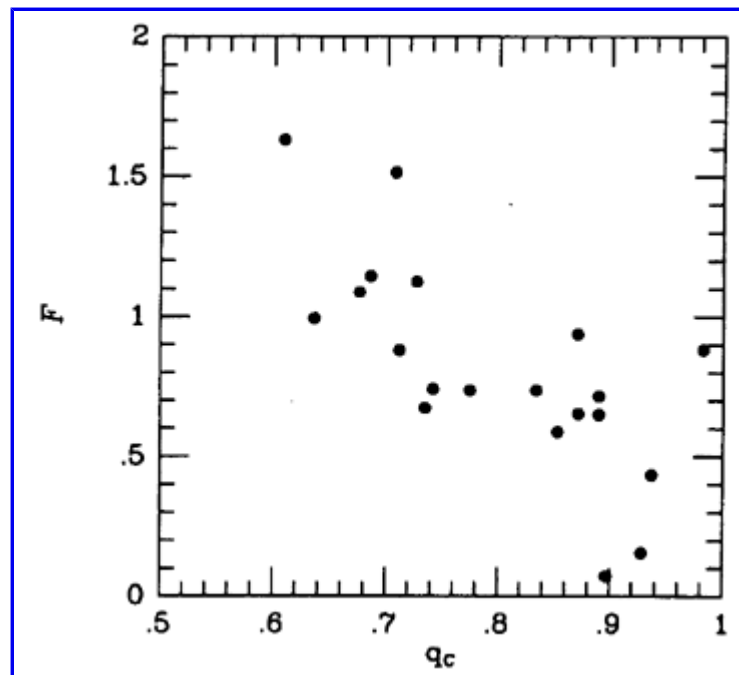


Figure 44. Quantification of distribution of HII regions around inner rings and the intrinsic shape of the ring. F is the relative 2θ Fourier amplitude of the $H\alpha + [NII]$ emission around the ring, and q_C is the deprojected continuum ring axis ratio. From [Crocker et al. \(1996\)](#).

2. In several galaxies where the red continuum image shows a broad, diffuse stellar outer ring of type R₁, the HII regions follow what appears to be an R'₂ pseudoring pattern. This was seen in [NGC 1326](#) (see [Figure 45](#)), [NGC 6782](#), [IC 1438](#), and [UGC 12646](#). The dichotomy suggests that in these galaxies, the R₁ component formed first and lasted long enough to leave a stellar remnant. The gas distribution has now evolved into the R'₂ phase, a sequence demonstrated by the test-particle models of [Byrd et al. \(1994\)](#); see [section 12.2](#).

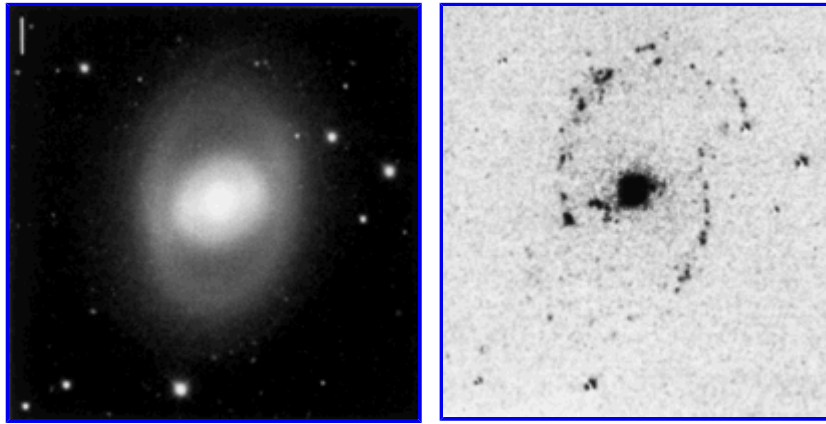


Figure 45. Distribution of HII regions in [NGC 1326](#), showing broad stellar outer R_1 ring in red continuum (left) and partial R_2 outer pseudoring in $H\alpha + [NII]$ (right), from [Crocker et al. \(1996\)](#). The HII regions in the outer arms do *not* line the R_1 feature but are displaced to the outside edge of this ring. This galaxy also illustrates the co-existence an old population R_1 ring and a star-forming nuclear ring (overexposed center).

3. Nuclear ring morphology shows an even greater range than found by [Pogge \(1989\)](#). In the nearly face-on galaxy [NGC 1317](#), [CBB](#) found that most of the HII regions are distributed in a *double nuclear ring/pseudoring pattern*. The inner nuclear ring is aligned parallel to a strong secondary bar, while the outer nuclear pseudoring is aligned parallel to a broad primary bar which itself is aligned perpendicular to the secondary bar (see [Schweizer 1980](#)). This links the double nuclear ring feature to an outer ILR.
4. HII region luminosity functions in ringed galaxies can be represented by power laws whose exponents are very similar to those found for non-ringed galaxies. In a few cases, a luminous nuclear ring produces a secondary peak in the luminosity function.
5. An unusual $H\alpha$ distribution was found in the large outer-ringed galaxy [NGC 1291](#). The primary bar, lens, and secondary bar regions of this galaxy are filled with a wispy pattern of diffuse ionized gas very reminiscent of what is seen in the bulge of [M31](#) ([Ciardullo et al. 1988](#)) and [M81](#) ([Devereux et al. 1995](#)).

Finally, we note the existence of HII regions connected with the subtle "dimpling" aspect of R_1 outer pseudorings in some galaxies. This has been noted in a study of the $(R_1)SAB(rs)a$ spiral [IC 4214](#) by [Buta et al. \(1996\)](#). Their $H\alpha$ distribution (based on Fabry-Perot interferometry) is shown in [Figure 46](#), and the arrows point to HII regions connected with weak dimples seen in blue light. These dimples are regions where the gas would be slowing down in the bar reference frame ([Schwarz 1981](#)), and perhaps bright HII regions might be expected in such regions depending on the gas available. This is yet another aspect of the distribution of HII regions in ringed galaxies which can be connected to internal dynamics. [IC 4214](#) is also discussed by [Buta & Crocker \(1991\)](#) and [Saraiva \(1996\)](#).

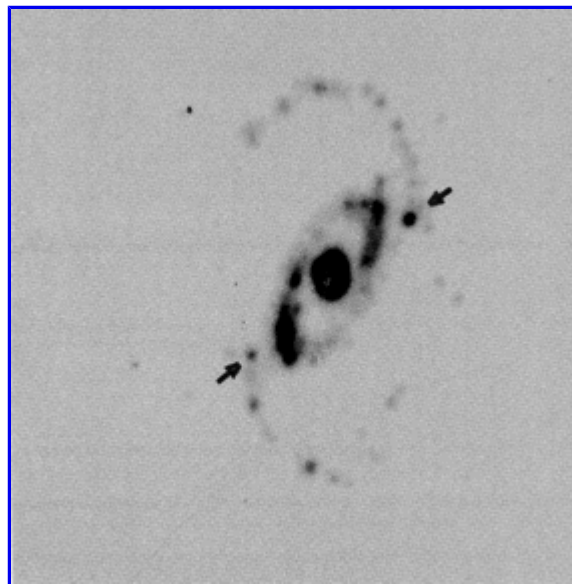


Figure 46. Dimple HII regions in [IC 4214](#) (arrows).

Nuclear Hotspots

A special topic in HII regions in ringed galaxies concerns the nature of nuclear "hotspot" HII regions compared to HII regions away from the nucleus. These hotspots are commonly found in nuclear rings, as we have noted. [Kennicutt, Keel, and Blaha \(1989\)](#) have made a spectrophotometric and radio continuum comparison between nuclei, hotspot, and disk HII regions to determine the mechanisms responsible for the ionization and the validity of assumptions concerning abundance determinations. These authors first of all determined that many of the hotspots seen in the nuclear rings are not HII regions but are continuum knots, i.e., star clusters or associations with no surrounding ionized cloud. The luminosities of disk HII regions and hotspot HII regions were found to be similar, but the hotspot HII regions were found to be more compact and had $H\alpha$ equivalent widths 7 times lower than disk HII regions of comparable luminosity (see also [McCall et al. 1985](#) and [Mayya 1994](#)). The stellar continua in the hotspots were also found to be more significant than in disk HII regions. Kennicutt *et al.* suggested that the optical and radio continuum properties of these regions are not easily explained in a simple picture whereby the hotspots are normal, photoionized HII regions located in an unusual environment.

[Korchagin et al. \(1995\)](#) have examined the star formation mechanism in hotspots. The most favored idea is that the high continuum emission reflects an accumulation of stars over many generations, so that star formation has to take place in hotspots over a period of time longer than the normal lifetime of a disk HII region. They conclude that hotspots are regions of self-regulated star formation where ultraviolet radiation from young, massive stars both triggers star formation and regulates it. The unique conditions at the centers of galaxies help to explain the behavior of the mechanism as compared to ordinary HII regions in the outer disk regions. Korchagin et al. conclude that the low equivalent widths and red optical colors of hotspots rule out an instantaneous burst interpretation but favor self-regulated sequential star formation lasting for 10-70 million years.

9.6. Neutral Hydrogen Emission from Ringed Galaxies

The distribution of HI has been mapped in several ringed galaxies. The first case so mapped was [NGC 4736](#) by [Bosma et al. \(1977\)](#). These authors found that the distribution of HI mimics the optical appearance of the galaxy in blue light, showing concentrations of gas in the inner and outer rings and deficiencies of gas in the region inside the inner ring and in the "gap" between the two rings. The HI surface density reaches a maximum at the radius of the inner ring and a secondary maximum at the outer ring. Evidence for a probable noncircular shape for the inner ring was presented.

[Mebold et al. \(1979\)](#) did low-resolution HI mappings of two early-type outer-ringed galaxies, [NGC 1291](#) and [1326](#). In each case, they determined that the kinematic line of nodes was nearly coincident with the major axis of the outer ring but not with the lens in the bar region. They suggested that the HI in both cases probably came from the outer rings, but could not resolve the exact location of the gas. This study suggested that [NGC 1291](#) is inclined only 6° to the line of sight, which implied that the outer ring is intrinsically oval with an axis ratio of 0.9 and is aligned perpendicular to the bar.

[Wevers \(1984\)](#) carried out a detailed HI and optical study of 16 northern spiral galaxies. Several galaxies in his study show ring or pseudoring-like patterns in the HI distribution which are not attributable merely to HI "holes". For example, [NGC 2903](#) shows a large outer HI pseudoring which has not been formally recognized in the galaxy's Hubble classification. The feature follows faint and extensive outer arms and produces a definite secondary maximum in the azimuthally-averaged surface density profile. The outer HI distribution Wevers found in [NGC 4258](#) resembles the R_2 morphology, and deep optical images may verify this. The inner ring of the tidally disturbed ringed, barred spiral [NGC 4725](#) (see [Haynes 1979](#)) is a clear, nearly closed enhancement of HI emission, coinciding also with the ring of HII regions found by [Buta \(1988\)](#).

[Knapp et al. \(1984\)](#) observed the HI distribution in [NGC 7013](#), type (R')SA(r)0/a. They found an HI distribution well-described by two rings coincident with the optical observed ring patterns. The surface density of HI in the inner ring was found to be higher than that in the outer pseudoring.

[Krumm et al. \(1985\)](#) detected an outer HI ring in the SB0 galaxy [NGC 4262](#). In this case, however, the outer ring has no optical counterpart and has a projected shape and velocity field suggesting that it is *not* coplanar with the main stellar disk. Krumm *et al.* suggest that the gas in this galaxy, which lies near the core of the Virgo Cluster, has probably been accreted as recently as 2×10^8 years ago. The accreted object could have been a gas-rich dwarf or an intergalactic HI cloud. Thus, the HI outer ring in [NGC 4262](#) is *not* likely to be a resonance ring with the stellar bar in the main disk, but is probably related more to polar ring galaxies. In a similar vein, [van Driel et al. \(1988\)](#) detected inner and outer HI rings in the nonbarred S0 galaxy [NGC 4203](#). The inner ring is nearly circular and may be connected to an HI hole, but the outer HI ring is a clear feature like that in [NGC 4262](#) and may be due to accretion. More recently, [Tilanus & Allen \(1993\)](#) discovered what is probably also an accretion HI ring around the main body of the large spiral [M83](#). These authors suggest that the HI ring and the large HI extent resulted from a past interaction with another galaxy.

[Van Driel, Rots, and van Woerden \(1988\)](#) obtained the HI distribution in two early-type galaxies with optical outer rings or pseudorings: [NGC 1291](#) and [NGC 5101](#). The observations of [NGC 1291](#) are at much higher resolution than those obtained by [Mebold et al. \(1979\)](#), and reveal a maximum of HI surface density in the region of the outer ring and lower surface density gas beyond this region (see [Figure 47](#)). The region of the bar and inner lens was found to be devoid of any HI gas. In this same region, CBB found wispy filaments of ionized gas reminiscent of what is seen in [M31](#), and [Bregman et al. \(1995\)](#) determined that the HI hole is also occupied by hot X-ray emitting gas. In [NGC 5101](#), van Driel et al. also found a deficiency of HI gas in the bar/lens region. The maximum of HI surface density in this galaxy follows the R_2 part of an R_1R_2 outer ring/pseudoring feature. A second partial HI ring not connected to optical structure was found outside this ring.

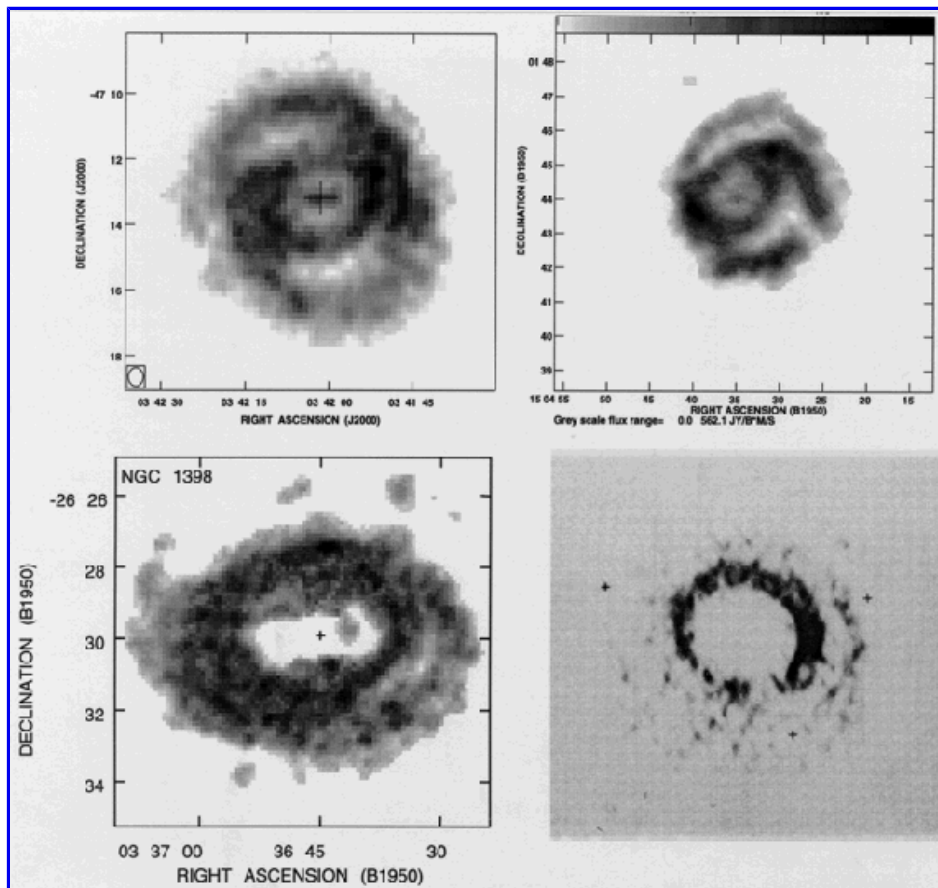


Figure 47. (*upper left*) HI distribution in ringed barred Sab spiral [NGC 1433](#) (from [Ryder et al. 1996](#)); (*upper right*) HI distribution in interacting ringed barred Sb spiral [NGC 5850](#) (from [Higdon et al. 1996](#)); (*lower left*) HI distribution in ringed barred Sab spiral [NGC 1398](#) ([Moore & Gottesman 1995](#)); (*lower right*) HI distribution in ringed barred S0/a galaxy [NGC 1291](#) (from [van Driel, Rots, and van Woerden 1988](#)).

[Van Driel & Buta \(1991\)](#) presented HI observations of three very dissimilar pseudoringed galaxies: [NGC 2273](#), [4826](#), and [6217](#). [NGC 2273](#) is a rare example of a double outer-ringed galaxy where the two rings are well-separated (see [Figure 22](#)). The galaxy also has a bright inner pseudoring and bar. Van Driel and Buta found that the HI in this galaxy is largely associated with the outermost outer ring, with little or no gas in the innermost outer ring and the inner pseudoring. The maximum in azimuthally-averaged HI surface density is between the two outer rings. In [NGC 6217](#), type (R'₁)SB(rs)bc, the outer HI distribution does not follow the R'₁, which is elongated perpendicular to the bar. Instead, it follows a ring-like distribution elongated along the bar, reminiscent of an R'₂ outer pseudoring. Deeper images than available to van Driel and Buta may reveal this feature.

The R'₁ outer ring of the unusual, ovaly-distorted galaxy [NGC 1808](#) is also a concentration of HI gas, as found by [Koribalski et al. \(1993\)](#). Unlike [NGC 4736](#), however, the HI gas in the outer ring region has a rounder distribution than the optical ring and inner disk, prompting these authors to conclude that the outer HI disk is significantly warped. This interpretation is disputed by [Bosma \(1996\)](#).

[Mulder \(1995; see also Mulder & van Driel 1993\)](#) has carried out a new HI study of [NGC 4736](#) with twice the resolution and better sensitivity of the study by [Bosma et al. \(1977\)](#). At a resolution of 13" × 20", the inner ring of the galaxy stands out as a clear enhancement of neutral gas and coincides almost precisely with the inner optical ring of HII regions. The azimuthally-averaged peak surface density in this ring is nearly 10M_⊙ pc⁻². The outer HI ring was found to be a more complete feature than before, and coincides very closely with the optical outer ring feature. Neutral gas was also found distributed within the intermediate oval distortion zone.

[Moore & Gottesman \(1995\)](#) carried out a study of the HI distribution in [NGC 1398](#), an excellent example of Hubble type SB(rs)ab. The outer arms have been interpreted as type (R₁R'₂) in the CSRG, though the R₁ component is very weak and the R'₂ component does not close completely into a ring. The HI in [NGC 1398](#) shows a strong central hole and little concentration of gas in the inner pseudoring zone (see lower left panel of [Figure 47](#)). Instead, the HI concentrates into an almost closed ring in the region of the outer arms, with more gas beyond.

Several other classic ringed barred spirals have recently been observed in HI: [NGC 5850](#) by [Higdon & Buta \(1996\)](#) and [NGC 1433](#) and [6300](#) by [Ryder et al. \(1996\)](#). The prototype SB(r)-type spiral [NGC 1433](#) is interesting in that it has nuclear, inner, and outer rings/pseudorings and is the nearest example of the class. The HI distributions in [NGC 1433](#) and [5850](#) are shown in [Figure 47](#). In both cases, the HI distribution mimics the optical structure of the galaxy very closely. Both the inner and outer pseudorings of [NGC 1433](#) are HI

surface density enhancements as are the secondary arcs off the leading sides of the inner ring (compare with [Figure 3](#)). The bar region, and the areas between the inner and outer rings along the bar minor axis line, are deficient in HI. *Ryder et al.* suggest that these latter gas-deficient regions are connected to the L4 and L5 Lagrangian points near corotation with the bar pattern speed (see [section 11.2](#)).

[Figure 48](#) shows the azimuthally-averaged HI surface density in [NGC 1433](#), from [Ryder et al. \(1996\)](#). This shows that each optical ring has an associated peak in HI surface density. The peaks are around $2\text{--}2.5 M_{\odot} \text{pc}^{-2}$, and do not necessarily coincide exactly with the ring radii.

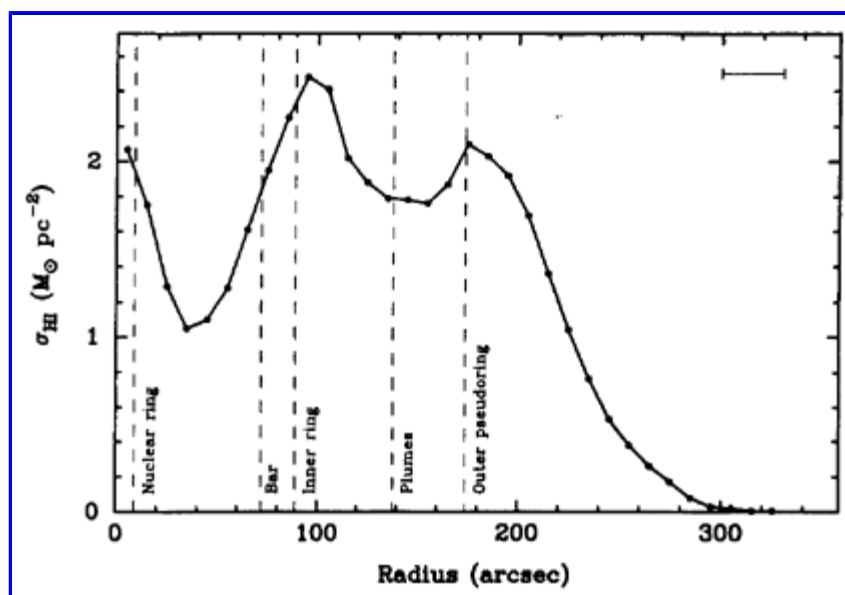


Figure 48. Azimuthally-averaged radial HI surface density profile for [NGC 1433](#), from [Ryder et al. \(1996\)](#).

[NGC 5850](#) is a ringed barred spiral which [Hubble \(1936\)](#) originally illustrated to define the SBb class of spirals. Like [NGC 1433](#), the inner ring is a clear concentration of neutral gas (see upper right panel of [Figure 47](#)). The gas distribution in this case shows a significant asymmetry. The galaxy is a member of the [NGC 5846](#) galaxy group ([de Vaucouleurs 1975b](#); [Turner & Gott 1976](#); [Haynes & Giovanelli 1991](#)), and may be suffering an interaction with another member of this group.

[NGC 6300](#) is an SB(rs)-type spiral with no nuclear or outer ring. In contrast to [NGC 1433](#), the HI distribution extends well-beyond the optical disk. Like [NGC 1433](#), however, the inner pseudoring is a region of enhanced neutral gas concentration, although the density peak is broader than the extent of the optical ring feature. [Ryder et al. \(1996\)](#) suggest that the galaxy is in a transition phase and has not fully developed its outer resonance ring. Also unlike [NGC 1433](#), [NGC 6300](#) exhibits a loose tail of gas on its western edge and a 20° warp in the position angle of the line of nodes.

Several early-to-intermediate Hubble type barred galaxies show a central hole in the HI distribution. These cases have been interpreted by [Koribalski \(1996\)](#) as caused by HI absorption against strong nuclear continuum emission. The continuum emission is connected to nuclear rings of star formation, such as have been detected in [NGC 7552](#) by [Forbes et al. \(1994a, b\)](#). Thus, [Koribalski](#) has suggested that HI holes trace the existence of nuclear rings in some galaxies.

[Mundell et al. \(1996\)](#) present interesting HI observations of the classic Seyfert galaxy [NGC 4151](#). The large-scale HI distribution of this galaxy shows two main outer HI arms which roughly follow an R^2 morphology. HI delineates the fat oval which acts as the bar of the system. An HI hole includes a nuclear ring discovered by [Vila-Vilaró et al. \(1995\)](#).

In summary, HI observations of optically ringed galaxies show that rings are usually zones of increased HI gas surface density. Thus, the gas needed for fueling the active star formation in these features is definitely present, although not all of the clear ring or pseudoring features seen in these galaxies necessarily have detectable HI. Also, some galaxies show HI outer rings having no optical counterpart.

9.7. CO, IR, and Radio Continuum Observations of Ringed Galaxies

Most molecular, IR, and radio continuum studies of ringed galaxies have focussed on those objects with the most intense rings of star formation. Of the three types of rings, nuclear rings are most commonly found in such studies because the gas density in these regions can be very high and the star formation rate may be much higher than elsewhere in the galaxies.

A particularly well-studied case is [NGC 1097](#). [Telesco & Gatley \(1981\)](#) showed that $10\mu\text{m}$ emission from the central region is ring-like and coincides with the optical nuclear ring. The total IR luminosity in the central $30''$ was estimated to be $\approx 10^{11} L_{\odot}$, most of which

originates in the nuclear ring. The IR emission was suggested to be due to a burst of star formation in the ring. Hummel, van der Hulst, and Keel (1987 = HHK; see also [Wolstencroft et al. 1984](#) and [Hummel et al. 1984](#)) obtained VLA radio continuum (1.5 and 4.9 GHz) and optical BV and $H\alpha$ observations of the nuclear ring. The radio continuum observations revealed a closed ring pattern nearly coincident with a ring of HII regions. The HII regions in the ring have a low excitation much like that in [NGC 3351](#) ([Rubin et al. 1975](#)). Detection of IR hydrogen recombination lines is the strongest indicator of a starburst in the [NGC 1097](#) ring according to [HHK](#). [HHK](#) compare the ring morphology in the different wavebands and separate the thermal and nonthermal radio emission. They find that one-third of the flux density from the ring at 4.9 GHz is thermal. The average extinction found is a factor of 3 at $H\alpha$. They find a smooth transition in the radio continuum emission from the dust lanes to the nuclear ring. From the ring $H\alpha$ flux, they found a star formation rate of $5 M_{\odot}$ per year, after a factor of ten correction for internal extinction. Geometrically, they deduced that the nuclear ring is elongated perpendicular to the bar in the galaxy plane.

The nuclear ring of [NGC 1097](#) has also been observed in the CO(1-0) emission line by [Gerin et al. \(1988\)](#). These authors determined that most of the CO emission comes from the nuclear ring and estimated a large molecular hydrogen mass of $1.3 \times 10^9 M_{\odot}$. They suggest that the high gas pileup there is due to the bar and possibly also to a small interacting companion, [NGC 1097A](#). Most importantly, they estimated the time-scale for consumption of all of this gas as a few hundred million years, similar to the time-scale for infall.

[Sofue \(1991\)](#) has reviewed CO observations of nuclear-ringed galaxies. Many CO-bright galaxies have a nuclear CO disk structure in the form of a ring, outside of which one normally finds dense molecular arms and sometimes bars. Sofue identifies two types of molecular nuclear rings: the first type has a radius of about 200 pc and a central cavity within the ring; the second type has a radius of 0.7-1 kpc. Examples of the first, compact type are [M82](#), [IC 342](#), [Maffei 2](#), and the Galaxy; these do not necessarily have optical counterparts. Examples of the second, broad type of ring are [NGC 1068](#) and [NGC 1097](#); in these cases, the nuclear rings are prominent in optical images.

Not surprisingly, one of the first star-forming rings to be studied for its molecular gas content was [NGC 4736](#). From a cut along the major axis, [Garman & Young \(1987\)](#) showed that the inner ring of this galaxy is a concentration of molecular gas. The central region of the galaxy was mapped more completely by [Gerin et al. \(1991\)](#), who detected CO(1-0) and CO(2-1) emission from the whole region of the ring and its interior. The molecular gas ring in [NGC 4736](#) coincides closely with the HI inner ring ([Mulder & van Driel 1993](#)). Gerin et al. determine that only 10% of the total hydrogen in the ring is in atomic form.

Radio continuum emission at 20 cm has been detected from the central regions of [NGC 4736](#) by [Duric & Dittmar \(1988\)](#). In this case the inner ring was detected as a weak secondary peak outside a bright central source of emission. Several compact sources, connected with bright HII regions or supernova remnants, were found along the ring.

[NGC 4736](#) is near enough that far-infrared observations can resolve the location of emitting dust. [Smith et al. \(1991\)](#) observed the galaxy at $100\mu\text{m}$ in a series of low-resolution scans across the nucleus and inner ring region. They determined that the emission from this region is definitely resolved and non-gaussian, with peaks at the nucleus and secondary peaks where the scans cross the inner ring. The flux density of $100\mu\text{m}$ emission from the ring was found to be ≈ 1.5 times that from the nuclear source. The $100\mu\text{m}$ ring emission was also found to be coincident with the well-known bright $H\alpha$ emission from the ring as well as the molecular gas ring. Smith et al. conclude that the far-IR emission from the ring comes from dust connected with the molecular gas ring. The total far-IR luminosity is about 100 times the $H\alpha$ luminosity. To explain this, Smith *et al.* concluded that the ring dust is being heated by massive young OB stars, while the nuclear emission is from dust heated by non-OB stars.

[Dahlem et al. \(1991\)](#) discuss the detection of a molecular gas nuclear ring in [NGC 1808](#), and conclude the gas is partly optically thin. This complex region has been studied in more detail by [Phillips \(1993b\)](#), who detected an $H\alpha$ nuclear ring and analyzed large-scale outflow connected with the nucleus and striking optical filaments.

[Garcia-Barreto et al. \(1991\)](#) obtained $H\alpha$, CO, radio continuum, and near IR observations of [NGC 1326](#). Virtually all of the CO and radio continuum emission was determined to come from the region of the bright nuclear ring of this galaxy. High resolution radio continuum emission maps revealed "hotspots" imbedded in diffuse emission in the nuclear ring. A large fraction of the radio continuum emission from the "hotspot" sources was determined to be thermal in nature. The CO mass in the region was determined to be $2.2 \times 10^8 M_{\odot}$.

[Combes et al. \(1992\)](#) observed CO (1-0) emission from the central region of [NGC 4314](#). They detected molecular gas on the *inner* side of the radio continuum nuclear ring, and concluded that the optical mini-spiral in this region is due to dust obscuration. Since the radio continuum ring coincides with recent star formation, the smaller H_2 nuclear ring implies that the ring is decreasing in diameter with time. Combes et al. suggest that dynamical friction of GMC's with bulge stars could account for this angular momentum loss. It would be a transient situation, seen after gas accretion in the ring has ceased. A similar explanation has been suggested for the nuclear dust ring in [NGC 7217](#), which lies on the inner edge of the stellar nuclear ring ([Buta et al. 1995b](#); [Figure 37](#)).

[Kenney et al. \(1992\)](#) brought attention to the phenomenon of "twin peaks" in barred spirals. In this structure, the CO emission in the bar has two bright peaks at the inner ends of the leading bar dust lanes. The prototype example is [NGC 3351](#), where the two bright peaks are symmetrically placed with respect to the nucleus and oriented perpendicular to the primary bar. The spots are connected with a bright nuclear ring, and Kenney et al. state that the peaks are where inward flowing gas from the bar region intersects the nuclear ring of gas. The phenomenon may be connected with orbit crowding near the ILR regions of the bar. [Kenney \(1996\)](#) illustrates some of the variation of CO morphology of conventional nuclear rings. In addition to twin peaks, the nuclear ring of [NGC 6951](#) appears as a CO spiral, while that in [NGC 4314](#) appears as a partial ring. He suggests that some of the variation is due to variations in central mass concentration and bar strength. Some barred spirals with particularly young central starbursts do not have ring-like CO distributions in the center of the bar. The

CO distribution in the nuclear ring of [NGC 4314](#) has been further studied by [Benedict et al. \(1996\)](#), who found the ring to be incomplete, clumpy (five distinct clumps), with an off-center minimum.

[Garcia-Burillo et al. \(1993a, b\)](#) have obtained the highest resolution CO(2-1) and CO(1-0) observations of the quintessential grand design spiral galaxy [M51](#). Their Figure 1 shows a clear ring of molecular gas in the central regions, a feature which would be classified as a nuclear ring. They state that the highest density of molecular gas is found in the ring, which corresponds to the beginnings of two spiral arms.

[Wilson et al. \(1991\)](#) discovered a nuclear ring in the Seyfert galaxy [NGC 7469](#) via radio continuum observations. Near-IR observations at $3.3\mu\text{m}$ by [Cutri et al. \(1984\)](#) had revealed a very concentrated source of emission and dust with a high temperature. These authors concluded that the dust must be heated by hot stars, not the Seyfert nucleus or clouds in the surrounding regions. The galaxy exhibits unidentified emission lines in the $8\text{-}13\mu\text{m}$ region typical of starbursts. Gas associated with hot stars in the central region is of low excitation compared to gas ionized by the Seyfert nucleus. IRAS properties of the system support the existence of nuclear HII regions. Strong ^{12}CO emission and an IR H_2 emission line suggest that there is definite molecular gas within a few arcseconds of the nucleus. [Cutri et al.](#)'s observations give definitive evidence of a circumnuclear starburst in [NGC 7469](#), but little information on its structure. [Wilson et al.](#)'s high resolution 6-cm observations detected a partial nuclear ring $1.5''$ from a strong compact source coincident with the Seyfert nucleus. The extended radio emission morphology seen is unlike most Seyfert nuclei. They use the ratio $\log[S_{60}/S_{1.4\text{ GHz}}] = 2.11\text{-}2.27$ to connect the emission mainly to a starburst. The emission-line morphologies are not like aligned narrow-line regions in Seyfert galaxies. Their radio map shows that much of the emission is from a ring of diameter 1 kpc ($H_0 = 75$). The size is typical of nuclear rings. The supernova rate was estimated to be 0.97 yr^{-1} .

[Forbes et al. \(1994a, b\)](#) reported the discovery of a radio continuum nuclear ring in the nearly face-on barred spiral [NGC 7552](#). The ring is not distinguishable in single color broad-band optical images because of dust, but its presence is detectable in 3cm and 6cm radio continuum images. The ring has dimensions $9'' \times 7''$ and shows no obvious central source. In $B - I$, a partial dust nuclear ring is evident with a blue break. $\text{H}\alpha$ emission is strongest in the blue break. In a $J - K$ color index map, the nuclear ring is seen with similar dimensions and shape to the radio continuum image. The ring is ≈ 1 kpc in diameter and is nearly circular in the galaxy plane. $U - B$ and $V - K$ colors of the ring region support a burst of star formation $< 5 \times 10^7$ years old. The K -band flux is dominated by red supergiants, and the SN rate was estimated to be 0.4 yr^{-1} . They connect the ring to an ILR and suggest that the nucleus is in a dormant (non-AGN) phase. They also suggest that the best wavelength regime to search for small-scale nuclear rings is in the radio regime. They state the nuclear rings may form a depository for inflowing material which is driven to the nucleus in cycles, and may act as "nozzle" for an outflowing superwind.

The spiral galaxy [M100 \(NGC 4321\)](#) is an example of a nuclear pseudoring that has been well-studied recently. As we have noted, this region shows a ring-shaped morphology in $\text{H}\alpha$ images ([Arsenault et al. 1988](#)). In broadband ($\approx V$) HST images distributed for publicity, this region is a grand-design spiral that mimics the large-scale structure of the galaxy. [Knapen et al. \(1995a\)](#) obtained K -band images of this region at good resolution and detected a bar within the pseudoring (see also [Pierce 1986](#)) and two short leading spiral arms. The latter were determined to be not due to dust, and were not distinguishable at shorter wavelengths. Two symmetrically-placed knots were also identified at the ends of the inner bar. [Knapen et al. \(1995b\)](#) attribute much of the structure seen in this region to a density wave driven by the primary bar of this galaxy. The nuclear pseudoring was connected to a double inner Lindblad resonance, which is the only way to explain the leading arms near the ends of the inner stellar bar. An important conclusion made by these authors is that the inner bar is not necessarily a "nuclear bar" decoupled from the primary bar (see [section 16](#)); the leading armlets cannot be explained in this context. The double ILR interpretation of the central structure of [M100](#) has been further supported by [Sakamoto et al. \(1995\)](#), who obtained high resolution CO data in this region. The CO distribution consists of two molecular spiral arms and a nuclear gas concentration. [Sakamoto et al.](#) interpret the molecular arms as due to orbit crowding of molecular clouds near the outer ILR, and the nuclear gas concentration as due to self-gravitating gas which fell into the center from the region of the inner ILR. [Sakamoto et al.](#) also determined that the nuclear bar is the dominant contribution to the potential, and that the molecular arms connected to the nuclear pseudoring are driven mainly by this small bar.

[Knapen \(1996a, b\)](#) has also discussed some of the general characteristics of nuclear rings in the near IR. In K -band images of the nuclear ring of [NGC 6951](#), star forming sites line the nuclear ring in much the same manner as in a $B - I$ color index map (see also [Friedli et al. 1996](#)). [Knapen](#) notes that this turns out to be the rule, while the structure in [M100](#) is the exception. He suggests the differences might be due to differences in the mass distribution in the central kiloparsec, such that the inner ILR might be closer to the center in some galaxies as opposed to [M100](#).

The recent availability of larger format near-IR arrays has led to JHK imaging of the global light distribution in some ringed galaxies. We show in [Figure 49](#) H -band ($1.6\mu\text{m}$) images of the inner regions of [NGC 3081](#) and the whole disk of [IC 4214](#). It is remarkable how prominent the inner ring of [NGC 3081](#) is in the near IR. If H -band surface photometry, as stated by [Benedict et al. \(1992\)](#), "best represents the distribution of red giants, supergiants, and low mass dwarfs" and essentially "traces stars only", then the inner ring has a clear old component and represents a true surface density enhancement in the old disk population. The structure of the ring is smooth but still shows traces of some of the smaller scale structure seen in blue light images. In [IC 4214](#), the near IR image shows all three of the prominent rings of the galaxy.

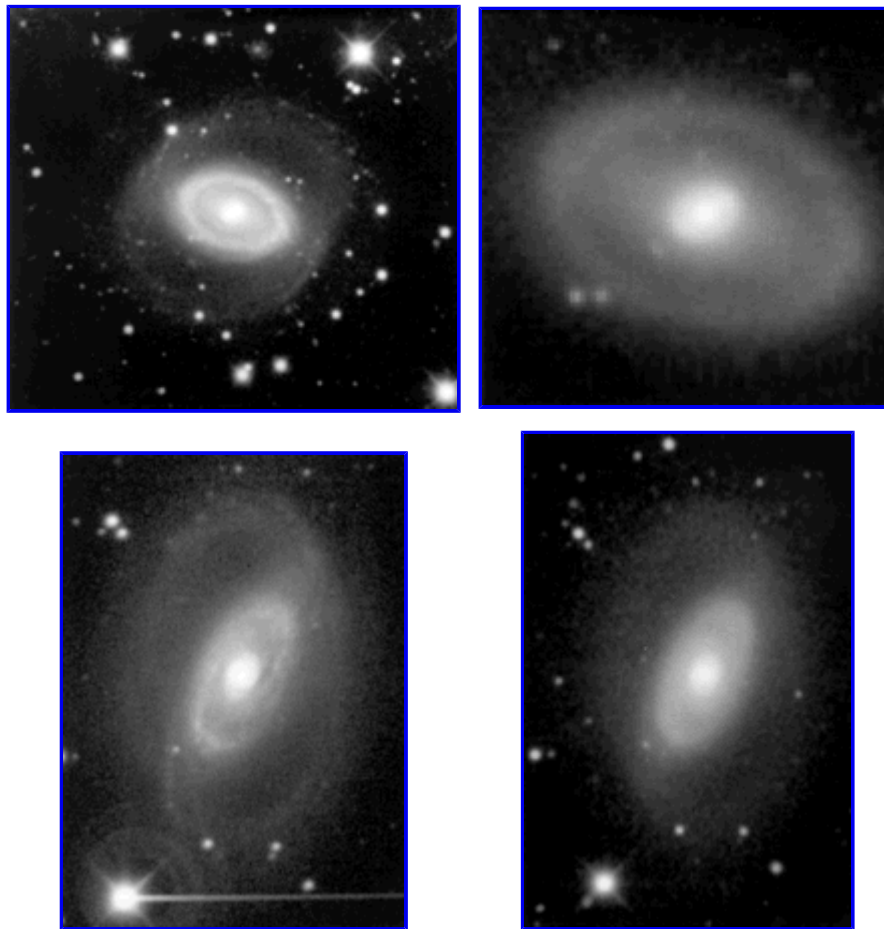


Figure 49. *B*-band (left) and *H*-band (right) images of the ringed, weakly-barred galaxies [NGC 3081](#) and [IC 4214](#). Only the inner ring region of [NGC 3081](#) is shown in *H*.

IRAS and Varieties

[Isobe & Feigelson \(1992\)](#) have derived far-IR luminosity functions of normal galaxies using a volume-limited sample and the technique of "survival analysis" as a means of allowing for the effects of censored data. The study used IRAS fluxes in the 12, 25, 60, and 100 μm passbands, and Gaussians were fitted to the integral luminosity function. In addition to examining for a possible dependence of this luminosity function on Hubble type (E-S0, early S, late S), they also considered the influence of family (SA, SAB, SB) and variety (r, rs, s). Among spirals, no difference was found between early and late types. However, differences were found among family and variety. The authors concluded that, contrary to previous studies, barred spirals are the least IR-luminous as a class. Galaxies of the inner ring variety were found to have significantly less IR emission than those of the (rs) variety, and the authors concluded that SAB(rs) galaxies have the highest IR luminosity among the class of normal galaxies. It was concluded that variety is more important than Hubble type or family in determining the IR emission of a galaxy, an unexpected result. They suggested that bars and rings may affect the dust distribution in a galaxy, by either reducing it or confining it, so that the efficiency of conversion of optical and UV photons to the IR is reduced.

These are interesting results, but we note that selecting galaxies on the basis of having inner rings is not necessarily the same as selecting them on the basis of having nuclear rings. [Hawarden et al. \(1986\)](#) found that barred spirals have higher far-IR luminosities than nonbarred or weakly barred galaxies, based on a different sample selection, and suggested that the enhancement was connected to the ability of a bar to transport large amounts of gas to the central regions where a circumnuclear starburst could take place. It is likely that if galaxies could be selected on the basis of the presence of a nuclear ring, then such galaxies would be IR-bright compared to non-nuclear-ringed galaxies. The IR emission from barred galaxies is further reviewed by [Hawarden et al. \(1996\)](#).

9.8. Kinematic Studies

Kinematic studies of ringed galaxies have been concerned with rotation curves, global velocity fields, and specific ring velocity fields. These studies have revealed a great deal of heterogeneity in the dynamical properties of these galaxies.

Velocity Fields

One of the first kinematic studies of a ringed galaxy was made by van der Kruit (1974, 1976a, b), who mapped the velocity field of the very bright inner ring of [NGC 4736](#) from optical emission lines seen in slit spectra. Evidence for noncircular motions was found on the southeast side of the ring, but little about the global velocity field could be deduced because of the faintness of any emission away from the ring. [Bosma et al. \(1977\)](#) later mapped the global HI velocity field of the galaxy, but these observations lacked sufficient resolution in the inner ring region. Another ringed galaxy which had early extensive kinematic studies was [NGC 3351](#), an SB(r)-type spiral in the Leo Group ([Rubin et al. 1975](#); [Peterson et al. 1976](#)). Emission line velocities were obtained for the inner and nuclear rings, and the outer arms, but the data were insufficient to plot a two-dimensional velocity field since the ionized gas was mostly confined to the two rings.

[Buta \(1984\)](#) obtained kinematic data for eight ringed galaxies over a range of types and bar strengths, and including [NGC 3351](#) and [4736](#). The results were described in several papers ([NGC 1433](#): [Buta 1986b](#); [NGC 7531](#): [Buta 1987a](#); [NGC 6300](#): [Buta 1987b](#); [NGC 1512](#), [3351](#), [4725](#), and [4736](#): [Buta 1988](#)). The velocity fields were derived from either slit spectroscopy or Fabry-Perot interferometry. The latter technique is especially good for giving more complete information on HII region distributions and velocity fields than slit spectra, and was used for [NGC 1433](#), [1512](#), [3351](#), [4725](#), [4736](#), and [7531](#). In [NGC 1433](#) and [1512](#), the velocity points detected were mainly associated with inner and nuclear rings. This localized nature of the HII region distribution precluded the construction of a serious dynamical model of these galaxies. In [NGC 3351](#) and [4725](#), more HII regions were detected beyond the inner rings, but again, little emission was found between the center and the inner rings.

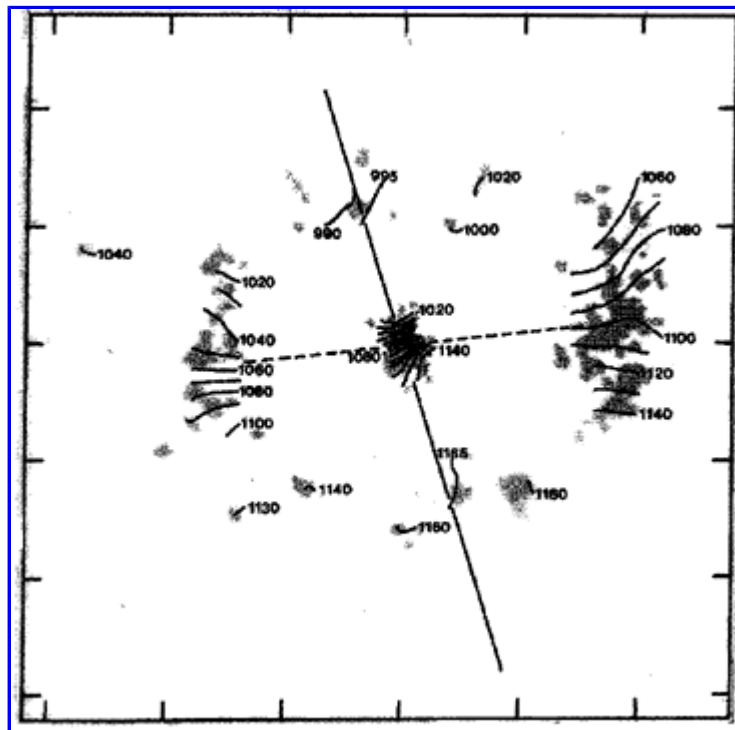


Figure 50. Velocity field of [NGC 1433](#) from TAURUS Fabry-Perot interferometry ([Buta 1986a](#)) and unpublished slit spectroscopy from C. J. Peterson. The shaded gray zones show where the velocity points are located. The dashed line is the bar axis and the solid line is the position angle of the line of nodes. Contours are labeled in km s^{-1} . This observation confirmed (1) the intrinsic oval shape of the inner ring, and (2) the intrinsic alignment of the ring with the bar axis. The tick marks are spaced by $50''$.

The velocity field of [NGC 1433](#) is the most interesting of these early ones studied because it immediately brings to light the possibility of intrinsic oval shapes of inner SB rings and intrinsic bar and inner ring alignment, aspects which had been suspected prior to 1964 by G. de Vaucouleurs (see [Figure 7](#)). [Kormendy \(1979a\)](#) had alternatively deduced from a survey of a small number of barred spirals that inner rings are nearly round, and [NGC 1433](#) provided a clear-cut test of either hypothesis. This galaxy's inner ring is highly elongated nearly along the strong bar in projection. If this apparent alignment were due purely to projection effects on a circular ring, then the line of nodes should be along the ring major axis. However, the observed velocity gradient is nearly perpendicular to this axis, meaning that the ring is intrinsically aligned with the bar (see [Figure 50](#)). A moderately high resolution HI velocity field of [NGC 1433](#), from [Ryder et al. \(1996\)](#), is shown in [Figure 51](#), and confirms the line of nodes previously found from the Fabry-Perot interferometry. [Buta & Purcell \(1996\)](#) and [Buta, Lewis, and Purcell \(1996\)](#) have obtained new $\text{H}\alpha$ velocity fields of five CSRG galaxies, [NGC 3081](#), [IC 4214](#), [IC 4290](#), [ESO 509-98](#), and [ESO 566-24](#), with the Rutgers Fabry-Perot interferometer at Cerro Tololo Inter-American Observatory. [Figure 52](#) shows a color-coded radial velocity map of [NGC 3081](#). This demonstrates the presence of a bounded zone of ionized gas in an oval structure associated with the bright blue light inner ring. The ring includes both discrete HII regions and diffuse ionized gas. The situation is similar to what was found for [NGC 4736](#) by [van der Kruit \(1976b\)](#). It is noteworthy that the inner edge of the ionized gas zone is less oval in projected shape than the outer edge; this was also seen in the shapes of isochromes of the ring in a $B - I$ color index map by [Buta \(1990a\)](#). The difference may

reflect a changing shape of the periodic orbits with radius in the galaxy plane.

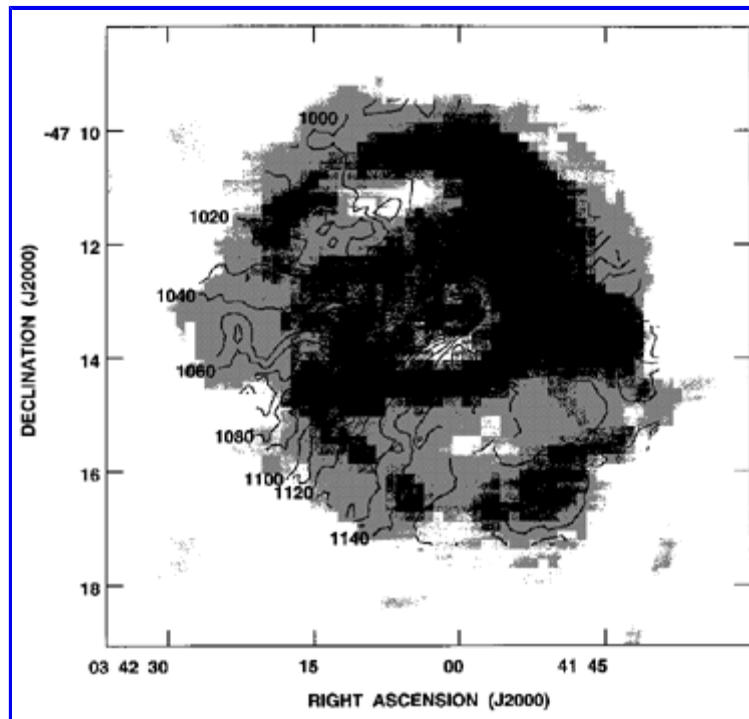


Figure 51. Velocity field of [NGC 1433](#) from HI interferometry ([Ryder et al. 1996](#)), covering the entire optical disk region.

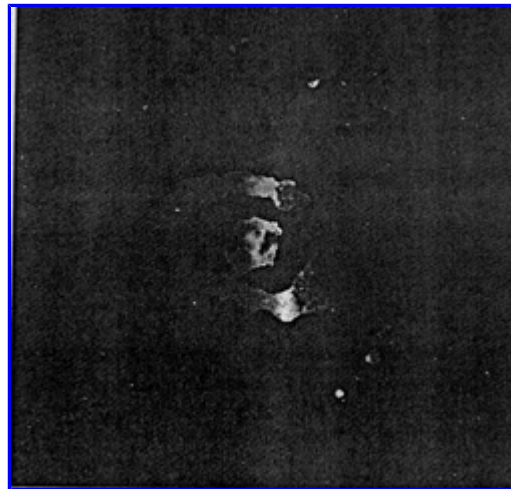


Figure 52. Color-coded (with red receding and blue approaching) velocity field of [NGC 3081](#), from unpublished Fabry-Perot interferometry by Buta and Purcell. The large elliptical zone is the inner ring. Few HII regions are beyond this region.

Rotation Curves

Optical rotation curves of ringed galaxies yield some curious coincidences. For example, in the weakly-barred spiral [NGC 7531](#), the very bright *inner ring* lies virtually exactly at the turnover radius ([Buta 1987a](#); see [Figure 53](#)). The same appears to be true for the *nuclear rings* of [NGC 7217](#) ([Peterson et al. 1978](#)), [NGC 1097](#) ([Wolstencroft & Schempp 1979](#)), [NGC 5728](#) ([Rubin 1980](#)), [NGC 1512](#) ([Buta 1988](#)), [NGC 1068](#) ([Telesco & Decher 1988](#)), and [ESO 565-11](#) ([Buta et al. 1995a](#)), and may be more generally true in the case of such rings as suggested by [Kenney et al. \(1993\)](#). The latter authors found that a starburst nuclear feature in [NGC 3504](#) lies very close to turnover in a CO rotation curve. The inner ring of [NGC 4736](#) lies well beyond turnover, however ([van der Kruit 1976b](#); [Buta 1988](#); [Mulder 1994](#)). We believe that the same will generally be true of most inner rings in SB galaxies. The nuclear rings of the SB galaxies studied lie well inside the bar, while the inner ring of [NGC 7531](#) surrounds the weak bar in the system. The turnover coincidence of the inner ring of [NGC 7531](#) and the nuclear rings of barred spirals is an important observation to be explained by dynamical models.

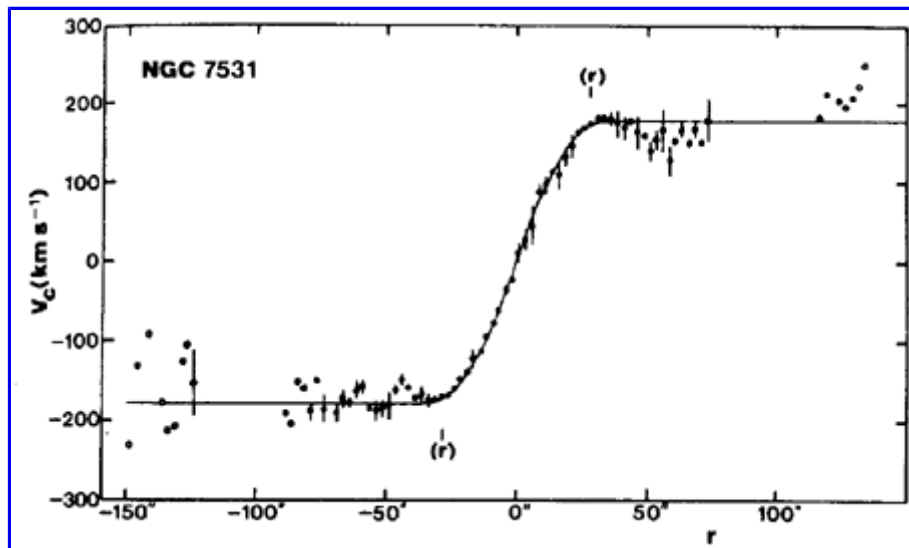


Figure 53. Rotation curve of [NGC 7531](#), from [Buta \(1987a\)](#). The inner ring is indicated by "(r)" and is the prototype "turnover ring", being located near the "turnover" radius of the rotation curve.

Another curious aspect of rings evident from rotation curves has to do with the total mass in the rings. Two interesting cases are [NGC 6300](#) and [7531](#). In [NGC 6300](#), the spiral inner pseudoring produces a large hump in an azimuthally averaged luminosity profile. The ring is also the location of a "step" in the rotation curve. [Buta \(1987b\)](#) transformed the light profile into a rotation curve (a "maximum disk" type solution) and found good agreement with the observed rotation curve. It appears that in this case, the pseudoring has significant self-gravity. Curiously, [Ryder et al. \(1996\)](#) observed [NGC 6300](#) in HI, but detected no hump in the ring region for a fixed inclination and line of nodes solution. H α rotation profiles at different position angles (also from [Buta 1987b](#)) show that the hump is not uniformly strong with azimuth, and the feature may be smoothed over in HI solutions.

[Buta \(1987a\)](#) showed, on the other hand, that a transformed *I*-band light profile of [NGC 7531](#) produced a rotation curve in very poor agreement with the observed rotation curve. In this case, the light profile predicts a large hump near the ring which is not observed, and a Keplerian fall-off almost immediately outside the ring. Thus, the inner ring of [NGC 7531](#), though conspicuous even in the *I*-band, may not contain a great deal of mass, or else the galaxy is dominated by dark matter even at these inner radii.

[Rubin \(1980\)](#) presented an interesting rotation curve for [NGC 5728](#), a large southern barred spiral with all three ring types (CSRG type (R₁)SAB(r,nr)a). Rubin noted an extreme mis-centering of the nuclear ring on the optical nucleus. The rotation curve showed a steep rise to maximum near the position of the nuclear ring, followed by an apparent decline in velocities and a subsequent rise in the region of an inner ring/lens zone. Rubin interpreted the peculiar rotation curve in terms of a two-component model consisting of a centrally condensed bulge and a constant density, uniformly rotating disk, and suggested that barred galaxies like [NGC 5728](#) in general rotate with constant angular velocity. However, it is now known that any rotation curve derived for a barred spiral will be aspect-dependent (e.g., [van Albada & Roberts 1981](#)). Also, Rubin chose orientation parameters for [NGC 5728](#) based on the appearance of the inner ring/lens zone, but it is clear now that this feature is intrinsically oval and misaligned with the true major axis of the galaxy by about 33° ([Schommer et al. 1988](#)).

[Figure 54](#) shows rotation curves for four CSRG galaxies from H α Fabry-Perot interferometry. The sample includes four distinctive types of ringed systems: [IC 4214](#): a tripled-ringed weakly-barred galaxy; [IC 4290](#), an SB(r)-type spiral with a very strong inner ring; [ESO 509-98](#), the prototype of the R₁R'₂ subclass of outer features; and [ESO 566-24](#), a very regular example of a four-armed, ringed barred spiral. Blue light images of all four galaxies are illustrated in [Buta & Crocker \(1991\)](#). In these cases the "normalcy" of the rotation curves is noteworthy. There are humps in the central regions of [IC 4214](#) and [ESO 566-24](#) due to rapid rotation in the region of a nuclear ring. The rotation curve of [IC 4290](#) is defined almost entirely by a slightly oval inner ring.

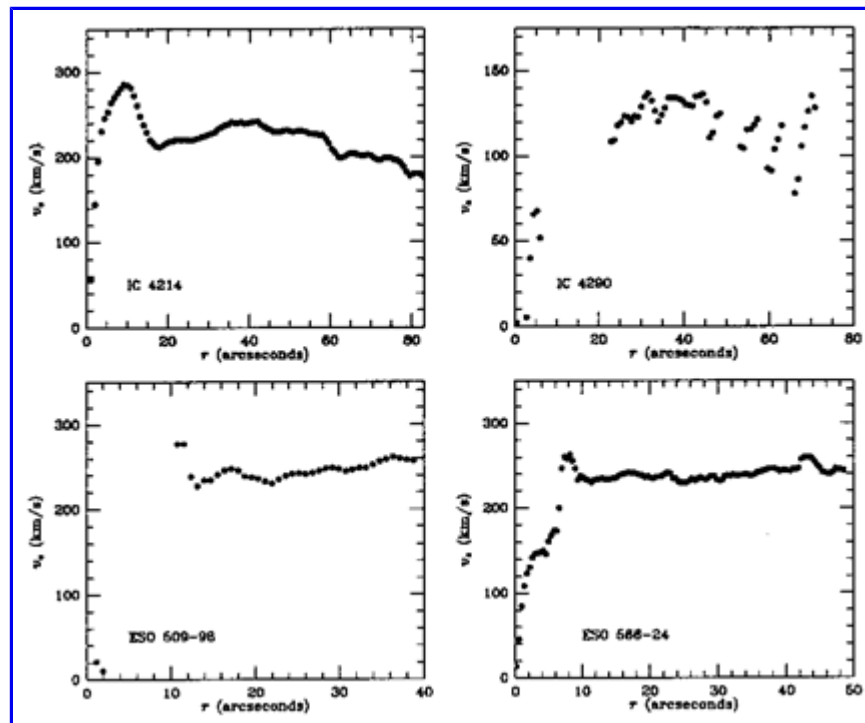


Figure 54. Rotation curves of four CSRG galaxies representing various classes of ringed systems, from [Buta et al. \(1996\)](#).

Velocity-Position Angle Diagrams

The velocity-position angle diagram is a useful tool for characterizing the motions within rings ([van der Kruit 1974](#)). Rings represent intense zones of H α emission in some galaxies, and since little emission may come from elsewhere in the disk, full dynamical models are usually precluded. Ring velocity-position angle diagrams provide a means of getting at dynamics in spite of the sparse amount of velocity information because noncircular motions can be detected in such diagrams.

The work of [van der Kruit \(1974\)](#) on [NGC 4736](#) suggested that noncircular motions in rings could be detected either as shifts of the apparent line of nodes or as asymmetries in the velocity-position angle diagram. Various ways of modeling the diagram include pure circular rotation, rotation plus expansion or contraction, resonance dispersion orbits, and uniformly precessing elliptical orbits. These kinds of models can fit the velocity-position angle diagrams of rings very well in some cases, but do not provide the most reliable interpretation of the dynamics.

An inner Lindblad resonance dispersion orbit ([Lindblad 1955](#); [Lindblad & Jörsäter 1981](#)) is an ordinary unperturbed galactic orbit which appears closed in a reference frame rotating at an angular velocity $\Omega_p = \Omega - \kappa / 2$ (Ω = mean circular angular velocity; κ = epicyclic frequency). [Lin \(1971\)](#) and [Mark \(1974a\)](#) had long ago suggested that inner rings of ionized gas and young stars could develop at this resonance, where the spiral density "wavelength" approaches zero (see also [Lindblad 1974](#)). The mass in the dispersion orbit is assumed to be small and not in itself capable of influencing the dynamics of the galaxy. A resonance dispersion orbit provided a popular interpretation of the "3 kpc" arm in the Galaxy ([Rougoor & Oort 1960](#)) in several early papers (e. g., [Shane 1972](#); [Simonson & Mader 1973](#)) and in [M51 \(Tully 1974\)](#).

A uniformly precessing ellipse model is an approximation to an orbit in a bar-perturbed potential. The precession rate would be the same as the bar pattern speed, and hence such a model allows an estimate of the bar pattern speed from a velocity-position angle diagram. The equations of such a model were derived from the solution to the equations of motion for a uniformly rotating disk ([Chevalier & Furenlid 1978](#)). A variation on this model which expresses radial and tangential velocity components as sinusoidal functions of azimuth around the ring was used by [Buta \(1986b, 1988\)](#).

[Van der Kruit \(1974\)](#) analyzed the velocity-position angle diagram of the inner ring of [NGC 4736](#) in terms of uniform circular rotation and uniform circular rotation with uniform radial expansion or contraction. In order to match the kinematic line of nodes with the observed major axis position angle of the ring, van der Kruit deduced that the ring must be expanding as well as rotating. The expansion velocity required was about 30 km s^{-1} . The radial term does not lead to an asymmetry in the velocity-position angle diagram, but shifts the apparent line of nodes by nearly 10° , owing to the fairly low inclination of 35° . A resonance dispersion orbit was also tried but found not to represent the observed velocity-position angle diagram.

The velocity-position angle diagrams of the inner and nuclear rings of [NGC 3351](#) were analyzed by [Rubin et al. \(1975\)](#) and [Peterson et al. \(1976\)](#). In this case, the velocities in the inner ring were found to be consistent with circular motions, but those in the nuclear ring could be

interpreted in terms of rotation plus a uniform *contraction* of 34 km s^{-1} . A precessing elliptical orbit was also tried for the nuclear ring and found to represent the data as well as a contracting ring model.

[Meaburn et al. \(1981\)](#) studied the motions within the nuclear pseudoring of [NGC 1097](#). Complex line profiles with multiple components were detected. The velocity-position angle diagram of the ring was analyzed in terms of circular motions, with the multiple components possibly due to different spirals in different planes or having different rotational velocities.

The problem with these early interpretations is that the results are very sensitive to the adopted orientation parameters of the parent galaxy. [Buta \(1988\)](#) presented a new analysis of the velocity field of the inner ring of [NGC 4736](#) based on a combination of $\text{H}\alpha$ Fabry-Perot interferometry data and the slit spectroscopy of [van der Kruit \(1976a\)](#). Models of pure circular rotation, rotation plus expansion, and a resonance dispersion orbit fit the data equally well with required line of nodes position angles of $116.^\circ5$, 125° , and 119° , respectively. Without independent knowledge of the line of nodes position angle, there is no way to choose between these models, and the case for an expanding circular ring in [NGC 4736](#) is weak. It is most likely that observed rings are elliptical or oval features rather than circular features, as shown by statistics in [section 9.3](#).

The best published cases of inner rings showing clear asymmetries (rather than just apparent line of nodes shifts) in the velocity-position angle diagram are [NGC 1433](#) ([Buta 1986b](#)) and [NGC 4725](#) ([Buta 1984, 1988; Wevers et al. 1984](#)). This is shown for [NGC 4725](#) in [Figure 55](#). In the case of [NGC 1433](#), the asymmetry is readily explained in terms of the elliptical shape of the inner ring. In spite of the low inclination of this galaxy, the deviations from circular motion are obvious in the velocity-position angle diagram and can be fitted by a rotating elliptical ring where the radial and tangential velocity components in the rotating frame vary sinusoidally with position angle in the galaxy plane. However, [NGC 4725](#), being more inclined and suffering interaction with a nearby companion, does not have sufficiently well-determined orientation parameters to yield a unique interpretation. The velocity-position angle diagram can be fit either by rotation plus uniform expansion (see right panel in [Figure 55](#)), or a precessing ellipse (see [Buta 1988](#)). In the expanding ring interpretation, the expansion velocity derived was $52 \pm 7 \text{ km s}^{-1}$ from optical interferometry and $40 \pm 13 \text{ km s}^{-1}$ from HI observations. However, no matter how well this kind of model may fit the data, it is unlikely that a large ring crossed by a bar is due to some kind of nuclear explosion (see [Sanders and Bania 1976](#)).

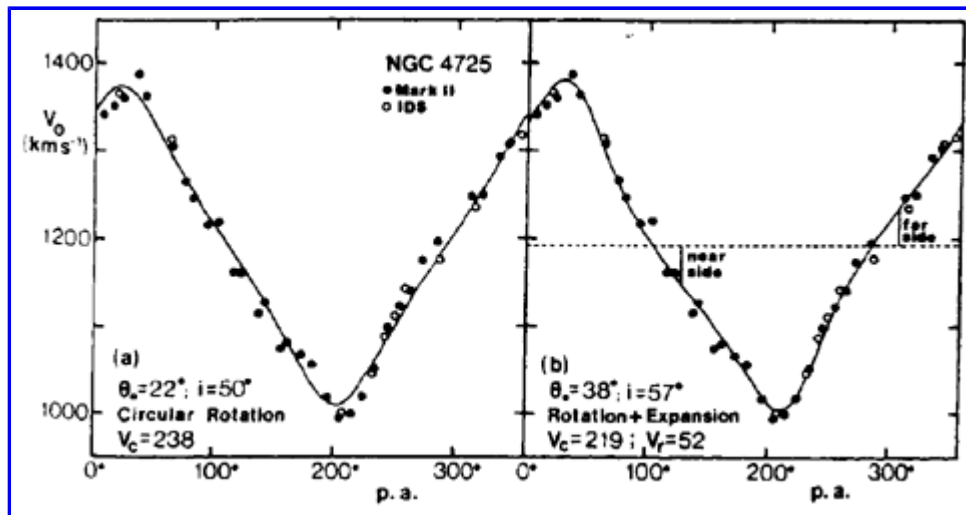


Figure 55. Velocity-position angle diagram of the inner ring of [NGC 4725](#). The solid curves are for pure circular rotation (left panel) and rotation plus uniform expansion (right panel). The orientation parameters used are indicated. "Mark II" and "IDS" refer to different data sets (see [Buta 1988](#)).

Although the inner rings of [NGC 1433](#) and [4725](#) display clear asymmetries in their velocity-position angle diagrams, the lack of asymmetry does not mean that there are no noncircular motions present. If an oval ring presents an aspect such that the observer is viewing the ring down its intrinsic major or minor axis, then the motion along the ring at the projected galaxy minor axis will be purely tangential, and no asymmetry will be seen in the velocity-position angle diagram. Two examples where this may be the case are the inner rings of [NGC 3351](#) and [4736](#) ([Buta 1988](#)).

Lindblad Precession Frequencies

Rotation curves derived for ringed or nonringed galaxies have been used to infer resonance locations by deriving the so-called Lindblad precession frequencies, $\Omega \pm \kappa / 2$, where Ω is the circular angular velocity and κ is the radial epicyclic frequency. We describe in this section a sampling of studies where these frequencies have been derived. In the linear theory, the location of the inner Lindblad resonance is where the pattern speed equals $\Omega - \kappa / 2$ and the location of the outer Lindblad resonance is where the pattern speed equals $\Omega + \kappa / 2$. Corotation is where the pattern speed equals the circular angular velocity in the disk. Since κ is derived from the radial derivative of the rotation curve, a smooth curve is often fitted to rotation curve points to reduce noise. These studies have usually not allowed for the effects of velocity dispersion on the observed rotation curve, especially in the inner regions, and treat the resonances as narrow in radius. [Contopoulos](#) (see discussion in [Pfenninger 1996](#)) discusses the nonlinear situation. Multiple-ringed galaxies are often the best choices for

such analyses, because one can check for consistency between the locations of the rings and a single pattern speed.

Buta (1987a) estimated the precession frequencies in the single-ringed galaxy NGC 7531 (see Figure 56), based on an analytic function fitted to the observed rotation curve. In this case the peak of $\Omega - \kappa / 2$ lies slightly outside the mean deprojected radius of the inner ring, but in any case the ring is located very close to the maximum of this function. The horizontal line in Figure 56 assumes the inner ring is located at ILR, which places corotation in the region of the faint outer arms.

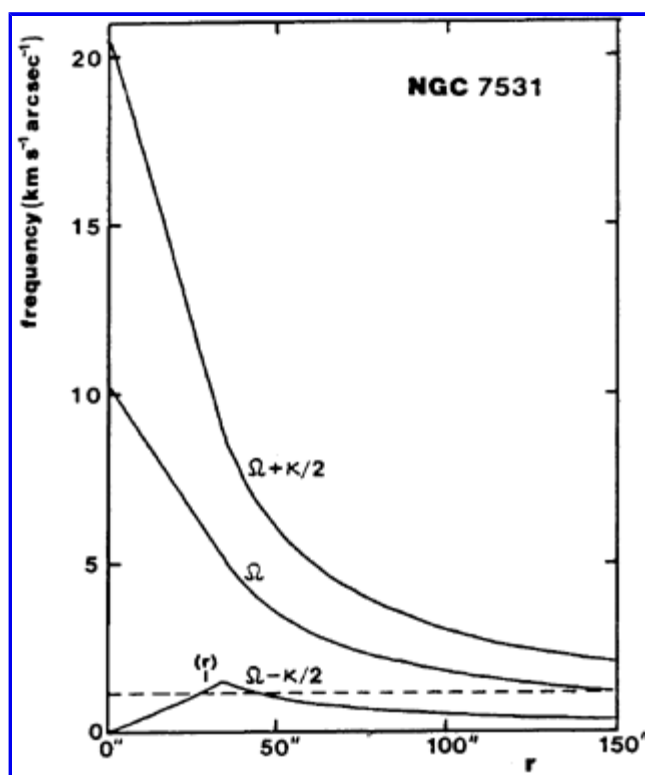


Figure 56. Lindblad precession frequencies in NGC 7531, from Buta (1987a). The horizontal line is for a pattern speed which places the inner ring (r) at ILR.

Telesco & Decher (1988) derived the precession frequencies for the well-known Seyfert 2 galaxy NGC 1068. Using a rotation curve based on a combination of stellar absorption line velocities over the region of the bright nuclear pseudoring, and gaseous emission line velocities outside this region, they deduce that for a pattern speed of $50 \text{ km s}^{-1} \text{ kpc}^{-1}$, the pseudoring of IR luminous star formation, brightest CO features, and the brightest non-nuclear HII regions lies between two ILR's. In their interpretation, the ends of the nuclear bar lie just inside the inner ILR of the system. They conclude that the luminous burst of star formation in the inner regions of NGC 1068 is due mainly to bar-driven gas flow and indirectly to the Seyfert activity in the nucleus. Their rotation curve did not extend far enough to deduce whether the location of the outer ring of NGC 1068 is consistent with the location of OLR for the same pattern speed.

Arsenault et al. (1988) derived a detailed rotation curve for M100 using a Fabry-Perot velocity field. By assuming that corotation lies at the ends of the weak primary bar, they deduced from the $\Omega - \kappa / 2$ curve that the nuclear pseudoring lies between the two ILR's of a double ILR. As we have already discussed in section 9.7, more recent and more detailed studies support this idea. This galaxy has no other rings.

Schommer et al. (1988) derived precession frequency curves for the barred Seyfert 2 galaxy NGC 5728. In this case, by assuming the bar ends at CR, they deduced that the nuclear ring of the galaxy is located just inside an ILR.

Devereux et al. (1992) used a combined optical/CO rotation curve to evaluate precession frequencies in the SB(r)b spiral NGC 3351. In order to connect the location of the bright nuclear ring to the region of the ILR's, the pattern speed was such that corotation was placed at 1.2 times the bar radius. This also placed the inner ring inside corotation.

From a combined high resolution CO and optical rotation, Kenney et al. (1993) deduced the precession frequencies in the (R')SAB(rs)ab spiral NGC 3504. In this case, by assuming corotation lies at the ends of the bar, they deduced that the partial nuclear ring and inner starburst in this galaxy lies between two possible ILR's and that the pattern speed is also consistent with the outer pseudoring being located near the outer Lindblad resonance.

Finally, Ryder et al. (1996) have used an HI rotation curve to deduce resonance locations in NGC 1433. Ryder et al. found reasonable consistency with a single pattern speed for the locations of the outer and inner pseudorings of this galaxy, with the outer pseudoring being located near the OLR and the inner pseudoring being located near the inner 4/1 resonance, where $\Omega_p = \Omega - \kappa / 4$. The resolution of the HI

rotation curve was not high enough to deduce whether the nuclear ring of this galaxy is connected to the region of the ILR's.

Complex Motions in Nuclear Ring Regions

The regions of nuclear rings in galaxies sometimes show complex velocities with large velocity dispersions, noncircular motions, and even multiple components. Virtually every example studied is characterized by rapid rotation, noncircular motions, and sometimes high velocity dispersion compared to HII regions away from the nuclear region. A representative case is [NGC 5728](#), a Seyfert 2 galaxy studied by [Schommer et al. \(1988\)](#), who mapped the velocity field of the nuclear ring with a Fabry-Perot interferometer. The emission map from this study revealed a bright nucleus and a bright arc or partial ring of emission. Strong noncircular motions were detected in a velocity cut along the kinematic major axis. Rapid rotation characterizes the region, and double-peaked line profiles were detected in the nucleus. The latter may be connected to the Seyfert activity, and not all nuclear rings include such an active nucleus.

Particularly interesting in this regard has been the detection of a nuclear gas ring in the Seyfert 1 galaxy [NGC 4151](#), by [Vila-Vilaró et al. \(1995\)](#). In this case, the ring appears red in color index maps owing to dust extinction. Gas motions in the ring were measured by [Robinson et al. \(1994\)](#), who detected a significant increase in the velocity dispersion in this region. Vila-Vilaró et al. suggest that the reddened arcs in the nuclear ring of [NGC 4151](#) are regions where gas from the leading regions of the bar encounter gas on the x_2 family of periodic orbits. This is very much like the origin of "twin peaks" CO emission from other barred galaxies ([section 9.7](#)). In addition, these authors identified a close alignment of the extended narrow line region with the nuclear gas ring, and suggest that the collimation of the AGN ionizing radiation field and the gas flows due to the bar potential are closely related. In the Seyfert 1.5 barred spiral galaxy [NGC 1365](#), the [OIII] emission lines reveal two components in the central regions: one component representing the circumnuclear ring in rotation, the other component the bipolar outflow of hot gas from the nucleus, forming a cone aligned along the minor axis ([Hjelm & Lindblad 1996](#), [Lindblad et al. 1996](#)), also roughly aligned with the nuclear ring.

This completes the main observational discussion. We now turn to the theoretical parts of this review.

10. THEORIES OF RING FORMATION

10.1. Some Historical Points

From the beginning, the problem of rings in galaxies has been associated with that of spiral arms, because like spiral arms, rings are very similar thin structures, more prominent in the blue, and the sites of star formation. Quite often, the rings are only pseudorings, clearly formed by spiral arms in the way of winding up into a ring (see [Figure 3](#) and [Figure 17](#)). It is then natural that early theories of rings closely accompanied theories of spiral structure. The same temptation to attribute them only to gas dynamics in a magnetic field, instead of gravitational dynamics, appeared from the 1930's-60's. However, as the idea of density waves was developed by Bertil Lindblad in the 1950s to explain spiral structure, he noticed the existence of "dispersion orbits" with $m = 2$ symmetry that precessed at a rate almost constant with radius ([Lindblad 1962](#), [1964](#)). From the epicyclic theory, we can consider stellar orbits as closed ellipses precessing at the rate $\Omega - \kappa / 2$, where κ is the epicyclic frequency. This precession rate appears to be almost constant in a certain range of radii in the Galaxy, which suggests that a ring could be formed by an accumulation of such dispersion orbits, slowly precessing as a whole around the galactic center (cf. the early N-body experiments of [P.O. Lindblad 1960](#)).

It is interesting to note that in the pre-density wave era, [Randers \(1940\)](#) proposed a theory of ring formation based on viscous torques. This theory was developed again in the 1970's and 80's for gas flows ([Icke 1979](#); [Lesch et al. 1990](#)), and we will discuss it in [section 12](#). The principle is that viscous torques act in regions of differential rotation, and accumulate matter where the angular velocity becomes constant, i.e., rings are expected at the turnover point of the rotation curves. Randers applied this theory to the stellar population, where he claimed that collisions and scatterings were equivalent to a viscosity effect. The problem of diffusion and heating of the stellar component was debated much later ([Wielen 1977](#); [Lacey 1984](#); [Zhang 1996](#)).

More recently, [Danby \(1965\)](#) discussed the existence of ringlike structures in barred galaxies, associated with the equipotential surfaces in the rotating frame of the bar; this might be the closest approach to the modern theory of ring formation, as resonant accumulation of gas in a non-axisymmetric potential.

The considerable success of the density wave theory of [Lin & Shu \(1964\)](#) led to the abandonment of the non-gravitational approaches, and the growing importance of N-body simulations focussed attention on bars, which were the only robust density waves found numerically in a self-consistent stellar disk (e.g. [Miller et al. 1970](#); [Hohl 1971](#)). With this advance, bars were no longer considered as solid body entities in rotation around the center, but as waves interacting with the rest of the disk and possibly triggering spiral structure. Simulations of gas flows in barred galaxies were initiated by [Sanders & Huntley \(1976\)](#), who showed convincingly that a long-lived spiral structure could be generated in the gas component by the stellar bar, owing to the properties of periodic orbits in a non-axisymmetric potential. No resonant rings were formed in these simulations, which could be an effect of the gas viscosity, as will be discussed in [section 12](#). The first work where resonance rings were formed, and explained through gravitational torques on the gas, was done by Schwarz ([1981](#), [1984b](#)), who modelled the gas component by ballistic particles undergoing collisions. This representation, which corresponds much better to the cloudy and clumpy interstellar medium, minimizes the artificial viscosity, and strongly helps the formation of highly contrasted rings.

We will discuss in detail the mechanism of ring formation in [section 11](#); since it is intimately linked to the bar, the dynamics of barred galaxies and their orbital structure will be detailed as a preliminary in [section 11](#). Let us first emphasize the observational facts that support the proposed mechanism.

10.2. Fundamental Clues from Observations

As was shown in the previous sections, and [section 9](#) in particular, rings are relatively narrow features, are always associated with gas, and are usually the site of enhanced star formation. *This suggests that gas is at the basis of ring formation.* The high velocity dispersion of the old stellar component will prevent it from forming very sharp structures. Even after young stars have formed out of the gas, they will acquire velocity dispersion in a time-scale of 10^9 yrs, and will no longer follow a thin ring morphology. *Gas is therefore necessary also for the persistence of a ring structure.*

We have also emphasized that rings are preferentially found in barred galaxies. They have a preferential orientation with respect to the bar, either parallel or perpendicular, and their sizes are also related to that of the bar. The inner ring is always encircling the bar, forming the famous θ -shape. All this already tells us that *the bar must be an essential element in ring formation.* Bars can be considered as long-lived density waves, and long-lasting modes. When a density wave of constant pattern speed is present in a galaxy, resonant phenomena with this forced pattern speed have time to develop and will be conspicuous. *The idea of rings formed at resonances with the bar is therefore entirely natural.*

A detailed color decomposition of an inner ring ([Buta 1991](#); see [section 9.4](#)) has shown that the ring is the superposition of two gaussians: a narrow blue one, containing the more recent stars, and a wider red one. The latter has about twice the width of the former. The mean central positions of the two gaussians coincide (see [Figure 40](#)), which means that the position of the inner ring has not significantly evolved from the time of its formation. The underlying pattern speed must therefore be nearly constant over the ring formation time.

11. DYNAMICS OF BARS

About two-thirds of spiral galaxies possess a non-axisymmetric distortion or a bar in their stellar component, although only one-third possess a really strong bar, of SB type (e.g. [de Vaucouleurs 1963](#)). Red or near-infrared photometry has revealed many bars and oval distortions in the old stellar component that were not visible on a blue photograph of the same galaxy, because of dust and star-formation regions ([Zaritsky & Lo 1986](#); [Rix & Rieke 1993](#)). A bar can be detected also by the cold gas component, which is a good tracer of faint perturbations in the potential (e.g. CO observations of [IC 342](#), [Ishizuki et al. 1990](#); [NGC 6946](#), [Ball et al. 1985](#); see also [Turner 1996](#)). It can therefore be concluded that a bar exists in the great majority of galaxies, and is not a peculiar structure, as was considered before the 1970's. Our own Galaxy appears barred from its kinematics and elliptical streamlines (e.g. [Peters 1975](#); [Mulder & Liem 1986](#)), and also from its boxy and asymmetric near-infrared contours ([Blitz & Spergel 1991](#)), and its micro-lensing efficiency ([Paczynski et al. 1994](#)). Our nearby companions are also barred ([M31](#), [Large](#) and [Small Magellanic Clouds](#), etc.).

Observed and dynamical properties of bars have recently been nicely reviewed by [Sellwood & Wilkinson \(1993\)](#). As far as rings are concerned, it is interesting here to note that barred galaxies might be the only objects where a long-lived, quasi-stationary, normal mode can be recognized. Bars are essentially composed of an old population, and the spiral waves in a barred galaxy are strongly influenced (maybe driven?) by the bar. In strong bars, the spiral arms appear always in the continuation of the bar, suggesting that they rotate with the same pattern speed. The presence of a grand-design spiral is about twice as frequent in barred galaxies than in nonbarred ones, as determined by [Elmegreen & Elmegreen \(1983\)](#). While nonbarred galaxies can be multi-armed or stochastic, most barred galaxies possess a two-armed regular density wave. Barred galaxies are therefore ideal for studying resonance phenomena.

11.1. Bar Formation

The bar instability was discovered in early N-body simulations of rotating stellar disks ([Miller & Prendergast 1968](#); [Hockney & Hohl 1969](#)). Because of these results, [Kalnajs \(1971, 1972\)](#) studied the stability of disks with respect to bar modes through a linear analysis, and made predictions about the eigenvalues and growth rates of the normal modes for a given density and velocity distribution. These have been verified by simulations in the linear regime (e.g. [Sellwood and Athanassoula 1986](#)).

Bars can be considered as long-lived modes, made by the superposition of leading and trailing waves, i.e. forming a standing wave. As such, the bar mode can grow through swing amplification, as outlined by [Toomre \(1981\)](#) for spiral density waves. The amplification of waves relies on the corotation region (CR), which separates the galaxy into two regions where the waves have opposite signs of energy and angular momentum (negative inside and positive outside CR). At CR a wave will be partially reflected and transmitted; the transmitted wave will carry energy of opposite sign as the incident wave, so that the reflected wave must have an increased amplitude to ensure conservation. The corotation amplifier, coupled with a feedback cycle that reflects the waves back to CR, can explain the growth of modes. Several feedback cycles were proposed, such as the WASER ([Mark 1974b](#)) based on long-trailing waves, while the swing involves the feedback of short leading waves. In the WKB theory, waves are, however, evanescent around CR, and tunnel through a forbidden zone ([Lin & Shu 1964](#)); the exponential decrease of wave amplitude in this region kills the amplifier, and the gain of the feedback cycles proposed is of the order of unity. Actual amplitude gain over a cycle relies on another kind of amplification, a positive feedback first identified by [Goldreich & Lynden-Bell \(1965\)](#) and [Julian & Toomre \(1966\)](#), and detailed by [Toomre \(1981\)](#), with the help of numerical simulations.

The amplification is due to a conspiracy between differential rotation, epicyclic oscillation, and self-gravity. Trailing density waves propagate radially towards the center, while leading waves propagate outwards. The leading wave packet becomes more and more open while traveling, due to differential shear, until it turns into a trailing wave. During this swing from leading to trailing, particles running on their epicyclic motion closely follow the wave, and strongly interact with it. Self-gravity contributes to gather particles, and amplify their density contrast. The wave energy is amplified at the expense of the rotational energy.

The trailing waves traveling inwards can be reflected in the center, while the leading waves give rise to trailing reflected waves, and transmitted waves at corotation. The reflection in the center occurs only if a wave can travel there without being damped at the inner Lindblad resonance. The problem of a possible Landau damping of waves at the inner resonance has long suggested that bars can only develop without this resonance. The pattern speed should then be high enough to prevent the resonance. This appears to be verified in N-body simulations in the linear regime, at the beginning of bar formation. But it does not seem to be the rule in the non-linear regime in N-body simulations, nor in the observations, when some hint can be gained of the bar pattern speed.

Another point of view to better understand the N-body problem is in terms of stellar orbits, and families of periodic orbits as will be described in the next section. Periodic orbits are closed orbits in the frame rotating with the bar. The stable ones trap regular orbits around them. They are thus the skeleton of the orbital structure of the disk. Periodic orbits are the fixed points that depend essentially on the symmetry of the potential, and not on the detailed mass distribution. In the potential of a rotating bar, the main family of orbits is elongated along the bar, supporting it, and we can understand under which conditions a self-gravitating system will become barred. When the mass concentration towards the center is strong enough, the elongated orbits will be replaced by periodic orbits perpendicular to the bar, and we can predict the dissolution of the bar. This approach can help to determine the pattern speed of realistic self-consistent bars. Such an approach has been developed by Contopoulos and collaborators (e.g. [Contopoulos & Papayannopoulos 1980](#)).

The consideration of near-resonant orbits aligned with the bar led [Lynden-Bell \(1979\)](#) to propose that bar instability could come from a kind of Jeans instability, trapping all elongated orbits and aligning their major axes. He studied the conditions under which an elongated closed orbit in the bar rotating frame will be forced to align with the bar, and therefore reinforce it, because of gravitational torques. He concluded that for this to occur, the precession rate of elongated orbits ($\Omega - \kappa / 2$) must increase with specific angular momentum, a condition that is fulfilled only in the central parts of galaxies where the velocity curve is rising. The pattern speed of the bar in this scenario must be lower than the peak of the $\Omega - \kappa / 2$ axisymmetric curve, which is not the case at the beginning of the bar instability in N-body simulations.

The development of the instability has now been followed through a wide series of N-body simulations (e.g. [Sellwood 1981](#); [Combes & Sanders 1981](#); [Sellwood & Wilkinson 1993](#)). In an initially axisymmetric stellar disk, first a transient two-armed spiral wave develops; since it is trailing, it transfers angular momentum outwards ([Lynden-Bell & Kalnajs 1972](#)). The bar then forms in two steps: first a short and weak bar forms, rotating with a high pattern speed which is always higher than the maximum of the precession rate $\Omega - \kappa / 2$. The bar, as a wave inside its corotation, has a negative angular momentum, and is amplified through the outwards transfer provided by the spiral arms. Then, the bar slows down, with a growing intensity, trapping more and more particles in its potential well. This can be understood in the frame of density wave theory as well as in stellar orbit theory. At the beginning, the perturbation is linear; for the swing amplifier to work, there should be no inner Lindblad resonance. This is fulfilled if the bar pattern speed is well over the $\Omega - \kappa / 2$ curve, justifying the fast rotation at the start.

In parallel, we can consider that the bar traps more particles in extending its length. Those particles, at larger radii, have lower precession rates, and it is likely that the global equalized rate, i.e. the pattern speed, will be lowered by the adjunction of these particles. As the pattern speed decreases, the bar loses angular momentum through the spiral wave.

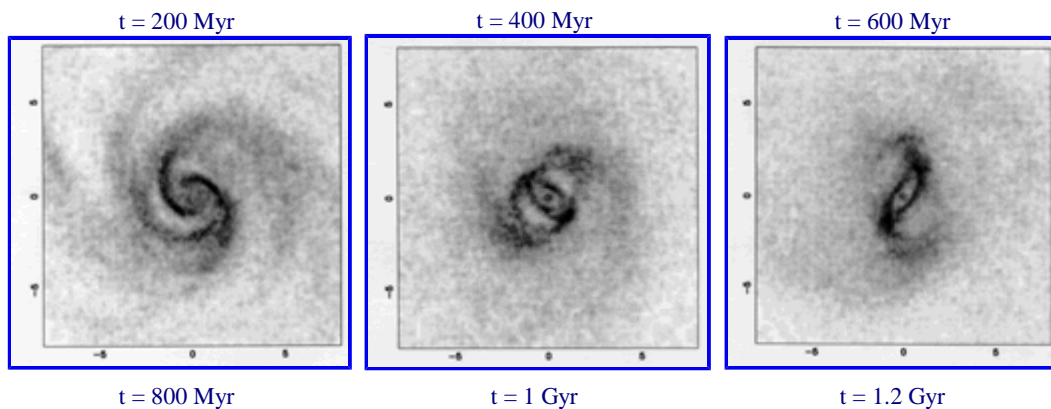
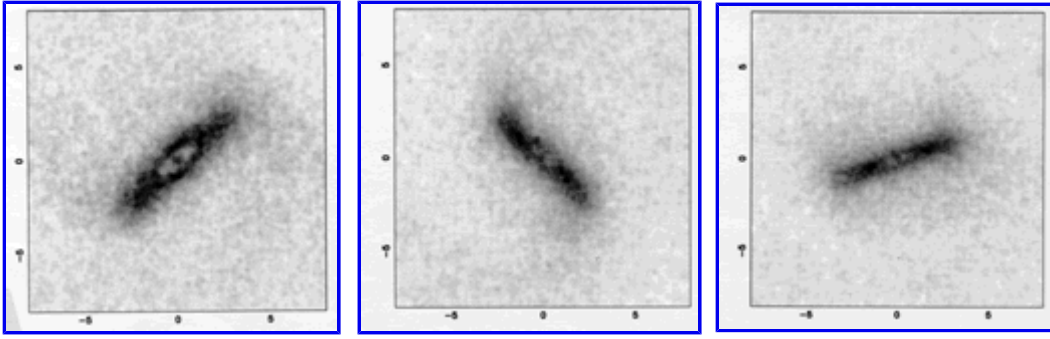


Figure 57. Example of bar formation in an N-body simulation, with stars only. The galaxy is plotted every 200 Myr.



Periodic orbits are parallel to the bar only inside corotation, as we shall see below. As Ω_b decreases, corotation propagates outwards, and the bar extension could be higher. Bar formation by trapping of orbits is illustrated in the N-body simulation of [Figure 57](#).

11.2. Orbits in a Barred Galaxy

Knowledge of the stellar orbits in a barred galaxy can help us to understand the dynamical properties of bars, their extension, and pattern velocity. It is also fundamental to understanding resonances, the behavior of the gas component, and therefore to explaining the existence of rings.

Bars are three-dimensional components, and they can be modeled as triaxial ellipsoids. Although the disks of spiral galaxies are very thin components, with axis ratios around 10, bars can be thicker because of vertical resonances (e.g. [Combes et al. 1990b](#)), and reveal box or peanut shapes when seen edge-on. In a first approach, we will describe the stellar orbits as if they were confined in the galaxy plane. This much simpler approach gives already most of the characteristics of bar dynamics and is sufficient to understand the gas behavior, since the gas disk is much thinner.

First, let us recall the characteristics of orbits in an axisymmetric potential $\phi(r)$ in the plane $z = 0$. A circular orbit has an angular velocity $\Omega^2 = 1/r d\phi/dr$. In linearizing the potential in the neighborhood of a circular orbit, the motion of any particle can be expressed in first order by an epicyclic oscillation, of frequency κ ,

$$\kappa^2 = d^2\phi/dr^2 + 3\Omega^2 = r d\Omega^2/dr + 4\Omega^2 \quad 6$$

The general orbit is therefore the combination of a circle and an epicycle, or a rosette, since there is no rational relation between the two periods.

The bar creates a bisymmetric gravitational potential, with a predominant Fourier component $m = 2$, which rotates in the galaxy with the pattern speed Ω_b . To be left with a potential independent of time, where the energy of particles is conserved, we must consider the orbits in the rotating frame. The equivalent potential in this frame is then:

$$\phi_{eq} = \phi(r, \theta) - 1/2 \Omega_b^2 r^2 \quad 7$$

in cylindrical coordinates (r, θ, z) , for $z = 0$.

The energy of a particle (per unit mass) in this frame is

$$E_J = 1/2 v^2 + \phi - 1/2 \Omega_b^2 r^2. \quad 8$$

It is an integral called the Jacobi integral. It is expressed as a function of the energy in the fixed frame E , as $E_J = E - \Omega_b L_z$, where L_z is the angular momentum, which is not an integral, since the potential is non-axisymmetric.

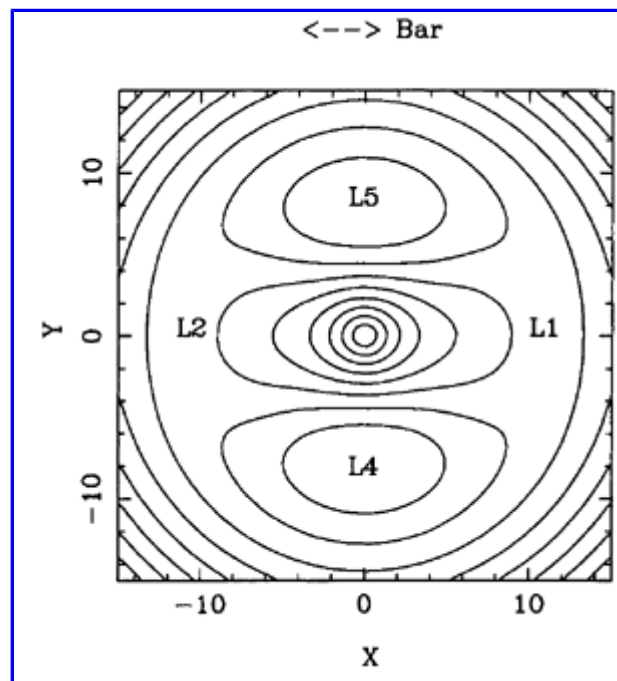


Figure 58. Equipotentials in the rotating frame of the bar. This picture already provides a good hint of some of the periodic orbit shapes.

The equipotentials in the rotating frame are given in [Figure 58](#). There exist 5 stationary points, known as Lagrangian points, L_1 to L_5 , where the derivative of ϕ_{eq} vanishes. L_3 is the central minimum, L_4 and L_5 are maxima, and L_1 and L_2 are saddle points. Only L_4 and L_5 are stable, i.e., a particle can oscillate around them with the epicyclic frequency. The four points, L_1 , L_2 , L_4 , and L_5 correspond to the corotation resonance with the bar. Although they are not located at the same galactocentric distance, they delineate an annular zone, called the corotation zone.

Lindblad Resonances

In the rotating frame, the effective angular velocity of a particle is $\Omega' = \Omega - \Omega_b$. There exists then regions in the galaxy where $\Omega' = \kappa / m$, i.e. where the epicyclic orbits close themselves after m lobes. The corresponding stars are aligned with the perturbation and closely follow it; they interact with it always with the same sign, and resonate with it. These zones are the Lindblad resonances, sketched with dashed circles in [Figure 59a](#). According to the relative values of Ω and κ in a realistic disk galaxy ([Figure 59b](#)), and because the bar is a bisymmetric perturbation, the most important resonances are those for $m = 2$. An obvious resonance is corotation, for which $\Omega = \Omega_b$ ($\Omega' = 0$).

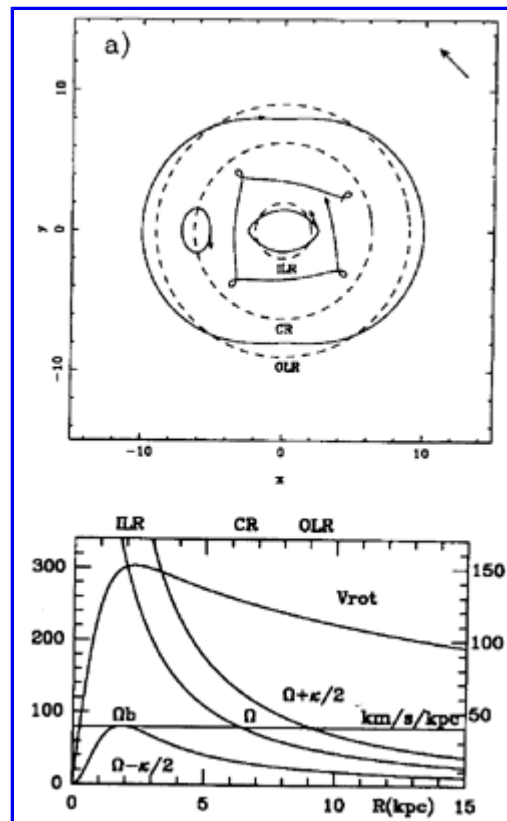


Figure 59. Lindblad resonances: a) resonant orbits in the rotating frame of the bar; b) rotation curve (left scale, km/s) and frequencies (right, km/s/kpc) used to model these orbits. The pattern speed of the bar is indicated.

Periodic Orbits

Periodic orbits in the bar rotating frame are orbits that close on themselves after one or more turns. Periodic orbits are the building blocks which determine the stellar distribution function, since they define families of trapped orbits around them. Trapped orbits are non-periodic, but oscillate about one periodic orbit, with a similar shape. The various families are best identified in surface of section diagrams, first used by Poincaré as early as 1899. This method consists of representing orbits of the 4-D phase-space (x, y, \dot{x}, \dot{y}) only by their intersection points with any plane of phase space, for instance $\dot{x} = 0$, and projecting these points in a 2-D space (for instance (y, \dot{y})). Periodic orbits appear then as single points, while trapped orbits are represented by invariant curves. The fact that points do not spread in space all over a given region, but follow an invariant curve, is the consequence of the existence of another integral besides Jacobi's. There can, however, exist irregular orbits, for which the intersection points are spread all over a sea in a stochastic manner. These ergodic orbits occur essentially when the potential presents strong asymmetries. For realistic galaxy potentials, ergodic orbits concern mainly regions outside corotation.

The periodic orbits are numerous (see the recent review by [Contopoulos & Grosbøl 1989](#)), and we will describe here the most important ones for the bar support, and for the ring formation mechanism:

1. the x_1 family (see [Figure 60](#)) is the main family supporting the bar. Orbits are elongated parallel to the bar, within corotation. They can look like simple ellipses, and with energy increasing, they can form a cusp, and even two loops at the extremities.

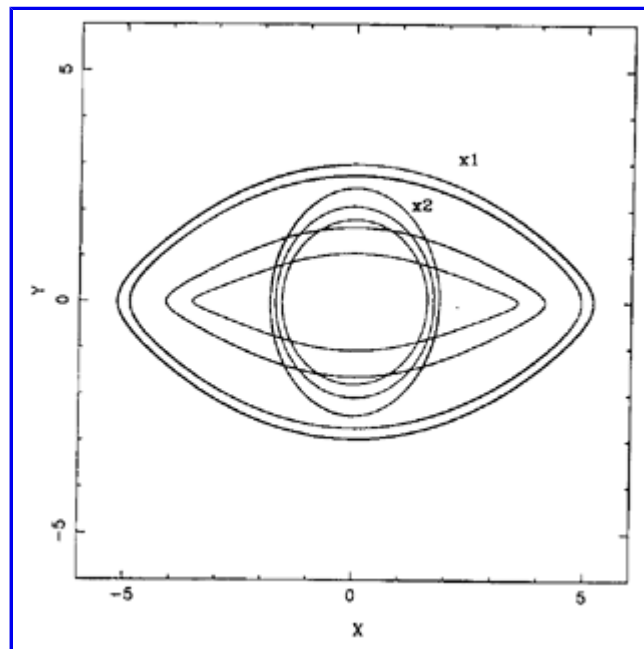


Figure 60. Shape of the main families of periodic orbits in a barred galaxy, (see e.g. [Contopoulos & Papayannopoulos 1980](#)). Some x_1 orbits parallel to the bar are represented, together with some x_2 perpendicular orbits, inside CR.

2. the x_2 family exists only between the two inner Lindblad resonances (ILR), when they exist. They are more round, and elongated perpendicular to the bar. In the same category of $2/1$ orbits (which close after one turn and two epicycles), there are also the x_4 retrograde orbits, and the x_3 unstable orbits, but with less impact for galaxies. The presence or not of nuclear rings appears to be related to the existence of an ILR, as we have discussed in sections [9.7](#) and [9.8](#), and which will be developed later. Even when there exist two ILR's in the axisymmetric sense, the existence of the x_2 family is not certain. When the bar is strong enough, the x_2 orbits disappear. The bar strength necessary to eliminate the x_2 family depends on the pattern speed Ω_b : the lower this speed, the stronger the bar must be.
3. Outside corotation, the $2/1$ orbits that are run in the retrograde sense in the rotating frame are perpendicular to the bar inside the outer Lindblad resonance (OLR), and parallel to the bar slightly outside ([Figure 61](#)). These orbits are also discussed by [Kalnajs \(1991\)](#). Their shape reveals a characteristic figure-eight, that is very similar to the dimpled shape of some outer rings in barred galaxies (see [section 4.1](#) and [Figure 18](#)). When the bar is strong, most orbits perpendicular to the bar between CR and OLR become unstable. That is why this region is often depopulated and, in real galaxies, never includes recent star formation.

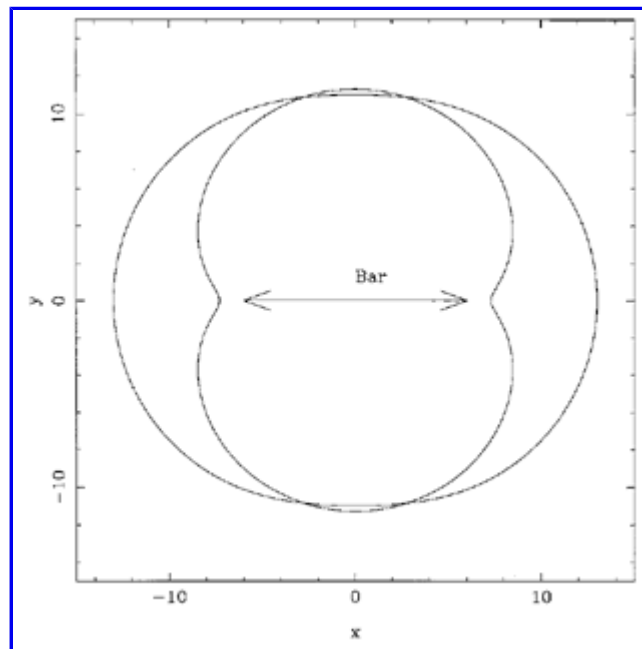


Figure 61. Shape of the two main families of periodic orbits near the outer Lindblad resonance (OLR). The orbit inside OLR is perpendicular to the bar, while the orbits outside OLR are parallel. The first one displays the characteristic dimpling that corresponds to observations of R₁ outer rings.

4. When getting towards corotation (CR) all higher order resonances $\omega' = \kappa / m$ with $m \geq 3$ are encountered. Spanning this region, on the inner or outer side of CR, the periodic families 6/1 and 4/1 are displayed in [Figure 62](#). The 4/1 resonant family is likely to play a role in the formation of inner rings.

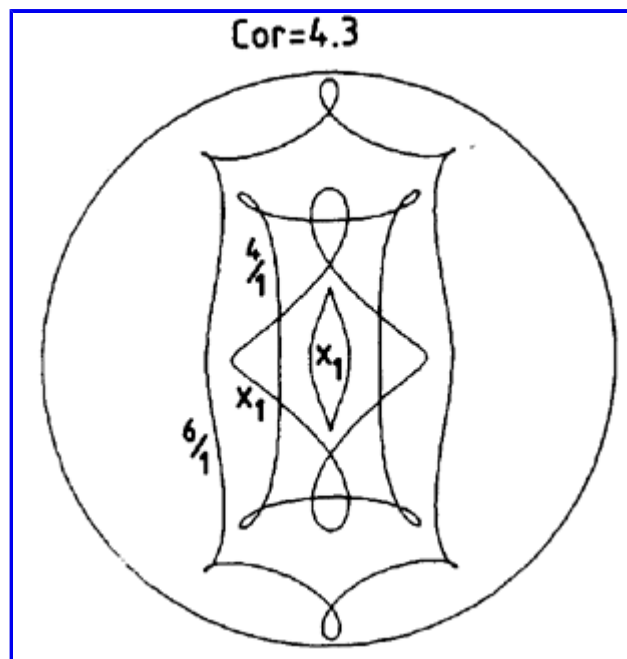


Figure 62. The 4/1 and 6/1 periodic orbits, from [Contopoulos & Grosbøl \(1989\)](#). The bar is vertical, and the circle indicates corotation.

5. Finally, circulating around the Lagrangian points L_4 and L_5 , one can distinguish the banana orbits or long period orbits (LPO), and the short period orbits (SPO).

Consequences for the Bar Dynamics

The main family of orbits building the bar is the x_1 family, elongated along it. We can note however that the stable direct periodic orbits have an orientation either parallel or perpendicular to the bar, and that their orientation rotates by 90° at each Lindblad resonance crossing. The x_2 family, when it exists between the two ILR's, tends to weaken the bar, if the concerned region is large enough. This suggests that a self-consistent bar can barely have one ILR; this is the same conclusion reached from the swing amplification and wave reflection mechanism to form the bar: the presence of ILR's tends to destroy the bar.

The existence of a small zone between the two ILR's where the orbits are not supporting the bar helps to understand the decoupling of a second pattern, rotating faster than the main bar, in the nuclear parts of some barred spiral galaxies. Examples of this decoupling into two patterns can be found in the "nuclear barred" galaxies (e.g. [de Vaucouleurs 1975a](#); [Jarvis et al. 1988](#); [Shaw et al. 1993](#); [Buta & Crocker 1993](#)). The nuclear bar often occurs inside the nuclear ring, corresponding to the ILR (see [section 16](#)).

Beyond corotation, the stable periodic orbits are also perpendicular to the bar, which suggests that a self-consistent bar cannot extend far beyond its own corotation. This has been verified in N-body simulations of barred galaxies (e.g., [Sellwood 1981](#); [Combes & Sanders 1981](#); [Sparke & Sellwood 1987](#)): the longest bars end just slightly before their corotation.

Approaching the corotation region, higher order resonances occur, and the periodic orbits become more and more complex and squarish. The observed shape of face-on early-type galaxy bars is indeed boxy, as was shown for [NGC 936](#) by [Kormendy \(1983\)](#), which compares very well with N-body models (e.g. [Miller & Smith 1979](#)). This squarish shape might measure the importance of the $4/1$ resonance, which will in turn have a strong consequence for inner rings encircling the bars.

11.3. Bars in Early and Late-type Galaxies

[Elmegreen & Elmegreen \(1985, 1989\)](#) have shown that the nature of bars changes along the Hubble sequence. First, spiral galaxies with early Hubble types tend to have bars that are longer relative to the size of the optical disk and the turnover radius of the rotation curve, compared to late-type barred galaxies; second, early-type bars are more uniform in intensity relative to the outer disk light profile, compared to bars in later Hubble types. The spirals surrounding these bars also differ, with a tendency toward grand design two-armed spirals occurring for the early types, while the later types have a more multiple-armed or flocculent structure, as in nonbarred galaxies. The bar and spiral-arm amplitudes differ along the Hubble sequence too, with stronger bars and radially decreasing spiral-arm amplitudes in early type SB or SAB galaxies, and weaker bars with radially increasing spiral-arm amplitudes in late types.

These observations suggest that bars in early-type galaxies extend to corotation, where they drive two-armed spirals at the same pattern speed out to the outer Lindblad resonance, and that bars in late-type galaxies could end well inside CR, possibly as far in as the inner Lindblad resonance for the outer spiral pattern, and that these outer spirals are not always driven by bar.

The problem of the extent of bars has long been debated in the literature. [Contopoulos \(1980\)](#) has argued that bars should extend up to their corotation, or slightly inside, up to the $4/1$ resonance: inside CR, the main stable periodic orbits are parallel to the bar, and bars are composed of slightly elongated orbits trapped around periodic orbits. Periodic orbits are perpendicular to the bar outside CR. Weak bars could still form by crowding effects in that case, but in the case of strong bars, orbits become stochastic outside corotation, which supports the bar confinement inside CR. In N-body simulations, no bar has been seen outside its corotation.

In the point of view developed by [Lynden-Bell \(1979\)](#), and further by [Pasha & Polyachenko \(1994\)](#) and [Polyachenko \(1994](#); see also [Polyachenko 1996](#) and [Polyachenko & Polyachenko 1996](#)), bars are made of near-resonant orbits at the inner Lindblad resonance. The predicted pattern speed is then always below the maximum of $\Omega - \kappa / 2$, since the precessing rate of an elongated orbit is lower than the nearly axisymmetric one, and the pattern speed is now an average of all precessing rates of the orbits in the bar. The bar is also predicted to end near ILR, far before the corotation radius. This scenario has not yet found support from N-body simulations.

[Petrou & Papayannopoulos \(1986\)](#) have also proposed that bars are shorter than their corotation. This was meant essentially to resolve the problem of the position of dust lanes in the concave side of the arms, in strongly barred galaxies. If dust lanes trace shocks experienced by the gas as it enters the arms, their position in the concave side means that the arms are inside corotation. Since they are outside the bar, the latter must end well inside its CR. They claim that in very strong bars, there can exist a $1/1$ resonance, and that orbits become stochastic outside the $1/1$ radius. The bar will then end at this radius, well inside CR. Other solutions have been proposed to solve the same problem; one of them is the existence of two different pattern speeds for the bar and the spiral ([Sellwood & Sparke 1988](#)).

[Combes & Elmegreen \(1993\)](#) have studied by N-body simulations the properties of bars along the Hubble sequence. Basically, two models of galaxies were used, differing by their bulge-to-disk mass ratio (less than 10% for late-types, and equal to 2 for early-types). In any case, the bar pattern speed adjusts as a compromise of the precession rates of all trapped orbits. It is always very near the maximum of the $\Omega - \kappa / 2$ curve, slightly higher at the beginning, and lower at the end of bar formation, when the bar reaches a steady-state ([Figure 63](#)).

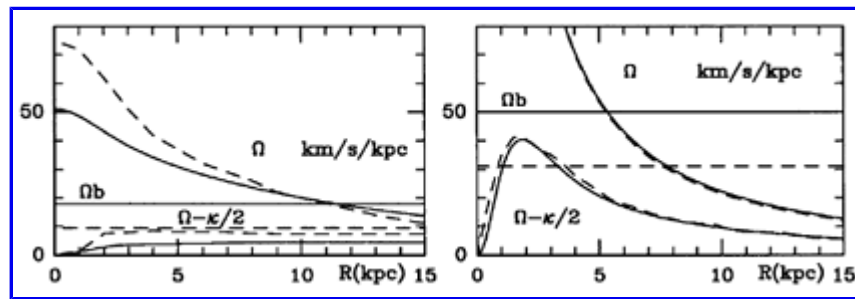


Figure 63. Rotation curves for late and early-type galaxy models, compared with the bar pattern speed. The initial values are full lines, while the final values are dashed lines. Left: late-type model; Right: early-type (from [Combes & Elmegreen 1993](#)).

For early-type galaxies, the bar ends slightly inside corotation, as was frequently observed in N-body simulations. The bar is strong, non-linear, and ergodicity outside CR prevents the bar extension. The bar saturates inside, trapping all possible orbits, which explains the flat-topped profile. Bar growth is slow, however, due to the massive bulge and its stabilizing effect.

For late-types, the bar ends far inside CR, at about the inner Lindblad resonance. The pattern speed is so slow (corresponding to the low precessing rates $\Omega - \kappa / 2$) that corotation is pushed outside of the optical disk. The bar stops growing because of a lack of particles outside corotation which can receive angular momentum (cutting the bar amplification mechanism). The bar has a radial exponential profile, following the optical disk profile, since its growth has prematurely ended (cf. [Figure 64](#)).

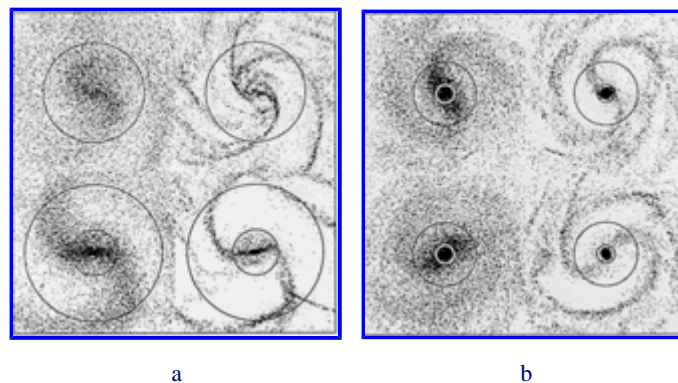


Figure 64. Locations of resonances (ILR and CR, circles) in late (a) and early-type (b) galaxies ([Combes & Elmegreen 1993](#)). In each case, stars are shown at left, and gas at right.

The shape of the bar for late-types is also found to be more squarish ($m = 4$ term larger than in early-types). This can be understood in terms of orbits, since the x_1 orbits supporting the bar are rounder when the axisymmetric background is stronger ([Contopoulos 1988](#)).

11.4. Pattern Speed Determination

If the dynamical theory predicts that rings should occur at Lindblad resonances, the determination of the pattern speed of the bar or spiral wave is essential to check the theory. Reciprocally, *rings are then a precious tool to measure the pattern speed, when the rotation curve is known*. It is, however, necessary to attribute each ring to the right resonance, and therefore to have a hint of the pattern speed order of magnitude.

The dispersion relation in spiral density wave theory ([Lin & Shu 1964](#)) tells us that the waves can exist between ILR and OLR; but there exists however a forbidden gap at CR when the Toomre Q parameter is larger than 1, and this at first oriented models of galaxies with corotation at the edge of optical disks ([Roberts et al. 1975](#)). But waves can tunnel through the gap, the presence of gas can enhance the spiral strength, and the spirals then extend up to OLR as revealed by simulations. The modal solutions also have corotation in the middle of the pattern ([Bertin et al. 1989](#)). The presence of outer rings in barred galaxies, thought to be associated with OLR, also contributed to change this view, and to put OLR at the edge of the optical disk (cf. [section 11](#)). Let us review several methods to determine the value of pattern speeds from observations (see also [Elmegreen 1996](#)).

One of the methods relies on morphology: the crossing of corotation is supposed to correspond to a gap in luminosity for the main arms; also interarm spurs should occur at the inner $4 / 1$ resonance, with roughly an $m = 4$ symmetry (e.g. [Elmegreen et al. 1992a](#)). This method requires very regular spiral structure.

A more straightforward method is based on the change of sign of radial streaming motions across corotation. However, many ambiguities arise when studying a strip along the minor axis. First there is no way to check that the position angle of the minor axis is right, since there are often twists in the outer regions (warps). And as soon as the strip is offset in angle, the tangential motions corrupt the analysis. [García-Burillo et al. \(1994\)](#) have shown through dynamical modelling that the turnover region for the radial streaming sense is very wide, and the method uncertain, when the amplitude of the wave is strong. A related method, also based on streaming motions but taking into account the "geometric phase" phenomenon, has been proposed by [Canzian \(1993\)](#). The map of residual velocities with respect to an axisymmetrical model should display a spiral pattern with one arm inside CR, and 3 arms outside (Figure 65). This has been applied to [UGC 2885](#) and [NGC 4321](#) (Figure 66), but also with some ambiguities.

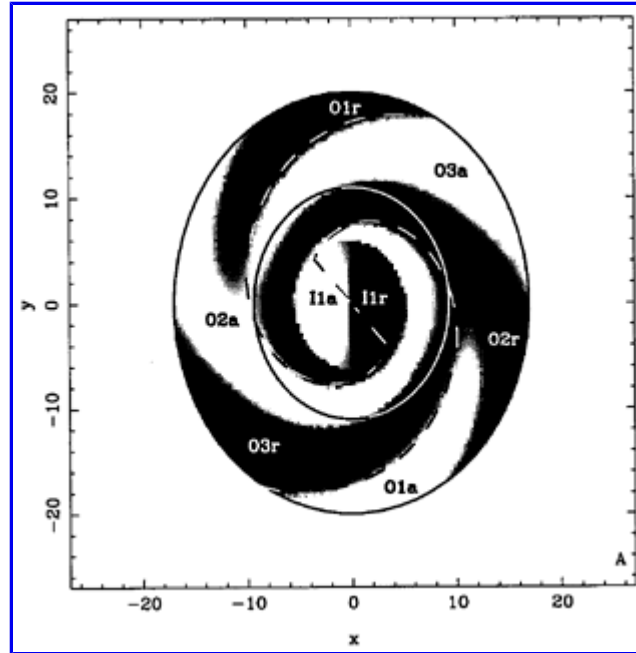


Figure 65. The "geometric phase" method for deriving a pattern speed, as developed by [Canzian \(1993\)](#). Here are plotted the residuals of the velocity field predicted for [NGC 4321](#), based on a model of its spiral structure ([Sempere et al. 1995a](#)): negative residuals are white (labeled "a" for approaching), positive residuals are black (labeled "r" for receding). The major axis of the galaxy is rotated to be vertical, and the inner full circle (ellipse in projection onto the plane of the sky) indicates corotation (arms labeled "1" inside CR and "0" outside CR). The dashed line marks the density maximum in the bar+spiral structure. The residual map reveals one arm inside CR and three outside CR.

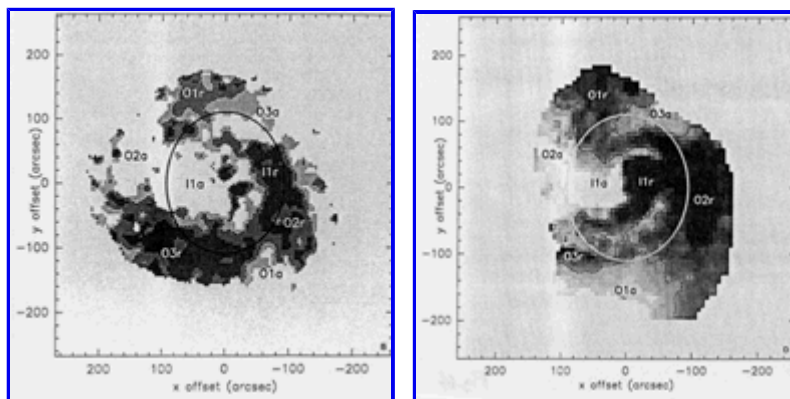


Figure 66. Canzian method to determine the location of corotation, applied to HI observations of [NGC 4321](#). The residual velocity map reveals a one-armed spiral structure inside CR, that shifts to a three-armed one outside CR (from [Sempere et al. 1995a](#)). Negative residuals are white (dashed contours), and positive are black (full contours). Here CR is in the middle of the disk, just outside the bar.

Another method, proposed by [Tremaine & Weinberg \(1984\)](#), is based on the assumption that the mass tracer, stars or gas, obeys a continuity equation. The method only requires the measurement of the surface brightness and the radial velocity along a strip parallel to the major axis. The continuity condition is best fulfilled for stars, but then the method requires absorption-line spectroscopy. The method has been applied to the gas in [NGC 5383](#), but without a firm conclusion. Recently [Merrifield & Kuijken \(1995\)](#) have succeeded in applying the method to the stars in the barred lenticular galaxy [NGC 936](#), yielding CR at the ends of the bar. This galaxy is a favorable case, since there is no gas which could be transformed into stars during a revolution, so the basic continuity assumption of the method is likely to be fulfilled.

Another method has been proposed by [García-Burillo et al. \(1993b\)](#), and consists of modelling the gas dynamical behavior in the potential derived from a red image of the galaxy. The resulting spiral structure appears to depend critically in shape and phase on the pattern speed. This has allowed the determination that CR is midway in the spiral in [M51](#) and [NGC 4321](#). The late-type galaxy [NGC 7479](#), on the contrary, appears to have a bar ending well inside its CR ([Sempere et al. 1995b](#)). A dynamical model of the central Milky Way based on orbit calculations has proposed that a bar exists with an OLR at 4 kpc ([Binney et al. 1991](#)). This value is discussed further by [Weinberg \(1992\)](#) and [Kalnajs \(1991\)](#).

11.5. Angular Momentum Transport

It is easy to show that to minimize its total energy, an isolated galaxy tends to transfer its angular momentum outwards (cf. [Lynden-Bell & Kalnajs 1972](#), hereafter LBK72). In fact, for a given total angular momentum, the least energy state corresponds to solid body rotation. But galaxies are in general in differential rotation, with their angular velocity Ω decreasing with radius. The exchange will tend to give angular momentum to the outer particles with the least Ω , and with the higher specific angular momentum.

[LBK72](#) remarked that only trailing waves can transfer angular momentum outwards, while leading waves have the opposite effect; this explains why trailing waves are preponderant in observed galaxies. Since angular momentum transfer, mediated by non-axisymmetric instabilities, is the motor of secular evolution of galaxies, and of the formation of bars and resonant rings, it is fundamental to summarize here the essential phenomena.

[LBK72](#) stated that, for a steady wave, stars can exchange angular momentum at resonances only: they emit angular momentum at inner Lindblad resonance, while they absorb angular momentum at corotation and outer Lindblad resonance. [LBK72](#) also showed that, while stars do not gain or lose angular momentum on average away from resonances, they are able however to transport angular momentum as lorries in their orbiting around the galactic center. When they are at large radii, they gain angular momentum, while they lose some at small radii: even if the net balance is zero, they carry angular momentum radially, and the sense of this lorry transport is opposite to that of the spiral wave. This phenomenon can then damp the wave, if the amplitude is strong enough. [LBK72](#) noticed that this damping phenomenon became negligible for small wavelengths, i.e. when $kr \gg 1$.

In a recent investigation, [Zhang \(1996\)](#) introduces an equivalent "dissipation" for the stellar component, corresponding to small-angle scatterings of neighboring stars in the spiral arms. This process transforms ordered motions into disordered ones (resulting in increased velocity dispersion, or large epicycle amplitudes), and when collective effects are taken into account, secular modifications of the stellar orbits can result: they can lose energy and angular momentum inside corotation. If this dissipation is taken into account, together with the phase-shift between the stellar density and the potential of the spiral wave, gravity torques are exerted by the wave on the stars, and stars gain or lose angular momentum, even away from resonances.

This angular momentum transfer between the wave and the stars helps the wave to grow in the linear regime, but soon due to the collective dissipation process, it will contribute to damping and saturation. The wave is not quite steady. [Zhang \(1996\)](#) has shown that the stellar density azimuthal profile steepens with time, indicating the presence of large-scale gravitational shocks. The result of the secular evolution is a global redistribution of mass: stars inside corotation lose angular momentum and move to smaller radii, which steepens the radial density profile in the disk. This has been observed during many N-body simulations of a stellar disk that has obtained a long-lived spiral pattern (e.g. [Donner & Thomasson 1994](#)).

Expressions for the Torque and Phase-shift

It is obvious that the torque exerted by the wave on particles is a second order term, since the tangential force $\delta V_1 / \delta \theta$ is first order, and has a net effect only on the non-axisymmetric term of the surface density $\sigma_1(r, \theta)$. The torque $T(r)$ applied by the wave on the disk matter in an annular ring of width dr , can be expressed by:

$$T(r) = r dr \int -\sigma_1(r, \theta) \delta V_1 / \delta \theta d \theta \quad 9$$

([Zhang 1996](#)). In this formula, it is easy to see that the torque vanishes if the density and potential spiral perturbations are in phase. But there must be a phase-shift in the general case, according to the Poisson equation. The potential is non-local, and is influenced by the distant spiral arms. So the sign and amplitude of the phase-shift depends on the radial density law of the perturbation. It has been shown by [Kalnajs \(1971\)](#) that the peculiar radial law in $r^{-3/2}$ for an infinite spiral perturbation provides exactly no phase-shift. The phase-shift is such that the spiral density leads the potential if the radial falloff is slower than $r^{-3/2}$, and the reverse if it is steeper.

Now in a self-consistent disk, the phase-shift given by the Poisson equation must agree with that given by the equations of motion. Through the computation of linear periodic orbits in the rotating frame, [Zhang \(1996\)](#) has found that the forcing consists of two terms in quadrature, and that the phase-shift δ of the orbit orientation with respect to the forcing potential has the expression:

$$\tan(m\delta) \approx -2\Omega / [(\Omega - \Omega_p)kr] \quad 10$$

This shows that in the WKB approximation, the phase-shift is negligible ($kr \gg 1$), and that it changes sign at corotation. The fact that the torque is a non-linear effect, and vanishing in the WKB approximation, may explain why it was neglected before, but it has a quite important effect in galactic conditions. Inside corotation, we expect that the density leads the potential, and the contrary outside corotation.

The amplitude of the density-potential phase-shift can be estimated through N-body simulations: [Figure 67](#) shows the results of a Fourier analysis of the $m = 2$ component, in a purely stellar simulation (2-D polar grid particle mesh with 10^5 particles). In this simulation, initial parameters were chosen such as to stabilize the stellar disk with respect to bar formation through the presence of an analytical bulge component of mass equal to the mass of the self-gravitating stellar disk. A bar eventually developed, but was delayed until 2×10^9 yrs, i.e. ≈ 20 dynamical times. In the mean time, a spiral wave developed, and remained for several dynamical times. Its power spectrum revealed a well-defined pattern speed, at least up to corotation (≈ 7 kpc). We can see in [Figure 67](#) that the phase-shift between stellar density and potential is quite high, up to 28° inside corotation, where it is most meaningful.

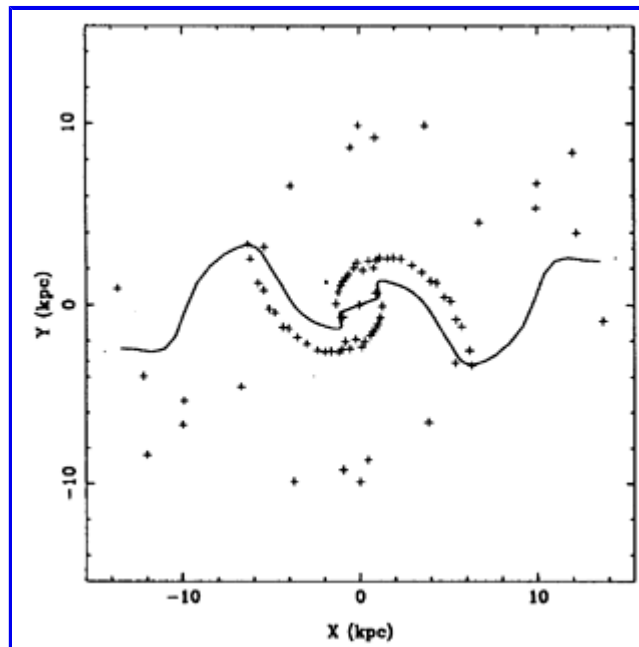


Figure 67. Results of the Fourier analysis of the stellar density (crosses) and potential (full line) in a purely stellar N-body simulation, while a spiral structure rotates in the disk. Plotted here are the phases of the pattern at each radius. The density leads the potential almost everywhere inside corotation. The perturbation is weaker outside corotation.

Consequences for Wave Growth

The exchange of angular momentum between the stars and the wave, which takes angular momentum to the stars inside corotation, and deposits it in the outer parts, helps the wave to grow spontaneously in the linear regime. But as soon as the amplitude of the wave is large enough to enter the non-linear regime, the angular momentum is transferred at an ever increasing rate to the particles in the disk; this no longer benefits the wave, whose amplitude levels off, but dissipation, through spiral arm shocks and particle scattering in the dense spiral arms, makes the wave weaken and fade. This collective dissipative process is induced by the phase-shift between particles and wave, which is nonexistent for a bar. The latter can therefore be robust and long-lived in a collisionless ensemble of particles (galaxy disk without gas).

Gas Component

The mechanism of the angular momentum transfer for the gas is the same as that previously described: the gas settles in a spiral structure which is not in phase with the potential ([Figure 68](#)). Gravity torques are exerted by the wave on the gas. The dissipation here is of course different, since the gas radiates away its energy. The gas component is then maintained cool and responsive to new gravitational instabilities. This is the source of more drastic secular evolution, with the possibility of the whole gas component inflowing towards the center.

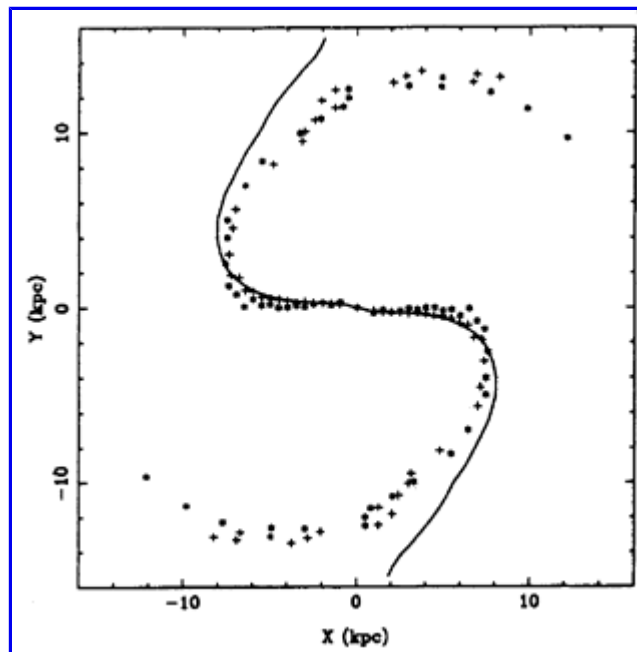


Figure 68. Same as [Figure 67](#) for an N-body simulation taking into account gas and stars, and where a bar develops. The phases of the gas pattern are indicated by asterisks, while crosses indicate the stars, and the full line the potential. Now the potential is in phase with the stellar density in the bar, and leads the density in the spiral outside corotation.

12. GAS FLOW IN BARRED GALAXIES

Numerous authors have investigated the behavior of gas in hydrodynamical models, since the early 1970's. Unfortunately, the results appear to depend on the details of the modelling, either as a continuous fluid, dominated by pressure forces, or as ballistic particles, experiencing a few dissipative collisions per orbit. Early simulations have nicely modelled the spiral structures and the associated shocks, but have overlooked ring formation.

12.1. Hydrodynamic Modeling

The most straightforward way to represent the interstellar medium (ISM) is as a continuous diffuse fluid, essentially governed by pressure forces. This simple model is based on the large-scale atomic gas observations (HI line at 21cm), although this quite diffuse phase appears to be composed of individual clouds at small-scale (see [Burton 1992](#) for a review). In fact, the ubiquity of the HI component is the source of heavy blending and saturation that makes the HI emission appear pervasive and continuous, washing out the discrete, cold and dense hydrogen clouds. Another view of the ISM is gained from molecular cloud studies, essentially from the CO line at 2.6mm, tracing the H₂ molecule that has no radio rotational line for symmetry reasons. Molecular clouds are highly clumpy, and show that most of the mass of the ISM has a very low volume filling factor. Current views of the ISM are therefore based on self-similar structures, a hierarchy of clouds over several orders of magnitude in scale ([Falgarone et al. 1992](#); [Pfenniger & Combes 1994](#)). These clouds are supported by gravity, and pressure forces could then concern only the smallest scale, much below the parsec size. There coexist several phases in the ISM, with different densities and temperatures, from the cold molecular component (10K), the warm neutral and ionized phases (8000K), to the hot coronal gas (10⁶ K) as emphasized by [McKee & Ostriker \(1977\)](#). However, most of the mass appears to be by far in the cold phase, and a view based on slightly dissipative ballistic clouds emerges. Energy is poured into this medium from the nuclear energy released in stars: supernovae explosions, stellar winds, bipolar flows, etc.

The continuous gas picture has also been favored by the observation of conspicuous dust lanes along spiral arms and bars. These very narrow features, where gas and dust appear to be compressed and the density enhanced, are highly suggestive of shocks. These large-scale shocks, however, do not concern most of the mass in the ISM. The hot phase, the coronal gas, is much too hot to be affected by shocks. The ensemble of molecular clouds could behave as a fluid, with clouds acting as "molecules" ([Cowie 1980](#)), but the collisional time-scale is larger than the crossing time of spiral arms, and the ensemble does not really act as a fluid ([Casoli & Combes 1982](#)). Only the warm and diffuse phase will be trapped in a shock, and its high compression will result in conspicuous thin dust lanes along the leading edges of the bar and spirals (e.g. [Elmegreen 1989](#)).

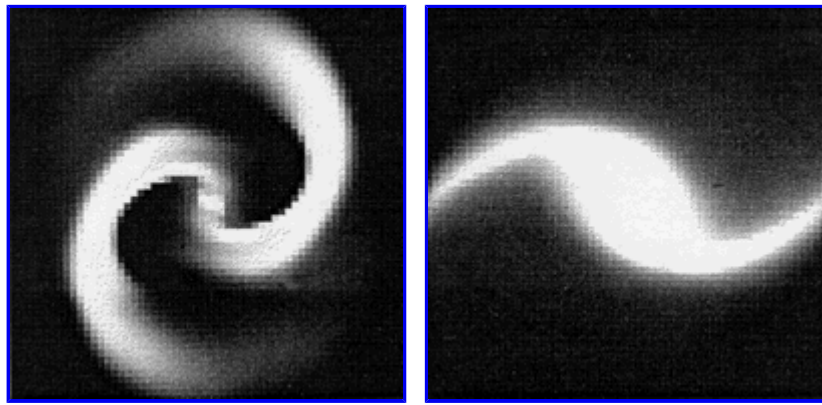


Figure 69. Hydrodynamic simulations reveal that a bar potential can drive spiral structure in the gas component, from [Sanders & Huntley \(1976\)](#). The gas spiral turns by 90° at each resonance. The model in the right panel includes an ILR, while that in the left panel does not. The bar is horizontal in each case.

The first attempts to simulate gas in barred galaxies were done with the continuous fluid model (e.g. [Sanders & Huntley 1976](#), with the beam scheme). The simulations treated gas as test particles moving in a fixed bar potential. The gas revealed a beautiful spiral structure driven by the bar (see [Figure 69](#)). This behavior can be interpreted with the help of the periodic orbit families in a bar potential. We know that the main stable orbits are either aligned parallel or perpendicular to the bar, and that they change orientations by 90° at each resonance. The gas will first tend to follow these orbits, but the streamlines of gas cannot cross. Since periodic orbits do cross, gas clouds can encounter enhanced collisions, such that their orbits are changed. Instead of experiencing sudden 90° turns, their orbits will smoothly and gradually turn, following the schematic diagram of [Figure 70](#): regularly tilted elongated orbits are a vivid illustration of density waves ([Kalnajs 1973](#)).

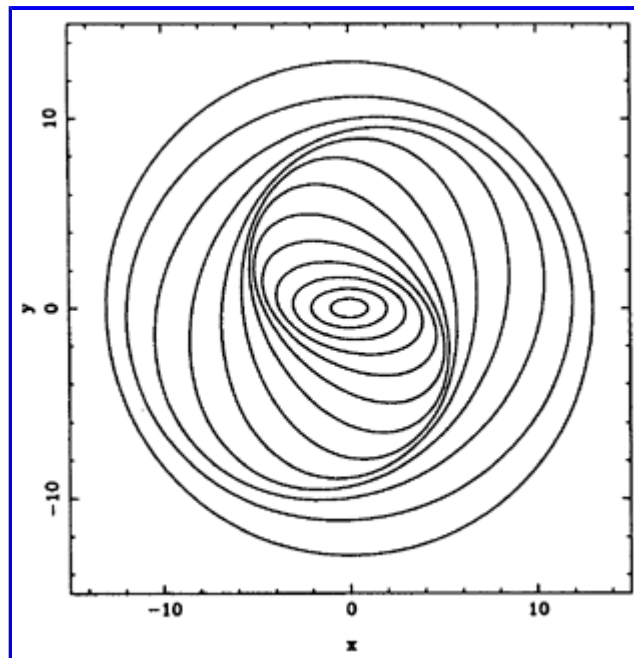


Figure 70. Elongated orbits, gradually tilted, illustrate how the gas streamlines can form the spiral wave (following [Kalnajs 1973](#)).

This interpretation predicts that the arms will be more wound when there exist more resonances; there will be a winding over 180° with only CR and OLR, with the gas aligned with the bar until corotation. When there exist 2 ILR's, the gas response can be perpendicular to the stellar bar. When there is barely one ILR, strong shocks can occur on the leading edge of the bar, corresponding to the offset dust lanes observed in barred galaxies ([Sanders & Tubbs 1980](#); [Schempp 1982](#)). Other continuous gas models have been widely used, with and without gas self-gravity; for example, SPH, finite difference codes, and flux-splitting second order schemes ([van Albada 1985](#); [Athanasoula 1992](#); [Wada & Habe 1992](#); [Friedli & Benz 1993](#); [Heller & Shlosman 1994](#); [Teuben 1996](#)). Although these hydrodynamical codes simulate successfully the spiral structure, they are affected by a high viscosity, in large part of numerical origin. In particular, an artificial viscosity is added in order to treat shock waves, and to spread the shock over a few resolution cells. Gas is driven to the central parts very quickly, in spiraling streamlines, and the long time-scale gas behavior cannot be reproduced. This long time-scale is required to form outer ring structures.

The other technique used in galaxy hydrodynamics modeling is the "sticky particle" approach, which involves an ensemble of gas clouds moving in ballistic orbits. The individual clouds are free to collide, without extra pressure and viscosity terms (Schwarz 1981, 1984a, b; Roberts & Hausman 1984; Combes & Gerin 1985; Palous et al. 1993; Byrd et al. 1994). In these models, dissipation does not dominate the dynamics, and the long-term behavior can be followed more realistically. There are no large-scale shocks, however. We note that the SPH technique, which considers individual particles with a finite size, is somewhat intermediate between the two approaches: it will approach the fluid behavior only asymptotically for large particle numbers.

12.2. Formation of Rings

The most successful theory is that *rings are formed by gas accumulation at Lindblad resonances, under the continuous action of gravity torques from the bar pattern*. This long-term behavior has been revealed essentially by the sticky particle simulations. Since the potential is non-axisymmetric, tangential forces are exerted on the gas. If the gas is moving on circular orbits, these forces will cancel out by symmetry, and no net torque will be produced. This is also the case for orbits aligned parallel or perpendicular to the bar. On the contrary, when the gas is distributed in a spiral shape, orbits are inclined with respect to the symmetry axis of the bar. This results in a net torque on the gas, which is schematically represented in Figure 71. The torque changes sign at each resonance, where the spiral turns by 90°. Between the ILR and corotation, the torque is negative, while between CR and OLR, the torque is positive. These torques tend to depopulate the corotation region, and to accumulate gas towards the Lindblad resonances, in the shape of rings. Indeed, these rings then are aligned with the symmetry axis of the bar, and *no net torque is acting on them*.

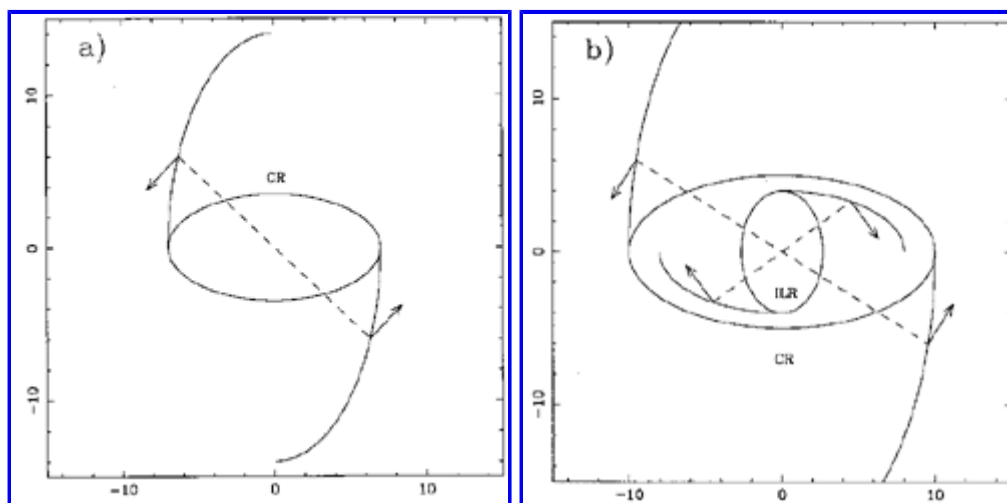


Figure 71. Schematic representation of the gravity torques exerted by the bar on the gaseous spiral: a) between CR and OLR, the gas acquires angular momentum and is driven outwards; b) between CR and ILR, the gas loses angular momentum (cf. Combes 1988).

Schwarz (1981, 1984b) was the first to demonstrate the efficiency of these gravity torques to form rings, via numerical simulations. He developed a sticky particle code, where gas clouds are test particles in a fixed barred potential, moving like free particles, except when their trajectories cross and inelastic collisions are introduced. The reduced viscosity of the code allows us to see gas being driven outwards, from CR to OLR, instead of being dominated by viscous torques, that would have driven all the gas towards the center, irrespective of its location in the galaxy. Figure 72 shows in a very convincing way the formation of outer rings. The time-scale for this formation is quite long, being proportional to the rotation period in the concerned radii, which at OLR is of the order of a few times 10^9 yrs. Of course, this time-scale is longer for a weaker bar, with weaker torques.

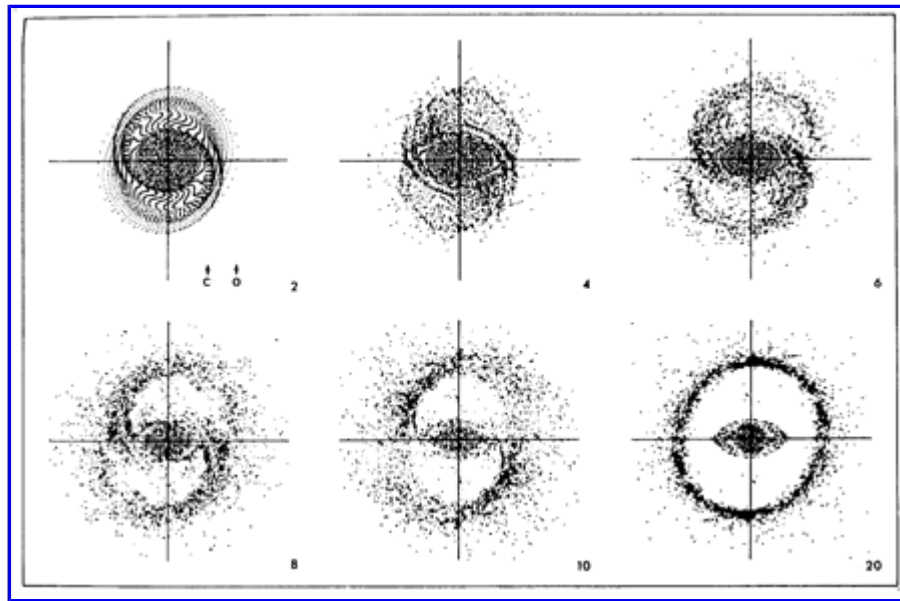


Figure 72. Simulations of sticky particles by Schwarz (1979, 1984b) revealing the formation of an outer ring at OLR.

Schwarz (1981) showed that two kinds of outer rings can be obtained, according to the initial distribution of the gas; both are shown in Figure 73. If the gas is more centrally concentrated, the outer ring is perpendicular to the bar, and takes the figure-eight shape characteristic of the $2/1$ resonant periodic orbits slightly inside OLR. If the gas distribution is initially more extended, then the outer ring is parallel to the bar, and takes the shape of the other $2/1$ resonant orbits slightly outside OLR. These two types of outer rings exist and have been called R'_1 and R'_2 , respectively, by Buta (1986a) and Buta & Crocker (1991); they were illustrated and discussed in section 4.1. It is noteworthy that Schwarz found the parallel-aligned variety of outer ring to be more robust than the perpendicular-aligned variety, stating that it was always favored when there was even a little gas outside the OLR. However, as was shown by Buta (1995), in real barred galaxies the R'_1 variety is more commonly observed than the R'_2 variety.

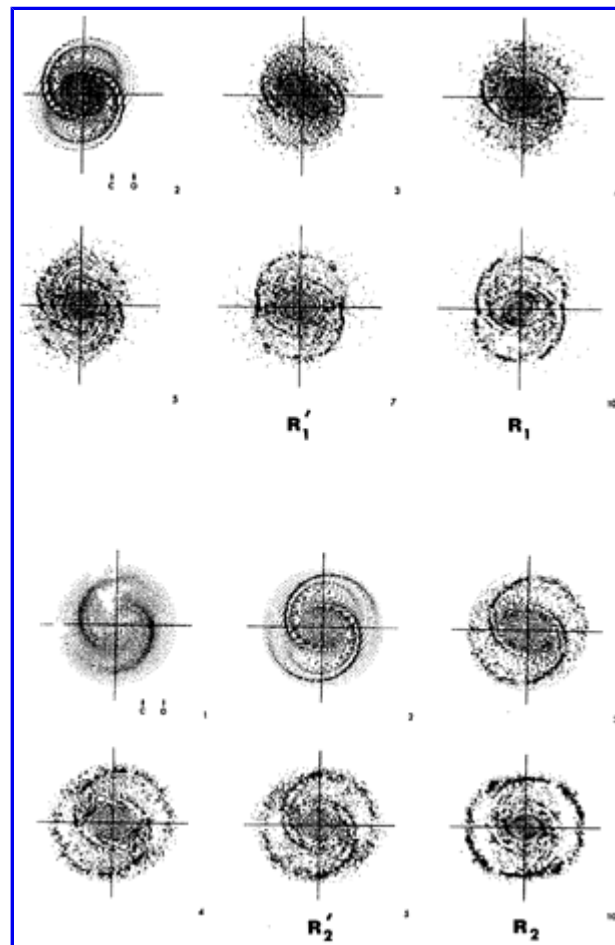


Figure 73. Simulations of sticky particles by [Schwarz \(1981\)](#) revealing the formation of two possible types of outer pseudoring at OLR. The two sets of simulations shown differ only in the assumed initial distribution of gas particles. The upper set led to formation of an R_1 -type outer ring, while the lower set led to formation of an R_2 -type outer ring. The outer rings slowly evolve from pseudorings. The number of bar rotations is at the lower right of each frame, and the locations of corotation (C) and OLR (O) are indicated.

The formation of outer rings and pseudorings has also been investigated by [Byrd et al. \(1994\)](#), who extended Schwarz's simulations by using a larger number of particles, an improved collision scheme which tracked individual particles to determine when they collide, and different rotation curves. They found that outer rings (mainly those of type R_2) are more easily produced with fast bars (since there is then enough matter at OLR). Besides also verifying Schwarz's results, this study identified a possible evolutionary sequence whereby outer rings begin as R_1 pseudorings, evolve into R_2 pseudorings, and then evolve into detached closed outer rings (see [Figure 74](#)). This study also helped to elucidate the possible origin of the R_1R_2 morphology which was discussed in [section 4.1](#). This combination morphology of the two ring types was not found in Schwarz's simulations, but traces of it are seen in Byrd et al.'s highest pattern speed simulation (see upper left frame of [Figure 74](#)). The general lack of formation of this type of structure in simulations might only be due to the non-introduction of star formation out of the gas in the models. Indeed, the ring formation only involves gas. The stellar component is not following the accumulation of gas at resonances, since the stellar orbits are parallel to the symmetry axis of the bar. But new stars will be formed out of the gas in rings, a process that will grow more effective as the gas density there is enhanced. When the gas is then locked up into stars, it will no longer be as sensitive to the gravity torques as in the simulations, and will stay in the rings formed. The remaining gas will then lose a little energy by dissipation, and falls on the next orbit in energy, which is inside OLR forming the R_1 ring.

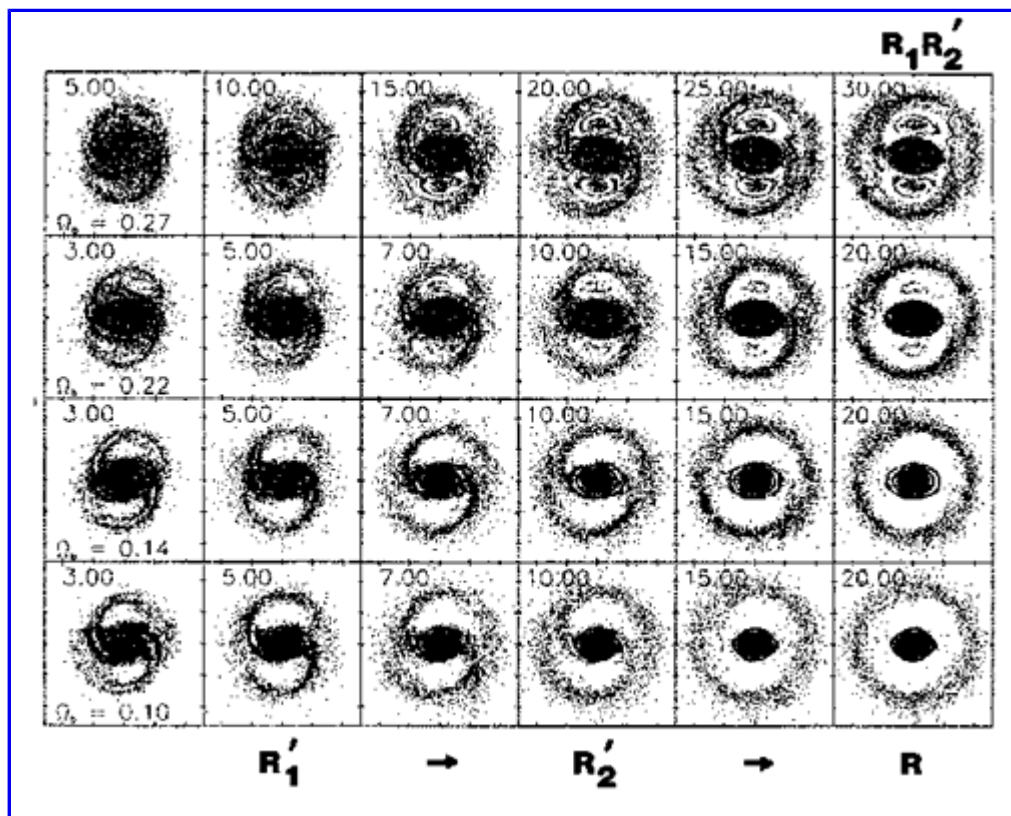


Figure 74. Time sequences in the evolution of a barred galaxy from [Byrd et al. \(1994\)](#). This demonstrates the possible evolution between the R_1 and R_2 subclasses of outer rings in the sense that the former precedes the latter in development. Each set of six frames is for a different dimensionless pattern speed indicated in the left panels. The time in bar rotations is indicated in each frame.

In support of these ideas, [Byrd et al. \(1994\)](#) pointed out the existence of a subtle dichotomy in the R_1R_2' galaxy IC 1438. In this galaxy, the R_1 component is most prominent in a near-IR image, while the R_2 component is most prominent in a blue light image or a $B - I$ color index map. The dichotomy suggests that the R_1 component formed first and left behind a stellar remnant. Such an arrangement seems to support the evolutionary sequence shown in [Figure 74](#), and the need for allowing for star formation to explain the R_1R_2' morphology in some cases. [Crocker et al. \(1996\)](#) also found evidence in support of the $R_1 \rightarrow R_2$ sequence in the distributions of HII regions in several early-type ringed galaxies with strong stellar R_1 components (see [section 9.5](#)).

With regard to the periodic OLR orbits that lead to the R_1 and R_2 rings, [Kalnajs \(1991\)](#) has proposed that the Hyades and Sirius star streams may be connected with crossing periodic orbits near the OLR in our Galaxy. The Sirius stream would be outside the OLR while the Hyades stream would be inside. This is interesting, and not unlikely given the location of the Sun at a radius comparable to some outer rings in galaxies.

A sticky-particle simulation which shows an especially well-defined inner ring was illustrated by [Simkin et al. \(1980\)](#); see [Figure 75](#). [Schwarz \(1984a, b\)](#) proposed that the inner ring in this and his other simulations corresponds to gas accumulated at the inner $4/1$ ultraharmonic resonance (UHR) just slightly inside corotation. In its motion towards the ILR due to the bar torque, some gas can stop at the UHR, where the orbits are parallel to the bar. The gas gathers into the largest periodic orbit near UHR which does not cusp and which does not intersect another orbit. The symmetry of the orbit then shields it from the torques. Formation of a UHR ring depends on the bar field being strong enough near UHR to cause spiral shocks. When the bar field near UHR is weak, the periodic orbits at UHR do not intersect, and no ring forms there.

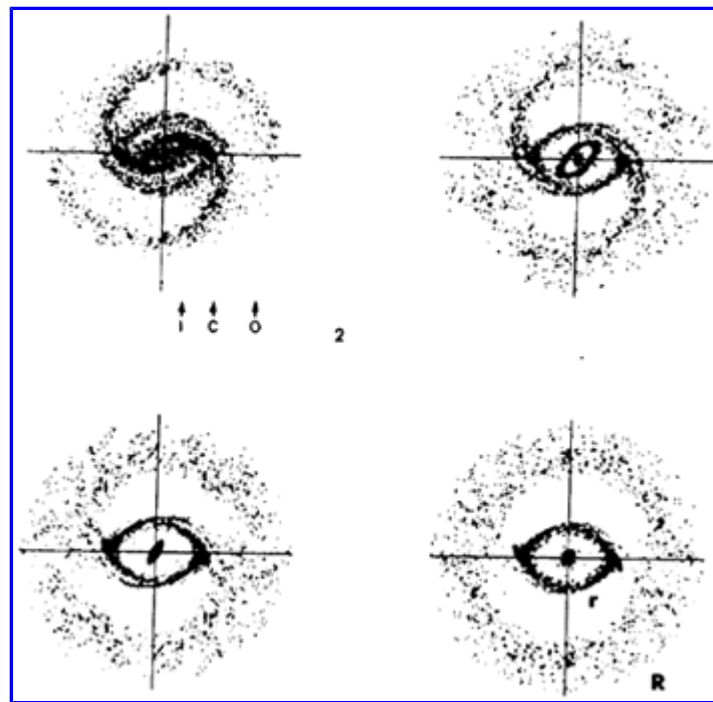


Figure 75. Simulation of an inner ring in an "inverted isochrone" potential from Schwarz (1979) and Simkin et al. (1980), showing the evolution from a spiral pseudoring (upper left) to a more closed ring pattern (lower right).

The simulated inner rings tend to be rather oval and sharp-cornered with a rough diamond shape and a pointy major axis. The UHR rings begin as pseudorings and develop a four-part structure before evolving into a pointy oval (as in Figure 75). Evidence that the UHR is the right interpretation for real inner rings and pseudorings comes from the shape of some of these rings, which are in general elongated along the bar (section 9.3), and which are sometimes pointy-ended as in NGC 6782 (see Figure 76) or sectioned into four parts as in NGC 1433 (Buta 1986b, see Figure 3). From Figure 75, the inner pseudoring in NGC 1433 could be in an earlier stage of development than the pointy oval inner ring in NGC 6782 or the inner ring in NGC 3081 (Figure 49). We have already pointed out, however, that the inner rings in these three galaxies are extreme in shape. Schwarz (1985) investigated a way of making the inner rings in his simulations come out rounder than in Figure 75. By adding a lens-like component to the background, he was able to achieve rounder, less pointy inner rings.

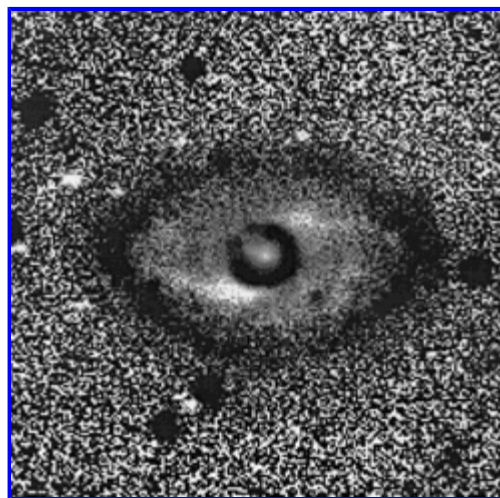


Figure 76. The inner ring of NGC 6782 is a pointy oval in this $B - I$ color index map, similar to what simulations have predicted for a ring formed at the inner $4/1$ UHR.

The ratio of radii of outer and inner rings in most barred galaxies that exhibit both types agrees well for $R(\text{OLR}) / R(\text{UHR})$ for flat rotation curves: the expected ratio is 2.6 compared to the observed average ratio of 2.2 (Athanasoula et al. 1982; Buta 1995, see Figure 27). We can see this characteristic ratio in the simulation in Figure 75.

Nuclear rings are even more easily formed, since the time-scale is quite short: a few 10^7 to 10^8 yrs (see [Figure 77](#)). They require the existence of at least one ILR. But various shapes can be obtained, according to the assumed pattern speed of the bar: the nuclear ring can be parallel to the bar, tilted in the leading direction, or even perpendicular to the bar ([Schwarz 1984b](#); [Combes & Gerin 1985](#); [Byrd et al. 1994](#)). Its ellipticity can take a wide range of values. In the long run, the inner rings are depleted to the benefit of nuclear rings. *The persistence of inner rings in observed galaxies suggests that fresh gas is continuously provided to the galaxy, either from the gas released from high mass star formation, or by continuous infall of external gas.*

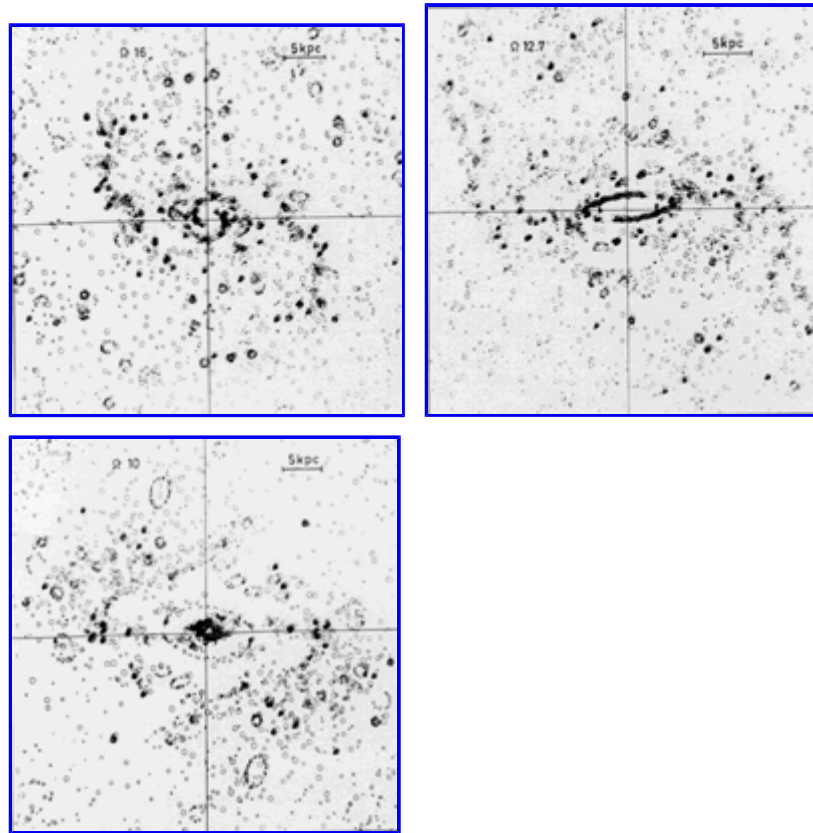


Figure 77. Formation of nuclear rings for different bar pattern speeds (from [Combes & Gerin 1985](#)). a) $\omega_b = 16$ km/s/kpc, there exists just one ILR, the nuclear ring is quite round; b) and c) $\omega_b = 12.7$ and 10 km/s/kpc, there exist two ILR's; note that the gas accumulates at the inner ILR to form the nuclear ring, since a leading spiral arm has developed in the very center (cf. [Figure 79](#)).

When there exist two ILR's, the gas accumulates at the inner ILR ([Combes & Gerin 1985](#); [Piner et al. 1995](#)), which can be very close to the center (inside 1 kpc, typically). This can be explained either by the gas dissipation, since viscous torques are becoming less negligible towards the center, or by gravity torques. In fact, the transient spiral that forms between the two ILR's is a mixture of leading and trailing waves, and close to the inner ILR, the leading one dominates. The gas distribution, which is very concentrated in the center, favors the leading wave, and the dominant torque is negative.

The nuclear rings are so small that they represent a huge accumulation of gas, with large surface densities. This leads to starbursts that are frequently observed as hot spots of giant HII regions, or non-thermal radio emission: typical examples are [NGC 1097](#) ([Hummel et al. 1984](#); [Gerin et al. 1988](#)), [NGC 4314](#) ([Wakamatsu & Nishida 1980](#); [Garcia-Barreto et al. 1991](#)), and others discussed in sections 9.5 and 9.7. Some nuclear rings are so small (of the order of 100 pc scale, e.g. [M82](#), [Lo et al. 1987](#)) that viscous torques, or even dynamical friction of giant molecular clouds (of mass up to $10^7 M_\odot$) on the bulge could produce large gas flows towards the center, and fuel an active nucleus. A correlation has been found between the existence of bars and activity in the nuclei ([section 8](#)), and in particular the presence of a nuclear ring (e.g., the jets in [NGC 1097](#), [Wolstencroft et al. 1984](#)). The presence of two ILR's, in shifting the gas response with respect to the stellar bar, enhances the negative gravity torques on the gas, that is now leading the bar. This considerably enhances the nuclear gas flows ([Combes 1994](#)). When the mass concentration is high enough in the center, another pattern can develop inside the nuclear ring, as will be described in [section 16](#).

12.3. Role of Viscosity

In the above dynamical mechanism for the formation of rings, gas plays the essential role, because of its dissipative character. Even

considering the case of a non-self-gravitating disk, spiral structure is hardly driven in the stellar component by a bar potential. Stellar particles will first follow a very transient spiral structure by crowding of orbits in the relaxation phase, and then will settle around the periodic orbits, aligned either parallel or perpendicular to the bar, but along its symmetry axes. There will then be no gravity torques exerted on the stars, and no angular momentum transfer. In a self-gravitating disk, gravitational instabilities contribute to heat the disk, so that a pure stellar disk soon becomes dynamically hot and cannot sustain a long lasting spiral structure. The dissipative gas component is therefore required to cool down the disk, and maintain the spiral structure. This induces a phase-shift between the density and the potential, and gravity torques act to transfer angular momentum, which is at the basis of ring formation.

But if dissipation is present, the action of viscous torques themselves could play a role in the radial flow of gas. The idea was already mentioned by [Randers \(1940\)](#), and has been widely developed in the context of accretion disks (e.g. [Frank et al. 1985](#)). [Lynden-Bell & Pringle \(1974\)](#) showed that the evolution of any gaseous disk can be characterized by an expansion of the outer parts, which carry most of the angular momentum, and consequently a collection of an ever increasing mass towards the center. At the limit, a negligible mass is ejected and takes away all the angular momentum. This comes from the fact that for a given total angular momentum, the least energy of a rotating disk is obtained for a uniform rotation.

Most galaxies are in differential rotation, and the angular velocity ω decreases with radius. In viscous exchanges (collisions) particles in the outer parts will gain angular momentum and energy, in order for the galaxy to tend to the uniform rotation state of least energy. But the specific angular momentum (per unit mass) is a monotonically increasing function of radius. Therefore, angular momentum is distributed to the regions of the disk that are already richer in angular momentum, and this is not a stable process. To remain in equilibrium, the matter that receives angular momentum has to increase its radius. This implies also that its speed ω decreases, and the system is going away from the desired uniform rotation state. The process is divergent, and no equilibrium will be reached until all the matter has fallen towards the center.

How does the viscosity act to make the system evolve this way? We have only advanced until now energetic principles. Viscosity (or equivalently here cloud collisions) produce shearing forces on each gaseous ring, that compose to produce a torque. Shearing forces tend to cancel the relative velocity between two adjacent gaseous rings. Since ω is decreasing with radius, the torque will transfer angular momentum to the outer parts. The ideal state, where there would be no viscous forces, is again the uniformly rotating disk. The analysis above demonstrates however that uniform rotation is unstable in the presence of viscosity.

Viscous torques then provide a mechanism to form gas rings in galaxies: [Icke \(1979\)](#) noticed that if the rotation is sufficiently uniform inside the turnover radius of the rotation curve (R_{\max}), then the shear is zero inside, and viscous torques external to the turnover radius will accumulate gas in a ring at R_{\max} .⁽⁴⁾ The ring is short-lived, however, since all the gas is bound to go towards the center. But the time-scale of this process is longer as the rotation is more uniform in the center. Simulations of the effect of viscous torques in galactic disks have succeeded in forming a gaseous ring at turnover ([Icke 1979](#); [Silchenko & Lipunov 1987](#); [Lesch et al. 1990](#)). The ring is smooth, with no sharp boundary, and is reminiscent of the molecular ring in the Milky Way, between 4 and 8 kpc. Its radius is shrinking with time. If it is possible that viscous torques can explain some of the rings observed, they cannot account for the presence of several sharp rings in the same galactic disk, and especially *not* the outer rings.

In addition, the efficiency of viscous torques has only been assumed in those simulations, but not firmly established. The physical nature of viscosity in gaseous galactic disks is not well known. To transfer angular momentum over large scales, large relative velocities are required. The molecular viscosity is of course negligible. But there are large random velocities between interstellar clouds, which are supported by star formation energy. These motions give rise to the turbulent viscosity. The estimation of the efficiency of viscous torques in galactic disks was attempted by [Lynden-Bell & Pringle \(1974\)](#), who concluded that viscosity had little importance over a Hubble time. The estimated time-scales were $\approx 10^9$ yrs at 1 kpc radius, and $\approx 10^{11}$ yrs at 10 kpc.

An interesting idea is that the viscosity is gravitational in origin: large-scale instabilities heat the gas component, and fuel small-scale random motions, like the local effective viscosity of [Lin & Pringle \(1987\)](#). The gas has the tendency to reduce its velocity dispersion by dissipation. When this dispersion δV falls below the critical value c_r necessary to ensure stability against axisymmetric perturbations (i.e., the parameter $Q = \delta V / c_r$ falls below 1), then instabilities occur in the disk, and stir up the random motions of the gas. This acts as a feedback mechanism to maintain large velocity dispersions.

Attempts to estimate the efficiency of viscous torques in gas simulations in galaxies have always led to the conclusion that gravity torques dominate over viscous torques in the transfer of angular momentum ([Combes et al. 1990a](#); [Barnes 1991](#)). The corresponding time-scale is one or two orders of magnitude shorter ([von Linden et al. 1994](#)). The best proof of the predominance of gravity torques is the formation of outer rings, by accumulation of gas at the OLR. The effect of the viscous torques is only to bring the gas towards the center, while in the simulations the gas is driven outwards, from CR to OLR.

⁴ We have already pointed out the existence of real "turnover" rings in galaxies in [section 9.8](#); however, the existence of these rings does not automatically support the viscous mechanism since the turnover radius is also the ILR in general. Therefore, the location of the inner/nuclear ring cannot discriminate the two theories. [Back](#).

12.4. Fueling the Nucleus

Gravity torques from the bar can drive very efficiently the gas towards the center, and it has been proposed that non-axisymmetric potentials are the main agent to bring gas towards active nuclei, to fuel their strong energetic activity (Simkin et al. 1980). However, as emphasized by Combes & Gerin (1985), the gas is in general efficiently driven to the inner Lindblad resonance, where it accumulates, but not to the very center. We can try to understand schematically, in terms of orbits, the sense of winding of gaseous spiral arms in the center, and consequently the sense of gravity torques.

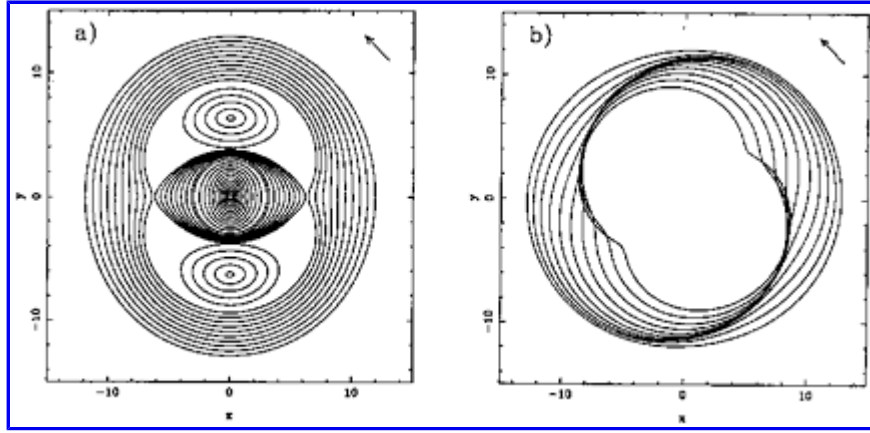


Figure 78. a) Periodic orbits in a $\cos 2\theta$ potential. Their orientation rotates by $\pi/2$ at each resonance. b) The gas tends to follow these orbits, but is forced to precess more rapidly while losing energy and angular momentum.

In a $\cos 2\theta$ bar potential, the main families of periodic orbits are aligned or anti-aligned to the bar, according to the position with respect to Lindblad resonances (see Figure 78). Due to cloud collisions, the gas component cannot follow these periodic orbits; instead, upon losing energy, the gas streams in elliptical trajectories at lower and lower radii, with their major axes leading more and more the periodic orbit, since the precession rate (estimated by $\Omega - \kappa/2$ in the axisymmetric limit, for orbits near ILR, and by $\Omega + \kappa/2$ near OLR) increases with decreasing radii in most of the disk. This regular shift forces the gas into a trailing spiral structure, from which the sense of the gravity torques can be easily derived. Inside corotation, the torques are negative, and the gas is driven inwards towards the inner Lindblad resonance (ILR). Inside ILR, and from the center, the precessing rate is increasing with radius, so that the gas pattern due to collisions will be a leading spiral, instead of a trailing one (see Figure 79). The gravity torques are positive, which also contributes to the accumulation of gas at the ILR ring. This situation is only inverted in the case of a central mass concentration (a black hole?), for which the precession rate $\Omega - \kappa/2$ is monotonically increasing towards infinity with decreasing radii. Only then, the gravity torques will pull the gas towards the very center, and "fuel" the nucleus.

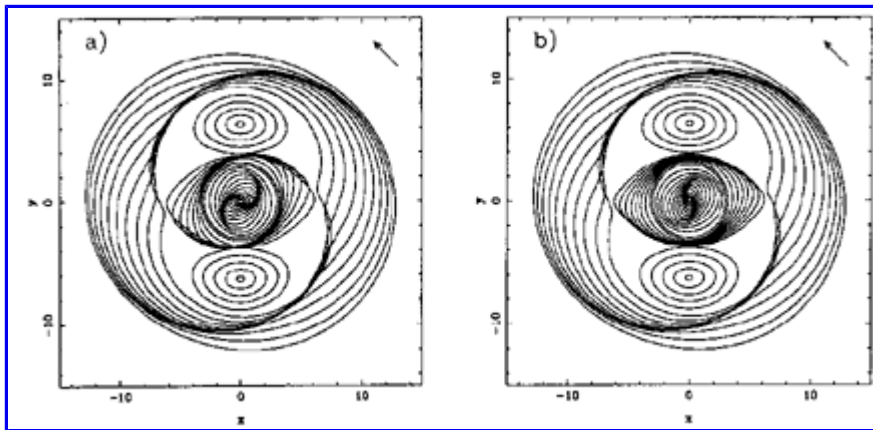


Figure 79. a) Without a central mass concentration, the gas winds up in a leading spiral inside the ILR ring; b) with a central mass concentration, the gas follows a trailing spiral structure.

What can form the active nucleus in the first place? It will be shown in the following sections that the accumulation of matter towards the center can produce a decoupling of a second bar inside the primary bar. This nuclear bar, and possibly other ones nested inside like Russian dolls, can take over the action of gravity torques to drive the gas to the nucleus, as first proposed by Shlosman et al. (1989).

13. SELF-GRAVITATING HYDRODYNAMICS

The formation of rings by gas accumulation at resonances, through the action of bar gravitational torques, has been illustrated beautifully by non-self-gravitating simulations of sticky particles. We have seen that somewhat different results are obtained when considering the gas as a continuous fluid, submitted to pressure forces and shocks. The differences between the two gas models are amplified by taking into account self-gravity. In the fluid picture, the fast infall of gas towards the center produces large central mass concentrations that modify the whole dynamics. This can perturb the orbital structure of the stellar component, shift the resonances, and destroy the bar (e.g., [Friedli & Benz 1993](#)). At this stage, the consideration of star formation is necessary, as a process that can lock the gas into a non-dissipative phase, and stop the gas infall ([Heller & Shlosman 1994](#)).

13.1. Stability

The gas component, even though it represents only a few percent of the total mass, has a considerable influence on the global stability of a galaxy. The gravitational coupling between gas and stars makes the ensemble unstable, even when each component would have been separately stable (e.g. [Jog & Solomon 1984](#); [Bertin & Romeo 1988](#); [Elmegreen 1994b](#)). The stability of a one-component infinitely thin stellar disk has been widely studied: the criterion introduced by [Toomre \(1964\)](#) indicates that stellar disks are stable against axisymmetric perturbations if the ratio Q of their radial velocity dispersion c_r to the critical dispersion $c_{\text{crit}} (= 3.36 G \mu / \kappa)$ is larger than 1. Here $\mu(r)$ is the disk surface density and $\kappa(r)$ is the epicyclic frequency. In fact, numerical simulations have shown that even when $Q > 1$, the stellar disk can be violently unstable with respect to non-axisymmetric perturbations, such as spirals or bars (e.g., [Sellwood & Wilkinson 1993](#)), together with z-instabilities (e.g. [Combes et al. 1990b](#)). These heat considerably the stellar disk, which can then no longer sustain spiral structure. Instabilities can be suppressed by reducing the effective self-gravity of the stellar disk, either through the addition of a hot bulge or halo ([Ostriker & Peebles 1973](#)), or through disk heating, i.e. increasing the initial velocity dispersion ([Athanasoula & Sellwood 1986](#)).

The stability of a two-fluid system with respect to axisymmetric perturbations has been studied by [Jog & Solomon \(1984\)](#), who showed that the star-gas system will be unstable if:

$$2 \pi G k \mu^* / (\kappa^2 + k^2 c^{*2}) + 2 \pi G k \mu_g / (\kappa^2 + k^2 c_g^2) > 1$$

where k is the wave number, μ^* and μ_g are the surface densities, and c^* and c_g are the velocity dispersions of stars and gas, respectively. This formula emphasizes the relative contribution of the two components, proportional to the surface density, and weighted with the inverse of the velocity dispersion. This shows why even a small fraction of gas, with a tiny velocity dispersion, can de-stabilize the ensemble. [Bertin & Romeo \(1988\)](#) and [Romeo \(1992\)](#) have shown that there exist two stability domains, corresponding to the two bumps of the Q parameter as a function of wavelength. At short wavelength, the system is unstable essentially because of the gas. With respect to the more common one-system stability regime, one can then consider a two-phase region, according to the surface density and velocity dispersion ratios between gas and stars: the gaseous and stellar regimes are reached successively, with increasing wavelength.

[Jog \(1992\)](#) also studied the growth of non-axisymmetric instabilities in a two-fluid system, and concluded again that the ensemble can be unstable, even if each component is separately stable with respect to non-axisymmetric perturbations.

The crucial importance of gas comes from its dissipation. In galaxy evolution, gravitational instabilities heat the disk, but the gas component remains cool, radiating away the excess heating due to the waves. The spiral structure can then be continuously renewed (e.g. [Miller et al. 1970](#); [Sellwood & Carlberg 1984](#)), even in the stellar disk. This is supported by observations, since spiral galaxies always possess gas, and early-type systems without gas are smooth and axisymmetric. Gas also has a damping effect on growing instabilities, because of its non-linear dissipation in shocks, and can then play a self-regulating role in spiral structure, as stressed by [Bertin & Romeo \(1988\)](#). While the gas is triggering spiral and bar instability when it represents only a few percent of the total mass, it can play the reverse role when its mass is above $\approx 10\%$. It is then unstable even to axisymmetric local perturbations. When the gas possesses too much self-gravity, it forms lumps through Jeans instability, and the lumpiness of the gas can scatter the stars, randomize their motions, and prevent any bar formation ([Shlosman & Noguchi 1993](#)).

13.2. Self-gravitating Rings and Nuclear Spirals

When more self-gravity is introduced in the gas component, the nuclear rings formed at ILR are much more unstable, and short-lived. This has already been shown in simulations of gas flow in a bar potential, when self-gravity of the gas is taken into account ([Fukunaga & Tosa 1991](#); [Wada & Habe 1992](#); see also [Elmegreen 1994a](#)). In the presence of an ILR, the gas accumulates in a ring towards the center, but the local instabilities it undergoes there make the ring fragment into clumps; the ring is also more elongated, and more asymmetric. Two big clumps gather at the end of the elongated ring, and re-inforce the bar potential. This produces more gravity torques, and a rapid loss of angular momentum for the gas in the ring. The ring collapses towards the center in a few rotations.

However, the results of these simulations are highly dependent on the fact that the stellar potential remains fixed and barred, with an imposed pattern speed. In fact the gas infall, when sufficiently massive, will perturb significantly the potential in the center, the pattern speed of the bar, and even can destroy the bar ([Friedli & Benz 1993](#)). A more likely behavior is the formation of two ILR's, due to the high mass concentration, the formation of a phase-shifted bar, due to the existence of perpendicular x_2 orbits ([Shaw et al. 1993](#); [Combes 1994](#)), or the formation of a secondary bar inside the primary one (see [section 16](#)). Both behaviors represent mechanisms to fuel the gas towards the nucleus, and extend towards the center the effects of the gravity torques from the primary bar. The actual behavior depends however on

the gas simulation code and on its assumed viscosity.

With the help of self-consistent simulations with stars and fluid-gas (through the beam-scheme hydrodynamical code, e.g., [Sanders & Prendergast 1974](#)), [Junqueira & Combes \(1996\)](#) have shown that a large mass concentration due to gas infall can both destroy the bar and help an $m = 1$ instability to grow. The latter phenomenon is quite stable, and prevents at the same time further gas infall.

Many galaxies are observed with their nuclei off-centered with respect to neighboring isophotes, and lopsided morphologies have been known for a long time ([Baldwin et al. 1980](#)). Asymmetric features are preferentially observed in the distribution of gas in late-type spiral galaxies. In a sample of 1700 galaxies, [Richter & Sancisi \(1994\)](#) have found that more than 50% of HI distributions are significantly asymmetrical. Stellar disks reveal also lopsidedness, in about 30% of cases, in the old population traced by the K -band (2.2μ , [Rix & Zaritsky 1995](#)). In several cases these features can be identified as one-armed spirals ($m = 1$ mode, e.g., [Phookun et al. 1992, 1993](#)). More frequently, nuclei of galaxies are observed displaced with respect to the gravity center, as in [M33](#), [M101](#) or [M31](#) ([Bacon et al. 1994](#)). Our own galaxy appears to experience such an off-centering, at least as far as the gas disk is concerned: about three quarters of the molecular mass of the nuclear disk is at positive longitude, and one quarter at negative longitude (e.g., [Bally et al. 1988](#)). Asymmetries are also seen at larger scale in atomic gas, while much of the neutral gas between a few hundred parsecs and 2 kiloparsecs from the nucleus lies in a tilted disk whose plane of symmetry is inclined by 20° with respect to the galactic plane (e.g., [Burton 1992](#)). Barred spiral galaxies can have their kinematical center displaced from the bar center ([de Vaucouleurs & Freeman 1973](#); [Marcelin & Athanassoula 1982](#); [Phookun et al. 1992](#); [Odewahn 1996](#)). It has been suggested by [Colin & Athanassoula \(1989\)](#) that offset bars can generate a one-armed structure in the disk.

The frequency of asymmetries and lopsidedness in spiral galaxies requires some efficient dynamical mechanism to generate and maintain them. The swing amplifier can play a role, but the dominant amplified mode depends essentially on the degree of self-gravity of the disk (e.g., [Jog 1992](#)): high disk-to-halo mass ratio, low velocity dispersion, and high gas fraction are favorable. One can remark also that a direct $m = 1$ mode is favored by the absence of damping at resonances, since there is no ILR possible ($\Omega - \kappa < 0$). Another mechanism can be the excitation of a leading $m = 1$ spiral by a retrograde companion ([Thomasson et al. 1989](#)). In that case, elongated orbits excited by the tide precess at a rapid and retrograde rate, and form a leading retrograde spiral. This occurs with a close interaction, when the disk of the target is embedded in a very massive halo. Since galaxies with leading arms are very rare, this might mean that the halo-to-disk mass within the visible disk is lower than unity for most spiral galaxies. It is a general observation that spiral galaxies with $m = 1$ structures display also higher order $m = 2, 3, \dots$ structures, and the sense of arms winding is usually the same for each set of structures. An interesting exception is [NGC 4622](#), which we discuss specially in [section 17.1](#). One of the results of the N-body simulations by [Zang and Hohl \(1978\)](#) is that the introduction of a significant fraction of counter-rotating stars can produce one-armed structures, in addition to the $m = 2$ instability. The $m = 1$ instability has been confirmed analytically by [Palmer & Papaloizou \(1990\)](#) in the case of equal numbers of direct and retrograde stars. However, one-armed spirals do not possess a larger fraction of stars in counterrotation than galaxies with two arms. Another possibility to trigger asymmetries and lopsidedness is infall of gas ([Sancisi et al. 1990](#); [Phookun et al. 1993](#)).

[Miller & Smith \(1992\)](#) have studied, through N-body simulations of disk galaxies, a peculiar oscillatory motion of the nucleus with respect to the rest of the axisymmetric galaxy. They interpret the phenomenon as a local instability, or overstability, of the center, but not in terms of a normal mode. Their models did not include any gas component. The presence of gas may change the picture considerably.

A qualitatively different mechanism has been studied in the context of massive gaseous disks around young stellar objects, i.e. nearly Keplerian disks, by [Adams et al. \(1989\)](#). They discovered numerically a family of unstable normal modes where the star did not lie at the center of mass of the system. The $m = 1$ instability arises essentially from the displacement of the central star from the center of mass of the system, which creates an effective forcing potential. [Shu et al. \(1990\)](#) presented an analytical description of a modal mechanism, the SLING amplification, or "Stimulation by the Long-range Interaction of Newtonian Gravity". This mechanism uses the corotation amplifier, where the birth of positive energy waves outside strengthens negative energy waves inside. In the SLING mechanism, a feedback cycle is provided by four waves outside corotation; long-trailing waves propagate from the OLR inward to the Q -barrier at CR where they refract in short trailing waves. These propagate outwards, cross the OLR, and reflect back to the outer edge of the disk. This is a critical point: the whole amplification mechanism depends on the reflecting character of this outer edge (cf. [Noh et al. 1992](#)). Then a short leading wave propagates inwards from the edge, through OLR, towards CR, where it refracts again into a long leading wave, which is then reflected at OLR. An essential point here is also the ability of waves not to be absorbed at OLR, which is why this mechanism applies to gaseous disks only. Using a WKBJ analysis, they derived from the dispersion relation, and the condition of a constructive reflection, the required pattern speed for these modes.

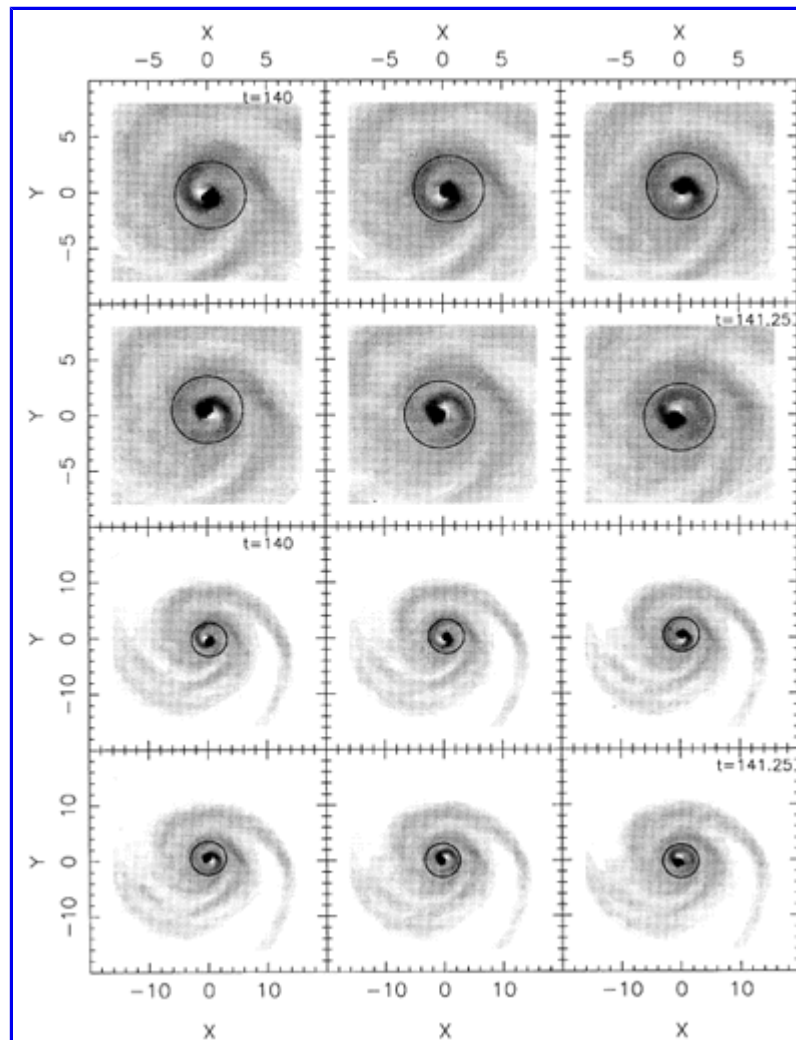


Figure 80. Development of a central $m = 1$ wave in the gas component, rotating at $\omega_p = 400 \text{ km s}^{-1} \text{ kpc}^{-1}$. The circle, at 3 kpc, indicates the OLR; from [Junqueira & Combes \(1996\)](#).

The same mechanism could be applied to massive gaseous disks in the central parts of galaxies possessing high central mass concentrations, as proposed by [Junqueira & Combes \(1996\)](#). At first, a bar instability accumulates gas towards the center, when it becomes unstable and forms an $m = 1$ spiral mode ([Figure 80](#)). The mode grows in a dynamical time, and remains quasi-steady until the end of simulations (during 2×10^9 yrs). The gaseous disk mass represents more than 25% of the central mass. In the density plots, the spiral is conspicuous until 3 kpc radius, and other more transient features, with much lower angular speeds, dominate at larger radii. The Fourier analysis of the total potential indicates a very high pattern speed of $\omega_p = 400 \text{ km s}^{-1} \text{ kpc}^{-1}$ for the central $m = 1$ spiral, which corresponds to the OLR at 3 kpc ([Figure 81](#)). This pattern speed is much higher than the speed at larger radii; there is no coupling between several modes, as was suggested for bars within bars. In the latter case, the corotation of the small bar is the inner resonance of the large one, and there exists a non-linear interaction between the two patterns ([Tagger et al. 1987](#)). A non-linear interaction between two modes with azimuthal mode numbers $m = n$ and $m = n + 1$ was proposed by [Laughlin & Korchagin \(1996\)](#) to trigger $m = 1$ instabilities in low-mass disks, and was confirmed through self-consistent hydrodynamic simulations.

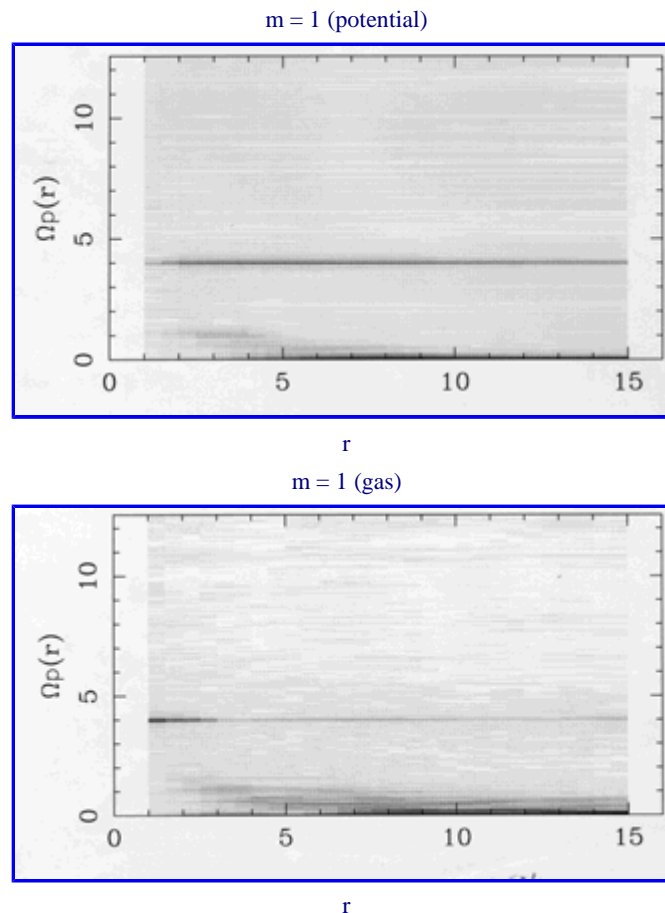


Figure 81. Power spectrum analysis for the gas density of [Figure 80](#) and for the corresponding total potential. The identified perturbation extends up to the outer parts of the disk.

The power spectrum analysis for the gas density of [Figure 80](#) and the corresponding total potential reveals that the influence of the fast-rotating $m = 1$ pattern extends towards the edge ([Figure 81](#)). This can be explained for the potential, since the $m = 1$ perturbation is a periodic move of the center of mass, and is instantaneously felt in the whole disk, but the signature in the gas density is more remarkable. The stellar component does not follow the $m = 1$ spiral with as much contrast, but the off-centering of its center of mass is also conspicuous. The two components oscillate in phase opposition, while the massive dark halo, represented by an analytical Plummer component, is nailed down to the center. The large gaseous condensations in the center of spiral galaxies can therefore give rise to new instabilities, and account for some of the observed off-centered nuclei or lopsided distributions.

14. PROBLEMS IN RING FORMATION

Although the formation of rings by gas accumulation at bar resonances has gained strong observational support, and is now widely accepted, there remain peculiar cases for which the standard model encounters some difficulties in its application. Let us summarize here the predictions of resonance theory: in a barred spiral disk, gas is subject to strong gravity torques from the total potential, and accumulates at one of the main resonances, where its trajectory follows the main periodic orbit family there. These are symmetrically oriented with respect to the potential, and subject to no net torque. Outer rings correspond to OLR, and the shape of the ring can be perpendicular to the bar, with dimples (R_1), if slightly inside OLR, or parallel to the bar slightly outside (R_2). The inner ring encircling the bar corresponds to the ultraharmonic resonance, the $4/1$, slightly inside corotation, while nuclear rings correspond to the ILR region. The relative positions of the rings are therefore constrained by the theory, once the rotation curve is known.

The theory also predicts that at equilibrium, rings are aligned with the bar; the rings are essentially composed of gas, and after star formation, of young stars. If the bar is long-lived, with the same pattern speed, the ring can survive also, although the old stars will diffuse out of the ring, after acquiring velocity dispersion through scattering by perturbations (giant molecular clouds, or gravitational instabilities in the rings themselves). When all the gas from the spiral arms has been depleted to the benefit of the rings, and when enhanced star formation has consumed all the gas in the rings, the latter should age and turn to "dead" (or quiescent) rings, with diffuse boundaries. Many diffuse and detached outer rings could be in such a phase, or individual rings within a galaxy, such as the inner and outer rings of [NGC 7702](#) and [1326](#), the nuclear ring of [NGC 5850](#), or the R_1 component of [IC 1438](#).

Let us remark first that the presence of barred galaxies without any ring is *not* actually a problem for the theory. Ring formation requires gas, which might not be present (for instance in lenticular galaxies). Outer rings require at least a few Gyrs to form, and the bar might be quite recent. Nuclear rings are the manifestation of the inner Lindblad resonance, which is present only in highly concentrated galaxies, and inner rings at UHR are favored in rather squarish potentials near corotation, possessing a strong $m = 4$ component.

14.1. Time-scales and the Co-existence of Rings

The first problem encountered is the frequent observation of simultaneous outer, inner, and nuclear rings in the same galaxy, in spite of their very different formation time-scales and lifetimes. An excellent example of this conundrum is [NGC 1326](#) (see [Figure 45](#)), which has a beautifully developed stellar outer R_1 ring and an intense nuclear ring of young stars and $H\alpha$ emission. Other examples include [NGC 3081](#), [NGC 5728](#), [NGC 6782](#), [IC 1438](#), and [IC 4214](#). The outer rings require, in a reasonably strong bar, at least 3×10^9 yrs to form, and can be maintained over a Hubble time if the galaxy has no close companion, while the nuclear rings form in typically 10^8 yrs, and their life-time can be as short as 10^8 yrs because of consumption by star formation and flow to the center through self-gravitating instabilities, dynamical friction, or dissipation. This problem has been encountered in simulations (e.g. [Gerin et al. 1991](#); [Byrd et al. 1994](#)), but underestimated, since star formation was not taken into account.

A possible solution to this problem is to take into account some gas accretion: either the gas locked up in stars, and then released by stellar winds, explosions, etc., or gas accreted from outside, from the atomic hydrogen clouds outside the optical disk, or from companions. The latter, however, will perturb the dynamics of the disk, modify the bar pattern speed ([Gerin et al. 1990](#), [Sundin et al. 1993](#)), or even destroy the bar ([Pfenniger 1991](#)). Only mild distortions are welcome, to replenish the gas content in the disk without destroying the outer ring. In any case, there should not be a true outer ring co-existing with a strong bar, or with a self-gravitating gaseous nuclear ring. Outer pseudorings do not need such a long time to form, and a non-self-gravitating gaseous nuclear ring in a weak bar is much more long-lived. Most cases observed with several rings indeed satisfy these conditions (e.g., [NGC 4736](#) with a weak bar ([Gerin et al. 1991](#)), or [IC 1438](#) with a low gas content ([Fisher & Tully 1981](#)). Also, some dead inner rings have been identified from their colors (e.g., that in [NGC 7702](#), [Buta 1991](#)). Some galaxies with very detached outer rings possess secondary lenses and secondary bars, rather than blue nuclear rings ([Buta & Crocker 1993](#)).

14.2. Bar-Ring Misalignment

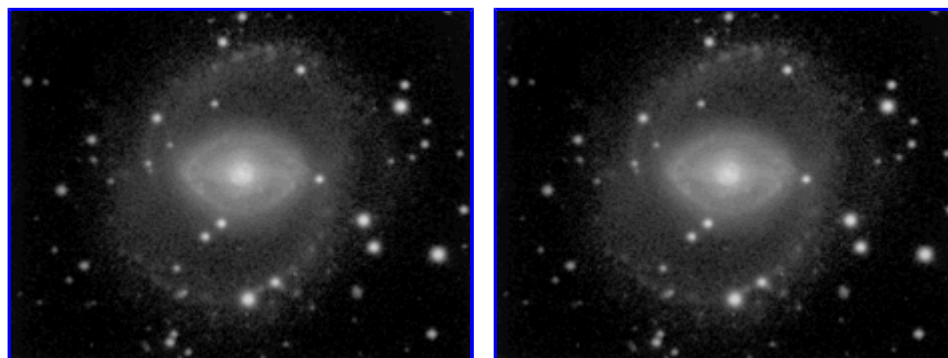


Figure 82. Top: Blue light image of [ESO 565-11](#), a kinematically and photometrically established case of intrinsic bar/ring misalignment, from [Buta et al. \(1995a\)](#). Bottom: Blue light image of [NGC 6782](#), an aligned bar/inner ring galaxy. Both galaxies also have nuclear rings and outer pseudorings of type R_1 .

Most inner and outer rings in barred galaxies are aligned with the bar ([section 9.3](#)). Exceptions do exist, however, like in [ESO 565-11](#) ([Buta et al. 1995a](#); see [Figure 82](#)) and others described by [Buta \(1995\)](#), but they are rare. Therefore, there is no incompatibility with the theoretical predictions that they should be transient features. Possible scenarios include a tidal interaction with a companion (see, for example, [Noguchi 1987](#)), since these galaxies are sometimes members of loose groups, or the relaxation of the disk through mass concentration driven by the bar. Indeed, as soon as a relatively high fraction of the gas has accumulated in the center, the potential and rotation curve are significantly modified, and so is the bar structure; a secondary bar can even decouple from the primary one, as developed in [section 16](#), and misaligned components are expected at the transition phase. A secondary bar can have a different pattern speed from the primary one, so that no alignment is expected between the two bars. For the peculiar case of [ESO 565-11](#), the bar is rather weak and of the "ansae" type, which indicates possibly a half-destroyed bar (cf. [section 15](#)). The nuclear ring is the site of a conspicuous starburst, so that the hypothesis of a recent gas concentration, and consequent relaxation of the potential is the most plausible. The galaxy is not yet highly concentrated, so that the decoupling of a secondary bar is unlikely.

As for the alignment of the nuclear bars, they are much more difficult to ascertain, and highly elongated nuclear rings are rare (see [section 9.3](#)). When elongated, they are in general misaligned with the main bar, as in [ESO 565-11](#). Due to the presence of two inner Lindblad resonances in highly concentrated galaxies, some phase-shift between the bar and the nuclear ring is expected (e.g., [Shaw et al. 1993](#)).

Also, a secondary wave with a different pattern speed may exist, which implies misalignment.

15. RINGS IN NON-BARRED GALAXIES

The standard mechanism to form rings, as we have described above, appears to require the presence of a bar. We can note however that in the presence of a steady spiral density wave, gravity torques will also drive the gas towards the center inside corotation, and outwards outside corotation, so that it could accumulate in rings at resonances. But the mechanism is not efficient, since spirals are not steady enough in the absence of bars. Recurrent spiral structure has been obtained in N-body simulations, but always with different pattern speeds (e.g., [Sellwood & Carlberg 1984](#)). First, not only do spiral instabilities heat the stellar medium, which becomes unresponsive, but also angular momentum is exchanged due to phase-shifts between density and potential, and rapid evolution occurs. On the contrary, a bar is very steady and robust in the stellar component.

The existence of rings in nonbarred galaxies is a common phenomenon (see [section 9.1](#) and [Buta 1995](#)). Some of them could be explained by the steady tidal action of a bound companion, since the non-axisymmetric perturbation is then very similar to that of a bar ([Combes 1988](#)); these are described in [section 17](#). Many cases could also be explained by the existence of a weak oval distortion, weak enough that the galaxy is classified SA. A very good example is the case of [NGC 7217](#), an isolated spiral which appears even on near-infrared photographs very axisymmetric, and which may be one of the most axisymmetric galaxies ever observed ([Buta et al. 1995b](#)). Yet the very faint $m = 2$ component discovered in the deprojected image is sufficient to explain the formation of the three rings observed in the galaxy with resonances. The nuclear, inner and outer rings of [NGC 7217](#) are well reproduced by a simulation of gas flow in the potential derived from the *I*-band image ([Buta et al. 1995b](#)). A noteworthy characteristic discovered by the latter authors is a large extended circular halo of light in the outer parts of the galaxy.

Another possibility for the ringed nonbarred galaxies is that the rings were formed while the galaxy was barred, but the bar has now been dissolved through either tidal interaction with a companion, or through gas accretion and mass concentration. This has been proposed in particular for [NGC 7217](#) ([Verdes-Montenegro et al. 1995](#); [Athanasoula 1996](#)), since about 20-30% of the stars have been observed in counter-rotation in this galaxy by [Merrifield & Kuijken \(1994\)](#). The progressive destruction of the bar could also explain the counter-rotation, through the librating/rotating separatrix crossing mechanism developed by [Evans & Collett \(1994\)](#): in the rotating frame of the bar, some particles were trapped librating about the bar. When the bar disappears, the trapped librating orbits are scattered almost equally into clockwise and anti-clockwise rotating loop orbits. Since not all particles were trapped with the bar, and due to the preferential sense of rotation, less than 50% of the stellar population is expected to be counter-rotating in the final nonrotating frame (which could correspond to the observed 25%).

If this mechanism is attractive to explain the counter-rotating phenomena, it raises however some problems for the survival of rings. The destruction of the bar must not be due to a violent event, because that would have destroyed also the rings; for this reason, the tidal action of a companion is not likely (see [section 17](#)). If it is the gas accretion that makes the galaxy axisymmetric, it must have occurred quite rapidly, otherwise the changing pattern speed of the decaying bar would have diluted the rings. But if the axisymmetrization is rapid, the velocity dispersion produced at the separatrix crossing is too high ([Evans & Collett 1994](#)).

15.1. Bar Destruction, Lens, and Oval Formation

Recent numerical simulations, and in particular those including the gas component, have promoted the idea that bars might be only a transient phase in the life of a galaxy. Bars can be easily destroyed by massive gas flow towards the center or by a satellite merger, and also can re-form since spiral disks are cooled down and made unstable to new perturbations by fresh gas accretion. The duty cycle of the strong bar phase could be of the order of 30% of the Hubble time, explaining the observed frequency of SB galaxies. This is in contrast with the view brought along by previous N-body simulations dealing with only the stellar component, where the bar is robust and lasts for more than a Hubble time.

The influence of a central mass concentration on bar strength was first studied for its relevance to AGN's: a sufficiently massive black hole in the nucleus of a barred galaxy can weaken and destroy the bar ([Norman et al. 1985](#); [Hasan and Norman 1990](#); [Pfenniger & Norman 1990](#)). The black hole acts as a scattering mass that can axisymmetrize the central disk. The bar favors elongated orbits in the center, with less angular momentum, which are more sensitive to the central mass than circular orbits. For high enough central masses, stochasticity develops in the stellar orbital structure, and the bar is no longer supported by the x_1 family of orbits. Through orbit computations, [Hasan & Norman \(1990\)](#) have determined the percentage of the remaining regular x_1 orbits, as a function of the black hole mass. This percentage falls significantly when the central mass reaches 5% of the total mass: the percentage of stochastic orbits is so large that the bar is significantly weakened, then destroyed for a mass fraction of 10%. Through self-consistent stellar simulations, [Nishida & Wakamatsu \(1996\)](#) have shown that a bar still forms with the same amplitude in a galaxy with an initial mass concentration as high as 5%, but its strength weakens in the long run, while a bar with no central mass concentration keeps its amplitude in a steady state through a Hubble time.

In normal spiral galaxies, there do not exist massive black holes as large as 5% of the total mass, i.e. $5 \times 10^9 M_{\odot}$. A very concentrated nucleus or bulge (of mass M_b , and size a_b) could play the role of the scattering mass, when the scattered velocity is of the order of the rotational velocity provided by the disk, i.e., $v \approx (GM_b / a_b)^{1/2} \approx V_{\text{rot}}$, and the ratio of scale-lengths between the disk and the central mass concentration is high enough (more than 5 typically). According to a recent compilation of observed profiles of spiral galaxies

(Courteau et al. 1996), this scale-length ratio is on average larger than 10; the condition of a required (M/r) ratio comparable for the bulge and the disk, i.e., $(M/r)_b \approx (M/r)_d$, translates then in terms of the surface densities $\mu_b \approx 10 \mu_d$, which is often observed in early-type galaxies. Another possibility is that the strong gas infall driven by the bar produces itself a sufficient mass concentration, as suggested by simulations (e.g., Friedli & Benz 1993). The fate of these gas concentrations, once star formation has occurred, is to contribute to the nucleus or bulge component anyway.

How fast does the bar destruction occur, and can we recognize such a phenomenon in the observations? In the case of a satellite merger, the event can be very sudden, and the effective dissolution of the bar occurs in about 20 Myr (Pfenniger 1991); it might be too rare to be observed, although it could be recognized through the presence of a close companion. In the case of gas infall towards the center, it depends essentially on the amount of gas present and the rate of accretion. If the latter is high enough, the decoupling of a secondary bar might be the first step in the dissolution of the primary one (Friedli & Martinet 1993). For a milder gas accretion, the bar dissolution can be a very long phenomenon, because of self-regulation. The processes could be at the origin of lens formation, and therefore easy to recognize (cf. Combes 1996). The regulation comes from the fact that the gas accretion destroying the bar is driven by the bar itself: in a first phase, the torques due to the strong initial bar drive the gas inwards, increasing significantly the central mass concentration. The central potential is modified, and so are the frequency curves ($\Omega, \Omega - \kappa / 2$), until the development of two inner Lindblad resonances, and the appearance of the family of x_2 perpendicular orbits in the center. This has the effect of weakening the bar in the very center. Progressively, if the central concentration builds up, stochasticity extends in the orbital structure, and the fading of the bar reduces the torques and the gas infall. Part of the gas coming from the outer parts of galaxies has now time to form stars in the disk, which re-establishes the mass balance between the nucleus and the disk. The central mass concentration loses its dynamical efficiency, and a new strong bar phase can occur through gravitational instability, which closes the cycle. To have several such cycles in a Hubble time requires however a substantial mass accretion, i.e., important gas reservoirs in the outer parts of galaxies (cf. Pfenniger et al. 1994).

The bar destruction process affects the orbital structure in such a way as to explain lens formation (Combes 1996). The main effect is to introduce stochasticity in the middle of the bar: close to the central mass concentration, the potential becomes axisymmetric and orbits remain regular; near the end of the bar, the bar potential is dominant, and the x_1 periodic orbits remain almost unperturbed. The chaotic region develops in the middle, corresponding to intermediate energies in the rotating frame. These orbits do not support the bar, and may contribute to a lens component. The regular orbits still trapped in the bar near its end might be at the origin of "ansae" condensations, that are sometimes observed in weak bars.

Chaotic orbits are bounded only by their limiting energy curve; in the bar rotating frame, the effective potential is $\phi(r) - 1/2 \Omega^2 r^2$, and is maximum at corotation. This plays the role of the last boundary for the chaotic region inside CR. Orbits with higher energies will eventually escape. This could be the origin of the sharp cut-off of the lens (e.g., Kormendy 1984). The observation that the lens and the bar have typically the same maximum size (the bar fills the lens along its intrinsic major axis) suggests that the lens ends also near corotation. An exception could be ESO 565-11, where the bar and lens are misaligned by 60° (Buta et al. 1995a).

Self-consistent simulations with stars and gas of the slow bar destruction by a central mass concentration illustrate the lens formation (Figure 83). In this particular case, the central mass concentration is 1% and the total gas mass is 0.5% of the total mass. A very thick oval forms through dissolution of the stellar bar, with the "ansae"-shape. The gas bar is thinner and longer. The half-destroyed bar remains for a 2×10^9 yrs time-scale.

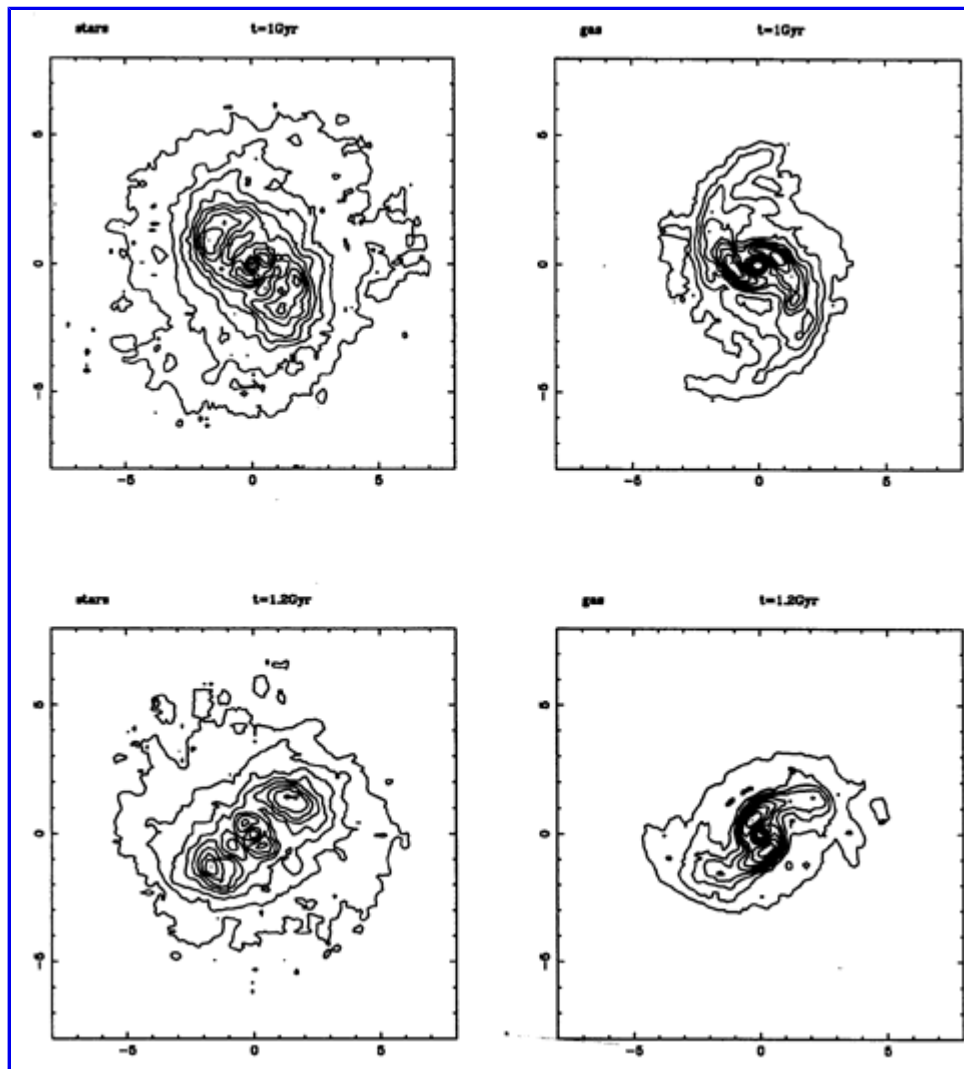


Figure 83. Isophotes of the results of N-body simulations with stars (left) and gas (right), starting with axisymmetric conditions, and a mass concentration of 1%. The bar stays half-dissolved for a time-scale of Gyrs. Note the "ansae" in the stellar distribution.

15.2. Evolution along the Hubble Sequence

We have already shown how non-axisymmetric perturbations, and in particular bars, can provoke rapid evolution of spiral disks, through angular momentum transfers. The presence of the dissipative gas component plays a fundamental role in this evolution. Tidal interactions by companions and mergers also contribute to a rapid evolution. Therefore, galaxies can change Hubble types frequently during their life-time, and the most likely sense of evolution is from late to early types ([Pfenniger 1993](#)). What are the consequences for secondary structures like rings and lenses?

The very existence of true detached outer rings in early-type galaxies already tells us that the evolution slows down at the end of the Hubble sequence. The formation time of these structures is a few Gyr, and the bar and its pattern speed must have been steady over this period of time. This is easy to understand since the gas fraction is very low in these early-types, and the gas component is the motor of the evolution. Early-type barred galaxies with massive bulges or high mass concentration should be in the process of slow bar dissolution, and should be accompanied by a lens. This appears to be the case since ~ 54% of SB0-a galaxies have lenses ([Kormendy 1979a](#)). Non-barred galaxies with rings can be interpreted as systems where the bar has been slowly dissolved, and axi-symmetric rings have survived, possibly maintained by the remaining oval distortion.

16. INTERACTIONS BETWEEN SEVERAL WAVES

The co-existence of several rings in the same barred galaxy, with relative radii compatible with what is expected for the various Lindblad

resonances, speaks *against* the existence of several patterns with different angular speeds in the galaxy. However, for certain peaked mass distributions, with high gradients of rotation frequencies, the whole spiral disk cannot participate in the same pattern, as shown in N-body simulations (Sparke & Sellwood 1987). Several pattern speeds can then co-exist, with non-linear interactions between the various waves (Tagger et al. 1987), so that mutual amplification can occur. The most frequent interactions will concern two $m = 2$ patterns (for instance a primary bar, and a nuclear bar or spiral), that interact at a common resonance (for example, the corotation of the nuclear pattern coincides with the ILR of the bar). In the overlap region, beat waves with multiplicity m equal to the sum and the difference of the two $m = 2$ modes, i.e. $m = 0$ and $m = 4$, will be generated, and their pattern speeds will be such that the overlapping region is also their OLR and ILR, respectively. The application of this mechanism to real galaxies could explain the observations of nuclear bars just inside nuclear rings, with arbitrary orientation.

16.1. Nuclear Bars inside Nuclear Rings

The presence of a possible second component in the center of barred galaxies has been recognized very early through the presence of a secondary bar (distinct position angle, and distinct ellipticity) in the photometry, or through central isophote twists. Already de Vaucouleurs (1974) had noticed such "bars within bars", and Sandage & Brucato (1979) high surface brightness nuclear bars, as independent entities. Kormendy (1982b) found that isophote twists are preferentially found in SB galaxies with strong central concentration, and that the second small bar is aligned nearly perpendicular to the main bar; he proposed that the triaxiality of bulges is the cause of the projected twists. More recently, Buta & Crocker (1991), Shaw et al. (1993), Wozniak et al. (1995), and Friedli et al. (1996) have shown that these twists are associated with nuclear rings, clearly traced by $B - I$, $B - V$, and even $J - K$ color index maps. The nuclear ring is always encircling the nuclear bar; sometimes the nuclear ring is itself elongated almost perpendicular to the main bar. These are cases where the twists cannot be attributed to a triaxial bulge seen in projection. Similar phenomena have been observed in the molecular component (e.g., Devereux et al. 1992, Kenney et al. 1992). Molecular bars perpendicular to the main bar are observed inside a nuclear ring. Sometimes only two peaks are prominent in the CO emission, at the crossing of the leading dust lanes parallel to the bar, and the smaller nuclear ring. These twin-peaks (Kenney 1991) represent the crossing zone between the x_1 and x_2 types of orbits.

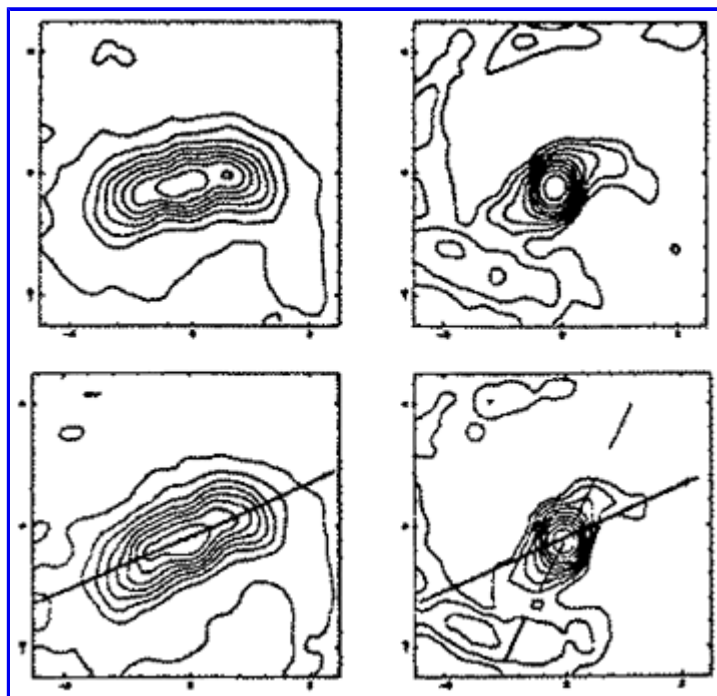


Figure 84. Density contours of the stellar component (left), the gas (right) in the less viscous model, where the existence of perpendicular orbits x_2 generates a twisted gas response.

Two main interpretations have been proposed for these isophote twists: first, in the presence of two inner Lindblad resonances, the family x_2 of perpendicular periodic orbits is the cause of phase-shifts in the gas component (Shaw et al. 1993); once enough gas is gathered in the center, a fraction of the stellar component follows its potential. This configuration remains for a short time, since strong gravity torques are present. Second, a nuclear bar can decouple from the main bar, with a larger pattern speed, as suggested by Shlosman et al. (1989), and simulated by Friedli & Martinet (1993). In that case, no preferential orientation is expected between the two bars, which represents better the observations (Buta & Crocker 1993). In both cases, this nuclear phenomenon requires a large mass concentration and large gradients of rotational velocities in the center, in order that there exist 2 ILR's. It requires also a significant gas fraction in the center, since a pure stellar disk will be too hot to participate in a second central pattern. Pure stellar N-body simulations do not reveal the nuclear bar decoupling, but a global gas mass fraction of 6% is enough to cool down the center, so that it can show this second pattern. The physical properties of the gas and the amount of dissipation assumed are the essential factors that determine the dynamical behavior between the two mechanisms outlined above (Combes 1994). With a small amount of dissipation, the gas settles in a phase-shifted bar, influenced by the existence of

perpendicular periodic orbits (Figure 84), while with a more viscous gas model, a rapidly rotating nuclear bar of stars and gas decouples from the main bar (Figure 85). In the simulations, where the nuclear bar rotates more rapidly than the primary bar, the corotation of the nuclear bar corresponds roughly to the ILR of the primary, so that the non-linear coupling between the two bars might be at work (Tagger et al. 1987).

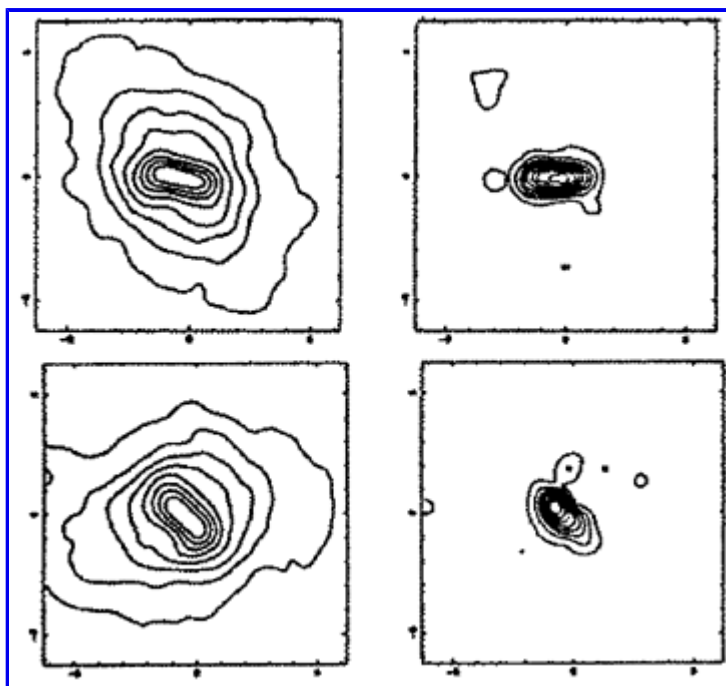


Figure 85. Density contours of the stellar component (left), the gas (right) in the viscous model, forming a nuclear bar. Time intervals are 60 Myrs.

Since the phase-shift between the gas density and the total potential is minimized in the case of the decoupled fast-rotating nuclear bar, gravity torques, and therefore gas infall, are also minimized, so that *the nuclear bar phase is less transient than the isophote twists phase*. The nuclear bar can survive a few rotations of the primary, which explains its frequent observation.

17. TIDAL INTERACTIONS AND RINGS

The influence of environment on the presence of rings was first studied by [Madore \(1980\)](#) who noted that galaxies with inner rings had significantly less close companions than average, about twice less.

[Elmegreen et al. \(1992b\)](#) studied in detail the influence of environment on outer rings and pseudo-rings in 153 bright spiral galaxies. The objects were selected from the catalog of bright ringed galaxies in [de Vaucouleurs & Buta \(1980a\)](#): 45 have semidetached outer ring (R) structures and 108 have outer pseudo-ring (R') structures. The environment of the objects was determined from the following catalogs: field ([Turner 1976](#)), pseudo-field (those galaxies that are relatively isolated but are suspected of being in groups, listed with an asterisk in the table by [Turner 1976](#)), groups ([Geller & Huchra 1983](#); [Turner & Gott 1976](#)), and binaries ([Peterson 1979](#) and [Turner 1976](#)).

A first interesting remark is that pure outer rings are much more frequent in early-type galaxies, such as SB0 and SB0/a (see also [section 9.1](#) and [Figure 24](#)). De Vaucouleurs and Buta's survey is heavily weighted toward these types, which comprise 24% of all the catalogued outer ring (R) galaxies, as compared to 7.9% for galaxies in general. It was found that a high fraction of these early barred galaxies in the field has an outer ring, $67 \pm 27\%$, while almost none of them has an outer ring in groups or binary systems.

The high fraction of extremely early barred galaxies with outer rings in the field may be interpreted in terms of the long formation time of detached outer rings with respect to the dynamical time. Because of their higher total mass, and higher average density, the internal dynamical time-scale of early-type galaxies is shorter, and they are dynamically more evolved: outer rings had more time to form, for a given bar strength, than in later-type galaxies. The low fraction of these early-type galaxies with detached outer rings in groups and binary systems implies that tidal interactions destroy the rings or prevent their formation.

The fraction of SB0 and SB0/a galaxies with outer *pseudo*-rings displays the opposite behavior as a function of environmental density. Now the fraction is zero in the field and increases with density, up to 15%. This result suggests that companions do not always destroy completely outer rings, but that some companions convert outer rings into outer pseudo-rings. There could still be some tidal destruction of rings (or inhibition of ring formation) too, because the fraction of SB0 and SB0/a galaxies with any type of outer ring (R or R') decreases with companion density, varying from 67% to an average of 15%. These numbers are consistent with a conversion of about 20% of the outer pure rings in binary SB0 and SB0/a galaxies into outer pseudo-rings, and a destruction of the other 80%. An alternative interpretation

could be that bars in binary galaxies are younger than bars in the field because the companions made the bars (i.e., [Noguchi 1987](#); [Combes 1988](#); [Elmegreen et al. 1990](#)). In this case, the younger bars have not had time to make pure outer rings but only outer pseudo-rings.

Another interesting result concerns the nonbarred galaxies. First the fraction of true outer rings in nonbarred galaxies is insignificant, which confirms the much larger efficiency of the bar in the ring formation. Secondly it is found that the fraction of late-type nonbarred galaxies with outer pseudo-rings decreases with environmental density from 25% to 5% from the field to binary systems. This suggests that companions either destroy or prevent the formation of pseudo-rings in nonbarred galaxies.

The decrease in pseudo-ring fraction with increasing environmental density among SA galaxies implies that the pseudo-rings are not made by tidal perturbations, but are made internally and then destroyed or altered by tidal perturbations. This helps to discriminate between the two possibilities opened by the results found on early-type galaxies, where the fraction of pseudo-rings increases with environmental density: these pseudo-rings must come from destroyed rings.

Computer simulations confirm the extreme fragility of outer rings with respect to tidal interactions (see [Figure 86](#)). Rings in barred galaxies are easily destroyed or converted into pseudo-rings by transient prograde interactions, and the same rings are converted into pseudo-rings by transient retrograde interactions. In a binary galaxy with a strong bar, where the ring formation time-scale can be about the same as the companion orbital period, a complete outer ring may have no time to form. Spiral structure will be generated at each encounter, and the incipient ring will only be able to form a pseudo-ring under the action of the unperturbed stellar bar. The companion may also change periodically the pattern speed of the bar ([Gerin et al. 1990](#), [Sundin et al. 1993](#)), which prevents the formation of a pure ring.

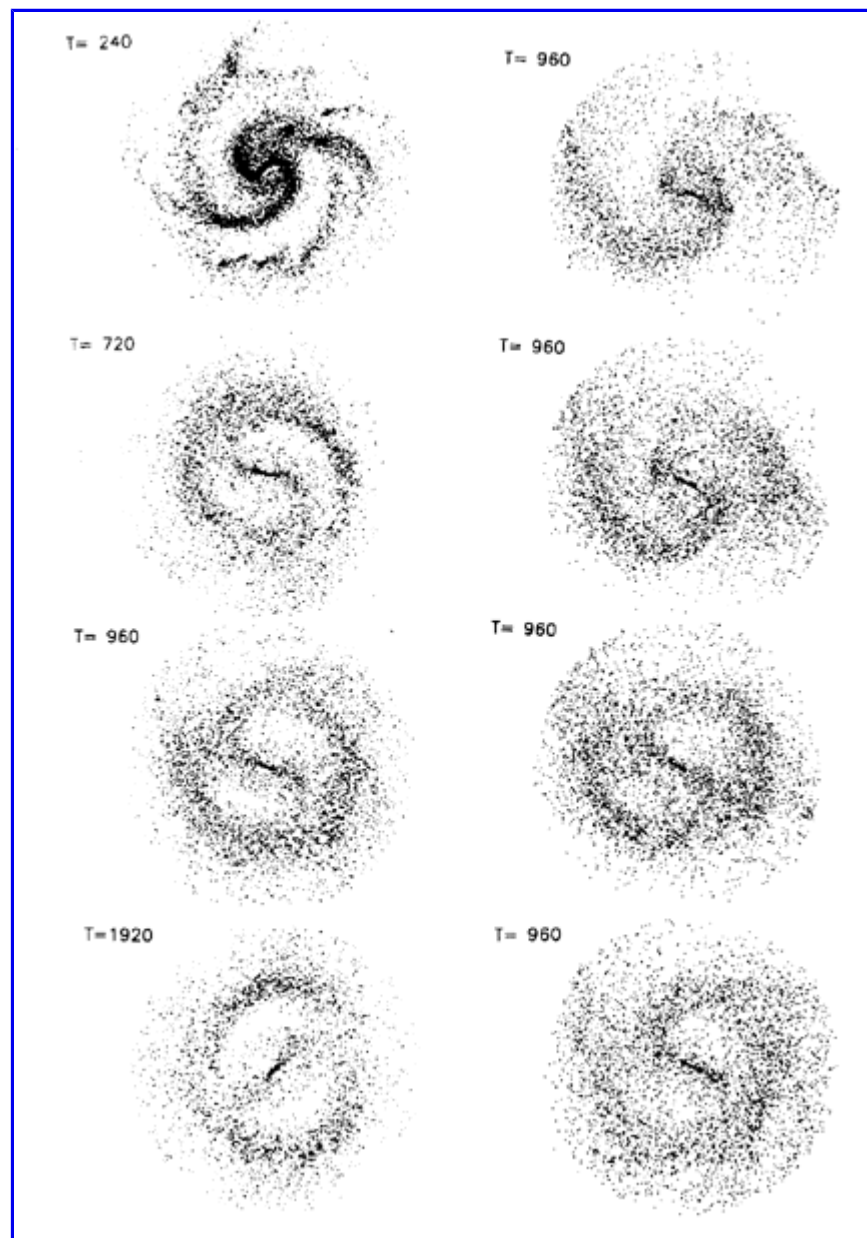


Figure 86. Formation of an outer ring (left), and its destruction by the tidal interaction with a companion (right), from [Elmegreen et al. \(1992b\)](#). Time is in Myrs. The gas component only is shown. The right column corresponds from top to bottom to a direct companion mass ratio of 0.5, 0.25, 0.12 and a retrograde passage with 0.5 mass ratio.

17.1. The Leading Arm Ringed Galaxy [NGC 4622](#)

The unusual nonbarred spiral [NGC 4622](#) provides an interesting possible example of a tidally generated ring. The inner ring of this galaxy marks the boundary between two different spiral patterns: a single inner arm winding counterclockwise, and two outer arms winding clockwise ([Buta et al. 1992](#); see [Figure 87](#)). This galaxy provides the best established case of leading spiral structure in a galaxy, but it has not been possible observationally to determine which set of arms is leading. On the basis of retrograde encounter models published by [Athanasoula \(1978\)](#), [Thomasson et al. \(1989\)](#), and [Noguchi & Ishibashi \(1986\)](#), it is likely that the inner, single arm has the leading sense. The galaxy is so far a unique example, and it leaves open the question of the nature of the ring. The outer arms of the galaxy are lopsided, and signal a probable interaction, possibly with a small galaxy 1.'85 to the east. Is the large inner ring of the galaxy possibly a consequence of the interaction as well? [Buta et al. \(1992\)](#) suggested that the ring may be a 1 / 1 resonance with the angular velocity of the companion at closest approach. The ring is off-centered and has an asymmetric azimuthal color index profile (see [Figure 36](#)).

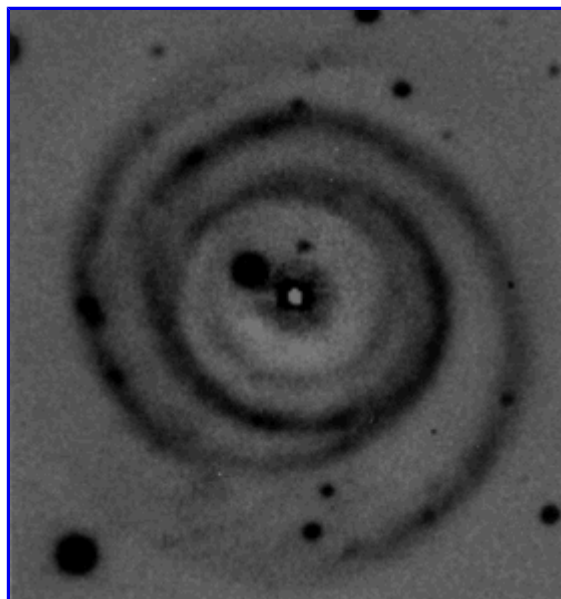


Figure 87. I-band image of [NGC 4622](#) after removal of the light of the bulge and background disk components, from [Buta et al. \(1992\)](#). The inner ring in this case separates regions of leading and trailing spiral arm structure in the disk.

[Byrd et al. \(1993\)](#) carried out N-body simulations to see if an encounter could explain the observed structure of [NGC 4622](#). Their best match is provided by a model where a low mass, small companion galaxy intrudes close to the nucleus of a larger disk galaxy. Both direct and retrograde encounters produced a similar structure, but a retrograde encounter model provided a better match and a longer-lasting leading arm. In order to work, the model required a halo-to-disk mass ratio of at least eight.

17.2. The One-armed Outer Ringed Galaxy [NGC 4378](#)

Another possible example of a tidally-generated ring in a nonbarred galaxy is provided by [NGC 4378](#), a low-inclination spiral in the direction of the Virgo Cluster. In blue-light images in [Sandage \(1961\)](#), [Rubin et al. \(1978\)](#), and [SB94](#), the spiral structure appears to be distinctly one-armed, and in the outer regions, this single arm appears to nearly close into an outer ring, hence the revised classification is (R)SA(s)a in RC3. Since the vast majority of outer pseudorings are defined by two spiral arms, the origin of this interesting structure was investigated by [Byrd et al. \(1994\)](#), who deduced from numerical simulations that, unlike the probable leading single arm in [NGC 4622](#), the arm in [NGC 4378](#) could be an impulsive *trailing* arm created by the grazing passage of a small companion. The actual trailing nature of the arm was recently confirmed by [Byrd et al. \(1996\)](#), who used optical broad-band images in conjunction with published kinematic data to deduce the near side of the galaxy's disk (following a technique described by [de Vaucouleurs 1958](#)). These broadband images also revealed asymmetry at very low light levels, suggesting that an interaction has indeed affected this galaxy. The Byrd, Freeman, and Howard simulations do not, however, explain why the single arm of [NGC 4378](#) closes into an outer ring.

17.3. Accretion Rings

It is now well-established that some ring features seen in galaxies may represent the result of the accretion of a gas-rich companion or tidal capture of material from a neighboring galaxy ([Schweizer et al. 1983](#)). Many galaxies of the polar-ring variety belong to this class (see atlas in [Whitmore et al. 1990](#)), and we have already pointed out probable accreted HI rings in [section 9.7](#). An especially interesting optical ring case is Hoag's Object ([Hoag 1950](#)), which at first sight looks like a nonbarred ringed galaxy. Photographs by Schweizer et al. ([1987b](#); see [Figure 88](#)) reveal an intricate structure in the bright ring, whose projected shape is nearly circular. The classification of the ring as "inner" or "outer" is unclear, but from its large diameter (about 31 kpc if $H_0 = 75$), it would be in the realm of outer rings. [Brosh \(1985\)](#) suggested that Hoag's object is indeed a "ringed galaxy", and that the ring formed when a bar was present, but the bar is now dissolved. [Schweizer et al. \(1987b\)](#) showed, however, that the inner core is an E0 galaxy, not a disk, and suggested the alternative interpretation that the ring resulted from an accretion event 2-3 Gyr ago. Schweizer et al. also used Hoag's Object to define a class called Hoag-type galaxies, which are neither obviously barred nor obviously inclined disks, and which have outer rings including a significant fraction of the total luminosity. They presented a list of seven additional possible candidates from a survey of about 70 objects, and estimated a frequency of 0.1%, indicating that the Hoag class is quite rare.

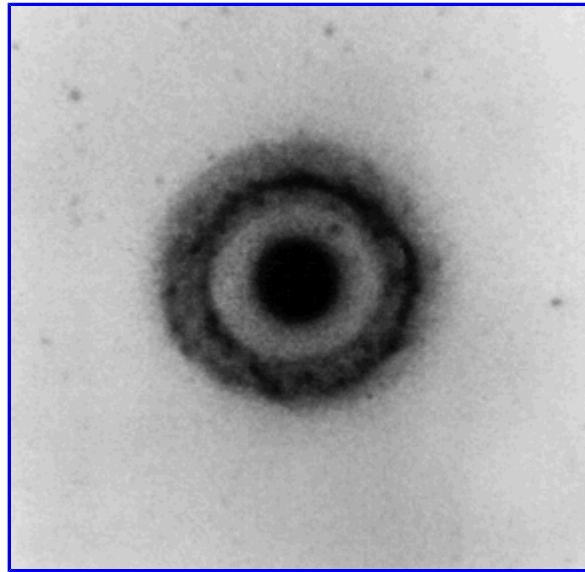


Figure 88. g-band image of Hoag's Object, from [Schweizer et al. \(1987b\)](#). The ring has a linear diameter comparable to large outer rings in barred galaxies. This is a possible face-on view of an accretion ring.

[Wakamatsu \(1990\)](#) observed one of these other candidates, [NGC 6028](#), and detected an oval structure in the central regions reminiscent of a bar. In fact, Wakamatsu examined the other galaxies in the Schweizer *et al.* list and determined that the only one lacking some elongation in the center was Hoag's Object. In [NGC 7742](#), another galaxy which bears a strong resemblance to Hoag's Object, [Wakamatsu et al. \(1996\)](#) also detected an oval central structure on a high resolution HST image. Wakamatsu suggested that the bar hypothesis is still viable for Hoag's Object because the galaxy lacks any evidence for tidal debris at low light levels. Thus, some of the rings in apparently "Hoag type" galaxies could still be resonance rings of the type we have been concerned with. Nevertheless, the possibility that nonbarred ringed galaxies may include both internally and externally-generated rings can certainly explain some of the larger dispersion in properties found for such rings compared to barred galaxies.

18. SINGLE RINGED, MULTI-ARMED SPIRAL GALAXIES

We have shown that orbit resonance theory provides a good explanation of the morphology and other characteristics of rings seen in many early-type barred galaxies. Often, such galaxies have more than one type of ring in co-existence as we discussed in [section 14.1](#), and the outer spiral pattern is defined by two main arms. Yet, there exist many examples of strong rings where the spiral structure beyond the ring is multi-armed. Examples illustrated here include [NGC 6902](#) ([Figure 4](#)), [IC 5240](#) ([Figure 8](#)), [NGC 2835](#) and [3124](#) ([Figure 11](#)), and [NGC 7217](#) ([Figure 5](#) and [Figure 37](#)). Other strong cases include [NGC 1640](#), [2307](#), [3450](#), and [3660](#) illustrated in [Buta \(1995\)](#). Except for [NGC 1640](#), the outer spiral patterns in these galaxies do not resemble one of the "OLR subclasses", and one may well question whether the inner rings in these cases are connected to the inner $4/1$ resonance. In most cases, there is either an obvious or a very weak bar inside the inner ring.

Multi-armed and flocculent galaxies have been reviewed by [Elmegreen \(1991\)](#) and simulated by [Elmegreen & Thomasson \(1993\)](#). The study by [Combes & Elmegreen \(1993\)](#) also provided some insight into these kinds of galaxies. [Elmegreen \(1991\)](#) points out that multi-armed galaxies have stellar spiral waves as seen in near-IR images, while flocculent spirals may not. He suggests that the former may either not have simple modes or may have several modes, while flocculent galaxies have such a high Q parameter that they cannot support stellar spirals while the gas can. [Elmegreen & Thomasson \(1993\)](#) used computer simulations to examine the effects of a Q barrier (a radius where Q increases rapidly) on the spiral structure. With a Q -barrier, well-developed two-armed spirals resulted, but without one, multi-armed and flocculent spirals were obtained. The difference between the latter two types of spirals was connected to the Q value of the stars. In an early-type galaxy simulation with gas, [Combes & Elmegreen \(1993\)](#) obtained nuclear and inner gas rings at the ILR and inner $4/1$ UHR, but a multiple-armed, almost flocculent spiral pattern outside the ring. In this case, they suggested that the bar was not strong enough to drive a coherent spiral outside CR.

It is likely that the inner rings seen in single-ringed, multi-armed or flocculent galaxies may be a mixture of inner $4/1$ UHR and ILR ring types. The inner ring of [NGC 2307](#) ([Buta 1995](#)) shows minor axis breaks, much like a simulated $4/1$ resonance ring. On the other hand, the turnover radius location of the inner ring of [NGC 7531](#), which is very much like [NGC 6902](#) and others in this category, suggests that the ring in that case is linked to an ILR. Thus, rotation curves may help to elucidate the nature of rings in such galaxies.

19. CONCLUSIONS

Many years ago, [Lindblad \(1974\)](#) stated that "It would be of the utmost importance for our understanding of density waves if we could identify the different resonance regions in the galaxies observed." We have never been closer to such a goal as we are now. We have shown in this review that the case for identifying observed rings and pseudorings in normal galaxies with dynamical orbit resonances associated with a bar is very strong. We have illustrated many different examples and highlighted the best and least understood cases. We have also shown that many rings are incredible star formation laboratories, and that in some galaxies a ring is the only place where major star forming events are taking place. Sophisticated modeling of individual galaxies is now necessary to further address the problems outlined in this review. The Hubble Space Telescope also has the capability to elucidate the structure in the ILR regions of barred galaxies in unprecedented detail. But the main interest of ringed and barred galaxies is what these objects tell us about how galaxies evolve. Identifying the locations of the main resonance regions in barred galaxies is one of the most important steps in understanding the dynamics of these objects.

We thank our many colleagues for their helpful discussions and collaborations over the years of research on galaxy structure and dynamics that led to this review. We also thank the authors who allowed us to use illustrations from their published works.

References

1. Adams, F. C., Ruden, S. P., and Shu, F. H. (1989), *ApJ*, **347**, 959.
2. Adams, T. F. (1977), *ApJS*, **33**, 19.
3. Appleton, P. N. and Struck-Marcell, C. (1996), *Fundamentals of Cosmic Physics*, in press.
4. Arimoto, N. and Yoshii, Y. (1986), *A&A*, **164**, 260
5. Arsenault, R. (1989), *A&A*, **217**, 66.
6. Arsenault, R., Boulesteix, J., Georgelin, V. and Roy, J.-R. (1988), *A&A*, **200**, 29.
7. Athanassoula, E. (1978), *A&A*, **69**, 395
8. Athanassoula, E. (1992), *MNRAS*, **259**, 345.
9. Athanassoula, E. and Sellwood, J. A. (1986), *MNRAS*, **221**, 213.
10. Athanassoula, E. (1996), in *Barred Galaxies*, R. Buta, D. A. Crocker, and B. G. Elmegreen, eds., ASP Conf. Ser. 91, San Francisco, p. 309.
11. Athanassoula, E. and Bosma, A. (1985), *Ann. Rev. Astron. Ap.*, **23**, 147.
12. Athanassoula, E., Bosma, A., Crézé, M., and Schwarz, M. P. (1982), *A&A*, **107**, 101.
13. Bacon, R., Emsellem, E., Monnet, G., and Nieto, J-L. (1994), *A&A*, **281**, 691.
14. Baldwin, J. E., Lynden-Bell, D., and Sancisi, R. (1980), *MNRAS*, **193**, 313.
15. Ball, R., Sargent, A. I., Scoville, N. Z., Lo, K. Y., and Scott, S. L. (1985), *ApJ*, **298**, L21.
16. Bally, J., Stark, A. A., Wilson, R. W., and Henkel, C. (1988), *ApJ*, **324**, 223.
17. Barnes, J. E. (1991), in *Dynamics of Galaxies and Their Molecular Cloud Distributions*, F. Combes and F. Casoli, eds., Kluwer, Dordrecht, p. 363.
18. Barth, A. J., Ho, L. C., Filippenko, A. V., Gorjian, V., Malkan, M., and Sargent, W. L. W. (1996), in *Barred Galaxies*, R. Buta, D. A. Crocker, and B. G. Elmegreen, eds., ASP Conf. Ser. 91, San Francisco, p. 94.
19. Barth, A. J., Ho, L. C., Filippenko, A. V., and Sargent, W. L. W. (1995), *AJ*, **110**, 1009.
20. Benedict, G. F. (1980), *AJ*, **85**, 513.
21. Benedict, G. F., Higdon, J. L., Tollestrup, E. V., Hahn, J. M., and Harvey, P. M. (1992), *AJ*, **103**, 757.
- 22.

- Benedict, G. F., Smith, B. J., and Kenney, J. D. P. (1996), in *Barred Galaxies*, R. Buta, D. A. Crocker, and B. G. Elmegreen, eds., ASP Conference Ser. Vol. 91, p. 227.
23. Bertin, G. and Romeo, A. B. (1988), *A&A*, **195**, 105.
24. Bertin, G., Lin, C. C., Lowe, S. A., and Thurstans, R. P. (1989), *ApJ*, **338**, 78.
25. Binney, J., Gerhard, O. E., Stark, A. A., Bally, J., and Uchida, K. I. (1991), *MNRAS*, **252**, 210.
26. Blitz, L. and Spiegel, D. N. (1991), *ApJ*, **370**, 205 and **379**, 631.
27. Boroson, T. (1981), *ApJS*, **46**, 177.
28. Bosma, A. (1996), in *Barred Galaxies*, R. Buta, D. A. Crocker, and B. G. Elmegreen, eds., ASP Conf. Ser. 91, San Francisco, p. 132.
29. Bosma, A., van der Hulst, J. M., and Sullivan, W. T. (1977), *A&A*, **57**, 373.
30. Bottinelli, L., Gouguenheim, L., Paturel, G., and de Vaucouleurs, G. (1980), *ApJ*, **242**, L153.
31. Bregman, J., Hogg, D. E., and Roberts, M. S. (1995), *ApJ*, **441**, 561.
32. Brosch, N. (1985), *A&A*, **153**, 199
33. Burbidge, E. M. and Burbidge, G. R. (1960), *ApJ*, **132**, 30.
34. Burton, W. B. (1992), in *The Galactic Interstellar Medium*, D. Pfenninger and P. Bartholdi, eds., Saas-Fee, Springer-Verlag, p. 1.
35. Buta, R., Mitra, S., de Vaucouleurs, G., and Corwin, H. G. (1994), *AJ*, **107**, 118.
36. Buta, R. (1984), University of Texas Publ. No. 23.
37. Buta, R. (1985), *Proc. Astr. Soc. Australia*, **6**, 56.
38. Buta, R. (1986a), *ApJS*, **61**, 609.
39. Buta, R. (1986b), *ApJS*, **61**, 631.
40. Buta, R. (1987a), *ApJS*, **64**, 1.
41. Buta, R. (1987b), *ApJS*, **64**, 383.
42. Buta, R. (1988), *ApJS*, **66**, 233.
43. Buta, R. (1989), in *The World of Galaxies*, H. Corwin and L. Bottinelli, eds., New York, Springer.
44. Buta, R. (1990a), *ApJ*, **351**, 62.
45. Buta, R. (1990b), *ApJ*, **354**, 428.
46. Buta, R. (1990c), *ApJ*, **356**, 87.
47. Buta, R. (1991), *ApJ*, **370**, 130.
48. Buta, R. (1995), *ApJS*, **96**, 39.
49. Buta, R. and Crocker, D. A. (1991), *AJ*, **102**, 1715.
50. Buta, R. and Crocker, D. A. (1992), *AJ*, **103**, 1804.
51. Buta, R. and Crocker, D. A. (1993), *AJ*, **105**, 1344.
52. Buta, R. and Purcell, G. B. (1996) in *Barred Galaxies*, R. Buta, D. A. Crocker, and B. G. Elmegreen, eds., ASP Conf. Ser. 91, San Francisco, p. 244.
53. Buta, R. and Williams, K. L. (1995), *AJ*, **109**, 543.

54. Buta, R. and de Vaucouleurs, G. (1982), *ApJ*, **48**, 219.
55. Buta, R., Crocker, D. A., and Byrd, G. G. (1992), *AJ*, **103**, 1526.
56. Buta, R., Lewis, M., and Purcell, G. B. (1996), in preparation.
57. Buta, R., Mitra, S., de Vaucouleurs, G., and Corwin, H. G. (1994), *AJ*, **107**, 118.
58. Buta, R., Purcell, G. B., and Crocker, D. A. (1995a), *AJ*, **110**, 1588.
59. Buta, R., van Driel, W., Braine, J., Combes, F., Wakamatsu, K., Sofue, Y., and Tomita, A. (1995b), *ApJ*, **450**, 593.
60. Byrd, G. G., Freeman, T., and Howard, S. (1993), *AJ*, **105**, 477
61. Byrd, G. G., Freeman, T., and Howard, S. (1994), *AJ*, **108**, 2078
62. Byrd, G., Buta, R., McCormick, D., Purcell, G. B., and Freeman, T. (1996), in *Structure and Evolution of Stellar Systems*, V. Orlov, ed., St. Petersburg Press, St. Petersburg, in press.
63. Byrd, G., Rautiainen, P., Salo, H., Buta, R., and Crocker, D. A. (1994), *AJ*, **108**, 476.
64. Canzian, B. (1993), *PASP*, **105**, 661.
65. Casoli, F. and Combes, F. (1982), *A&A*, **110**, 287.
66. Chevalier, R. A. and Furenlid, I. (1978), *ApJ*, **225**, 67.
67. Ciardullo, R., Rubin, V. C., Jacoby, G. H., Ford, H. C., and Ford, W. K. (1988), *AJ*, **95**, 438.
68. Colin, J. and Athanassoula, E. (1989), *A&A*, **214**, 99.
69. Combes, F. (1988), in *Galactic and Extragalactic Star Formation*, R. E. Pudritz and M. Fich, eds., Dordrecht, Kluwer, p. 475.
70. Combes, F. (1994), in *Mass-Transfer Induced Activity in Galaxies*, I. Shlosman, ed., Cambridge, Cambridge Univ. Press, p. 170.
71. Combes, F. (1996), in *Barred Galaxies*, R. Buta, D. A. Crocker, and B. G. Elmegreen, eds., ASP Conference Ser. Vol. 91, p. 286.
72. Combes, F. and Elmegreen, B. G. (1993), *A&A*, **271**, 391.
73. Combes, F. and Gerin, M. (1985), *A&A*, **150**, 327.
74. Combes, F. and Sanders, R. H. (1981), *A&A*, **96**, 164.
75. Combes, F., Debbasch, F., Friedli, D., and Pfenniger, D. (1990b), *A&A*, **233**, 82.
76. Combes, F., Dupraz, C., and Gerin, M. (1990a), in *Dynamics and Interactions of Galaxies*, R. Wielen, ed., Springer, New York, p. 205.
77. Combes, F., Gerin, M., Nakai, N., Kawabe, R., and Shaw, M. A. (1992), *A&A*, **259**, 27.
78. Contini, T., Davoust, E., and Considère, S. (1995), *Astrophys. Let. and Comm.*, **31**, 223.
79. Contopoulos, G. (1980), *A&A*, **81**, 198.
80. Contopoulos, G. (1988), *A&A*, **201**, 44.
81. Contopoulos, G. and Grosbøl, P. (1989), *A&A*, Rev. **1**, 261.
82. Contopoulos, G. and Papayannopoulos, T. (1980), *A&A*, **92**, 33.
83. Contopoulos, G. (1979), in *Photometry, Kinematics, and Dynamics of Galaxies*, D. S. Evans, ed., Univ. Texas, Austin, p. 425.
84. Corwin, H. G., de Vaucouleurs, A., and de Vaucouleurs, G. (1985), *Southern Galaxy Catalogue*, Univ. Texas Mono. in Astronomy No. 4.
- 85.

- Courteau, S., de Jong, R. S., and Broeils, A. H. (1996), *ApJ*, **457**, L73.
86. Cowie, L. L. (1980), *ApJ*, **236**, 868.
87. Crocker, D. A., Baugus, P. D., and Buta, R. (1996), *ApJS*, **105**, 353 (CBB)
88. Curtis, H. D. (1918), *Pub. Lick Obs.* XIII, Part I, 11.
89. Cutri, R. M., Rudy, R. J., Rieke, G. H., Tokunaga, A. T., and Willner, S. P. (1984), *ApJ*, **280**, 521
90. Dahlem, M., Wielebinski, R., Koribalski, B., and Mebold, U. (1991), in *Dynamics of Galaxies and Their Molecular Cloud Distributions*, F. Combes and F. Casoli, eds., Kluwer, Dordrecht, p. 283.
91. Danby, J. M. A (1965), *AJ*, **70**, 501.
92. de Vaucouleurs, G. (1956), *Mem. Comm. Obs.*, **3**, No. 13.
93. de Vaucouleurs, G. (1958), *ApJ*, **127**, 487.
94. de Vaucouleurs, G. (1959a), *Handbuch der Physik*, **53**, 275.
95. de Vaucouleurs, G. (1959b), *Ann. Obs. Houga*, **2**, No. 2.
96. de Vaucouleurs, G. (1963), *ApJS*, **8**, 31.
97. de Vaucouleurs, G. (1970), in *The Spiral Structure of Our Galaxy*, W. Becker and G. Contopoulos, eds., Reidel, Dordrecht, p. 88.
98. de Vaucouleurs, G. (1974), in *The Formation and Dynamics of Galaxies*, *IAU Symp.* 58, J. R. Shakeshaft, ed., Reidel, Dordrecht, p. 335.
99. de Vaucouleurs, G. (1975a), *ApJS*, **29**, 193.
100. de Vaucouleurs, G. (1975b), in *Galaxies and the Universe, Stars and Stellar Systems, Vol. IX*, A. Sandage, M. Sandage, and J. Kristian, eds., p. 557.
101. de Vaucouleurs, G. (1977), in *The Evolution of Galaxies and Stellar Populations*, B. M. Tinsley and R. Larson, eds., Yale Univ. Obs., New Haven, p. 43.
102. de Vaucouleurs, G. (1979), *ApJ*, **227**, 380.
103. de Vaucouleurs, G. and Buta, R. (1980a), *AJ*, **85**, 637.
104. de Vaucouleurs, G. and Buta, R. (1980b), *ApJS*, **44**, 451.
105. de Vaucouleurs, G. and de Vaucouleurs, A. (1964), *Reference Catalogue of Bright Galaxies*, Univ. Texas Mono. in Astr. No. 1.
106. de Vaucouleurs, G. de Vaucouleurs, A., and Corwin, H. G. (1976), *Second Reference Catalogue of Bright Galaxies*, Univ. Texas Mono. Astr. No. 2.
107. de Vaucouleurs, G., de Vaucouleurs, A., Corwin, H., Buta, R., Paturel, G., and Fouqué, P. (1991), *Third Reference Catalogue of Bright Galaxies*, Springer-Verlag, New York (RC3).
108. de Vaucouleurs, G. and Freeman, K. C. (1973), *Vistas in Astr.*, **14**, 163
109. Devereux, N., Jacoby, G. H., and Ciardullo, R. (1995), *AJ*, **110**, 1115.
110. Devereux, N. A., Kenney, J. D. P., and Young, J. S. (1992), *AJ*, **103**, 784.
111. Donner, K. J. and Thomasson, M. (1994), *A&A*, **290**, 785.
112. Duric, N. and Dittmar, M. R. (1988) *ApJ*, **332**, L67
113. Elmegreen, B. G. (1989), *ApJ*, **342**, L67.
114. Elmegreen, B. G. (1991), in *Dynamics of Galaxies and Their Molecular Cloud Distributions*, F. Combes and F. Casoli, eds., Kluwer, Dordrecht, p. 113.

115. Elmegreen, B. G. (1994a), *ApJ*, **425**, L73.
116. Elmegreen, B. G. (1994b), *ApJ*, **427**, 384.
117. Elmegreen, B. G. (1996), in *Barred Galaxies*, R. Buta, D. A. Crocker, and B. G. Elmegreen, eds., ASP Conference Ser. Vol. 91, p. 197.
118. Elmegreen, B. G. and Elmegreen, D. M. (1983), *ApJ*, **267**, 31.
119. Elmegreen, B. G. and Elmegreen, D. M. (1985), *ApJ*, **288**, 438.
120. Elmegreen, B. G. and Elmegreen, D. M. (1989), *ApJ*, **342**, 677.
121. Elmegreen, B. G. and Thomasson, M. (1993), *A&A*, **272**, 37.
122. Elmegreen, B. G., Elmegreen, D. M., and Montenegro, L. (1992a), *ApJS*, **79**, 37.
123. Elmegreen, D. M. (1996), in *Barred Galaxies*, R. Buta, D. A. Crocker, and B. G. Elmegreen, eds., ASP Conference Ser. Vol. 91, p. 23.
124. Elmegreen, D. M., Elmegreen, B. G., Combes, F., and Bellin, A. D. (1992b), *A&A*, **257**, 17.
125. Elmegreen, D. M., Elmegreen, B. G., and Bellin, A. D. (1990), *ApJ*, **364**, 415.
126. Evans, N. W. and Collett, J. L. (1994), *ApJ*, **420**, L67.
127. Falgarone, E., Puget, J-L., and Perault, M. (1992), *A&A*, **257**, 715.
128. Fasano, G., Amico, P., Bertola, F., Vio, R., and Zeilinger, W. W. (1993), *MNRAS*, **262**, 109
129. Fisher, J. R. and Tully, R. B. (1981), *ApJ*, **47**, 139.
130. Forbes, D., Kotilainen, J. I., and Moorwood, A. F. M. (1994a), *ApJ*, **433**, L13.
131. Forbes, D., Norris, R. P., Williger, G. M., and Smith, R. C. (1994b), *AJ*, **107**, 984.
132. Frank, J., King, A. R., and Raine, D. J. (1985), *Accretion Power in Astrophysics*, Cambridge University Press, Cambridge.
133. Freeman, K. C. (1975), in *Dynamics of Stellar Systems*, IAU Symposium 69, A. Hayli, ed., Reidel, Dordrecht, p. 367.
134. Friedli, D. and Benz, W. (1993), *A&A*, **268**, 65.
135. Friedli, D. and Martinet, L. (1993), *A&A*, **277**, 27.
136. Friedli, D., Wozniak, H., Rieke, M., Martinet, L., and Bratschi, P. (1996), *A & AS*, **118**, 461.
137. Fukunaga, M. and Tosa, M. (1991), *PASJ*, **43**, 469.
138. Gallagher, J. S. and Wirth, A. (1980), *ApJ*, **241**, 567.
139. Garcia-Barreto, J. A., Downes, D., Combes, F. *et al.* (1991), *A&A*, **244**, 257.
140. Garcia-Baretto, J. A., Carillo, R., Venegas, S., and Escalante-Ramirez, B. (1996), in *Barred Galaxies*, R. Buta, D. A. Crocker, and B. G. Elmegreen, eds., ASP Conference Ser. Vol. 91, p. 76.
141. García-Burillo, S., Guélin, M., and Cernicharo, J. (1993a), *A&A*, **274**, 123.
142. García-Burillo, S., Combes, F., and Gerin, M. (1993b), *A&A*, **274**, 148.
143. García-Burillo, S., Sempere, M. J., and Combes, F. (1994), *A&A*, **287**, 419.
144. Garman, L. E. and Young, J. S. (1987), *A&A*, **154**, 80.
145. Geller, M. and Huchra, J. (1983), *ApJS*, **52**, 61.
- 146.

- Gerin, M., Casoli, F., and Combes, F. (1991), *A&A*, **251**, 32.
147. Gerin, M., Combes, F., and Athanassoula, E. (1990), *A&A*, **230**, 37.
148. Gerin, M., Combes, F., and Nakai, N. (1988), *A&A*, **203**, 44.
149. Goldreich, P. and Lynden-Bell, D. (1965), *MNRAS*, **130**, 125.
150. Hasan, H. and Norman, C. (1990), *ApJ*, **361**, 69.
151. Hawarden, T. G., Huang, J. H., and Gu, Q. S. (1996), in *Barred Galaxies*, R. Buta, D. A. Crocker, and B. G. Elmegreen, eds., ASP Conference Ser. Vol. 91, p. 54.
152. Hawarden, T. G., Mountain, C. M., Leggett, S. K., and Puxley, P. J. (1986), *MNRAS*, **221**, 41P.
153. Haynes, M. P. (1979), *AJ*, **84**, 1830.
154. Haynes, M. P. and Giovanelli, R. (1991), *AJ*, **102**, 841.
155. Heller, C. H. and Shlosman, I. (1994), *ApJ*, **424**, 84.
156. Higdon, J. L. and Buta, R. (1996), in *Barred Galaxies*, R. Buta, D. A. Crocker, and B. G. Elmegreen, eds., ASP Conf. Ser. 91, San Francisco, p. 470.
157. Higdon, J. L., Buta, R., and Purcell, G. B. (1996), in preparation
158. Hjelm, M. and Lindblad P.O. (1996), *A&A*, **305**, 727
159. Ho, L., Filippenko, A., and Sargent, W. L. W. (1996), in *Barred Galaxies*, eds. R. Buta, D. A. Crocker, and B. G. Elmegreen, ASP Conf. Series Vol. 91, p. 188.
160. Hoag, A. A. (1950), *AJ*, **55**, 170
161. Hockney, R. W. and Hohl, F. (1969), *AJ*, **74**, 1102.
162. Hohl, F. (1971), *ApJ*, **168**, 343.
163. Hubble, E. (1926), *ApJ*, **64**, 321.
164. Hubble, E. (1936), *The Realm of the Nebulae*, Yale Univ. Press, Yale.
165. Hummel, E., van der Hulst, J. M., and Dickey, J. M. (1984), *A&A*, **134**, 207.
166. Hummel, E., van der Hulst, J. M., and Keel, W. C. (1987), *A&A*, **172**, 32. (HHK)
167. Icke, V. (1979), *A&A*, **78**, 21.
168. Ishizuki, S., Kawabe, R., Ishiguro, M. *et al.* (1990), *Nature* **344**, 224.
169. Isobe, T. and Feigelson, E. D. (1992), *ApJS*, **79**, 197.
170. Jarvis, B. J., Dubath, P., Martinet, L., and Bacon, R. (1988), *A & AS* **74**, 513.
171. Jog, C. J. (1992), *ApJ*, **390**, 378.
172. Jog, C. J. and Solomon, P. M. (1984), *ApJ*, **276**, 114.
173. Julian, W. H., and Toomre, A. (1966), *ApJ*, **146**, 810.
174. Junqueira, S. and Combes, F. (1996), *A&A*, **312**, 703.
175. Kalnajs, A. J. (1971), *ApJ*, **166**, 275.
176. Kalnajs, A. J. (1972), *ApJ*, **175**, 63.
177. Kalnajs, A. J. (1973), *Proc. Astron. Soc. Australia* **2**, 174.

178. Kalnajs, A. J. (1991), in *Dynamics of Disc Galaxies*, B. Sundelius, ed., Göteborg, Sweden, p. 323.
179. Keeler, J. E. (1908), Pub. Lick Observatory, VIII.
180. Kenney, J. D. P. (1991), in *Dynamics of Disc Galaxies*, B. Sundelius, ed., Göteborg, Sweden, p. 171.
181. Kenney, J. D. P. (1996), in *Barred Galaxies*, R. Buta, D. A. Crocker, and B. G. Elmegreen, eds., ASP Conference Ser. Vol. 91, p. 150.
182. Kenney, J. D. P., Wilson C. D., Scoville N. Z., Devereux N. A., and Young J. S. (1992), *ApJ*, **395**, L79.
183. Kenney, J., Carlstrom, J. E., and Young, J. S. (1993), *ApJ*, **418**, 687.
184. Kennicutt, R. C. (1994), in *Mass-Transfer Induced Activity in Galaxies*, I. Shlosman, ed., Cambridge Univ. Press, Cambridge, p. 131
185. Kennicutt, R. C., Edgar, B. K., and Hodge, P. W. (1989), *ApJ*, **337**, 761.
186. Kennicutt, R. C., Keel, W. C., and Blaha, C. A. (1989), *AJ*, **97**, 1022.
187. Kent, S. M. (1985), *ApJS*, **59**, 115.
188. Kent, S. M. (1986), *AJ*, **91**, 1301.
189. Knapen, J. H. (1996a), in *Barred Galaxies*, R. Buta, D. A. Crocker, and B. G. Elmegreen, eds., ASP Conference Ser. Vol. 91, p. 416.
190. Knapen, J. H. (1996b), in *Barred Galaxies and Circumnuclear Activity*, A. Sandqvist, S. Joersaeter, and P. O. Lindblad, eds., Springer, in press.
191. Knapen, J. H., Beckman, J. E., Shlosman, I., Peletier, R. F., Heller, C. H., and de Jong, R. S. (1995a), *ApJ*, **443**, L73
192. Knapen, J. H., Beckman, J. E., Heller, C. H., Shlosman, I., and de Jong, R. S. (1995b), *ApJ*, **454**, 623
193. Knapp, G. R., van Driel, W., Schwarz, U. J., van Woerden, H., and Gallagher, J. S. (1984), *A&A*, **133**, 127.
194. Korchagin, V., Kembhavi, A. K., Mayya, Y. D., and Prabhu, T. P. (1995), *ApJ*, **446**, 574.
195. Koribalski, B. (1996), in *Barred Galaxies*, R. Buta, D. A. Crocker, and B. G. Elmegreen, eds., ASP Conference Ser. Vol. 91, p. 172.
196. Koribalski, B., Dahlem, M., Mebold, U., and Brinks, E. (1993), *A&A*, **268**, 14.
197. Kormendy, J. (1977), *ApJ*, **214**, 359.
198. Kormendy, J. (1979a), *ApJ*, **227**, 714.
199. Kormendy, J. (1979b), in *Photometry, Kinematics, and Dynamics of Galaxies*, D. S. Evans, ed., Univ. Texas, Austin, p. 341.
200. Kormendy, J. (1981), in *Structure and Evolution of Normal Galaxies*, S. M. Fall and D. Lynden-Bell, eds., Cambridge University Press, Cambridge, p. 85.
201. Kormendy, J. (1982a), in *Morphology and Dynamics of Galaxies*, L. Martinet and M. Mayor, eds., Geneva Obs., Sauverny, p. 113.
202. Kormendy, J. (1982b), *ApJ*, **257**, 75.
203. Kormendy, J. (1983), *ApJ*, **275**, 529.
204. Kormendy, J. (1984), *ApJ*, **286**, 116.
205. Kostiuk, I. (1975), *Comm. Special Astrophysical Obs.*, No. 13, p. 45
206. Krumm, N., van Driel, W., and van Woerden, H. (1985), *A&A*, **144**, 202.
- 207.

- Lacey, C. G. (1984), *MNRAS*, **208**, 687.
208. Larson, R. B. and Tinsley, B. M. (1978), *ApJ*, **219**, 46.
209. Lassell, W. (1866), *Mem. RAS*, **36**, 33.
210. Laughlin, G. and Korchagin, V. (1996), *ApJ*, **460**, 855.
211. Leitherer, C. and Heckman, T. (1995), *ApJS*, **96**, 9.
212. Lesch, H., Biermann, P. L., and Crusius, A. *et al.* (1990), *MNRAS*, **242**, 194.
213. Lin, C. C. (1971), *Highlights of Astr.*, **2**, 88.
214. Lin, C. C. and Shu, F. H. (1964), *ApJ*, **140**, 646.
215. Lin, D. N. C. and Pringle, J. E. (1987), *MNRAS*, **225**, 607.
216. Lindblad, B. (1955), *Stockholm Obs. Ann.* **18**, no. 6.
217. Lindblad, B. (1962), *IAU Symp.* 15, p. 164
218. Lindblad, B. (1964), *Astrophys. Norv.* **9**, 103.
219. Lindblad, P. O. (1960), *Stockholm Obs. Ann.* **21**, no. 4.
220. Lindblad, P. O. (1974), in *The Formation and Dynamics of Galaxies*, *IAU Symp.* 58, J. R. Shakeshaft, ed., Reidel, Dordrecht, p. 399.
221. Lindblad, P. O. and Jörsäter, S. (1981), *A&A*, **97**, 56
222. Lindblad, P. O., Hjelm M., Högbom J., Jörsäter, S., Lindblad P.A.B., Santos-Lleo M. (1996), *A&AS*, **120**, 403.
223. Lo, K. Y., Cheung, K. W., Masson, C. R., Phillips, T. G., Scott, S. L., and Woody, D. P. (1987), *ApJ*, **312**, 574.
224. Lucy, L. B. (1974), *AJ*, **79**, 745.
225. Lundmark, K. (1926), *Arkiv For Matematik, Astronomi Och Physik*, Band 19B, No. 8.
226. Lynden-Bell, D. (1979), *MNRAS*, **187**, 101.
227. Lynden-Bell, D. and Kalnajs, A. J. (1972), *MNRAS*, **157**, 1 (LBK72).
228. Lynden-Bell, D. and Pringle, J. E. (1974), *MNRAS*, **168**, 603.
229. Madore, B. (1980), *AJ*, **85**, 507.
230. Marcelin, M. and Athanassoula, E. (1982), *A&A*, **105**, 76.
231. Mark, J. W-K. (1974a), in *The Formation and Dynamics of Galaxies*, *IAU Symp.* 58, J. R. Shakeshaft, ed., Reidel, Dordrecht, p. 418.
232. Mark, J. W-K. (1974b), *ApJ*, **193**, 539.
233. Mayya, Y. D. (1994), *AJ*, **108**, 1276.
234. McCall, M. L., Rybski, P. M., and Shields, G. A. (1985), *ApJS*, **57**, 1.
235. McKee, C. F. and Ostriker, J. P. (1977), *ApJ*, **218**, 148.
236. Meaburn, J., Terrett, D. L., Theokas, A., and Walsh, J. R. (1981), *MNRAS*, **195**, 39.
237. Mebold, U., Goss, W. M., van Woerden, H., Hawarden, T. G., and Siegman, B. (1979), *A&A*, **74**, 100.
238. Merrifield, M. R. and Kuijken, K. (1994), *ApJ*, **432**, 575.
- 239.

- Merrifield, M. R. and Kuijken, K. (1995), *MNRAS*, **274**, 933.
240. Meurer, G. R., Freeman, K. C., Dopita, M. A., and Cacciari, C. (1992), *AJ*, **103**, 60.
241. Miller, R. H. and Prendergast, K. H. (1968), *ApJ*, **151**, 699.
242. Miller, R. H. and Smith, B. F. (1979), *ApJ*, **227**, 785.
243. Miller, R. H. and Smith, B. F. (1992), *ApJ*, **393**, 508.
244. Miller, R. H., Prendergast, K. H., and Quirk, W. J. (1970), *ApJ*, **161**, 903.
245. Moles, M., Márquez, I., and Pérez, E. (1995), *ApJ*, **438**, 604.
246. Moore, E. M. and Gottesman, S. T. (1995), *ApJ*, **447**, 159.
247. Morgan, W. W. (1958), *PASP*, **70**, 364.
248. Mulder, P. S. (1995), PhD Thesis, University of Groningen.
249. Mulder, P. S. and van Driel, W. (1993), *A&A*, **272**, 63.
250. Mulder, W. A. and Liem, B. T. (1986), *A&A*, **157**, 148.
251. Mundell, C. G., Pedlar, A., Shone, D. L., Asif, M. W., Robinson, A., and Axon, D. J. (1996), in *Barred Galaxies*, R. Buta, D. A. Crocker, and B. G. Elmegreen, eds., ASP Conference Ser. Vol. 91, p. 242.
252. Nishida, M. T. and Wakamatsu, K. (1996), *AJ*, in press.
253. Noguchi, M. (1987), *MNRAS*, **228**, 635.
254. Noguchi, M. and Ishibashi, S. (1986), *MNRAS*, **219**, 305
255. Noh, H., Vishniac, E. T., and Cochran, W. D. (1992), *ApJ*, **397**, 347.
256. Norman, C., May, A., and van Albada, T. S. (1985), *ApJ*, **296**, 20.
257. Odewahn, S. C. (1996), in *Barred Galaxies*, R. Buta, D. A. Crocker, and B. G. Elmegreen, eds., ASP Conference Ser. Vol. 91, p. 30.
258. Ohta, K., Hamabe, M., and Wakamatsu, K. (1990), *ApJ*, **357**, 71.
259. Ostriker, J. P. and Peebles, P. J. E. (1973), *ApJ*, **186**, 467.
260. Paczynski, B., Stanek, K. Z., Udalski, A., Szymanski, M., Kaluzny, J., Kubiak, M., Mateo, M., and Krzeminski, W. (1994), *ApJ*, **435**, L113.
261. Palmer, P. L. and Papaloizou, J. (1990), *MNRAS*, **243**, 263.
262. Palous, J., Jungwiert, B., and Kopecky, J. (1993), *A&A*, **274**, 189.
263. Parsons, C. (1926), *The Scientific Papers of William Parsons, Third Earl of Rosse 1800-1867*, The County Press, London.
264. Pasha, I. I. and Polyachenko, V. L. (1994), *MNRAS*, **266**, 92.
265. Pedreros, M. and Madore, B. F. (1981), *ApJS*, **45**, 541.
266. Perrine, C. D. (1922), *MNRAS*, **82**, 486.
267. Peters, W. L. (1975), *ApJ*, **196**, 617.
268. Peterson, C. J., Rubin, V. C., Ford, W. K., and Thonnard, N. (1976), *ApJ*, **208**, 662.
269. Peterson, C. J., Rubin, V. C., Ford, W. K., and Thonnard, N. (1978), *ApJ*, **219**, 31.
270. Peterson, S. D. (1979), *ApJS*, **40**, 527.

271. Petrou, M. and Papayannopoulos, T. (1986), *MNRAS*, **219**, 157.
272. Pfenniger, D. (1991), in *Dynamics of Disk Galaxies*, B. Sundelius, ed., Göteborg, Sweden, p. 191.
273. Pfenniger, D. (1993), in *Physics of Nearby Galaxies: Nature or Nurture?*, T. X. Thuan, C. Balkowski, J. Tran Thanh Van, eds., Editions Frontieres, Gif-sur-Yvette, p. 519.
274. Pfenniger, D. (1996), in *Barred Galaxies*, R. Buta, D. A. Crocker, and B. G. Elmegreen, eds., ASP Conference Ser. Vol. 91, p. 449.
275. Pfenniger, D. and Combes, F. (1994), *A&A*, **285**, 94.
276. Pfenniger, D. and Norman, C. (1990), *ApJ*, **363**, 391.
277. Pfenniger, D., Combes, F., and Martinet, L. (1994), *A&A*, **285**, 79.
278. Phillips, A. C. (1993a), PhD Thesis, University of Washington
279. Phillips, A. C. (1993b), *AJ*, **105**, 486.
280. Phillips, A. C. (1996), in *Barred Galaxies*, R. Buta, D. A. Crocker, and B. G. Elmegreen, eds., ASP Conference Ser. Vol. 91, p. 44.
281. Phillips, A. C., Illingworth, G. D., MacKenty, J. W., and Franx, M. (1996), *AJ*, **111**, 1566
282. Phookun, B., Mundy, L. G., Teuben, P., and Wainscoat, R. J. (1992), *ApJ*, **400**, 516.
283. Phookun, B., Vogel, S. N., and Mundy, L. G. (1993), *ApJ*, **418**, 113.
284. Pierce, M. J. (1986), *AJ*, **92**, 285.
285. Piner, B. G., Stone, J. M., and Teuben, P. J. (1995), *ApJ*, **449**, 508
286. Pogge, R. W. (1989), *ApJS*, **71**, 433.
287. Pogge, R. W. and Eskridge, P. B. (1993), *AJ*, **106**, 1405.
288. Polyachenko, V. L. (1994), in *Physics of the Gaseous and Stellar Disks of the Galaxy*, I. R. King, ed., ASP Conference Ser. Vol. 66, p. 103.
289. Polyachenko, V. L. (1996), in *Barred Galaxies*, R. Buta, D. A. Crocker, and B. G. Elmegreen, eds., ASP Conference Ser. Vol. 91, p. 406.
290. Polyachenko, E. V. and Polyachenko, V. L. (1996), in *Barred Galaxies*, R. Buta, D. A. Crocker, and B. G. Elmegreen, eds., ASP Conference Ser. Vol. 91, p. 476.
291. Randers, G. (1940), *ApJ*, **92**, 235.
292. Reynolds, J. H. (1921), *MNRAS*, **81**, 601.
293. Richter, O-G. and Sancisi, R. (1994), *A&A*, **290**, L9.
294. Rix, H-W. and Rieke, M. J. (1993), *ApJ*, **418**, 123.
295. Rix, H-W. and Zaritsky, D. (1995), *ApJ*, **447**, 82.
296. Roberts, W. W. and Hausman, M. A. (1984), *ApJ*, **277**, 744.
297. Roberts, W. W., Roberts, M. S., and Shu, F. H. (1975), *ApJ*, **196**, 381.
298. Robinson, A., Vila-Vilaró, B., Axon, D. J., Pérez, E., Wagner, S. J., Baum, S. A., Boisson, C., Durret, F., González-Delgado, R. M., and Moles, M. (1994), *A&A*, **291**, 351.
299. Romeo, A. B. (1992), *MNRAS*, **256**, 307.
- 300.

- Rougoor, G. and Oort, J. H. (1960), *Proc. N. A. S.*, **46**, 1.
301. Rubin, V. C. (1980), *ApJ*, **238**, 808.
302. Rubin, V. C., Ford, W. K., and Peterson, C. J. (1975), *ApJ*, **199**, 39.
303. Rubin, V. C., Ford, W. K., Strom, K. M., Strom, S. E., and Romanishin, W. (1978), *ApJ*, **224**, 782.
304. Ryder, S. D. and Dopita, M. A. (1993), *ApJS*, **88**, 415.
305. Ryder, S. D., Buta, R. J., Toledo, H., Shukla, H., Staveley-Smith, L., and Walsh, W. (1996), *ApJ*, **460**, 665.
306. Sakamoto, K., Okumura, S., Minezaki, T., Kobayashi, Y., and Wada, K. (1995), *AJ*, **110**, 2075.
307. Sancisi, R., Broeils, A., Kamphuis, J., and van der Hulst, T. (1990), in *Dynamics and Interactions of Galaxies*, R. Wielen, ed., Springer, New York, p. 304.
308. Sandage, A. (1961), *The Hubble Atlas of Galaxies*, Carnegie Inst. of Wash. Publ. No. 618.
309. Sandage, A. (1975), in *Galaxies and the Universe, Stars and Stellar Systems, Vol. IX*, A. Sandage, M. Sandage, and J. Kristian, eds., p. 1.
310. Sandage, A. and Bedke, J. (1994), *The Carnegie Atlas of Galaxies*, Carnegie Inst. of Wash. Publ. No. 638.
311. Sandage, A. and Brucato, R. (1979), *AJ*, **84**, 472.
312. Sandage, A. and Tammann, G. A. (1981), *A Revised Shapley-Ames Catalog of Bright Galaxies*, Carnegie Institute of Washington Publ. No. 635 (first edition).
313. Sandage, A. and Tammann, G. A. (1987), *A Revised Shapley-Ames Catalog of Bright Galaxies*, Carnegie Institute of Washington Publ. No. 635 (second edition).
314. Sanders, R., and Bania, T. M. (1976), *ApJ*, **204**, 341.
315. Sanders, R. H. and Huntley, J. M. (1976), *ApJ*, **209**, 53.
316. Sanders, R. H. and Prendergast, K. H. (1974), *ApJ*, **188**, 489.
317. Sanders, R. H. and Tubbs, A. D. (1980), *ApJ*, **235**, 803.
318. Saraiva, M. F. (1996), in *Barred Galaxies*, R. Buta, D. A. Crocker, and B. G. Elmegreen, eds., ASP Conference Ser. Vol. 91, p. 120.
319. Schempp, W. V. (1982), *ApJ*, **258**, 96.
320. Schommer, R. A. (1976), *BAAS*, **8**, 314.
321. Schommer, R. A., Caldwell, N., Wilson, A. S., Baldwin, J. A., Phillips, M. M., Williams, T. B., and Turtle, A. J. (1988), *ApJ*, **324**, 154.
322. Schwarz, M. P. (1979), PhD Thesis, Australian National University.
323. Schwarz, M. P. (1981), *ApJ*, **247**, 77.
324. Schwarz, M. P. (1984a), *Proc. Astr. Soc. Australia*, **5**, 464.
325. Schwarz, M. P. (1984b), *MNRAS*, **209**, 93.
326. Schwarz, M. P. (1984c), *A&A*, **133**, 222.
327. Schwarz, M. P. (1985), *Proc. Astr. Soc. Australia*, **6**, 202.
328. Schweizer, F. (1976), *ApJS*, **31**, 313.
329. Schweizer, F. (1980), *ApJ*, **237**, 303.
- 330.

- Schweizer, F., Whitmore, B. C., and Rubin, V. C. (1983), *AJ*, **88**, 909
331. Schweizer, F., Ford, W. K., Jedrzejewski, R., and Giovanelli, R. (1987b), *ApJ*, **320**, 454.
332. Schweizer, F., van Gorkom, J., and Seitzer, P. (1987a), *ApJ*, **338**, 770.
333. Searle, L., Sargent, W. L. W., and Bagnuolo, W. G. (1973), *ApJ*, **179**, 427.
334. Selby, S. M. (1973), *Standard Mathematical Tables*, 21st edition, Chemical Rubber Co., Cleveland, p. 394.
335. Sellwood, J. A. (1981), *A&A*, **99**, 362.
336. Sellwood, J. A. and Athanassoula, E. (1986), *MNRAS*, **221**, 195.
337. Sellwood, J. A. and Carlberg, R. G. (1984), *ApJ*, **282**, 61.
338. Sellwood, J. A. and Sparke, L. S. (1988) *MNRAS*, **231**, 25P.
339. Sellwood, J. A. and Wilkinson, A. (1993), *Rep. Prog. Phys.* **56**, 173.
340. Sempere, M. J., Combes, F., and Casoli, F. (1995b), *A&A*, **299**, 371.
341. Sempere, M. J., Garcia-Burillo, S., Combes, F., and Knapen, J. (1995a), *A&A*, **296**, 45.
342. Sersic, J. L. (1958), *Observatory*, **78**, 125.
343. Sersic, J. L. and Pastoriza, M. G. (1965), *PASP*, **77**, 287.
344. Sersic, J. L. and Pastoriza, M. G. (1967), *PASP*, **79**, 152.
345. Shane, W. W. (1972), *A&A*, **16**, 119.
346. Shapley, H. and Ames, A. (1932), *Harvard Ann.*, **88**, No. 2.
347. Shapley, H. and Paraskevopoulos, J. S. (1940), *Proc. Nat. Acad. Sci.*, **26**, 31.
348. Shaw, M. A., Combes, F., Axon, D. J., and Wright, G. S. (1993), *A&A*, **273**, 31.
349. Shlosman, I. and Noguchi, M. (1993), *ApJ*, **414**, 474.
350. Shlosman, I., Frank, J., and Begelman, M. C. (1989), *Nature*, **338**, 45.
351. Shu, F., Tremaine, S., Adams, F. C., and Ruden S. D., (1990), *ApJ*, **358**, 495.
352. Silchenko, O. K. and Lipunov, V. M. (1987), *Astrofizica* **26**, 443.
353. Simkin, S. M. (1967), *AJ*, **72**, 1032.
354. Simkin, S. M., Su, H. J., and Schwarz, M. P. (1980), *ApJ*, **237**, 404.
355. Simonson, S. C. and Mader, G. L. (1973), *A&A*, **27**, 337.
356. Smith, B. J., Lester, D. F., Harvey, P. M., and Pogge, R. W. (1991), *ApJ*, **373**, 66.
357. Sofue, Y. (1991), in *Dynamics of Galaxies and Their Molecular Cloud Distributions*, F. Combes and F. Casoli, eds., Kluwer, Dordrecht, p. 287.
358. Sparke, L. S. and Sellwood, J. A. (1987), *MNRAS*, **225**, 653.
359. Storchi-Bergmann, T., Wilson, A. S., and Baldwin, J. A. (1996), *ApJ*, **460**, 252
360. Su, H. J. and Simkin, S. M. (1980), *ApJ*, **238**, L1.
361. Sundin, M., Donner, K. J., and Sundelius, B. (1993), *A&A*, **280**, 105.
362. Tagger, M., Sygnet, J. F., Athanassoula, E., and Pellat, R. (1987), *ApJ*, **318**, L43.

363. Telesco, C. M. and Decher, R. (1988), *ApJ*, **334**, 573.
364. Telesco, C. M. and Gatley, I. 1981, *ApJ*, 247, L11.
365. Teuben, P. (1996), in *Barred Galaxies*, R. Buta, D. A. Crocker, and B. G. Elmegreen, eds., ASP Conference Ser. Vol. 91, p. 299.
366. Thomasson, M., Donner, K. J., Sundelius, B., Byrd, G. G., Huang, T. Y., and Valtonen, M. J. (1989), *A&A*, **211**, 25.
367. Tilanus, R. P. J. and Allen, R. J. (1993), *A&A*, **274**, 707.
368. Toomre, A. (1964), *ApJ*, **139**, 1217.
369. Toomre, A. (1981), in *Structure and Evolution of Normal Galaxies*, S. M. Fall and D. Lynden-Bell, eds., Cambridge Univ. Press, Cambridge, p. 111.
370. Tremaine, S. (1995), *AJ*, **110**, 628.
371. Tremaine, S. and Weinberg, M. D. (1984), *ApJ*, **282**, L5.
372. Tully, R. B. (1974), *ApJS*, **27**, 415.
373. Turner, E. (1976), *ApJ*, **208**, 20.
374. Turner, J. L. (1996), in *Barred Galaxies*, R. Buta, D. A. Crocker, and B. G. Elmegreen, eds., ASP Conference Ser. Vol. 91, p. 143.
375. Turner, E. and Gott, J. R. (1976), *ApJS*, **32**, 409.
376. van Albada, G. D. (1985), *A&A*, **142**, 491.
377. van Albada, G. D. and Roberts, M. S. (1981), *ApJ*, **246**, 740.
378. van der Kruit, P. C. (1974), *ApJ*, **188**, 3.
379. van der Kruit, P. C. (1976a), *A&AS*, **25**, 527.
380. van der Kruit, P. C. (1976b), *A&A*, **52**, 85.
381. van Driel, W. and Buta, R. (1991), *A&A*, **245**, 7.
382. van Driel, W., Rots, A. H., and van Woerden, H. (1988), *A&A*, **204**, 39.
383. van Driel, W., van Woerden, H., Gallagher, J. S., Schwarz, U. J. (1988), *A&A*, **191**, 201.
384. Véron-Cetty, M. P. and Véron, P. (1991), *A Catalogue of Quasars and Active Nuclei*, ESO Scientific Report 10, Garching.
385. Verdes-Montenegro, L., Bosma, A., and Athanassoula, E. (1995), *A&A*, **300**, 65.
386. Vila-Vilaró, B., Robinson, A., Pérez, E., Axon, D. J., Baum, S. A., González-Delgado, R. M., Pedlar, A., Pérez-Fournon, I., Perry, J. J., and Tadhunter, C. N. (1995), *A&A*, **302**, 58.
387. von Linden, S., Lesch, H., and Combes, F. (1994), in *Mass-Transfer Induced Activity in Galaxies*, I. Shlosman, ed., Cambridge Univ. Press, Cambridge, p. 189.
388. Vorontsov-Velyaminov, B. A. (1987), *Extragalactic Astronomy*, Harwood Academic Publishers, New York.
389. Vorontsov-Velyaminov, B. A., Arkhipova, V. P., and Krasnogorskaya, A. A. ([1962](#), [1963](#), [1964](#), [1968](#), [1974](#)), *Morphological Catalogue of Galaxies*, Parts 1-5, Moscow Univ. Press, Moscow.
390. Wada, K. and Habe, A. (1992), *MNRAS*, **258**, 82.
391. Wakamatsu, K. (1990), *ApJ*, **348**, 448.
392. Wakamatsu, K. and Nishida, M. T. (1980), *PASJ* **32**, 389.
393. Wakamatsu, K., Hamabe, M., Nishida, M. T., and Tomita, A. (1996), in *Barred Galaxies*, R. Buta, D. A. Crocker, and B. G.

- Elmegreen, eds., ASP Conf. Series Vol. 91, p. 83.
394. Weinberg, M. D. (1992), *ApJ*, **384**, 81.
395. Wevers, B. M. H. R. (1984), PhD Thesis, University of Groningen.
396. Wevers, B. M. H. R., Appleton, P. N., Davies, R., and Hart, L. (1984), *A&A*, **140**, 125.
397. Whitmore, B. C. and Schweizer, F. (1995), *AJ*, **109**, 960.
398. Whitmore, B., McElroy, D., and Schweizer, F. (1987), *ApJ*, **314**, 439.
399. Whitmore, B. C., Lucas, R. A., McElroy, D. B., Steiman-Cameron, T. Y., Sackett, P. D., and Olling, R. P. (1990), *AJ*, **100**, 1489.
400. Whitmore, B. C., Schweizer, F., Leitherer, C., Borne, K., and Robert, C. (1993), *AJ*, **106**, 1354.
401. Wielen, R. (1977), *A&A*, **60**, 263.
402. Wilson, A. S., Helfer, T. T., Haniff, C. A., and Ward, M. J. (1991), *ApJ*, 381, 79.
403. Wolstencroft, R. D. and Schempp, W. V. (1979), *New Zealand J. of Science*, **22**, 325.
404. Wolstencroft, R. D., Tully, R. B., and Perley, R. A. (1984), *MNRAS*, **207**, 889.
405. Wozniak, H., Friedli, D., Martinet, L., Martin, P., and Bratschi, P. (1995), *A&AS*, **111**, 115.
406. Zang, T. A. and Hohl, F. (1978), *ApJ*, **226**, 521.
407. Zaritsky, D. and Lo, K. Y. (1986), *ApJ*, **303**, 66.
408. Zhang, X. (1996), I *ApJ*, **457**, 125, and II, in press.